Dottorato di ricerca in Fisica

Ciclo XXX

Criticality Hypothesis in the Brain: from Neutral theory to Self-Organization and Synchronization

Coordinatore:
Chiar.mo Prof. Cristiano Viappiani

Tutor:
Chiar.ma Prof.ssa Raffaella Burioni

Tutor esterno:
Chiar.mo Prof. Miguel Angel Muñoz Martinez

Dottorando: Serena Di Santo

Contents

Chapter 1

Introduction

1.1 Motivation and Objectives

Beyond any doubt, the human brain is one of the most exciting subjects we can set to study. This magnificent organ is able to perform the most awesome tasks, such as storing information, making decisions, learning from the outcomes of its decisions, creating a set of conventions with other individuals in order to establish a communication, as a basis for coordinating cooperation and so on. Moreover, it can develop sophisticated thoughts, combine feelings and logics to create pictures of reality –for example through music, art or philosophy– feel emotions, elaborate on them while resting or dreaming, regulate tens of contradictory drives while working on different layers of consciousness...

Last decades have witnessed a spectacular improvement of functional and structural imaging techniques and the development of new methods of measure,

allowing us to boost formidably the resolution and the quality of recordings of electrochemical activity across neural units. All theese efforts allow us to gain insights into the physiological mechanisms ruling such an intricate machine, but of course a long way remains before this approach can try to explain phenomena as complex as the ones named above. There is still a big gap to fill before understanding how such a huge variety of abilities can emerge from the cooperation of a collection of cells exchanging electrical signals. Nevertheless it is certainly an extraordinary challenge to try to characterize the dynamics of activity in the brain and to address the question of which types of collective behaviors it is possible to reproduce from an ensemble of model-neurons and what are the minimal ingredients to be considered in the model to generate relevant emergent phenomena, explaining at least simple experimental observations.

One fascinating idea that emerged in Neuroscience, in parallel with other biological fields, is that this amazing complexity of performances must arise from the cooperation between units interacting efficiently at a wide scale. Such a long-range dynamics could spontaneously emerge as a consequence of the system being posed in the vicinity of the critical point of a phase transition. Moreover, if the system operates in a critical regime, it is conceivable that it might feature some self-regulatory mechanism guiding it and keeping it close to such a regime, under standard –healthy– conditions. Much work has been done after the proposal of this scenario, and many controversies emerged – of which we will try to give a glimpse along this thesis – but very often it is not even clear which are the two phases separated by the alleged phase tran-

sition. Along this PhD thesis we will explore this subject, trying to develop general schemes in order to shed light on the, so-called, *criticality hypothesis*. We will not claim that the brain is critical, nor that it's not, but we will present several possible interpretations to the phenomenology reported by experiments, adopting a neutral point of view. To the best of our knowledge, at present there exist no "smoking gun" experiment allowing to confirm or disprove the criticality hypothesis in Neuroscience: empiric evidence from larger systems, more accurate measurements, and less ambiguous analyses would be highly needed to prove or exclude such a scenario [1]. From a more general (and *critical*) point of view, asking whether biological systems are critical or not may be misleading, on the one hand because unveiling that the system is critical (or not), would not guarantee any practical implications on the system, on the other hand, because it is almost trivial that, if one wants to fit a complex phenomenon into a simple model, the only point where a match can be found is where the simple model develops complexity, i.e. in the critical point [2, 3]. However, the collection of many small pieces of information suggesting similarities between experimental reports and features of criticality cannot be neglected. Moreover, criticality might be considered as a very general mechanism through which Nature develops rich patterns, hence its apparent "obviousness" is a strength, rather than a weak point. These and more interesting reflexions about criticality in living systems can be found in [1].

Here, in particular, we clarify some crucial issues related, e.g., to the features of the existing models, to the methods used in experimental measurements and to the very essential features of the dynamics, which we think that can signif-

icantly improve the contents of the discussion on the criticality hypothesis.

1.2 Background context: Criticality in Neuroscience

Interesting phenomena in Biological systems are usually collective features emerging from the interactions among many constituents. During the last decades, Statistical Physics has proven more and more useful to collaborate with biology in solving problems concerning the study of life and living organisms [4]. One tremendously simple observation is that biological systems are nor simple, ordered and symmetric as a crystal, nor completely random or chaotic and disordered. Moreover, such living systems usually show spatial and temporal long range correlations, high sensitivity to stimuli, and the ability to adapt to perform a wide variety of complex tasks. All those hints readily suggest that living systems might be operating close to the critical point of some phase transition, hypothetically meaning that millions of years of evolution have selected for tuning "life" –or some aspects of it– to the point that maximizes complexity, variability and repertoire of behaviors.

According to this hypothesis, some living structures tend to achieve an optimal trade-off between robustness (resilience to external perturbations, a property of ordered phases) and flexibility (responsiveness to environmental stimuli, a trademark of disordered phases). From a statistical physics point of view, a most favorable balance between two competing tendencies can be accomplished

by keeping the system's dynamical state at the borderline of an order-disorder phase transition.

In 1990 Christopher Langton [5] proposed a way to parametrize the space of all possible cellular automata, evidencing the existence of a phase transition between highly ordered (deterministic) and highly disordered (chaotic) dynamics. He showed that optimal conditions for the support of transmission, storage and processing of information, are achieved in the vicinity of the transition point. Cellular automata in the vicinity of such a critical point appear to be non-degenerative, constructive, and open ended: they were demonstrated to be capable of universal computation, being equivalent to Universal Turing Machines. This means that in order for physical systems to support primitive functions required for computation (transmission, storage and modification of information), they must operate at the "edge of chaos", i.e. they must be hovering over some kind of phase transition.

Langton's idea was received with enthusiasm by Per Bak and colleagues [6], whose research aimed at finding a model for a general mechanism encoded in natural systems, allowing them to self-adjust to the vicinity of a phase transition, without the need of any external experimentalist who tunes the system to the critical point. They came up with a toy-model, for piles of grains of "sand" arriving at a threshold level and toppling, by redistributing grains to the neighbors in a 2D lattice. Cascades of toppling events, named avalanches, showed power law distribution of size and duration, fulfilling finite size scaling. Subsequently, further theoretical work [7, 8] established clearly that the sandpile undergoes a proper dynamical phase transition and identified

the specific universality class it belongs to. We refer to the Appendix A for a brief presentation of the Self-Organized Criticality (SOC) paradigm.

Nevertheless, both edge-of-chaos and SOC frameworks encountered the disapproval of a section of the complex systems community, since they seemed to be destined to stay confined to the realm of simple toy-models, not apt for describing any real natural system.

After a pioneering experiment performed in 2003 by John Beggs and Dietmar Plenz [9], the perspective of the criticality hypothesis spread into Neuroscience and the paradigm of SOC got rejuvenated. Beggs and Plenz were able to measure spatially distributed electrical activity on a slice of rat neocortex, through an array of microelectrodes superimposed to the slice, detecting the activity of small communities of neurons. This allowed them to measure the statistics of clusters of activity –from there on named *neuronal avalanches*–, which resulted free of any characteristic scale, both in time and in space extension, with a behavior very similar to sandpile's avalanches. On one hand, the work of Beggs and Plenz inspired a whole new research line in experimental neurophysics, aiming at checking their findings in a vast variety of experimental settings, across scales and species [10, 11, 12, 13, 14, 15, 16]. An important remark to stress is that, under un-healthy or pathological conditions, the features of criticality fade away [17], giving a hint for a natural parametrization of the alleged phase transition, or at least suggesting possible candidates for the subcritical and supercritical regimes –which, in this case, might be more than unaccessible imaginary phases of the parameter space– and thus conferring a much stronger basis to the idea of optimality achieved in the vicinity of a phase

transition. On the other hand, it found a solid and most appropriate theoretical support in Langton's result, since the cerebral cortex certainly requires optimal computational capabilities, in a sense most pertinent with the one it was originally proposed for. Moreover it is worth to note that, in the perspective of artificial neural networks, it has also been suggested in recent years that criticality features result essential for optimal deep-learning proficiency [18, 19] .

1.3 Outline of the work

The appearance of scale-invariant episodes of collective activity in networks of synthetic units is rationalized under several distinct frameworks (both critical and not) during this thesis, posing new and fascinating questions that may contribute to clarify crucial issues on the criticality hypothesis in the cortex and its implications for function and learning.

From a statistical physics point of view, several models have been developed [20, 21], which claimed to reproduce self-organization to criticality, relying on neurophysiologically plausible models of neurons or communities of neurons and synapses.

In particular, we analyze in depth the model of Millman et al. [21], which claims to reproduce self-organized criticality with its concomitant self-similar activity patterns in a whole set of parameter space corresponding to the "Up" state. In **Chapter 2** we clarify that self-organzied criticality cannot be pos-

sibly obtained in a state of sustained collective activity and we show that the interesting model proposed by Millman et al. reports scale free distributed *coexisting* avalanches, as a consequence of "neutrality" of the avalanches (no avalanche expands or shrinks in a preferential way with respect to the others). Moreover the scale-invariance is lost if precise causal information –of which neuron provokes the firing of which– is removed from the picture and it is worth to stress that this type of information is mostly unaccessible in real experiments. Thus, Millmann's model, although apparently physiologically accurate at a single-unit scale, is not apt to reproduce empirical results on emergent collective behaviors.

As reported in Millman model and in every biologically-inspired model of neurons (see Perceptron, Leaky Integrate and Fire, Wilson-Cowan, Brunel, Hodgkin and Huxley models etc.[1]), an essential feature of neural units is to integrate the inputs arriving from neighboring presynaptic active sites and produce a (significative) response only if/when such an input is sufficiently high. This very basic property, at a coarse grained level, gives rise to a positive feedback loop such that activity fosters the generation of further activity: a feature that suggests a scenario in which either the system is very active, or it is mostly silent. This observation naturally suggests the possibility that neural systems are posed in the vicinity of a first order (discontinuous) phase transition[2], which will be a recurrent theme throughout this thesis.

[1] We refer to Appendix B for a short presentation of some models in neuroscience, which are most relevant for a comprehensive view on this thesis

[2] This is also strongly evoked by the observation of states characterized by a clear alternation between periods of high and low activity.

We construct a general theory for self-organization to an abrupt phase transition, closely following the footprints for the origin of SOC, but introducing a *facilitation* mechanism mimicking the positive feedback discussed above (**Chapter 3**). Not only we succeed in creating the theory for the so-called "Self-Organized Bistability" (SOB), but we uncover that such theory shows a phenomenology whose details are consistent with the empirical observations in neural experiments, paving the way for a new rationale for neuronal avalanches, apparently more relevant than SOC. Moreover, we think that this new paradigm might find realizations in several fields, given that multistability is shown by a vast variety of systems.

Next, keeping in mind the SOB paradigm, we propose to answer the question: if neural systems are settled in the vicinity of a phase transition, which sort of phase transition is it? In **Chapter 4** we construct a parsimonious stochastic mesoscopic theory for a cortical network, being at the same time biologically consistent and minimal. We follow the Landau-Ginzburg approach, building our model from essential principles/symmetries, inspired to the physiology of neurons or groups of neurons. Such a model also provides us with a comprehensive view on other relevant models in neuroscience [21, 20, 22, 23, 24, 25] and naturally reconciles the community studying criticality in the brain and neuronal avalanches, to the (more traditional) one investigating macroscopic oscillatory electrical signals (as stemming e.g. from EEG) as a result of synchronization of neural units.

Moreover, since neuronal avalanches are empirically found to be consistent the universality class of the un-biased branching process –a feature which is

common to all mean-field systems with absorbing states– in **Chapter 5** we propose to derive those exponents, under a simple and unified perspective. The Langevin equation of four different universality classes (directed percolation, dynamical percolation, compact directed percolation and conserved directed percolation), crucially involving a square-root multiplicative stochastic term, can be analyzed by mapping them into random walkers confined to the origin by a logarithmic potential. This point of view allows us to have a compact visual of the difference between random walk and branching process, unfolding the common existing confusion between the avalanches generated by the two processes. Moreover it also allows to report on the emergence of non-universal continuously-varying exponent values stemming from the presence of small external driving –that might induce avalanche merging– and might account for deviations from the un-biased branching process exponents.

Chapter 6 is specifically addressed to examine the experimental method of measuring avalanches introduced by Beggs and Plenz [9], which is naturally inherited by most of the computational analyses in literature. We synthetically present some preliminary studies designed to check the accuracy of the method for distinguishing between critical and not critical regimes. More specifically, we compare the avalanches deriving from clustering algorithms inspired by the experimental procedure to the avalanches defined in more traditional and intuitive ways in simple dynamical known models. We suggest that,under certain conditions and, in particular in the presence of noise, the experimental procedure might detect signs of criticality even far away from the phase transition.

Finally, in **Chapter 7**, we explore another mechanism that has proven useful

to describe power-law distribution of avalanches, stemming from the condition of balance between excitation and inhibition, but, importantly, not requiring criticality. Self-similar bursts of activity can emerge in finite-size systems of spiking neurons because of the *reactiveness* of the mean field dynamics. In fact, in presence of excitatory and inhibitory components, the Jacobian of the linearized dynamics results to be non-normal, and, in particular when excitation and inhibition are balanced, this gives rise to extraordinary long transient behaviors. The introduction of noise on top of such non-normal dynamics, stabilizes the transient behavior, which effectively amplifies the fluctuations generated by the noise, so that the dynamics results in scale invariant bursts of collective spiking events. We analyze in detail this intriguing mechanism, both analytically and numerically, in order to identify the role of each ingredient and clarify their interplay, and we build a zero-dimensional model that reproduces the behavior of the system.

In summary, in this thesis we present a set of models and analysis techniques aimed at shedding further light on the fascinating topic of brain dynamics and the possibility of emerging criticality, which also pervades other fields of Biology.

1.4 List of Publications

- Di Santo, Serena; Burioni, Raffaella; Vezzani, Alessandro; Muñoz Martínez, Miguel Angel. 2016. *Self-organized bistability associated with first order phase transitions.* Phisical Review Letters. 126, 240601.

- Di Santo, Serena; Villegas Góngora, Pablo; Burioni, Raffaella; Muñoz Martínez, Miguel Angel. 2017. *Simple unified view of branching process statistics: Random walks in balanced logarithmic potentials.* Physical Review E. 95: 032115.

- Martinello, Matteo; Hidalgo, Jorge; Maritan, Amos; Di Santo, Serena; Plenz, Dietmar; Muñoz Martínez, Miguel Angel. 2017. *Neutral theory and scale free neural dynamics.* Phys. Rev. X 7, 041071.

- Di Santo, Serena; Villegas Góngora, Pablo; Burioni, Raffaella; Muñoz Martínez, Miguel Angel. 2018. *Landau-Ginzburg theory of cortex dynamics: scale free avalanches emerge at the edge of synchronization.* 2018. PNAS. doi: 10.1073/pnas.1712989115

- Di Santo, Serena; Villegas Góngora, Pablo; Burioni, Raffaella; Muñoz Martínez, Miguel Angel. 2018. *On the possibility of self-organization to bistability in the brain.* 2017. In preparation.

- Di Santo, Serena; Villegas Góngora, Pablo; Burioni, Raffaella; Muñoz Martínez, Miguel Angel. 2018. *Non-critical amplification of fluctuations in simple models of persistent neural dynamics.* 2017. In preparation.

1.5 Resumen en Castellano

La observación de que los sistemas biológicos a menudo muestran correlaciones de largo alcance tanto a nivel espacial como temporal, que son capaces de responder a una amplia gama de estímulos y son capaces de adaptarse para realizar una gran variedad de funciones, sugirió la hipótesis de que operan cerca del punto crtico de una transición de fase, lo que les daría un equilibrio óptimo entre robustez (estabilidad con respecto a perturbaciones externas, propiedad típica de las fases ordenadas) y flexibilidad (capacidad de responder a estímulos ambientales, propiedad típica de fases desordenadas). Esta hipótesis también se ha establecido en el campo de las redes neuronales, en particular después de un experimento pionero de 2003, en el que se midió la actividad eléctrica del neocortex de roedores con resoluciones espaciales y temporales que han permitido identificar clusters de actividad. Esto condujo a la definición de avalanchas neuronales, que, en condiciones fisiológicas, presentan tamaños y duraciones distribuidas de acuerdo con leyes de potencia, sto es, invariantes de escala.

El debate sobre la hipótesis de que la invarianza de escala en estas distribuciones es un síntoma de criticidad sigue abierto y en esta tesis el asunto se investiga en detalle, a partir de principios simples y tratando de unificar varios modelos existentes en la literatura. Este trabajo muestra que algunos modelos de inspiración neurofisiológica reproducen las distribuciones de avalanchas medidas empricamente, no tanto como una consecuencia de la supuesta criticidad hacia la cual se organiza el sistema, sino como consecuencia de un principio de

neutralidad entre las cascadas de eventos, en virtud del cual cada una tiene la misma probabilidad de expandirse y contraerse en comparación con las demás. El enfoque introducido permite subrayar cómo el protocolo experimental para medir avalanchas implique una aproximación en la evaluación de la causalidad de los eventos registrados, la cual debe tenerse en cuenta a la hora de interpretar los resultados experimentales. Las señales neuronales se estructuran en una alternancia de estados de actividad muy alta o muy baja ("Up and Down states"). Este comportamiento biestable sugiere analizar la posibilidad de que un sistema se autoorganice en un punto de transición no del segundo, sino de primer orden. Repasando las etapas de la teoría de criticidad autoorganizada (SOC), se desarrolla una teoría general para la autoorganización en un punto de coexistencia de fases –candidata para encontrar aplicaciones en varios campos de investigación– , que muestra invarianza de escala en combinación con eventos anormales que involucran a todo el sistema.

A menudo, en el ámbito del debate sobre la hipótesis de criticidad en el cerebro, no se especifica claramente la naturaleza de la transición de fase que genera la criticidad, y la referencia común al SOC o al branching process implica una transición entre estado absorbente y estado activo, estados que no reflejan con claridad posibles condiciones patológicas. Una descripcin minimal à la Landau-Ginzburg nos permite crear una teoría simple con un pequeño número de parámetros, pero de inspiración fisiológica, que muestra una transición de fase de sincronización –más plausible desde un punto de vista biológico– en la que medimos (según el protocolo experimental) avalanchas que reproducen muchos de los comportamientos observados en los experimentos. Además anal-

izamos en detalle un mecanismo propuesto en la literatura como alternativa a la criticidad para la generación de avalanchas neuronales, que tiene su fundamento en una fuerte inestabilidad producida por el balance entre excitación y inhibición. Explicamos el papel de los diversos componentes del modelo (dinámica determinística non normal, ruido demográfico y ruido térmico) con la ayuda de experimentos numéricos y técnicas analíticas. Finalmente, se presenta un enfoque analítico superuniversal (que incluye al menos 4 clases de universalidad) para el cálculo de los exponentes de las distribuciones de avalanchas en las transiciones de fase de no equilibrio.

Chapter 2

Neutral theory of neural avalanches

2.1 Introduction

Scale-free distributed events or bursts of "activity" such as earthquakes, vortex avalanches in superconductors, and Barkhaussen noise are common place in Nature (see e.g. [26, 27]) and are often ascribed to their underlying dynamics being poised at a critical point. The paradigm of "self-organized criticality" was developed to explain how and why natural systems could self-tune to the vicinity of critical points [26, 28, 29]: in this context, scale-free distributed avalanches turn out to be the fingerprint of critical points of a phase transition into quiescent (or "absorbing") states [30, 31]. Despite the success and conceptual beauty of this framework, not all scale-invariant episodes of activity can be

ascribed to underlying criticality [32, 33]; for instance, power-law distributed excursion sizes and times can also emerge from unbiased random walks [34] (see Chapter 5), self-organization to the edge of a discontinuous phase transition (see Chapter 3), the Yule-Simon or "the rich gets richer" process [33] and, as discussed here, neutral dynamics [35, 36]. In the present Chapter, we explore the possibility that avalanches measured in the most relevant existing models in neurophysical literature could be scale-free as a result of an underlying neutral dynamics –i.e. that each single event of activity is indistinguishable from others and can potentially propagate through the network in a marginal way, i.e. without an intrinsic tendency to either expand or contract– alternatively to being self-organized to the edge of a phase transition. That is, we explore whether scale-free avalanches could stem from the neutral competition of activity (generated from different sources or stimuli) for available space. We put forward a subtle but important difference between such causal avalanches and existing empirically measured ones, and discuss how neutral patterns of activity –i.e. coexisting causal avalanches of many different shapes, sizes and durations– could be exploited by real neural systems for efficient coding, optimal transmission of information and, thus, for memory and learning [37].

2.2 Main Results

2.2.1 Computational model and its phenomenology

Designing a model of leaky integrate-and-fire neurons regulated by synaptic plasticity, Millman, *et al.* [21] were able to capture the empirical observation of bistability in cortical networks, i.e. the existence of two well differentiated stable patterns of cortical activity, called Up and Down states (see e.g. [38, 39] and references therein, as well as [20, 40] for related and rather interesting models). Briefly, the model of Millman, *et al.* consists of N leaky integrate-and-fire excitatory neurons forming a directed random Erdős-Rényi network with average connectivity K. Neurons integrate synaptic inputs from other neurons and fire action potentials, which rapidly deplete the synaptic resources. These resources recover at a slow time scale, thereby limiting the overall level of activity in the network (see Appendix B.4). When not specified, model parameters were taken as in [21]: $K = 7.5$, $n_r = 6$, $R = 2/3$ GΩ, $C = 30$ pF, $V_r = -70$ mV, $\theta = -50$ mV, $w_{\mathrm{e}} = 95$ pA, $w_{\mathrm{in}} = 50$ pA, $p_r = 0.25$, $\tau_{rp} = 1$ ms, $\tau_s = 5$ ms and $\tau_R = 0.1$ s.

The model can be tuned by controlling e.g. its average synaptic strength. For weak synaptic strengths, a quiescent phase with very low levels of activity, the Down state, exists, whereas a second, stable state with high firing rates, the Up state, emerges for large synaptic strengths (see Fig. 2.1A). For intermediate strengths, spontaneous fluctuations allow for rapid Up and Down states alternations (see Fig. 2.1B). This phenomenology –which could also be repro-

duced by keeping synaptic strength fixed and varying the synaptic recovery time or some other parameter of the model– corresponds to a discontinuous phase transition (see Fig. 2.1 and Fig. 1 in [21]) and therefore lacks the critical point characteristic of continuous transitions. However, remarkably, when tracking cascades of neuronal firing based on participating neurons, i.e. causal avalanches (see below), the model was shown to exhibit scale-free distributions of sizes and durations during Up-states, with associated exponents $\tau \approx 3/2$ and $\alpha \approx 2$, i.e. the hallmark of neuronal avalanches measured in brain activity. Accordingly, Millman *e*t al. considered the Up state as "self-organized critical", in contrast to the Down state which was "subcritical" with causal cascades that were not scale-free [21]. Given that critical dynamics emerge at continuous phase-transitions, the presence of scale-invariant avalanches within the Up state in the absence of any such transition in this model is unusual. This observation prompted us to identify possible alternative mechanisms for the emergence of scale-free avalanches.

2.2.2 Causal avalanches

Following [21], we tracked causal cascades/avalanches [1]. Each one is initiated when an external input depolarizes a neuron's membrane potential above threshold to fire an action potential, it unfolds as the membrane potential of a postsynaptic neuron surpasses threshold, as a result of a synaptic input from

[1]Here, we use indistinctly the terms "avalanche" and "cascade". See [41] for a recent and interesting analysis of causal avalanches on complex networks.

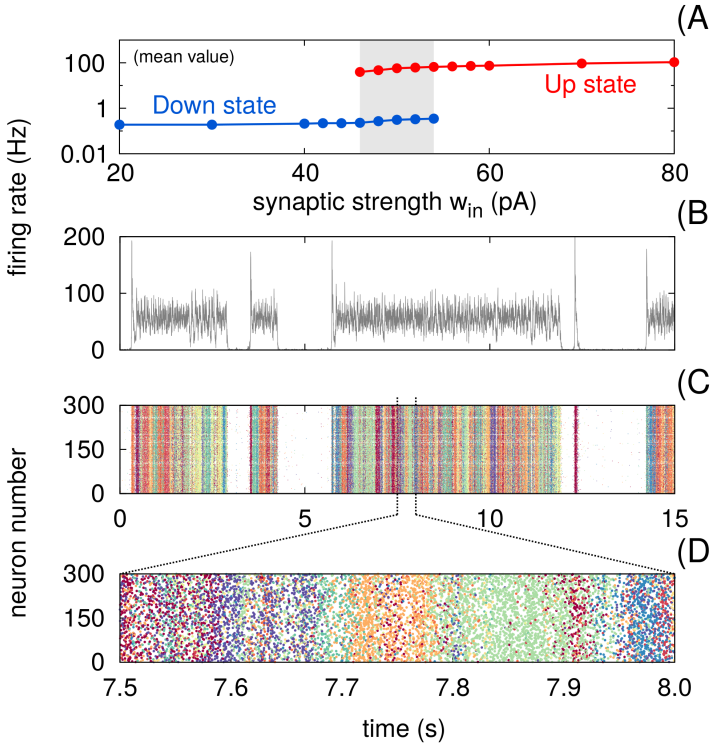

Figure 2.1: Numerical integration of the model of Millman *et al.* [21] with $N = 300$ neurons. (A) Bifurcation diagram of the mean firing rate as a function of the synaptic strength parameter, w_{in}. For low values of w_{in}, the stable state is a quiescent state with very low levels of activity (Down state), whereas for large values of w_{in}, the system exhibits high levels of activity (Up state). Both states coexist for intermediate strength values (shaded region), allowing for Up-and-Down transitions. Importantly, the transition is discontinuous. (B) Time series of the network firing rate for $w_{\text{in}} = 50$ pA illustrate the system's bistability, with eventual (stochastic) jumps between Up and Down states. (C) Raster plot (for the same times as above) in which distinct colors are used for different causal avalanches. Each avalanche is started when a neuron fires owing to an external input and is defined as the subsequent cascade of activated neurons firing as a consequence of such initial event [21] (see Section "Causal avalanches"). (D) Raster plot zoom (broken lines) demonstrating the intermingled and temporally overlapping organization of different causal avalanches. Model parameters have been set as in [21].

active neurons in the cascade, and stops when this does not happen [2]. The size of a cascade is the total number of action potentials triggered, while the cascade duration is the timespan between its initiation and the time of its last action potential [21]. Avalanches were analyzed separately for Up and Down states in a network with $N = 3000$ neurons, using different values of the external firing rate, f_e; in particular we analyzed the slow-driving case $f_e \to 0$ in which new cascades arrive at a slow pace.

Our results are in perfect agreement with the phenomenology found in [21]: cascades in the Down state do not exhibit scale invariance but instead have a characteristic scale (see Section D.1.2). In contrast, cascades during Up-states distribute in size and duration according to power-laws with exponent close to $\tau = 3/2$ and $\alpha = 2$, respectively (see Fig. D.1A). As already observed in [21], these results are quite robust, do not depend on how deep into the Up state (i.e. how far from the transition point) simulations are run, nor on simulation details, nor do they change upon introducing inhibitory neurons (see Section D.1.3).

2.2.3 Time-correlated avalanches from time binning

A key point of the previous analysis is that causal information between activation events (i.e. "who triggers who") is essential to define avalanches. However, in empirical analyses it is not clear whether events occurring nearby in time

[2] Usually many inputs contribute to the firing of a given neuron; each neuron firing is ascribed to the avalanche having produced the *last* or final input making it go over threshold [21].

–usually ascribed to the same avalanche in statistical analyses– are actually causally connected or not. The standard approach, that has been successfully used in the analysis of experimental data, where causal information of event propagation is typically not accessible [9, 10], consists in defining cascades from a series of discrete supra-threshold events, by choosing a discrete time bin Δt. An avalanche is defined as a sequence of successive time windows with at least one event in each that is preceded and ended by an empty bin. Following [9, 10] –where it was shown that scaling relations obtained with different time bins Δt could be collapsed– we take Δt to be equal to the average inter-event interval (IEI), defined as the average time interval between successive events[3]. Using this binning procedure in timeseries from the computational model, we find that cascade duration and size distributions obtained from Up states are exponentially distributed with a characteristic scale, showing no signs of scale-invariant behavior (see Fig. D.1B). Distributions did not change qualitatively for different values of Δt. Thus, in the model of Millman *et al.*, cascades based on temporal proximity differ significantly from cascades based on causal information. This finding is in contrast to the established scale-free avalanche distributions that emerge from experimental data based on temporal proximity.

In the model of Millman *et al.*, causal avalanches can (and do) coexist in time (see Fig. 2.1C and D); thus, the temporal proximity approach does necessarily fail to uncover true causal avalanches. Summing up, our observations, together

[3]Even though the IEIs can vary for different experimental situations, size and duration distributions have been claimed to exhibit universal behavior with exponent $\tau \approx 3/2$ and $\alpha \approx 2$, respectively, provided that data are binned using the IEI.

with the lack of a continuous phase transition, question the origin of scale invariance within Up states and its actual relationship with empirically found (time-correlated) scale-free avalanches. To shed light on this problem, in the next section we analyze a minimal model which captures the main ingredients for activity propagation, showing that the observed scale-free causal avalanches in the model of Millman *et al.* stems from an underlying neutral dynamics [35, 36].

2.2.4 Neutral (causal) avalanches in a minimal model for activity propagation

In archetypical models of activity propagation such as the contact process, directed percolation and the susceptible-infected-susceptible model [44, 45], "active" sites propagate activity to their nearest neighbors or become deactivated at some transition rates. As a result, depending on rate values, there exist a quiescent and an active phase, as well as a critical point separating them [44, 45]; avalanches triggered from a single initial event, exhibit scale invariance only at criticality (see Figure D.3 in Section D.1.4) and, if they are triggered at a sufficiently slow rate, they do not overlap.

In contrast, within the framework of neutral dynamics (that we are about to define), multiple avalanches can propagate simultaneously. The difference between critical and neutral avalanches can be vividly illustrated by considering a variant of the contact process, consisting of many different but equivalent "species" (or "labels" or "colors" or "types"). This model can be studied

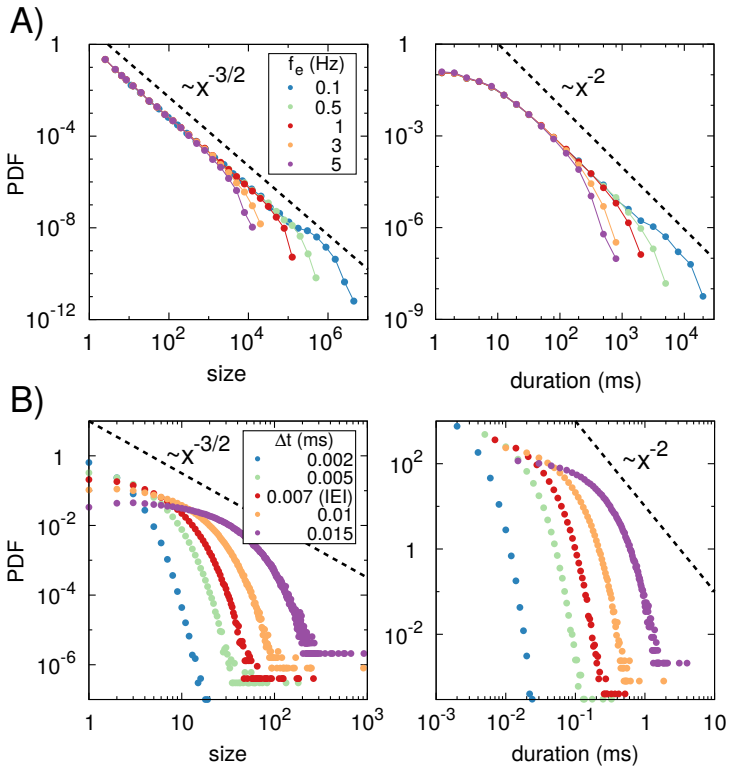

Figure 2.2: Avalanche size and duration distributions within the Up-state phase in the model of Millman *et al.* [21] using two different methods (double logarithmic plot). (A) Causal avalanches were defined using the same criterion as in [21], for several values of the external input f_e, confirming the observation that sizes and durations are power-law distributed with the same exponents of an unbiased branching process, i.e. $\tau = 3/2$ and $\alpha = 2$, respectively [42, 43]. (B) "Time-correlated" avalanches, defined with the standard temporal binning method [9] (which estimates causality by temporal proximity), using five different time intervals Δt to bin the data, including one coinciding with the average interevent interval (IEI) as usually done in the analyses of empirical data [9], for $f_e = 5$ Hz; in this case distributions do not obey a power-law distribution but have a characteristic scale. In all cases, simulations were performed in a network of $N = 3000$ neurons (model parameters as in [21]).

with parameters (rates) arbitrarily far from the phase transition to explore the statistics of causal avalanches. More specifically, we consider a network

with N nodes that can be either active (A) or inactive (I). Here we discuss the case of a fully-connected architecture –for which mathematical analysis is simpler– but almost identical results are obtained for a directed random-network, with the very same structure as employed in the model of Millman *et al.* (see Figure D.4 of Section D.1.4). At every time, each single active site is assigned to a unique individual avalanche/species k (the one from which it derives) and labeled by A_k. More specifically, the dynamics is as follows: i) a new avalanche, with a new label, is initiated by the spontaneous activation of an inactive site at small driving rate ϵ; ii) active sites propagate the activity to neighboring inactive places at rate λ, and iii) active sites become inactive at rate μ. This is equivalent to the following set of reactions for $k = 1, ..., M(t)$:

$$\begin{array}{ccc} I & \xrightarrow{\epsilon} & A_{M(t)+1} \\ A_k + I & \xrightarrow{\lambda} & A_k + A_k \\ A_k & \xrightarrow{\mu} & I \end{array} \tag{2.1}$$

where $M(t)$ is the total number of avalanches triggered up to time t. This dynamical process is *neutral* (or symmetrical) among species/avalanches as rates do not depend on label k (see Appendix A.4 for an extended presentation of neutral theories). The duration (resp. size) of an avalanche k is the time elapsed (resp. total number of activations) between its spontaneous generation and the extinction of its label. Observe that different avalanches can coexist (all the most in the active phase, as in the model of Millman *et al.*) and that the total number of coexisting avalanches can vary in time. The state of the system is determined by $M(t)$ and the number of $k-$type active sites,

$n_k(t)$, or, equivalently, their corresponding densities $\rho_k(t) = n_k(t)/N$. The total density of active sites is defined as $\rho(t) = \sum_{k=1}^{M(t)} \rho_k(t)$. Importantly, just ignoring species labels, one realizes that the system of Eq. (2.1) is nothing but the standard contact process (with a non-vanishing rate for spontaneous activation ϵ). Therefore, in the slow-driving limit $\epsilon \to 0$, the system exhibits a continuous phase transition for the total activity density at the critical point given by $\lambda_c = \mu$ [44, 45].

We performed computer simulations of the dynamics described by Eq.(2.1) by means of the Gillespie algorithm [46] in a fully-connected network of size $N = 10^4$. Parameter values are chosen for the system to lie well inside the active phase, $\lambda = 2$, $\mu = 1$ (i.e. $\lambda = 2\lambda_c$), and ϵ taking small values such as $10^{-1}, 10^{-2}, 10^{-3}$ and 10^{-4}. Typical timeseries for individual avalanches, ρ_k, as well as for the total activity, ρ, are depicted in Fig. 2.3A.

Observe that the steady-state overall density (gray color) coincides, on average, with that of the contact process in the infinite size limit, $\rho^* \simeq 1 - \mu/\lambda + \epsilon\mu/(\lambda(\lambda - \mu))$ (see Section D.1.1 for the derivation of this equality). On the other hand, individual avalanches (colored curves in Fig. 2.3A) experience wild fluctuations as a function of time. The statistics of avalanches is illustrated in Fig. 2.3B revealing that avalanche sizes and durations are power-law distributed with exponents $\tau = 3/2$ and $\alpha = 2$ in the limit of small spontaneous activation rate $\epsilon \to 0$. Remarkably, scale-free avalanches appear all across the active phase, $\lambda > \lambda_c$ (see Figure D.5 of Section D.1.4).

2.2.5 Analytical approach

To shed light on this result, we study analytically this simplified model in the large network-size limit. Starting from the master equation associated to Eq.(2.1), performing a system-size expansion for large but finite system sizes [47], the dynamics of a newly-created avalanche is described by the following equation:

$$\dot{\rho}_k = (\lambda(1-\rho) - \mu)\,\rho_k + \sqrt{\frac{1}{N}\,(\lambda(1-\rho) + \mu)\,\rho_k}\,\xi_k(t), \tag{2.2}$$

with the initial condition $\rho_k = 1/N$, and where $\xi_k(t)$ represents a zero-mean Gaussian white noise of unit variance (to be interpreted in the Itô sense [47]). If the system is very large, and *when the rates lie within the active phase* (i.e. $\lambda > \mu$), the total activity density exhibits very small fluctuations, remaining quite stable around the steady-state value, as illustrated by the gray-colored timeseries in Fig. 2.3A.

To understand the variability of individual avalanches, let us assume that in the steady state $\rho(t) \simeq \rho^*$, that introduced in Eq. (2.2) leads to:

$$\dot{\rho}_k = -\frac{\mu}{\lambda - \mu}\epsilon\rho_k + \sqrt{\frac{\mu}{N}\left(2 - \frac{\epsilon}{\lambda - \mu}\right)\rho_k}\,\xi_k(t). \tag{2.3}$$

In the limit $\epsilon \to 0$, the deterministic/drift term in Eq.(2.3) vanishes, and the dynamics of avalanche k can be simply written as:

$$\dot{\rho}_k = \sqrt{\rho_k}\;\xi_k(\hat{t}), \tag{2.4}$$

where for simplicity in the notation, a factor $2\mu/N$ has been reabsorbed into the time scale $\hat{t}$. Eq.(2.4) represents a freely-moving random-walk with demographic fluctuations, as profusely analyzed in Chapter 5. It describes the evolution of a species density in any neutral-type of dynamics –as further discussed in Appendix A.4. In other words, once an avalanche starts, its statistics is entirely driven by neutral demographic fluctuations, without any net tendency to either expand or contract, *regardless of the distance to the critical point* [4]. Furthermore, the avalanche exponents associated with this neutral, noise-driven, dynamics are $\alpha = 2$ and $\tau = 3/2$. Actually, the previous reasoning holds all across the active (Up) phase; on the other hand, in the quiescent (Down) state, the steady state activity ρ^* goes to 0, as the deterministic driving force in Eq.(2.2) is negative, leading to subcritical avalanches, as indeed reported in [21].

Thus, a simple approach allowed us to explicitly show that neutral dynamics among coexisting dynamically-indistinguishable avalanches leads to scale-free distributions all across the active (Up) phase, i.e. arbitrarily far away from the edge of the phase transition, where many different causal avalanches can simultaneously coexist, and with no relationship with self-organized criticality.

Our claim, relying on universality arguments, is that the same conclusion extends to the active phase of the model of Millman *et al.*; for such a case detailed analytical calculations would be much more difficult to perform, but it seems rather plausible that the effective dynamics is also neutral as in the case of

[4] Not surprisingly, Eq.(2.4) corresponds also to the mean-field description of an unbiased branching process [42].

the simple model discussed here, and that many neutral causal avalanches co-exist, thus strongly supporting that as a matter of fact the scale-free causal avalanches in the model of Millman *et al.* stem from neutral dynamics and not from the model being self-organized to the critical point of any (non-existing) continuous phase transition.

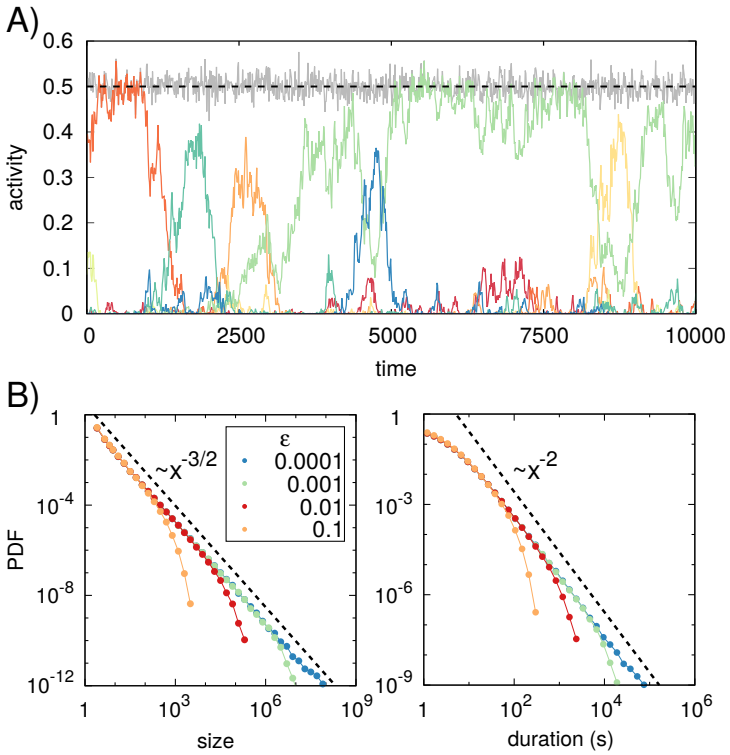

Figure 2.3: Causal avalanches in a minimal model for propagation activity, defined as cascades of events initiated from the spontaneous activation of one unit, without overlap between avalanches (i.e. a given node cannot be simultaneously part of more than one avalanche). (A) The activity of each avalanche is defined as the density of active elements in the system belonging to that avalanche, identified with different colors in the plot. The global activity density is represented with the gray-colored line. Parameters of the model are taken deep inside the active phase, $\lambda = 2$, $\mu = 1$, for a system size $N = 10^4$ and small spontaneous activation rate $\epsilon = 10^{-3}$. Whereas the global activity exhibits slight fluctuations around its steady-state value $\rho^* \simeq 1 - \mu/\lambda$ (represented by the dashed line), individual avalanches can exhibit wild variability. (B) Avalanche size and duration distributions for different values of ϵ (other parameters as in (A), i.e. deep inside the active phase). Avalanche statistics exhibit robust power-law scaling –limited by system size– with the same exponents of the neutral theory for avalanche propagation (marked with dashed lines for comparison).

2.3 Summary and Conclusions

A remarkable observation –that has elicited a great deal of interest– is that neural activity in the brain of mammals, including humans, occurs in the form of neuronal avalanches consisting of outbursts of neural activity intervened by periods of relative quiescence, across many resolution scales in a robust way [9, 48]. For *in vitro* studies of relatively small networks it seems plausible to assume that events occurring during one of such outbursts are causally connected, so that activity emerges at some location and transiently propagates through the network, causing a cascade of co-activations. However, there is no clear empirical validation that this is actually the case; diverse causally-connected cascades could, in principle, occur simultaneously, hindering their experimental discrimination as individual avalanches. Obviously, the situation is much more involved in large neural networks as analyzed *in vivo* at diverse scales of resolution, e.g. from local field potential measurements, magneto-encephalography, functional magnetic resonance imaging, etc. There is no well-accepted empirical procedure to actually disentangle causal influences, nor to discern whether different causal cascades of activations overlap (as they probably do in functional brains). Developing a protocol to fill such a gap is a task of utmost importance for the coming future (see [41]). In the absence of a better indicator, events of activity are customarily clustered together as individual avalanches, relying on a criterion of temporal proximity.

It remains to be fully elucidated what is the true nature of scale-free avalanches in actual neural systems. To shed light on this, here we scrutinized the most

commonly referred model –introduced by Millman and coauthors [21]– justifying the emergence of power-law distributed avalanches in networks of integrate-and-fire neurons with synaptic plasticity. First of all, we reproduced the findings in [21], and confirmed that the model exhibits two different phases in parameter space, an Up-state characterized by large average firing rates and a Down-one with small firing, separated by a discontinuous phase transition. We carefully analyzed the dynamics within the active phase, and corroborated that diverse avalanches can coexist, and that their sizes and durations are scale-free (with exponents, 3/2 and 2, respectively) if and only if precise information on which neuron triggers the firing of which –which is accessible in computational models– is used to identify (causal) avalanches [41]. On the other hand, a different analysis –which is the one customarily applied to empirical data– based on defining avalanches through a time-binning procedure, blind to detailed causal information between activation events, does not reveal any trace of scale-freedom in avalanche distributions.

These observations naturally pose two important questions. First, if this model is not self-organized to the edge of a phase transition, where do the computationally-reported scale-free (causal) avalanches within this model stem from? And second, does this model constitute a faithful representation of actual neural dynamics, including the experimentally observed scale-invariant avalanches?

To answer the first question we designed a simplified dynamical model with an overall phenomenology very similar to that of the model of [21]: i.e. it exhibits scale-invariant causal avalanches all along its active phase, regardless of the

distance to a phase-transition point (which actually can be either a continuous or a discontinuous one depending on model details). This simplified model –a variant of the contact process with many different types of active sites– allowed us to uncover that scale-invariant avalanches within the active phase stem from the neutral dynamics among diverse coexisting (causal) avalanches. In particular, if new seeds of activity are injected at a very slow rate in a system with recurrent background activity (i.e. in its active phase) each one does not have a net drift toward contracting or expanding in the background of recurrent activity in which it unfolds; its dynamics just follows demographic fluctuations, much as in neutral theories of population genetics. Moreover, the branching ratio is equal to unity, and causal avalanches are power-law distributed (as in the unbiased branching processes), without the model being posed at the edge of a phase transition. In summary, the observed scale-invariance in a well-accepted computational model for neuronal dynamics as well as in a simplified model stems from the neutrality or symmetry between diverse co-existing cascades of causally-related events which coexists in a background of recurrent activity.

Further results, details and comments can be found in Appendix D.1.

Chapter 3

Self-organized bistability

3.1 Introduction

As already mentioned in this Thesis, Self-organized criticality elucidates the conditions under which physical and biological systems tune themselves to the edge of a second-order phase transition, with scale invariance. In this Chapter, we propose and analyze a theory for the self-organization to the point of phase-coexistence in systems exhibiting a first-order phase transition, motivated by the empirical observation of bimodal distributions of activity in neuroscience and other fields.

Indeed, multistability –understood as the existence of diverse stationary states under a fixed set of conditions– is ubiquitous in physics and in biology [49, 50, 51]. Bistable switches are a common theme in the regulation of cellular processes such as cycles, differentiation and apoptosis [52] and, often, genes are

expressed in huge episodic bursts interspersed with periods of quiescence [53]. The cerebral cortex exhibits bistability during deep sleep, with an alternation between high or low levels of neural activity [54, 55, 39]. Real neural networks, both *in vitro* and *in vivo* have been reported to exhibit power-law distributed avalanches of activity –interpreted to be a sign of underlying criticality– [9]; however, when inhibitory mechanisms are repressed or under epileptic conditions [56], very large events (beyond the expectations of criticality) appear, and size-distributions become bimodal, suggesting some kind of underlying bistability.

Here we are interested in spatially extended noisy systems –such as the whole cortex or gene-expression patterns across tissues– for which a statistical mechanics framework is most appropriate. In this context, bistability is tantamount to the existence of a first-order phase transition at which two phases coexist [50]. A cornerstone result of equilibrium thermodynamics, the *Gibbs' phase rule*, establishes that two phases can coexist only at a single transition point of a one-dimensional parameter space [50] (see however, [57]). Thus, if biological systems operate in regimes of bistability, there should exist mechanisms by which they self-tune to the edge of a first-order phase transition. This idea resembles the rationale behind self-organized criticality (SOC) [6, 26, 28, 58, 30], which explains why critical-like phenomena are ubiquitous despite the fact that second-order phase transitions, with their associated criticality, power-laws and scaling, occur only at singular points of phase spaces. SOC toymodels, such as sandpiles [6, 59, 60]), illustrate how self-tuning to criticality may occur (see Appendix A.3). Theoretical progress [61, 7, 30, 31]

allowed for a rationalization of how SOC works, by relating it to a standard second-order phase transition [50, 62].

The purpose of the present Chapter is to formulate a general theory of *self-organized bistability* (SOB) or self-organized phase coexistence by extending the ideas of self-organization to bistable systems.

3.2 Main Results

3.2.1 "Facilitated" sandpiles.

Early experimental attempts aimed at observing scale-invariant (SOC) avalanches in real sandpiles did not find the expected power-law distributions. Instead, they found anomalously large quasi-periodic avalanches, that exceeded the expectations for large events in SOC (see, e.g. Figure 4 in [63]). The reason for this is that real sandgrains have a tendency to keep on moving once they start doing so, dragging other grains, and *facilitating* the emergence of huge avalanches. To mimic this effect in a highly-stylized way, we consider the Manna sandpile and modify it with a facilitation mechanism. In particular, we let sites that receive grains simultaneously from more than one neighbor (e.g. from 2) to temporarily (one timestep) decrease their instability threshold (e.g. to $z = 1$). This type of cooperative activation is expected to generate discontinuous transitions [62].

Steady-state avalanche-size distributions $P(s)$ for this facilitated sandpile are

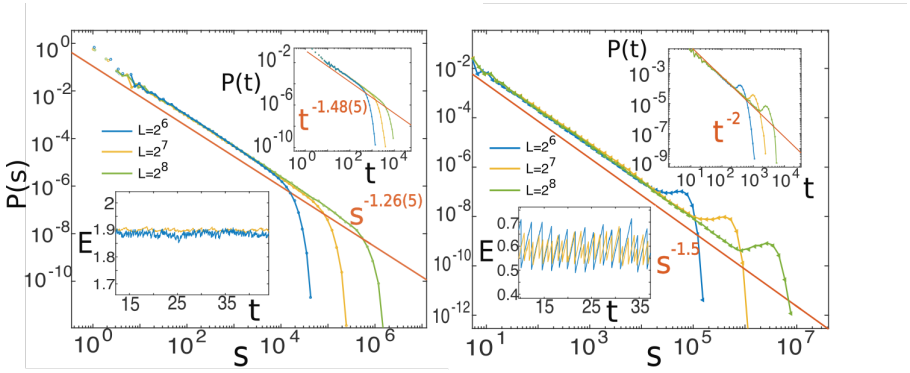

Figure 3.1: Avalanche size distributions for the (LEFT) standard 2-dimensional Manna sandpile model and the (RIGHT) facilitated sandpile model (time distributions for the 2 cases are shown in the upper insets). Observe the difference in the avalanche exponents, corresponding to the so-called Manna class in the standard (SOC) case ($\tau \approx 1.26$, $\tau_t \approx 1.48$) versus ($\tau \approx 3/2$, $\tau_t \approx 2$) for the facilitated sandpile. In the facilitated case there are bumps of anomalously large avalanches or "kings" [64]. The lower insets illustrates that"energy" time series are much more sawtooth-like in the facilitated than in the SOC case owing to the existence of "kings".

plotted in Fig.3.1 for different linear system sizes, L. Two facts are in blatant contrast with usual sandpile results (also portrayed in Fig.3.1): **(i)** the distributions are *bimodal* and consist of two different types of avalanches: "regular ones" and huge avalanches or "kings" [64] –corresponding to the bumps in the distributions– which reverberate through the whole system, and **(ii)** regular avalanches are (nearly) power-law distributed, but with an exponent $\tau \approx 1.5$ significantly different from the value $\tau = 1.26(5)$ of standard sandpiles [65]. The relative abundance of regular and king avalanches can be altered by changing model details. In any case, the resulting bimodal distributions stem from the self-organization to a state of bistability, as will shall show by putting these findings onto a much general framework: the theory of SOB.

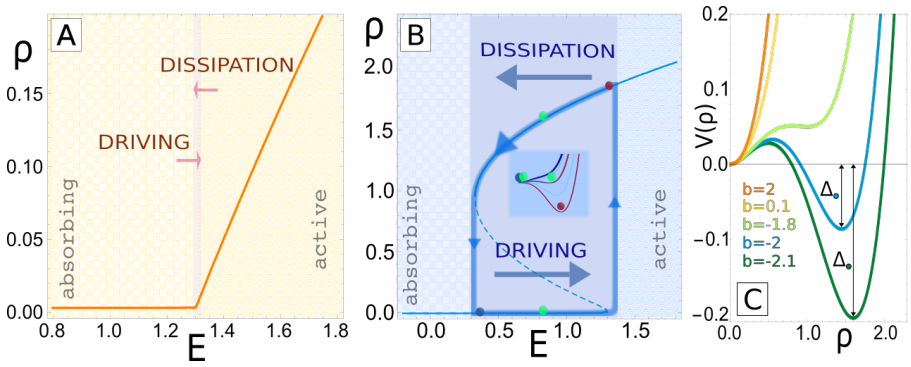

Figure 3.2: Sketch of how –within mean-field theory– the self-organization mechanism (alternating driving and dissipation at infinitely separated timescales) tunes to (A) the critical point of a second-order phase transition (SOC) or (B) to the hysteretic loop of a first-order one. In inset in (B) sketches the shape of the potential V and the position of the minima (color code as in the dots of the main plot) as E is changed. (C) Potential, $V(\rho)$ for different values of b, both positive (one minimum) and negative (two minima). For $b < 0$, the potential depth at the active minima, Δ, grows with $|b|$. Parameters: $a = -1.3$, $\omega = c = 1$.

3.2.2 SOB: mean-field picture

To construct a mean-field theory of SOB, one needs to replace the model showing a continuous transition (see Appendix A.3), by its counterpart for a discontinuous one: $\dot{\rho}(t) = a\rho - b\rho^2 - c\rho^3$, with $b < 0$ and $c > 0$ (the r.h.s. derives from the potential $V(\rho)$ shown in Fig.3.2, and can be obtained from the continuous-transition case by assuming an additional facilitation effect). Indeed, to implement a positive feedback (facilitation) one needs to increase the a, in the presence of activity, as $a \to a + \alpha\rho$, where α is some constant shifting $-b$ toward larger values $b \to -b + \alpha$. Also, an additional cubic term is included to avoid $\rho \to \infty$. For the above equation, there is a regime of bistability for the active and absorbing states, the domains of attraction of

which are separated by the *spinodal* line (dashed line in Fig.2B). Coupling, as in SOC, this dynamics to that of an energy field, E fostering the creation of further activity ($\dot{\rho}(t) = (a + \omega E)\rho - b\rho^2 - c\rho^3$), with dynamics $\dot{E} = h - \epsilon\rho$ (where $\omega > 0$ is a constant and the double limit $h, \epsilon \to 0$, $h/\epsilon \to 0$ should be considered –see Appendix A.3), the system follows a limit cycle (the hysteretic loop in Fig.2): a departure from the absorbing/active state is observed only when local stability is lost (ending points of the spinodal line). Therefore, within the mean-field approximation, a self-organizing mechanism identical to that of SOC leads to cyclic bursts of activity –i.e. a sort of phase alternance [1]– rather than to a unique point.

3.2.3 SOB: beyond mean-field

To investigate how this simple mean-field picture changes in spatially-extended noisy systems, in full analogy with the mean-field case, we propose the following equations for discontinuous transitions:

$$\begin{aligned} \partial_t \rho(\vec{x}, t) &= [a + \omega E(\vec{x}, t)]\rho - b\rho^2 - c\rho^3 + D\nabla^2\rho + \sigma\eta(\vec{x}, t) \\ \partial_t E(\vec{x}, t) &= D\nabla^2\rho(\vec{x}, t), \end{aligned} \tag{3.1}$$

with $b < 0$ and $c > 0$. In what follows, we vary b (keeping other parameters fixed) to explore whether diverse regimes emerge. Direct numerical integration of Eq.(3.1) can be performed in a very efficient way using the split-step integration scheme of [67]. Simulations are started by either low or high densities to

[1] This switching is not to be confused with stochastic resonance [66] which is a noise induced phenomenon.

enable the system to reach different homogeneous steady states, which are separated by a spinodal line. Results, summarized in Fig.3.3, confirm that both the size of the jump and the bistability region shrink upon reducing $|b|$ and that they shrink significantly with respect to their mean-field values (Fig.3.2). Remarkably, for small values, e.g. $b = -0.1$, the transition becomes continuous, even if the mean-field approximation predicts a discontinuous one. As discussed in [68], fluctuation effects typically soften the discontinuity, shrink bistability regions, and can even alter the order of the phase transition, leading to noise-induced criticality. For values of $|b|$ larger than a certain (unspecified) tricritical value $|b_T|$ the transition remains discontinuous [69]. We have also verified that there exists a point of true phase coexistence within the bistability regime, i.e. a *Maxwell point* (defined as the value of $\bar{E}$, E_M, at which a flat interface separating two halves of the system, one in each phase, does not move on average, while, for $\bar{E} < E_M$ (resp. $\bar{E} > E_M$) the absorbing (active) phase invades the other one; see dashed lines in Fig.3.3). Moreover, the observed metastability region shrinks upon enlarging system size.

Having characterized the fixed-energy ensemble, we now let the system self-organize by switching on slow driving and boundary dissipation as in SOC, and allow the system to reach its steady state. As illustrated in Fig.3.3, we observe different scenarios depending of the value of $|b|$: *(i) Noise-induced critical regime–* For sufficiently small values of $|b|$ (such as $b = -0.1$) the transition becomes continuous and the phenomenology is as in SOC (scale-invariant avalanches with $\tau \approx 1.26$ and $\tau_t \approx 1.48$). *(ii) King-avalanche dominated regime–* In the opposite limit of large values of $|b|$ (e.g. $b = -2$), we

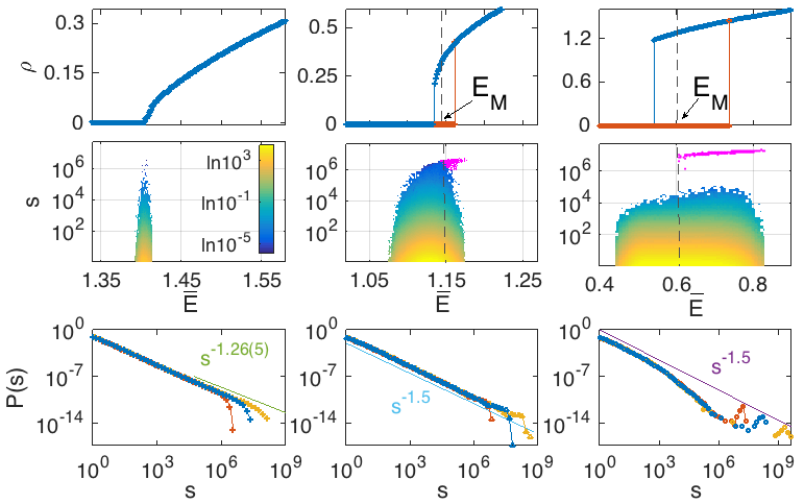

Figure 3.3: The three rows show: (Upper) steady state density ρ as a function of E in the fixed-E ensemble, (Central) color-temperature plot of the conditional size distributions $P(s|\bar{E})$ as a function of E; king avalanches plotted with a distinct color (magenta), and (Lower) $P(s)$ for different system sizes; for large $|b|$, king avalanches coexist with smaller ones. The three columns show three different values of $b < 0$, ($b = -0.1$, $b = -1$ and $b = -2$, respectively) representatives of different regimes. System size in the first two rows is $L^2 = 2^{12}$, and $L^2 = 2^{12}, 2^{14}, 2^{16}$ in the bottom one. Parameter values: $a = -1.3$, $\omega = c = D = \sigma = 1$.

observe large peaks in $P(s)$ and $P(t)$ for large events or "kings", coexisting with smaller (regular) avalanches which are exponentially truncated above a characteristic cutoff time/size, and are responsible for large energy-dissipation events. *(iii) Hybrid regime*– For intermediate values of $|b|$ (e.g. $b = -1.0$), one has a situation similar to that of the facilitated sandpile (Fig..3.1), in which power-law distributed regular avalanches (with $\tau \approx 3/2$ and $\tau_t \approx 2$) coexist with kings. In cases *(ii)* and *(iii)*, $E(t)$ exhibits characteristic sawtooh-like profiles (as the facilitated sandpile of Fig.3.1) which –as revealed by the presence of a clear peak in their power spectra (not shown)– are quasi-periodic,

i.e. E cycles between high and low values (the larger $|b|$ the larger the excursions). Indeed, Fig.3.3 (central) shows the conditional distribution $P(s|\bar{E})$, illustrating that avalanches can be triggered at diverse values of $\bar{E}$. However, even if for any finite system, SOB leads to excursions all through the bistability region, we have verified that such regions (and excursions) shrink upon enlarging system size; thus, in the thermodynamic limit, $\bar{E}$ self-tunes in SOB systems to a unique point of phase coexistence –the Maxwell point– much as in SOC [31] and unlike the mean-field picture.

Let us now describe the properties of regular and king avalanches. For regular ones, recall that right at the Maxwell point $\bar{E} = E_M$ both phases are equally stable, and thus the dynamics is as in the so-called compact directed percolation [70] or voter model, in which a stable phase tries to invade an equally stable one, giving rise to a complex dynamics at the boundaries separating both. This type of dynamics is well-known to lead to $\tau = 3/2$ and $\tau_t = 2$ in two (or larger) dimensions [70, 65, 35], [2], so that –as $\bar{E}$ wanders around E_M– one could anticipate that $P(s) \sim s^{-3/2}$ for regular avalanches, with some cut-off that depends on $|b|$ (see below).

As illustrated in Fig.3.3, king avalanches (magenta color) can be triggered whenever $\bar{E}$ is above the Maxwell point of the fixed-energy diagram (Fig.3.3), i.e. $\bar{E} \geq E_M$ (and not only when $\bar{E}$ reaches the limit of instability of the absorbing state, as happens in the mean-field picture). The reason for this lies in the existence of a nucleation process [49] as we describe now. Imagine that, after driving the system, a large fluctuation creates a large droplet of activity –

[2] With the possibility of logarithmic corrections in two dimensions.

of linear size/radius R– in an otherwise absorbing configuration. To investigate the fate of such a droplet in a simple though approximate way, we switch off noise by fixing $\sigma = 0$ in Eq.(3.1). In this deterministic approximation, one can safely define a free energy which has two additive contributions: one for the space integral of the potential $V(\rho)$ (shown in Fig.3.2C), and a surface tension term proportional to $D \int d\vec{x}(\nabla\rho)^2$. When $\bar{E} > E_M$, the potential at the active steady state ($\rho > 0$) is negative ($\Delta < 0$) and thus, deeper than that at 0 (Fig.3.2C). Thus, the creation of an active droplet leads to a competition between the gain of bulk free energy and the penalty associated with the formation of an interface between the active and absorbing states. Equating these two trends, one obtains a critical radius $R_c \approx 2D/\Delta$ above which the bulk contribution dominates and the droplet expands ballistically and compactly through the whole system [49], giving rise to a "king avalanche". This heuristic argument does not strictly apply in the presence of (multiplicative) noise for which a free energy cannot even be defined. However, recent analytical work has shown that the most probable path to jump from active to inactive states in this type of bistable noisy systems involves the creation of a critical droplet that then expands ballistically through the system [71], putting under more solid grounds our heuristic approach. Finally, observe that the larger $|b|$ the smaller R_c, and the stronger the cut-off for regular avalanches.

To visualize these effects, we have kept track of different avalanches –both regular and kings– and computed their averaged shape [72]; this is close to a semicircle for regular avalanches, as correspond to random-walk like processes [72], while kings, after a transient time, have a radically different triangu-

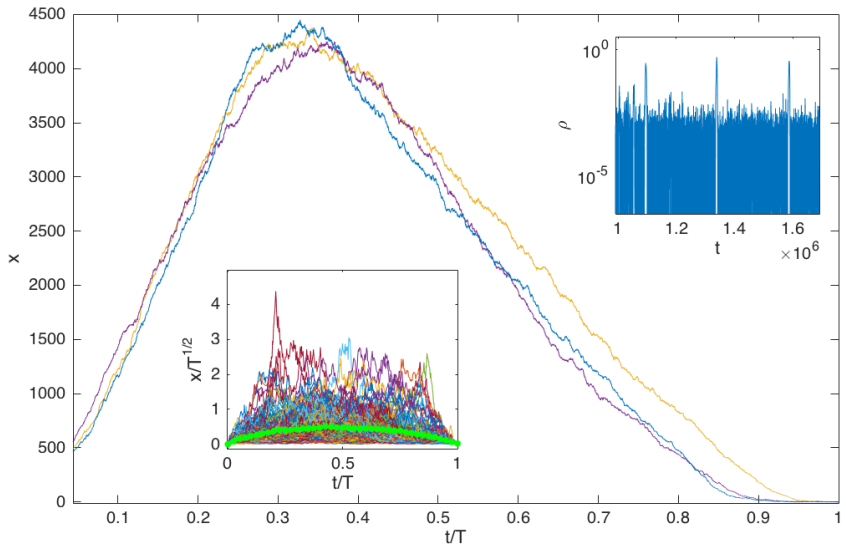

Figure 3.4: Different averaged shapes of regular an king avalanches. The inset shows regular avalanches (rescaled by the square-root of time) as a function of the re-scaled time. The green curve stands for their average. Main figure: shape of three different king avalanches, showing a characteristic triangular shape (linear growing followed by linear shrinking). The rightmost inset show the activity time-series fro which these data have been extracted, illustrating the presence of quasi-periodicity.

lar shape (with linear growth stemming from ballistic expansion, followed by ballistic extinction stemming from large energy dissipation) – see Fig.3.4.

3.2.4 Effects of varying the Diffusion Coefficient

Here we briefly present a calculation that allows us to show that the discontinuity as well as the bistability region decrease by decreasing the diffusion coefficient D. First of all, by assuming that the activity field is homogeneous in space we can approximate the diffusion term in equation 3.1 as $D\nabla^2\rho \sim 4D(\langle\rho\rangle - \rho)$.

This approximation will work better for bigger values of the diffusion coefficient. We will treat the expected value of the activity as a constant h, write down the expression for the stationary probability distribution (which will contain h) and set up the self-consistency equation $\langle\rho\rangle = \int_0^\infty \rho P(\rho)d\rho = h$, which has an explicit dependence on D. The Fokker-Plank equation (interpreted with Itō convention) that describes the time evolution of the probability density function of the activity field reads:

$$\dot{P}(\rho,t) = -\frac{\partial}{\partial\rho}[(\tilde{a}\rho + b\rho^2 - c\rho^3 + 4Dh)P(\rho,t)] + \frac{\sigma^2}{2}\frac{\partial^2[\rho P(\rho,t)]}{\partial\rho^2}, \qquad (3.2)$$

where $\tilde{a} = a+\omega E-4D$. By imposing the probability current to vanish we find the stationary probability density $P(\rho,t) \sim \exp[\frac{2}{\sigma^2}(\tilde{a}\rho+\frac{b}{2}\rho^2-\frac{c}{3}\rho^3+4Dh\ln\rho)-\ln\rho]$.

3.3 Summary and Conclusions

In summary, we have defined the concept of "self-organized bistability" (SOB) by extending well-known ideas of self-organization to critical points to systems exhibiting bistability and phase coexistence and provided an explanation for the emergence of bimodal distributions –combining aspects of scale invariance and bistability– as often observed in biological problems. Our goal here is not that of analyzing a specific example of a real system exhibiting SOB – of which we believe there are plenty of instances– but rather to characterize the general mechanism, much as done in SOC. The most promising specific

example to be pursued is that provided by real neural networks (for which synaptic resources play the role of E and neural activity that of ρ), in which avalanches appear to be distributed with exponents $\tau \approx 3/2$ and $\tau_t \approx 2$ [9]. These values –at odds with the expectations of SOC in either 2 or 3-dimensional systems– are usually justified by making assumptions about the architecture of the underlying network of connections, a hypothesis which is not always obvious. Furthermore, anomalously large (king) events, inconsistent with the predictions from criticality, appear when inhibitory mechanisms are repressed or under epileptic conditions [56] and a non-trivial temporal organization of neural avalanches [73] has been reported to exist. Thus, we suggest that it should be carefully scrutinized under which circumstances cortical networks (which are known to have facilitation mechanisms) are not self-organized to a critical point (SOC) –as usually considered– but to a region of bistability (SOB) with its concomitant mean-field like avalanche exponents, the natural possibility of king avalanches, and a non-trivial temporal organization. In future work, we shall extend our theory in a number of ways, including self-organization in the absence of conservation laws and/or of infinitely separated time-scales, as well as allowing for global rather than point-like driving; these extensions will hopefully allow for a more direct connection with biological systems.

Chapter 4

Synchronization Phase Transition

4.1 Introduction

Scale-free synchronized outbursts of neural activity recorded by Beggs and Plenz [9] has been taken as empirical evidence backing the criticality hypothesis, i.e. the conjecture that the awake brain might extract essential functional advantages –including maximal sensitivity to stimuli, large dynamical repertoires, optimal computational capabilities, etc.– from operating close to a critical point, separating two different phases [74, 48, 75, 2].

In order to make further progress, it is of crucial importance to clarify the nature of the phase transition marked by such an alleged critical point. It is usually assumed that it corresponds to the threshold at which neural activity

propagates marginally in the network, i.e. to the critical point of a quiescent-to-active phase transition [9], justifying the emergence of branching-process exponents [45, 44]. However, several experimental investigations found evidence that scale-free avalanches emerge in concomitance with collective oscillations, suggesting the presence of a synchronization phase transition [76, 77].

From the theoretical side, on the one hand, very interesting models accounting for the self-organization of neural networks to the neighborhood of the critical point of a quiescent-to-active phase transition have been proposed [20, 78, 21, 79]. These approaches rely on diverse regulatory mechanisms [80], such as synaptic plasticity [81], spike-time-dependent plasticity [82], excitability adaptation, etc. to achieve network self-organization to the vicinity of a critical point. These models have in common that they rely on an extremely large separation of dynamical timescales (as in models of self-organized criticality[1] [26, 28]) which might not be a realistic assumption [20, 56, 83, 79]. Some other models are more realistic from a neurophysiological viewpoint [21, 15], but they give rise to scale-free avalanches if and only if causal information –which is available in computational models but not accessible in experiments (see Chapter ch:neutral)– is considered. Thus, in our opinion, a sound theoretical model justifying the empirical observation of putative criticality is still missing. On the other hand, from the synchronization viewpoint, well-known simple models of networks of excitatory and inhibitory spiking neurons exhibit differentiated synchronous (oscillatory) and asynchronous phases, with a synchronization phase transition in between [23, 84, 22, 85]. However, avalanches

[1] See Appendix ap:ASOC.

do not usually appear (or are not searched for) in such modeling approaches (see, however, [16, 86, 87]).

Concurrently, during deep sleep and also under anesthesia the cortical state has long been known to exhibit, so called, "up and down" transitions between states of high and low neural activity, respectively [88, 89], which clearly deviate from the possible criticality of the awake brain, and which have been modeled on their own [54, 55, 21]. Thus, it would be highly desirable to design theoretical models describing within a common framework the possibility of criticality, oscillations, and up-down transitions.

Our aim here is to clarify the nature of the phases and phase transitions of dynamical network models of the cortex by constructing a general unifying theory based on minimal assumptions and allowing us, in particular, to elucidate what the nature of the alleged criticality is.

To construct such a theory we follow the strategy pioneered by Landau and Ginzburg. Landau proposed a simple approach to the analysis of phases of matter and the phase transitions they experience. As we briefly review in Appendix A.1.3, it consists in a parsimonious, coarse-grained, and deterministic description of states of matter in which –relying on the idea of universality– only relevant ingredients (such as symmetries and conservation laws) need to be taken into account and in which most microscopic details are safely neglected [90, 50]. Ginzburg went a step further by realizing that fluctuations are an essential ingredient to be included in any sound theory of phase transitions, especially in low-dimensional systems. The resulting Landau-Ginzburg theory, includ-

ing fluctuations and spatial dependence is regarded as a *meta-model* of phase transitions and constitutes a firm ground on top of which the standard theory of phases of matter rests [50]. Similar coarse-grained theories are nowadays used in interdisciplinary contexts – such as collective motion [91], population dynamics [68], and neuroscience [92, 93, 94]– where diverse collective phases stem out of the interactions among many elementary constituents. In what follows we propose and analyze a Landau-Ginzburg theory for cortical neural networks –which can be seen as a variant of the well-known Wilson-Cowan model (see Appendix ap:BWC) including, crucially, stochasticity and spatial dependence– allowing us to shed light from a very general perspective on the collective phases and phase transitions that dynamical cortical networks can harbor. Employing analytical and, mostly, computational techniques, we show that our theory explains the emergence of scale-free avalanches, as episodes of marginal and transient synchronization in the presence of a background of ongoing irregular activity, reconciling the oscillatory behavior of cortical networks with the presence of scale-free avalanches. Last but not least, our approach also allows for a unification of existing models describing diverse specific aspects of the cortical dynamics, such as up and down states and up-and-down transitions, within a common mathematical framework, and is amenable of future theoretical (e.g. renormalization group) analyses.

4.2 Main Results

We construct a mesoscopic description of neuronal activity, where the building blocks are not single neurons but local neural populations. These latter can be thought as small sections of neural tissue [95, 96] consisting of a few thousand cells (far away from the large-network limit), and susceptible to be described by a few variables. Even though this effective description is constructed here on phenomenological bases, more formal mathematical derivations of similar equations from microscopic models exist in the literature (see e.g. [97]). In what follows, first (i) we model the neural activity at a single mesoscopic "unit", then (ii) we analyze its deterministic behavior as a function of parameter values, and later on (iii) we study the collective dynamics of many coupled units.

4.2.1 Single-unit model

At each single unit we consider a dynamical model in which the excitatory activity, ρ, obeys a Wilson-Cowan equation [98] (that, following the Landau approach, we truncate to third order in a series expansion) [2]:

$$\dot{\rho}(t) = \big[-a + R(t) + b\rho(t) \big] \rho(t) - \rho^3(t) + h \tag{4.1}$$

[2] We keep up to third order to include the effect of the sigmoid response function; a variant of the model considering the non-truncated Wilson-Cowan equation leads to almost identical results; see Section D.3.5

where $a > 0$ controls the spontaneous decay of activity, which is partially compensated by the generation of additional activity at a rate proportional to the amount of available *synaptic resources*, $R(t)$; he quadratic term with $b > 0$, controls non-linear integration effects[3]; finally, the cubic term imposes a saturation level for the activity, preventing unbounded growth, and h is an external driving field.

A second equation is employed to describe the dynamics of the available synaptic resources, $R(t)$, through the combined effect of synaptic depression and synaptic recovery, as encoded in the celebrated model of Tsodyks and Markram (TM) for synaptic plasticity [81, 25]:

$$\dot{R}(t) = \frac{1}{\tau_R}(\xi - R(t)) - \frac{1}{\tau_D} R(t)\rho(t), \tag{4.2}$$

where τ_R (resp. τ_D) is the characteristic recovery (depletion) time, and ξ is the baseline level of non-depleted synaptic resources. Importantly, we have also considered variants of this model, avoiding the truncation of the power-series expansion, or including an inhibitory population as the chief regulatory mechanism: either of these extensions leads to essentially the same phenomenology and phases as described in what follows, supporting the robustness of the forthcoming results (see Appendix D.3.5).

[3]Single neurons integrate many presynaptic spikes to go beyond threshold, and thus their response is non-linear: the more activity the more likely it is self-sustained [95]. As a matter of fact, the Wilson-Cowan model includes a sigmoid response function with a threshold, implying that activity has to be above some minimum value to be self-sustained, and entailing $b > 0$ in the series expansion (see Appendix D.3).

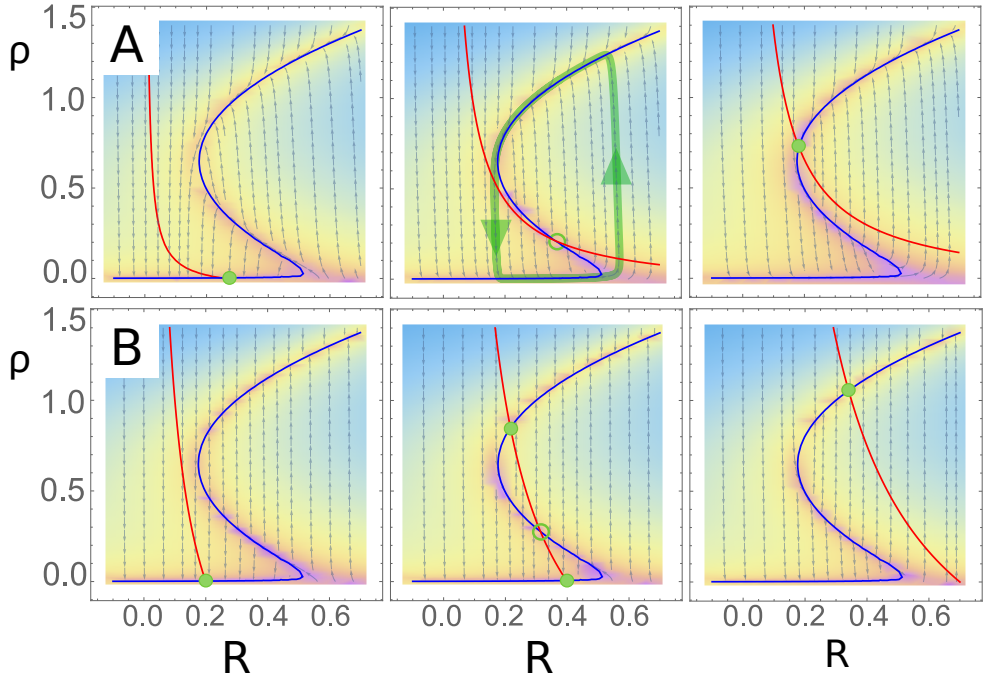

Figure 4.1: Phase portraits and nullclines for the (deterministic) dynamics, Eqs.(D.13) and (4.2). Nullclines are colored in blue ($\dot{\rho} = 0$) and red ($\dot{R} = 0$), respectively; fixed points (ρ^*, R^*) –at which nullclines intersect– are highlighted by green full (empty) circles for stable (unstable) fixed points. Background color code (shifting from blue to purple) represents the intensity of the vector field $(\dot{\rho}, \dot{R})$, whose direction is represented by small grey arrows. A trajectory illustrating a limit cycle is showed in green in (A). The system exhibits either (A) an oscillatory regime or (B) a region of bistability, in between a down (left) and an up (right) state. It is possible to shift from case (A) to case (B) and viceversa by changing just one parameter; e.g. the timescale of resources depletion, τ_D^{-1} (0.016 and 0.001 for cases (A) and (B), respectively). Other parameter values: $h = 10^{-3}, a = 0.6, b = -1.3, \tau_R = 10^3$; control parameter, from left to right, $\xi = 0.3, 1.6, 2.3$ in the upper panel and $\xi = 0.2, 0.4, 0.7$ in the lower one.

4.2.2 Mean-field analysis

We analyze, both analytically and computationally, the dynamics of the single unit, as given by Eqs.(D.13) and (4.2). We obtain the fixed points (ρ^*, R^*) of the dynamics –i.e. the possible steady-states at which the system can settle– as a function of the baseline-level of synaptic resources, ξ, which plays the role of a control parameter (all other parameters are kept fixed to reasonable values, as summarized in the caption of Fig.4.1). For small values of ξ, the system falls into a quiescent or *down* state with $\rho^* \approx 0$ and $R^* \approx \xi$ [4]. Instead, for large values of ξ there is an active or *up* state with self-sustained spontaneous activity $\rho^* > 0$ and depleted resources $R^* < \xi$. In between these two limiting phases, two alternative scenarios can appear, depending on some parameter values, as illustrated in Fig.4.1 and summarized in the phase diagram of Appendix ap:Csynchro) can appear depending on the time scales τ_D and τ_R:

(A) A stable limit cycle (corresponding to an unstable fixed point, with complex eigenvalues) emerges for intermediate values of ξ (in between two Hopf bifurcations) as illustrated in Fig.4.1A. This Hopf-bifurcation scenario has been extensively discussed in the literature (see e.g. [99]) and it is at the basis of the emergence of oscillations in neural circuits.

(B) An intermediate regime of bistability including three fixed points is found for intermediate values of ξ (in between two saddle-node bifurcations): the up and the down ones, as well as an unstable fixed point in between (as illustrated in Fig.4.1B). This saddle-node scenario is the relevant one in models [54, 40, 21]

[4] Deviations from $\rho^* = 0$ stem from the small but non-vanishing external driving $h \neq 0$.

describing transitions between up (active) and down (quiescent) states as they occur in the brain during sleep or under anesthesia [88, 89]

Two remarks are in order. The first is that one can shift from one scenario to the other just by changing one parameter, e.g. the synaptic depletion timescale τ_D [5]; the second and important one is that none of the two scenarios exhibits a continuous transition (transcritical bifurcation) separating the up from the down regimes; thus, at this deterministic level there is no precursor of a critical point for marginal propagation of activity.

4.2.3 Stochastic network model

We now introduce stochastic and spatial effects in the simplest possible way. For this, we consider a network of N nodes coupled following a given connection pattern, as described below. Each network node represents a mesoscopic region of neural tissue or "unit" as described above. On top of this deterministic dynamics, we consider that each unit (describing a finite population) is affected by intrinsic fluctuations [97, 93, 100]. More specifically, Eq.(D.13) is complemented with an additional term $+A(\rho)\eta(t)$ which includes a (zero-mean, unit-variance) Gaussian noise $\eta(t)$ and a density-dependent amplitude $A(\rho)$[6] i.e. a multiplicative noise [47].

[5] Note that the slope of the the nullcline deriving from Eq.(4.2) (red in Fig.4.1) is proportional to τ_D: if it is small enough, there exists only one unstable fixed point, giving rise to a Hopf bifurcation; otherwise the nullclines intersect at three points, generating the bistable regime.

[6] In the limit of slow external driving and up to leading order in an expansion in powers of ρ, this can be written as $A(\rho) = \sigma\sqrt{\rho(t)}$, where σ is a noise amplitude; this stems from the fact that the spiking of each single neuron is a stochastic process, and the overall fluctuation of the density of a collection of them scales with its square-root, as dictated by the central

At macroscopic scales, the cortex can be treated as a two-dimensional sheet consisting mostly of short-range connections [101][7]. Although long-range connections are also known to exist, and small-world effects have been identified in local cortical regions [103], here we consider a two-dimensional square lattice (size $N = L^2$) of mesoscopic units as the simplest way to embed our model into space. Afterward, we shall explore how our main results are affected by the introduction of more realistic network architectures including additional layers of complexity such as long-range connections and spatial heterogeneity.

Following the parsimonious Landau-Ginzburg approach adopted here, the coupling between neighboring units is described up to leading order by a diffusion term. This type of diffusive coupling between neighboring mesoscopic units stems from electrical synapses [95, 104], has some experimental backing [105], and has been analytically derived starting from models of spiking neurons [92] [8]. Thus, finally, the resulting set of coupled stochastic equations is:

$$\begin{cases} \dot{\rho}_i(t) = (-a + R_i + b\rho_i)\rho_i - \rho_i^3 + h + D\nabla^2\rho_i + \sigma\sqrt{\rho_i}\eta_i \\ \dot{R}_i(t) = \frac{1}{\tau_R}(\xi - R_i) - \frac{1}{\tau_D}R_i\rho_i \end{cases} \tag{4.3}$$

where, for simplicity, some time dependences have been omitted; $\rho_i(t)$ and $R_i(t)$ are, respectively, the activity and resources at a given node i (with $i = 1, 2, ...N$) and time t, $D\nabla^2\rho_i \equiv D\sum_{j\in n.n.i}(\rho_j - \rho_i)$, describes the diffusive

limit theorem [47] (see also [97] for a detailed derivation of the square-root dependence).

[7] This type of approach is at the bases of, so-called, neural-field models, with a long tradition in neuroscience [102].

[8] More elaborated approaches including coupling kernels between different regions, as well as asymmetric ones, are also often considered in the literature (e.g. [94]), but here we stick to the simplest possible coupling.

coupling of unit i with its nearest neighbors j, with (diffusion) constant D. The physical scales of the system are controlled by the values of the parameters D and σ; however, given that, as illustrated in Appendix ap:Csynchro, results do not change qualitatively upon varying parameter values (as long as they are finite and non-vanishing), here we take $D = \sigma = 1$ for the sake of simplicity.

Eq.(4.3) constitutes the basis of our theory. In principle, this set of equations is amenable to theoretical analyses, possibly including renormalization ones [50]. However, here we restrict ourselves to computational studies aimed at scrutinizing what is the basic phenomenology, leaving more formal analyses for the future. In particular, we resort to numerical integration of the stochastic equations Eq.4.3, which is feasible thanks to the efficient scheme developed in [67] to deal with multiplicative noise. We consider $\delta t = 0.01$ as an integration timestep and keep, as above, all parameters fixed, except for the baseline level of synaptic resources, ξ, which works as a control parameter.

4.2.4 Phases and phase transitions: Case A

We start analyzing a sets of parameters lying within case A above. We study the possible phases that emerge as ξ is varied. These are illustrated in Fig. 4.2 where characteristic snapshots, overall-activity time series, as well as raster plots are plotted.

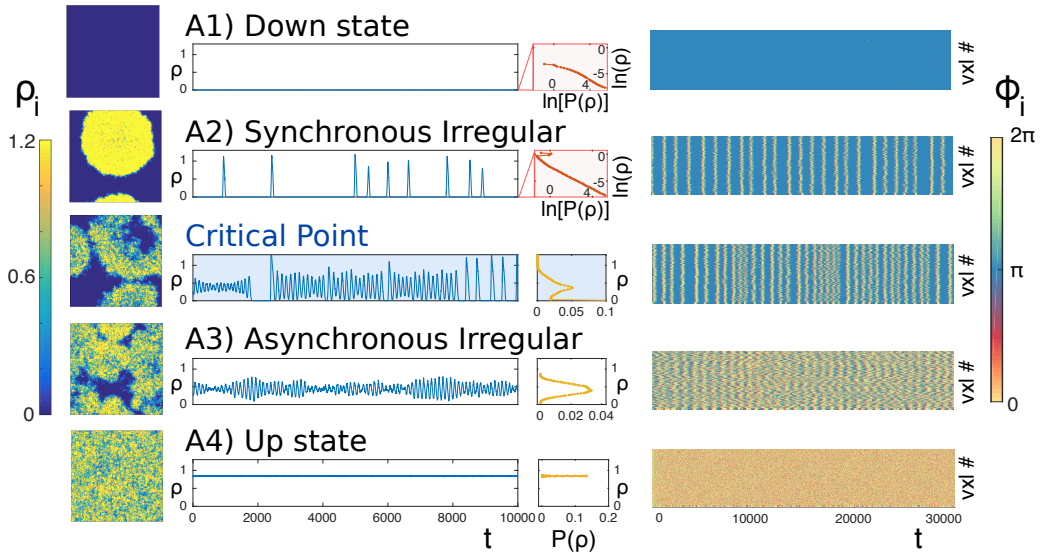

Figure 4.2: Illustration of the diverse phases emerging in the model (case A). The baseline of synaptic resources, ξ, increases from top to bottom: $\xi = 0.4$ (down-state), $\xi = 1.2$ (synchronous regime), $\xi = 2.47$ (critical point for the considered size, $N = 128^2$), $\xi = 2.7$ (asynchronous phase), and $\xi = 5$ (active phase). *First column:* Snapshots of typical configurations; the color code represents the level of activity at each unit as shown in the scale. The network-spiking or synchronous irregular case, is characterized by waves of activity growing and transiently invading the whole system, before extinguishing the resources and coming to an end. On the other hand, in the nested-oscillation or asynchronous irregular regime multiple traveling waves coexist, interfering with each other. In the up-state waves are no longer observed and a homogeneous state of self-sustained activity is observed. *Second column:* Timeseries of the overall activity averaged over the whole network. In the down state activity is almost vanishing. In the synchronous phase macroscopic activity appears in the form of almost synchronous bursts, interspersed by almost silent intervals. At the critical point network spikes begin to superimpose, giving rise to complex oscillatory patterns (nested oscillations) and marginally self-sustained global activity all across the asynchronous regime; finally, in the up state the global activity converges to steady-state with small fluctuations.

Figure 4.2: *Third column:* Steady state probability distribution $P(\rho)$ for the global activity: in the down state and the network spiking regime the distributions are shown in a double-logarithmic scale; observe the approximate power-law for very small values of ρ stemming from the presence of multiplicative noise (see Chapter 5). *Fourth column:* Illustration of the different levels of synchronization across phases: a sample of 200 randomly chosen units are mapped into oscillators using their *analytic-signal representation* (see Methods); the plot shows the time evolution of their corresponding phases $\phi_k^{\mathcal{A}}$. Observe the almost periodic behavior in the synchronous phase, which starts blurring at the critical point, and progressively vanishes as the control parameter is further increased. Parameter values: $a = 1, b = 1.5, \tau_R = 10^3, \tau_D = 10^2, h = 10^{-7}$.

(A1) Down-state phase

If the baseline level ξ is sufficiently small (i.e. $\xi \lesssim 0.75$), resources R are always scarce and the system is unable to produce self-sustained activity (i.e. it is hardly excitable) giving rise to a down-state phase, characterized by very small stationary values of the network time-averaged activity $\bar{\rho} \equiv \frac{1}{T}\int_0^T dt \frac{1}{N}\sum_{i=1}^N \rho_i(t)$ for large times T (see Fig.4.2a). The quiescent state is disrupted only locally by the effect of the driving field h, which creates local activity, hardly propagating to neighboring units.

(A2) Synchronous irregular (SI) phase

Above a certain value of resource baseline ($\xi \gtrsim 0.75$) there exists a wide region in parameter space in which activity generated at a seed point is able to propagate to neighboring units, triggering a wave of activity which transiently invades the whole network until resources are exhausted, activity ceases, and the

recovery process restarts (see Fig. 4.2b). Such waves or "network-spikes" appear in a non-periodic fashion, with an average separation time that decreases with ξ. In the terminology of Brunel [22], this corresponds to a *synchronous irregular* (SI) state/phase, since the collective activity is time-dependent and individual spiking is irregular (as discussed below). This wax-and-wane state resembles the huge bursts of anomalous synchronous activity as they appear in e.g. epileptic tissues [106].

(A3) Asynchronous irregular (AI) phase

For even larger values of resource baseline ($\xi \gtrsim 2.15$), the level of synaptic recovery is sufficiently high so that network-regions depleted of resources recover fast enough as to become susceptible of propagating new waves before activity has extinguished in the network. Thereby, diverse spatially extended waves coexist in the network, giving rise to a collective complex oscillatory pattern (see Fig. 4.2d; which is strikingly similar to, e.g. EEG data of $\alpha-$rhythms [107]). The amplitude of these oscillations, however, decreases upon increasing network size (as many different local waves are averaged and deviations from the mean tend to be washed away). This regime can be assimilated to an *asynchronous irregular* (AI) phase of Brunel [22] (see below).

(A4) Up-state phase

For even larger values of ξ, plenty of synaptic resources are available at all times, giving rise to a state of perpetual activity with small fluctuations around

the mean value (Fig. 4.2e), i.e. an up state. Let us finally remark, that as explicitly shown in the Section D.3.9, the AI phase and the Up-state cannot be distinguished in the infinite network-size limit, in which there are so many waves to be averaged that a homogeneous steady state emerges on average in both cases.

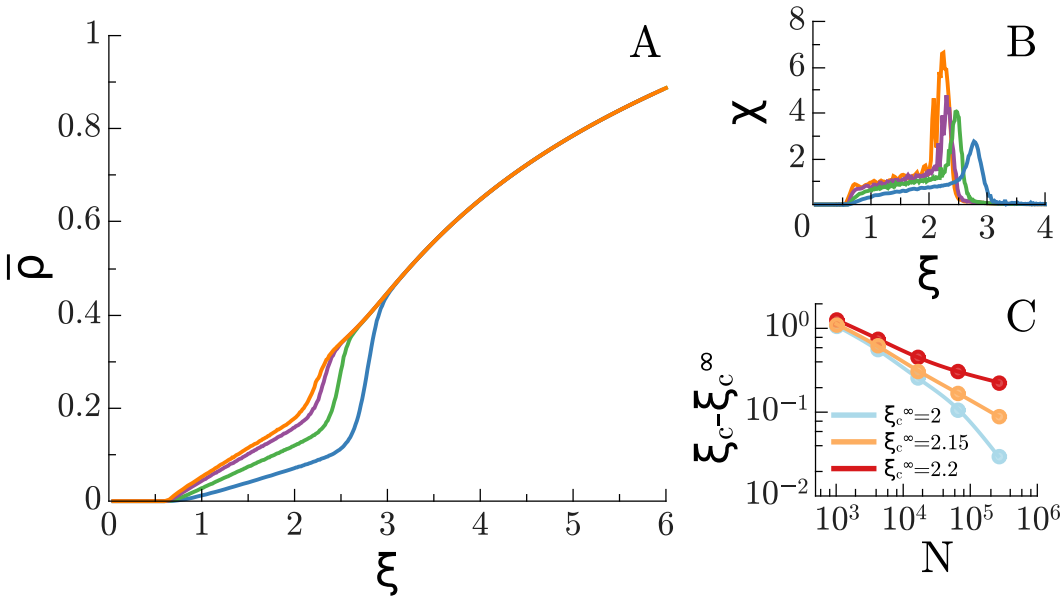

Figure 4.3: Overall network activity state (case A) as determined by the network time-averaged value $\bar{\rho}$ ($h = 10^{-7}$). (A) Order parameter $\bar{\rho}$ as a function of the control parameter ξ for various system sizes $N = 64^2, 128^2, 256^2, 512^2$ (from bottom to top); observe that $\bar{\rho}$ grows monotonically with ξ and that an intermediate regime, in which $\bar{\rho}$ grows with system size, emerges between the up and the down states. (B) Inset: Standard deviation of the averaged overall activity in the system multiplied by $\sqrt{N}$; $\Xi = \sigma_\rho \sqrt{N}$ (see main text); The point of maximal variability coincides with the point of maximal slope in (A) for all network sizes N. (C) Finite-size scaling analysis of the peaks in (B). The distance of the size-dependent peak locations $\xi_c(N)$ from their asymptotic value for $N \to \infty$, ξ_c^∞, scales as a power law of the system size, taking $\xi_c^\infty \approx 2.15$, revealing the existence of true scaling as corresponds to criticality.

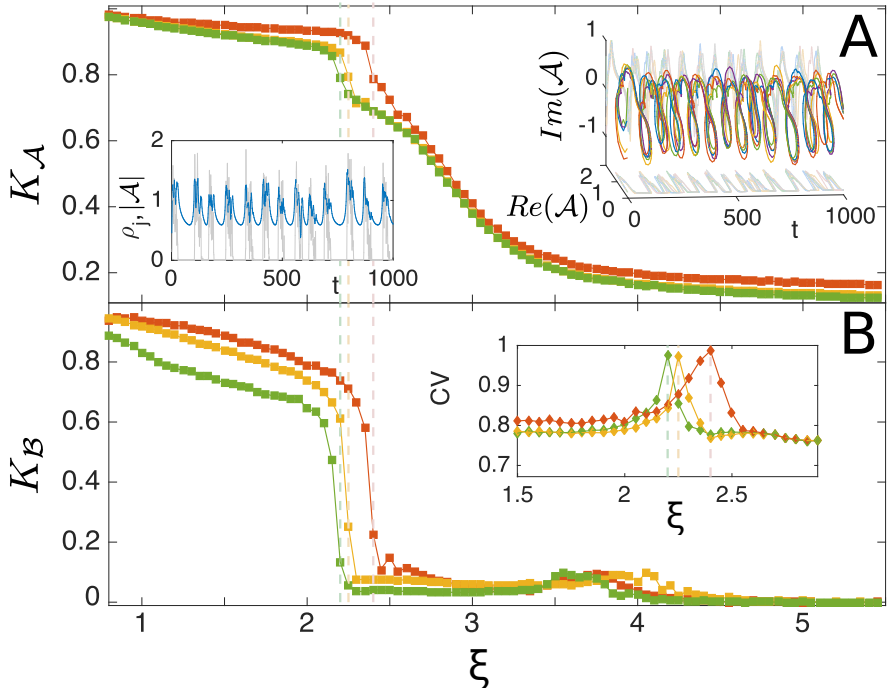

Figure 4.4: **Synchronization transition elucidated by measuring the Kuramoto parameter** as estimated using (A) the analytic signal representation $\mathcal{A}_k(t)$ of activity time series $\rho_k(t)$ at different units k and for various system sizes ($N = 128^2$ (red), 256^2 (orange), 512^2 (green)). For illustrative purposes, the top right inset of (A) shows the analytical representation (including both a real and an imaginary part) of 5 sample units as a function of time; the inset on the left shows the time evolution of one node (gray) together with the amplitude of its analytic representation (blue) Both insets, vividly illustrate the oscillatory nature of the unit dynamics. (B) Results similar to those of (A), but employing a different method to compute time-dependent phases of effective oscillators (see Methods). This alternative method captures more clearly the emergence of a transition; the point of maximum slope of the curves corresponds to the value of the transition points $\xi_c(N)$ in (A). The inset in (B) shows the coefficient of variation CV (ratio of the standard deviation to the mean) of the times between two consecutive crossings of the value 2π; it exhibits a peak of variability at the critical point $\xi_c(N)$.

Phase transitions

Having analyzed the possible phases, we now discuss the phase transitions separating them. For all the considered network sizes the time-averaged overall activity, $\bar{\rho}$, starts taking a distinctively non-zero value above $\xi \approx 0.75$ (see Fig.4.3), reflecting the upper bound of the down or quiescent state (transition between A1 and A2). This phase transition is rather trivial and corresponds to the onset on network spikes i.e. oscillations (whose characteristic time depends on various factors, such as the synaptic recovery time [108] and the baseline level of synaptic resources).

More interestingly, Fig.4.3 also reveals that $\bar{\rho}$ exhibits an abrupt increase at (size-dependent) values of ξ, between 2 and 3, signaling the transition from A2 to A3. However, the jump amplitude decreases as N increases, suggesting a smoother transition in the large-N limit. Thus it is not clear *a priori*, using $\bar{\rho}$ as an order parameter, whether there is a true sharp phase transition or there is just a crossover between the synchronous (A2) and the asynchronous (A3) regimes. To elucidate the existence of a true critical point, we measured the standard deviation of the network-averaged global activity $\bar{\rho}$, σ_ρ. Direct application of the central limit theorem [47] would imply that such a quantity should decrease as $1/\sqrt{N}$ for large N and thus, $\chi \equiv \sqrt{N}\sigma_\rho$ should converge to a constant. However, Fig. 4.3B shows that χ exhibits a very pronounced peak located at the (N-dependent) transition point between the A2 and the A3 phases; furthermore its height grows with N –i.e. it diverges in the thermodynamic limit– revealing strong correlations and anomalous scaling, as occurs

at critical points. Also, a finite-size scaling analysis of the value of ξ at the peak (for each N), i.e. $\xi_c(N)$, reveals the existence of finite-size scaling, as corresponds to a *bona fide* continuous phase transition at $\xi_c^{\infty} \simeq 2.15(5)$ in the infinite-size limit (see Fig. 4.3C). Moreover, a detrended fluctuation analysis [109, 110] of the timeseries reveals the emergence of long-range temporal correlations right at ξ_c (see Appendix D.3.8), as expected at a continuous phase transition.

To shed further light on the nature of such a transition, it is convenient to employ a more adequate (synchronization) order-parameter. In particular, we consider the Kuramoto index K –customarily employed to detect synchronization transitions [111]– defined as $K \equiv \frac{1}{N}\left\langle \left| \sum_{k=1}^{N} e^{i\phi_k(t)} \right| \right\rangle$ –where i is the imaginary unit, $|\cdot|$ is the modulus of a complex number, $\langle\cdot\rangle$ here indicates averages over time and independent realizations, and k runs over units, each of which is characterized by a phase, $\phi_k(t) \in [0, 2\pi]$, that can be defined in different ways. For instance, an effective phase $\phi_k^{\mathcal{A}}(t)$ can be assigned to the time-series at unit k, $\rho_k(t)$, by computing its *analytic signal representation*, which maps any given real-valued timeseries into an oscillator with time-dependent phase and amplitude (see Appendix D.3). Using the resulting phases, $\phi_k^{\mathcal{A}}(t)$, the Kuramoto index $K_{\mathcal{A}}$ can be calculated. As illustrated in Fig. 4.4A, it reveals the presence of a synchronization transition: the value of $K_{\mathcal{A}}$ clearly drops, at the previously determined critical point $\xi_c(N)$. An alternative method to define a time-dependent phase for each unit (details discussed in Appendix D.3) reveals even more vividly the existence of a synchronization transition at $\xi_c(N)$ as shown in Fig. 4.4B. Finally, we have also estimated the coefficient of vari-

ation (CV) of the distance between the times at which each of these effective phases crosses the value 2π; this analysis reveals the presence of a sharp peak of variability, converging for large network sizes to the critical point $\xi_c^{\infty} \approx 2.15$ (see inset of Fig. 4.4B).

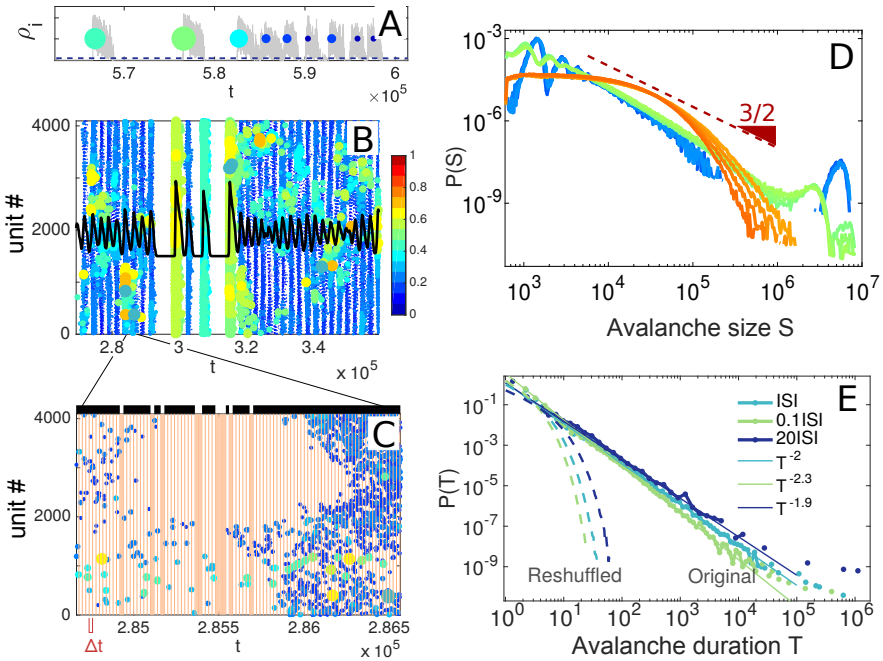

Figure 4.5: Avalanches measured from activity time series. (A) Illustration of the activity timeseries $\rho_i(t)$ (gray color) at a given unit i. By establishing a threshold value θ (dashed red line, close to the origin) a single "event" or "unit spike" is defined by convention at the time of the maximal activity in between two threshold crossings (n.b. the forthcoming results are robust to changes in this criterion; see Section D.3.10); a weight equal to the area covered in between the two crossings is assigned to each event (note the color code). This allows us to map a continuous time-series into a discrete series of weighted events. The time distance between two consecutive events is called *inter-event interval* (ISI). (B) Raster plot for a system with 64 units, obtained using the procedure above for each unit. Observe that large events coexist with smaller ones, and that these last ones, occur in a rather synchronous fashion. The overall time-dependent activity is marked with a black curve. (C) Zoom of a part of (B) illustrating the time resolved structure and using a time binning Δt equal to the network-averaged IEI. Shaded columns correspond to empty time bins, i.e. with no spike. Avalanches are defined as sequences of events occurring in between two consecutive empty time bins and are represented by the black bars above the plot. (D) Avalanche-size distribution (the size of the avalanche is the sum of the weighted spikes it comprises) for diverse values of ξ (from 1.85 to 2.05, in blueish colors, from 2.7 to 2.9 in greenish colors, and from 3.3 to 3.45 in orangish colors) measured from the raster plot $\Delta t = IEI$.

Figure 4.5: The (red) triangle, with slope 3/2 is plotted as a reference, illustrating that, near criticality, a power law with an exponent similar to the experimentally measured one is recovered. Away from the critical point, either in the synchonous phase (blueish colors) and the asynchronous one (orangish) clear deviations from power-law behavior are observed. Observe the presence of "heaps" in the tails of the distributions, especially in the synchronous regime; these correspond to periodic waves of synchronized activity (see Section D.3.10); they also appear at criticality, but at progressively larger values for larger system sizes. (E) Avalanche-duration distribution, determined with different choices of the time bin. The experimentally measured exponent 2 is reproduced using $\Delta t = IEI$, whereas deviations from such a value are measured for smaller (larger) time bins, in agreement with experimentally reported results. After reshuffling times, the distributions become an exponential, with characteristic timescales depending on Δt (dashed lines).

Thus, recapitulating, the phase transition separating the down state from the synchronous irregular regime (A1-A2 transition) is trivial and corresponds to the onset of network spikes, with no sign of critical features. In between the asynchronous and the up state (A3-A4) there is no true phase transition, as both phases are indistinguishable in the infinitely-large-size limit (see Appendix D.3.9). On the other hand, different measurements clearly reveal the existence of a bona fide synchronization phase transition (A2-A3) at which non-trivial features characteristic of criticality emerge.

4.2.5 Avalanches

For ease of comparison with empirical results, we define a protocol to analyze avalanches that closely resembles the experimental one, as introduced by Beggs and Plenz [9]. Each activity timeseries of an individual unit can be mapped into a series of discrete-time "spikes" or "events" as follows. As illustrated in Fig.4.5A, a "spike" corresponds to a period in which the activity at a given unit is above a given small threshold in between two windows of quiescence (activity below threshold).[9] Hence, as illustrated in Fig.4.5B, the network activity can be represented as a raster plot of spiking units. Following the standard experimental protocol a discrete time binning Δt is chosen and each individual spike is assigned to one such bin. An avalanche is defined as a consecutive sequence of temporally-contiguous occupied bins preceded and ended by empty bins (see Fig.4.5B and C). Quite remarkably, using this pro-

[9]Results are quite robust to the specific way in which this procedure is implemented. See Appendix ap:Csynchro section as well as the caption of Fig.4.5 and Appendix D.3.10.

tocol several well-known experimental key features of neuronal avalanches can be faithfully reproduced by tuning ξ to a value close to the synchronization transition. In particular: (i) The sizes and durations of avalanches of activity are found to be broadly (power-law) distributed at the critical point; these scale-invariant avalanches coexist with anomalously large events or "waves" of synchronization, as revealed by the "heaps" in the tails of the curves of in Fig.4.5D and E.

(ii) Changing Δt, power-law distributions with varying exponents are obtained at criticality (the larger the time bin, the smaller the exponent) as originally observed experimentally by Beggs and Plenz (Fig.4.5E).

(iii) In particular, when Δt is chosen to be equal to the ISI (inter-spike time interval, i.e. the time interval between any two consecutive spikes), avalanche sizes and durations obey –at criticality– finite-size scaling with exponent values compatible with the standard ones, i.e. those of an unbiased branching process (see Fig.4.5B and C as well as Appendix D.3.10).

(iv) Reshuffling the times of occurrence of unit's spikes, the statistics of avalanches is dramatically changed, giving rise to exponential distributions (as expected for an uncorrelated Poisson point process) thus revealing the existence of a non-trivial temporal organization in the dynamics (Fig.4.5E).

(v) Away from the critical point, both in the sub-critical and in the super-critical regime, deviations from this behavior are observed; in the subcritical or synchronous regime, the peak of periodic large avalanches becomes much more pronounced, while in the asynchronous phase, such a peak is lost and

distribution functions become exponential ones with a characteristic scale (see Fig.4.5D).

Summing up, our model tuned to the edge of a synchronization/desynchronization phase transition reproduces all chief empirical findings for neural avalanches. These findings strongly suggest that the critical point alluded by the criticality hypothesis of cortical dynamics does not correspond to a quiescent/active phase transition –as modeling approaches usually assume– but to a synchronization phase transition, at the edge of which oscillations and avalanches coexist.

It is important to underline that our results regarding the emergence of scale-free avalanches are purely computational. To date, we do not have a theoretical understanding of why results are compatible with branching-process exponents. In particular, it is not clear to us if a branching process could possibly emerge as an effective description of the actual (synchronization) dynamics in the vicinity of the phase transition, or whether the exponent values appear as a generic consequence of the way temporally-defined avalanches are measured (see [87]). These issues deserve to be carefully scrutinized in future work.

4.2.6 The role of heterogeneity

Thus far we have described homogeneous networks with local coupling. However, long-range connections among local regions also exist in the cortex, and mesoscopic units are not necessarily homogeneous across space [112, 103].

These empirical facts motivated us to perform additional analysis of our theory, in which slightly modified substrates are employed. First, we considered small-world networks, and verified that our main results (i.e. the existing phases and phase transitions) are insensitive to the introduction of a small percentage of long-range connections (see Appendix D.3.7). However, details such as the boundaries of the phase diagram, the shape of propagation waves, and the amplitude of nested oscillations do change. Recent experimental analyses have scrutinized the effect of network heterogeneity in cultures of rat cortical neurons *in vitro* [113]. In particular, Okujeni *et al.* where able to control the level of clustering by experimentally modifying the level of a given enzyme (protein Kinase C) that promotes neuronal aggregation. In this way, progressively more clustered networks were generated as the level of protein was increased (see Fig. 1 in [113]).

Keeping fixed other experimental conditions, Okujeni *et al.* found that in the case in which neurons are more homogeneously distributed in the substrate networks spikes appear much more sporadically than when the network is highly clustered (see Fig. 4.7, which is adapted from [113]), and that network spikes appear more clustered in time in this latter case. Thus, in conclusion, clustering promotes the generation of spontaneous network activity. In order to model these experimental results, we developed a heterogeneous network in which we keep fixed the mean value of the parameter a (that controls the decay of the activity at each single unit), but inducing some areas with low local values of a_1, i.e. with a smaller propensity for activity to decay (red nodes in Fig. 4.6), while in the rest of the network larger values of a, a_2, are

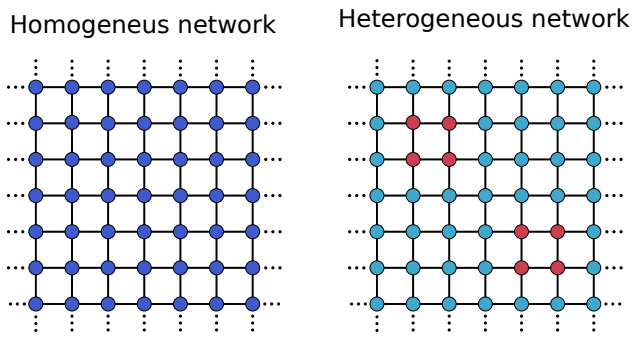

Figure 4.6: Sketch of the considered networks: homogeneous to the left and heterogeneous/clustered to the right. In both cases the network-average value of the activity-decay parameter a is taken to be equal. However, while in the homogeneous case the value of a is constant across the network, in the heterogeneous one there are some areas (marked with red nodes) with a lower value of a.

considered (keeping the network-average value of a constant). As shown in Figure 4.7, the lower the local value of a_1, the more facilitated the emergence of spontaneous activity, leading the system closer and closer to the critical point or the asynchronous irregular phase, and reproducing quite remarkably the chief experimental observations of Okujeni *et al.*

Thus, in conclusion, our general model, equipped with an additional layer of network heterogeneity is able to reproduce specific empirical results. To further explore the influence of network architecture onto dynamical phases, in future work we will extend our model employing empirically-obtained large-scale networks of the human brain, as their heterogeneous and hierarchical-modular architecture is known to influence dynamical process operating on them [103, 114].

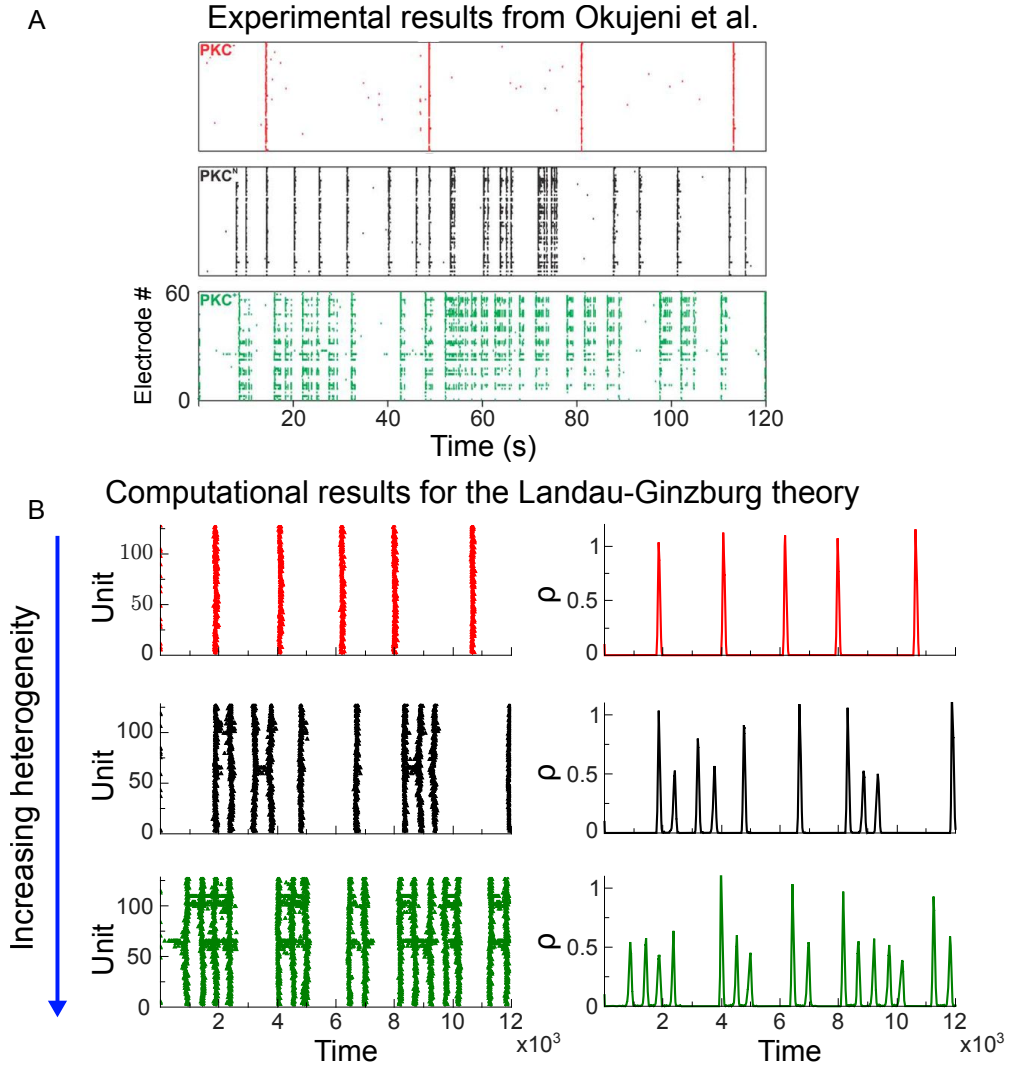

Figure 4.7: Temporal series for different level of network clustering. Panel A shows the experimental results of Okujeni [113] (adapted figure from the original paper) for increasing levels of aggregation in a neural network. Panel B shows three temporal series for different levels of network clustering and a fixed value of $\xi = 1.2$. In the first one (red) the network is homogeneous with $a_1 = a_2 = 1$. Observe that smaller values of a_1 produce a more active network, in particular for $a_1 = -0.7$ (black) and $a_1 = -0.928$ (green). In both cases, the clustering facilitate the spontaneous activity. Other parameter values: $b = 1.5, \tau_D = 10^2, \tau_R = 10^3, h = 10^{-7}$.

4.2.7 Phases and phase transitions: Case B

We discuss the much simpler scenario for which the deterministic/mean-field dynamics predicts bistability, i.e. case B above, which is obtained e.g. considering a slower dynamic for synaptic-resource depletion. In this case, the introduction of noise and space, does not alter the deterministic picture. Indeed, computational analyses reveal that there are only two phases: a down state and an up one for small and large values of ξ, respectively. These two phases have the very same features as their corresponding counterparts in case A. The phase transition between them is discontinuous (much as in Fig. 1B) and thus, for finite networks, fluctuations induce spontaneous transitions between the up and the down state when ξ takes intermediate values, in the regime of phase coexistence. Thus, in case B, our theory constitutes a sound Landau-Ginzburg description of existing models, such as those in [21, 54, 55], describing up and down states and up-and-down transitions.

4.2.8 Large separation of timescales: self-organized bistability

Remarkably, this set of equations 4.3 exhibits profound analogies with the theory of SOB, as introduced in the previous Chapter. We want to discuss here if SOB can be encompassed by a synaptic plasticity mechanism, thus proving relevant in neuroscience. An important point to stess is that while in SOB the background field is conserved in the bulk (only driving events and boundary dissipation make the total integral value fluctuate in time), the above

equation for $\dot{R}(t)$ is not conserved in general. However, it includes a (positive) term for the charging/recovery of resources which is tantamount to driving in SOB as well as a (negative) term for the activity-dependent consumption of resources. The limit of SOB can be recovered for infinitely slow synaptic dynamics $1/\tau_R \to 0$ and $1/\tau_D \to 0$, while $\tau_D/\tau_R \to 0$. In fact, while the synaptic timescales become larger and larger, the dependence on the control parameter ξ becomes weaker and weaker. Moreover, in the mean-field picture, the relation between the two timescales is such that the slope of the nullcline $\dot{E} = 0$ goes to zero in the thermodynamic limit, making sure that (for any –reasonable– value of the parameter ξ) only one unstable fixed point exists.

In Fig.4.8 we plot a measure of avalanches statistics, showing that SOB behavior is finely reproduced: the dynamics consists of avalanches of activity (measured as activity over threshold, as usually done in absorbing/active phase transitions) occurring in between two consecutive quiescent (down) periods, with the usual branching-process universality class exponents, interspersed with anomalously large or "king avalanches", much as in SOB. However, this extreme separation of timescales does not seem to be neuro-physiologically realistic. In fact, if we take as a reference the neural activity timescale, which is of the order of the millisecond, the self-organization limit would be reproduced for synaptic timescales of the order of 10 to 1000 seconds, whereas, in neurophysiological measurements, such scales are comprised between few tens and few hundreds of milliseconds [99, 115, 116]. Moreover an additional caveat is that finite size scaling would be correctly reproduced if synaptic timescales scaled with the system size, which is biologically unplausible [83]. Given the

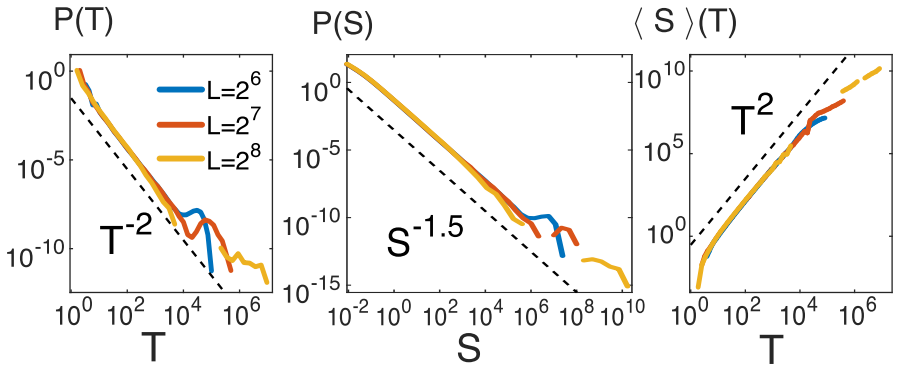

Figure 4.8: Avalanche distributions in the limit of extremely slow synaptic-resources dynamics, for the spatially extended noisy system ($\sigma = D = 1$). Probability distribution for avalanche durations T (left), avalanche sizes S (center) and average avalanche size as a function of duration (right) in double logarithmic scale, for square-lattice systems of sizes: $N = 2^{12}, 2^{14}$ and 2^{16}. The dashed lines are plotted as a guide to the eye, and have the slopes corresponding to the expectations for an unbiased branching process ($-2, -3/2$ and 2, respectively) as experimentally observed. The "bumps" in the blue curves, correspond to anomalously large events, i.e. synchronized spiking events, occurring in the SI phase. The cut-offs/bumps change with N obeying finite-size scaling as in the theory of self-organized bistability (see Chapter 3). Parameters: $b = -0.5$ $a = 1$, $h = 10^{-7}$.

variety of synaptic timescales measured both locally and temporally [117], it is possible that self-organization cannot be achieved without including in the picture further mechanisms, such as neuromodulation, inhibition, spike timing-dependent plasticity, which regulate the synaptic timescales, allowing biological neural networks to span from up/down states to scale-invariance plus oscillatory behavior to self-organization to criticality.

4.3 Summary and Conclusions

Aimed at shedding light on the issues concerning the criticality hypothesis in the brain and in particular establishing what these phases are, and what the nature of the putative critical point is, here we followed a classical statistical-physics approach: following the parsimony principle of Landau and Ginzburg in the study of phases of the matter and the phase transitions they experience, we proposed a simple stochastic mesoscopic theory of cortical dynamics that allowed us to classify the possible emerging phases of cortical networks under very general conditions. For the sake of specificity and concreteness we focused on a regulatory dynamics –preventing the level of activity to explode– controlled by synaptic plasticity (depletion and recovery of synaptic resources), but analogous results can be obtained considering e.g. inhibition as the chief regulatory mechanism. As a matter of fact, our conclusions are quite robust and general and do not essentially depend on specific details of the implementation, the nature of the regulatory mechanism, or the network architecture.

Importantly, taking advantage of experience from the theory of phase transitions, we introduce two additional key ingredients: intrinsic stochasticity stemming from the non-infinite size of mesoscopic regions, and spatial dependence. In this way, our theory consists of a set of stochastic Wilson-Cowan equations and can be formulated as a field theory, employing standard techniques [118].

Using our Landau-Ginzburg approach, we have shown that the stochastic and spatially extended neural networks can harbor two different scenarios depending on parameter values: case (A) including a limit cycle at the deterministic

level and the possibility of oscillations and case (B) leading to bistability (see Fig.4.1).

In the simpler case (B) our complete theory generates a down and a homogeneous up-state phase, with a discontinuous transition separating them, and the possibility of up-down transitions when the system operates in the bistability region. In this case, our theory constitutes a sound mesoscopic description of existing microscopic models for up-and-down transitions [21, 54, 40, 24] as observed in the cortex during deep sleep or under anesthesia [88, 89].

On the other hand, in case (A), we find diverse phases including oscillatory and bursting phenomena: down states, synchronous irregular, asynchronous irregular, and active states[10].

Within our framework, it is possible to define a protocol to analyze avalanches, resembling very closely the experimental one [9, 11, 10, 14, 15]. Thus, in contrast with other computational models, causal information is not explicitly needed/employed here to determine avalanches –they are determined from raw data– and results can be straightforwardly compared to experimental ones for neuronal avalanches, without conceptual gaps (see Chapter 2).

The model reproduces all the main features observed experimentally: (i) power-law distributed avalanche sizes and durations emerge only at the critical point of the synchronization transition, while deviations from such a behavior occur away from the critical point, in either phase. (ii) The corresponding exponent

[10] As a side remark, note that, in the search of a mesoscopic description of cortical networks of spiking neurons, we constructed a coarse-grained model for the network activity. However, our analyses readily revealed the "spiking" nature of the activity dynamics, underlying the fundamental role of oscillations and partial synchronization in neural dynamics across scales.

values depend on the time bin Δt, required to define avalanches, but (iii) fixing the time bin Δt to coincide with the inter-event interval, IEI, the same statistics as in empirical networks, i.e. the critical exponents compatible with those of an unbiased branching process (see Chapter 5) are obtained; and finally (iv) scale-free distributions disappear if events are reshuffled in time, revealing a non-trivial temporal organization.

Thus, the main outcome of our analyses is that the underlying phase transition at which scale-free avalanches emerge does not separate a quiescent state from a fully active one but a synchronization transition, separating regimes in which mesoscopic units tend to become active synchronously or asynchronously, respectively. This is a crucial observation, as most of the existing modelling approaches for critical avalanches in neural dynamics to date rely on a continuous quiescent/active phase transition, and this is not a pertinent choice as we have argued above.

Let us also remark that –consistently with our findings– the amazingly detailed model put together by the Human Brain Project consortium seems to suggest that the model best reproduces experimental features when tuned near to its synchronization critical point [119]. In such a study, the concentration of Calcium ions, Ca^{2+} needs to be carefully tuned to its actual nominal value to set the network state. Similarly, in our approach, the role of the calcium concentration is played by the parameter ξ, regulating the maximum level reachable by synaptic resources. Interestingly, the calcium concentration is well-known to modulate the level of available synaptic resources (i.e. neurotransmitter release from neurons; see e.g. [81, 25, 96]), hence, both quantities play a similar

role.

Summing up, our Landau-Ginzburg theory with parameters lying in case (B) constitutes a sound description of the cortex during deep sleep or during anesthesia, when up and down transitions are observed. On the other hand, case (A) when tuned close to the synchronization phase transition can be a sound theory for the awaked cortex, in a state of alertness. A detailed analysis of how the transition between deep-sleep (described by case (B)) and awake (or REM sleep, described by case (A)) may actually occur in these general terms is beyond our scope here, but let us remark that, just by modifying the speed at which synaptic resources recover it is possible to shift between the two cases, making it possible to speculate on how such transitions could be easily induced.

A simple extension of our theory, including spatial heterogeneity has been shown to be able to reproduce remarkably well experimental measurements of activity in neural cultures with structural heterogeneity, opening the way to more stringent empirical validations of the general theory proposed here.

Chapter 5

A simple unified view of branching process statistics: random walks in balanced logarithmic potentials

5.1 Introduction

The work presented in this Chapter is intended to help avoiding the frequent confusion we have encountered in the neuroscience literature about branching processes and their relation with random walks. It can also be useful for interpreting empirical results, in particular in understanding non-universal continuously-varying exponents. In fact, as already mentioned above, neuronal

avalanches distributions are found to be compatible with branching process exponents. Although a mean field scenario is not adequate to describe the emergence of avalanching behavior in the cerebral cortex, since spatial effects must be crucial, we want to clarify under a simple, general and super-universal analytical perspective how those exponents emerge in systems with absorbing states.

Directed percolation (DP) is the paradigmatic example of a very large class of systems –including catalytic reactions, growing interfaces in random media, damage spreading, epidemic dynamics, and turbulence, to name but a few– exhibiting a phase transition separating a quiescent or absorbing state from an active one [120, 42, 44, 45, 121, 122]. The essence of this very robust universality class –which, curiously enough, had to wait long for experimental backing [123]– is parsimoniously encoded in the following Langevin equation [124, 125, 45, 121, 122]

$$\dot{\rho}(\mathbf{r},t) = a\rho(\mathbf{r},t) - b\rho^2(\mathbf{r},t) + D\nabla^2\rho(\mathbf{r},t) + \sqrt{\rho(\mathbf{r},t)}\eta(\mathbf{r},t), \qquad (5.1)$$

where $\rho(\mathbf{r},t)$ is the density of activity at coordinates $\mathbf{r}$ and time t, a is the control parameter regulating the distance to the critical point, b and D are constants, and $\eta(t)$ is a Gaussian white noise of variance σ^2. Critical exponents, scaling functions, and, in general, all critical features can be obtained using Eq.(5.1) as a starting point. The most preponderant aspect of this equation, distinguishing it from other classes, as for instance the Ising class [50], is the $\sqrt{\rho}$ factor in the noise amplitude. This square-root noise term stems from the "demographic" nature of the particle-number fluctuations; and it imposes

that there are no fluctuations in the absence of activity, as corresponds to the absorbing state [1].

The same type of demographic noise also appears in other slightly different universality classes, such as (i) the *voter-model* or neutral class describing the dynamics of neutral theories in which two symmetric competing states are possible [129, 120, 130, 131]; in this class there is no deterministic force except for diffusion, and the noise amplitude is different from zero only at the interfaces separating the two absorbing states e.g. at $\rho = 0$ and $\rho = 1$, i.e. $\dot{\rho}(\mathbf{r},t) = D\nabla^2\rho(\mathbf{r},t) + \sqrt{\rho(\mathbf{r},t)(1-\rho(\mathbf{r},t))}$ [131]; (ii) the *dynamical percolation* class [132, 133] –in which re-activation of sites cannot occur and, as a consequence, the non-linear term in Eq.(5.1) needs to be replaced by a non-Markovian term $-\rho(\mathbf{r},t)\int_{-\infty}^{t} dt'\rho(\mathbf{r},t')$ keeping track of past activity while the noise term remains unchanged, and (iii) the *Manna* class of systems with many absorbing states such as sandpiles in which an additional conservation law –that can be encapsulated in an additional term $-\rho(\mathbf{r},t)\int_{-\infty}^{t} dt\nabla^2\rho(\mathbf{r},t)$ [7, 31]– exists, while the noise term remains as in directed percolation.

All systems with absorbing states, including the four classes discussed above, and some other more infrequent ones, not specified here– share the common feature of exhibiting avalanching behavior, meaning that if the absorbing state is perturbed by a localized seed of activity, this can trigger a cascade of events before falling back again into the absorbing state. It is common knowledge

[1] Another group of universal behavior is that of systems with noise proportional to the activity (rather that to the square-root of the activity); these encode a different type of processes where the most dominant fluctuations are not demographic, but associated to spatio-temporal variability in the overall parameters [126, 127, 128].

that avalanches turn out to be scale invariant at critical points; in particular, the avalanche-size (S) and avalanche-duration (T) probability distribution functions can be written at criticality as

$$\begin{aligned} P(S) &\sim S^{-\tau}\mathcal{G}_{\mathcal{S}}(S/S_C) \\ F(T) &\sim T^{-\alpha}\mathcal{G}_{\mathcal{T}}(T/T_C), \end{aligned} \tag{5.2}$$

where $\mathcal{G}_{\mathcal{S}}(S/S_C)$ and $\mathcal{G}_{\mathcal{T}}(T/T_C)$ are cut-off functions, and the cut-off scales, S_C and T_C, depend only on system size right at the critical point, and on the distance to criticality away from it [134]. Similarly, the averaged avalanche size scales with the duration as $\langle S\rangle \sim T^{\gamma}$, where the exponent γ needs to obey the scaling relation [135, 136],

$$\gamma = \frac{\alpha - 1}{\tau - 1}. \tag{5.3}$$

In particular, for avalanches propagating in high dimensional systems (or in densely connected networks) mean-field exponent values $\tau = 3/2$, $\alpha = 2$ and $\gamma = 2$ are obtained for all systems with absorbing states. A compilation of avalanche exponents for different dimensions and universality classes, as well as scaling relationships, can be found in [65, 137, 138, 139].

5.2 Main Results

5.2.1 Computation of exponent values for the mean field case

In order to explicitly compute these exponent values, textbooks usually resort to the (Galton-Watson) branching process [140, 42, 141, 120]. In this, each node of a tree has two branches emerging out of it; from an occupied/active node at time/generation n each of its two out-branches (at time/generation $n+1$) are occupied/active with probability p or left empty with complementary $(1-p)$. Observe that this is just a variant of directed percolation running on a regular tree (see Figure 5.1). For illustration and completeness, we now present a very simple derivation of its associated avalanche distribution functions.

To compute $P(S)$ –where S is the total number of occupied/active nodes before the process comes to its end– one just needs to evaluate the total number of connected trees of size S, which is nothing but the Catalan number [142]

$$C(S) = \frac{1}{S}\binom{2S}{S-1}, \tag{5.4}$$

and multiply it for the probability of each one to occur, $p^{S-1}(1-p)^{S+1}$. Evaluating the resulting expression $P(S,p) = (2S)!/((S+1)!S!)p^{S-1}(1-p)^{S+1}$ in the Stirling approximation for $S >> 1$, one readily obtains

$$P(S,p) = \frac{\mathcal{N}}{\sqrt{\pi}} S^{-3/2}(4p(1-p))^S, \tag{5.5}$$

where $\mathcal{N}$ is a normalization constant; in particular, this becomes a power law at the critical point $p = 1/2$: $P(S, 1/2) = \frac{\mathcal{N}}{\sqrt{\pi}} S^{-3/2}$, implying $\tau = 3/2$. The exponent γ can also be derived using the statistics of branch lengths in Catalan trees of a given size [143], leading readily to the result $\gamma = 2$; and from this, using the scaling relation Eq.(5.3), one obtains $\alpha = 2$.

5.2.2 A general unifying view

These results for the branching-process avalanche statistics can be derived in a more systematic way –for different types of underlying regular or random tree topologies– within the generating function formalism [34, 144, 43]; indeed, already back in 1949 Otter computed the solution for the case of a Poissonian distribution of branches per node [145]. Given that the result, e.g. a power-law with exponent 3/2 for the size distribution, is much more general than any specific branching process in any specific tree-like topology, it is appealing from a theoretical point of view to derive an even more general proof of these results, covering all cases at once. From a slightly different perspective, relying on field theory and scaling arguments [146, 65, 147] the whole set of exponent values can be obtained for each specific universality class, but again, the result –being common to all classes, i.e. *super-universal*– should be amenable for a more generic explanation.

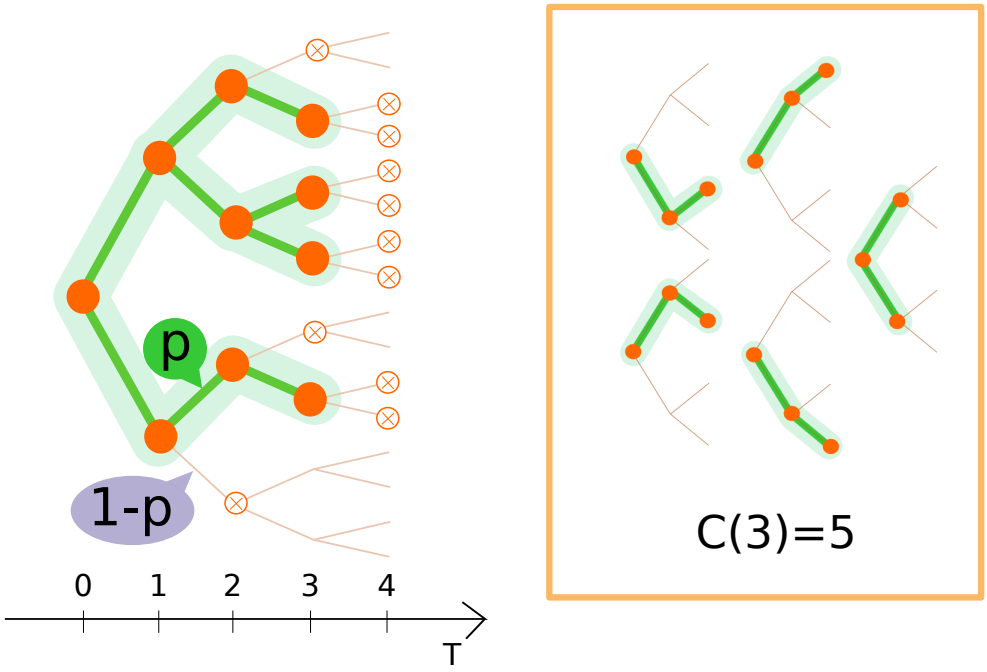

Figure 5.1: Left: Illustration of a realization of the un-biased branching process, showing (highlighted) an avalanche of size $S = 10$ and duration $T = 3$, together with the structure of the underlying rooted binary tree on top of which it unfolds. Right: Visualization of the 5 possible paths of $S = 3$ as counted by the Catalan number $C(3) = 5$.

5.2.3 Random walk in a logarithmic potential

The common feature shared by all the Langevin equations of the different classes of systems with absorbing states, as already mentioned above, is the presence of a demographic, square-root, noise amplitude. As a matter of fact –as illustrated in more detail in Section D.4.1– in the mean-field limit it is easy to derive a common and unique effective Langevin equation for all classes of systems with absorbing states at criticality, as

$$\dot{\rho} = \sqrt{\rho}\ \xi(t), \tag{5.6}$$

where ρ is the overall activity and $\xi(t)$ is a Gaussian white noise with zero mean and $\langle \xi(t)\xi(t')\rangle = 2\sigma^2\delta(t-t')$ which needs to be interpreted in the Itô sense in order to guarantee that $\rho = 0$ is an absorbing state [148, 47]. We refer to Eq.(5.6) as "demographic random walker" (DRW). To avoid the complications of the Itô calculus, we write the equivalent equation in the Stratonovich interpretation [148, 47]:

$$\dot{\rho} = -\frac{\sigma^2}{2} + \sqrt{\rho}\eta(t) \tag{5.7}$$

where now $\langle \eta(t)\eta(t')\rangle = \frac{\sigma^2}{2}\delta(t-t')$. Using now standard calculus to change variables to $x = \sqrt{\rho}$ directly gives [2]

$$\dot{x} = -\frac{\sigma^2}{4x} + \eta(t). \tag{5.8}$$

[2] An alternative approach to analyze Langevin equations such as Eq.(5.6) consists in reabsorbing the noise amplitude into the time-scale, leading to a standard random walk with a different "clock" [58]. Another interesting possibility is deriving these results from a more general fractional Brownian motion [149].

The resulting equation is just a particular case of a one-dimensional random walker (RW) moving in a logarithmic potential $U(x) = \lambda \log x$, i.e.

$$\frac{dx}{dt} = -\frac{dU(x)}{dx} + \eta(t) = -\frac{\lambda}{x} + \eta(t), \tag{5.9}$$

where λ is a positive constant and, in general, $\langle \eta(t)\eta(t') \rangle = 2\mu\delta(t - t')$, with μ a generic positive constant. Observe tha Eq(5.8) corresponds to the particular case, $\lambda = \mu = \sigma^2/4$ –that we call *balanced*– in which the ratio between the amplitudes of the logarithmic potential and the noise-correlation amplitude, μ, is equal to unity: $\beta \equiv \lambda/\mu = 1$. This perfect balance between the deterministic-force and stochastic coefficients is essential for what follows, as we shall see. More in general, let us remark that, in the presence of an external field –allowing for the spontaneous generation of activity at a fixed rate h– Eq.(5.7) needs to be complemented with an additional $+h$ term. Upon changing variables, this implies $\beta = 1 \to 1 - h/\mu$, in Eq.(5.9) and thus, in the presence of external driving, the perfect balance between coefficients breaks down.

To compute avalanche exponents from Eq.(5.9), let us define an avalanche as a random walk $x(T)$, starting at $x(t = 0) = 0^+$ and returning for the first time to the origin at time T, $x(T) = 0$ (see Figure 5.2). The distribution or its return times is nothing but $F(T)$ as defined in Eq.(5.2). The problem of computing such a return-time distribution for the random walk in a logarithmic potential, i.e. by Eq.(5.8), was solved by A. Bray [150] and revisited by F. Colaiori in the context of Barkhaussen crackling noise [72]. The solution requires writing down the equivalent Fokker Planck equation for the Langevin dynamics, with

a delta-like initial condition centered at a value slightly larger than $x = 0$, and computing the probability flux F at the origin as a function of the time T (more detailed sketch of the analysis is presented in Section D.4.2 for the sake of completeness). The resulting first-return probability distribution function is

$$\begin{aligned} F(T) &= \frac{4\mu\epsilon^{2\nu}}{\Gamma(\nu-1)}(1+\beta)(4\mu T)^{-\nu-1}e^{-\frac{x^2}{4\mu T}} \\ &\sim T^{-\nu-1} = T^{-\frac{3+\beta}{2}}, \end{aligned} \tag{5.10}$$

where $\nu = (1+\beta)/2$, implying $\alpha = \frac{3+\beta}{2}$. Observe that, in the limit of vanishing potential amplitude, $\lambda = 0$, this result reproduces the statistics of a freely-moving random walk, $F(T) \sim T^{-\frac{3}{2}}$, while in the opposite perfectly-balanced limit, $\lambda = \mu$ (i.e. $\beta = 1$) the result is $F(T) \sim T^{-2}$ in agreement with the expectations for the un-biased branching process. It is noteworthy that –despite the fact that the random walk in a logarithmic potential gives a non-universal avalanche duration exponent– for the undriven DRW case, in which the logarithmic potential derives from a change of variables in Itô calculus, there exists a perfect balance between the coefficients of the equation; they both depend on the noise amplitude and, compensating each other, they generate the universal value $\alpha = 2$. However, as said above, in the presence of an external field, $\beta = 1 - h/\mu$ breaking down the perfect balance between coefficients, non-universal continuously-varying avalanche exponents appear (see Figure 5.3); in particular,

$$\alpha = 2 - \frac{h}{2\mu}. \tag{5.11}$$

In any possible discrete/particle model with absorbing states, this change of exponents stems from the fact that –owing to the external driving– avalanches from different initial seeds (each of them spontaneously generated by the external driving field) can merge, which allows their combination to survive longer and be larger, thus leading to smaller effective exponents α and τ (see Table 1).

5.2.4 Derivation of avalanche exponents

Turning back to the general discussion, using the above result together with simple scaling, we can readily derive the associated avalanche size exponent, τ. In order to have a unified notation let us use a generic variable $v(t)$, which can be in particular, $x(t)$ for the RW, or $\rho(t)$ for the DRW. The size of any given avalanche is defined as the area under the curve defined by the random walk, i.e. $S = \int_0^T v(t)\, dt$, and we are interested in the distribution of such sizes as a function of T, $P(S|T)$. Given that the typical displacement of a random walk in time t scales as $v \sim \sqrt{t}$, for the DRW (for which there is an additional square-root factor) we have $v \sim \sqrt{v}\sqrt{t}$, and thus, $v \sim t$; hence, we can write, in general, $v \sim t^{\phi}$, with $\phi = 1/2$ and $\phi = 1$ for the RW and the DRW (either driven or undriven), respectively.

It is natural to define a new rescaled variable $\tilde{v}(t/T) = v(t)/T^{\phi}$ which describes a random excursion in the interval $[0, 1]$. In these terms,

$$S = \int_0^T v(t)dt \;\sim\; T^{\phi+1} \int_0^1 \tilde{v}(z)dz. \tag{5.12}$$

Thus, the average avalanche size, $\langle S \rangle$ obtained averaging over all possible avalanche shapes, $\tilde{v}(z)$, scales also with $T^{\phi+1}$, implying $\gamma = \phi + 1$.

Using the previous result, $P(S|T)$ can be written as a scaling form $P(S|T) = T^{-\gamma}\mathcal{G}\left(S/T^{\gamma}\right)$ where the factor $T^{-\gamma}$ comes from the normalization condition, and the unspecified scaling function $\mathcal{G}$ obeys $\mathcal{G}(z) \geq 0$ for all z and $\int_0^\infty \mathcal{G}(z)dz = 1$. Having computed the conditional probability $P(S|T)$, we can explicitly obtain $P(S)$ as

$$\begin{aligned} P(S) &= \int_0^\infty dT P(S|T)F(T) \\ &\sim C\int_0^\infty dT\ T^{-\gamma}T^{-\alpha}\mathcal{G}\left(S/T^{\gamma}\right) \\ &\sim CS^{-(\gamma+\alpha-1)/\gamma}\int_0^\infty duu^{\frac{(\alpha-1)}{\gamma}}\mathcal{G}\left(u\right), \end{aligned} \tag{5.13}$$

and, thus, $\tau = (\gamma+\alpha-1)/\gamma$ (which is nothing but the scaling relation Eq.(5.3)). Plugging the value of α and γ derived above one obtains the well-known result $\tau = 4/3$ for the standard random walk [3] and

$$\tau = \frac{3}{2} - \frac{h}{4\mu}, \tag{5.14}$$

for the DRW, which reduces to the well-known result $\tau = 3/2$ for the un-driven case. Table 1 contains a summary of the exponents for the different cases.

Results beyond critical exponents have also been obtained in the literature, for example, the average shape of random-walk excursions is a semi-circle for

[3] In the case of the standard RW case the scaling function $\mathcal{G}_{\mathcal{RW}}$ has been exactly derived (see e.g. [151]), but its specific form is not essential for our purposes here.

	Unbiased RW	Demographic RW	Driven Demographic RW
$P(T) \sim T^{-\alpha}$	$\alpha = 3/2$	$\alpha = 2$	$\alpha = 2 - h/2\mu$
$P(S) \sim S^{-\tau}$	$\tau = 4/3$	$\tau = 3/2$	$\tau = 3/2 - h/4\mu$
$P(S\|T) \sim T^{-\gamma}$	$\gamma = 3/2$	$\gamma = 2$	$\gamma = 2$

Table 5.1: Summary of the avalanche exponents for standard RW, for the demographic RW and for the driven demographic RW (in the presence of an external field, allowing for the spontaneous generation of activity at a fixed rate h).

standard un-biased random walkers [136] while it is a parabola for demographic walkers [152]. This can be easily seen by rescaling the walks to $\tilde{v}$ and the times to t/T to collapse curves as described above. In this way $\tilde{v}(t/T) = \mathcal{F}(t/T)$ where $\mathcal{F}(t/T)$ is a scaling function. Given that, $v(t) \sim t^{\gamma-1}$, dividing by $T^{\gamma-1}$, $\tilde{v}(t/T) \sim (t/T)^{\gamma-1}$, at least for small times, $t << T$. Considering that a similar relation holds for the reverse time walk starting from $t/T = 1$, then the avalanche shape is $\mathcal{F}(t/T) = [(t/T)(1 - t/T)]^{\gamma-1}$ which is a semicircle for $\gamma = 3/2$ (RW) and a parabola for $\gamma = 2$ (DRW and driven DRW).

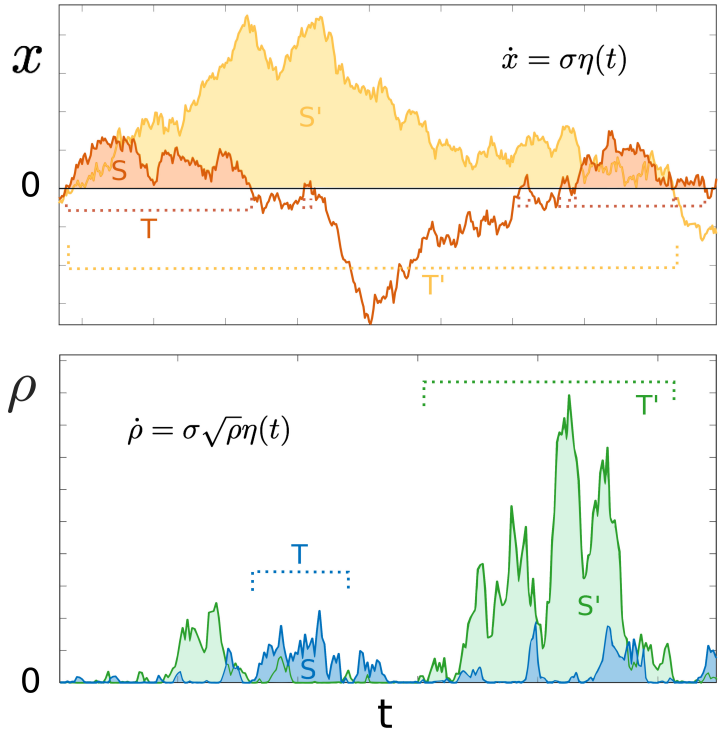

Figure 5.2: Illustration of the time evolution of a standard random walk (RW) and a demographic random walk (DRW); each color corresponds to a different realization. Upper panel: standard RW that, in principle, can freely cross the origin. Avalanches start and end when the walker crosses the origin. Lower panel: the DRW can be represented as a stochastic RW moving in a balanced logarithmic potential that keeps the walker bounded to the origin. Since the variable is always strictly positive, the avalanches can be defined as the activity over a threshold $\epsilon \to 0$.

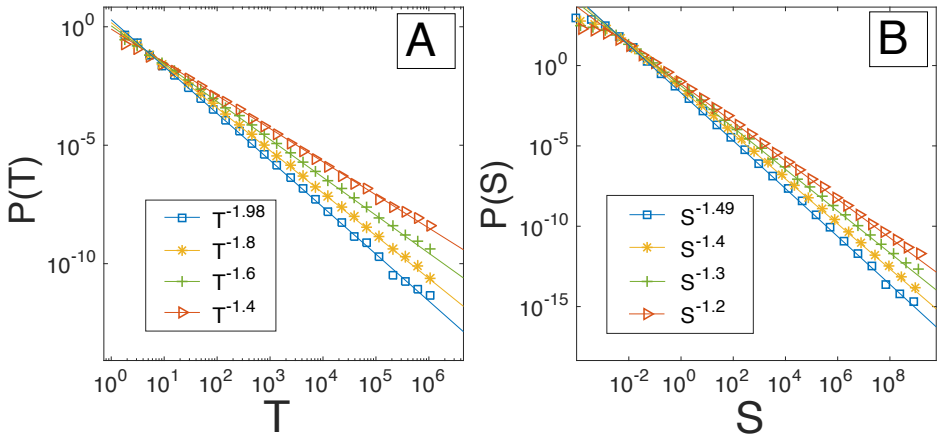

Figure 5.3: Size-avalanche and duration-avalanche distributions for the un-driven demographic random walk as described by Eq.(5.6), as well as for diverse values of the external driving field (marked with symbols) $h = 0.01$ (blue squares), $h = 0.1$ (yellow stars), $h = 0.2$ (green crosses) and $h = 0.3$ (red triangles), with reference curves (solid lines) $t^{-2+h/(2\mu)}$ and $s^{-3/2+h/(4\mu)}$ (as derived in the text), respectively, illustrating the agreement with theoretical predictions.

5.3 Summary and Conclusions

In summary, we have explicitly shown that the mean-field values of avalanche exponents in systems with absorbing states can be computed in a general way by mapping them into a random walk confined by a logarithmic potential, Eq.(5.8). Of course, this same conclusion could have been reached by arguing in a heuristic way that all of high-dimensional processes involving absorbing states should be effectively described by an un-biased branching process, and then constructing a continuous description of it (i.e. a Fokker-Planck or equivalently a Langevin equation) which would be nothing but Eq.(5.6).

An interesting corollary is that the exponents do change in the presence of spontaneous creation of activity, even if the rate is arbitrarily small. This result, which stems from the marginality of the associated logarithmic potential could be relevant to understand empirical results; for instance in cortical networks, avalanches of neural activity have been reported to exhibit branching process statistics [9]; still inspection of some of the most careful estimations reveals possible deviations from $\tau = 3/2$ [48], which could be potentially ascribable to a non-vanishing inherent spontaneous-activation.

Chapter 6

On Beggs-Plenz measure of avalanches

6.1 Introduction

In this Chapter we analyze in more detail the method used by Beggs and Plenz [9] to define avalanches, i.e. the conventionally used experimental protocol to identify avalanches starting from a raster plot. As we have already seen in Chapter 2, defining avalanches in different ways may lead to completely different results. Moreover, one of the main sources of disappointment on the criticality hypothesis in the brain stems from the fact that the exponents of the power laws describing the length and duration of neuronal avalanches –i.e. the key piece of information used to infer the generating process– depend on a parameter: the time bin used for the clustering procedure. The lack of a strong

physical criterion to set this parameter shed skepticism on the universality of the measure and, consequently, on the critical hypothesis. In the Beggs-Plenz procedure the time-bin is fixed to the average inter event interval in neuronal LFP recordings, which is considered a plausible intrinsic timescale defined by the system itself. Anyways, some authors [153] remark that "it is perhaps not so surprising, for example, that selecting the time bin size as the average inter event interval in neuronal LFP recordings results in an exponent close to the theoretical exponent of the branching process universality class, as in this way each event will be followed by, on average, one more event in the next bin". That means that there is a possibility that neuronal avalanches are power-law distributed, with the exponents of the branching process, as a consequence of the procedure used for their definition, which might create an effective process with branching ratio 1, i.e. an artificial critical branching process. Moreover, some authors thoroughly suggest that the measure of avalanches of activity in cortical signals is misleading, since originally avalanches are measured for systems undergoing an absorbing transition, while electric macroscopic activity might emerge as the result of a synchronisation of microscopic units, so that –as we discussed in Chapter 4– if any transition exists, it is not between a quiescent and an active state, but instead between a synchronous and an asynchronous phase [119, 22]. In the next sections we briefly go through the Beggs-Plenz protocol, then apply it to measure avalanches generated from various processes (Contact Process, Brunel model, an artificial stochastic distribution of spikes), in the attempt to understand whether or not this measure is able to distinguish between critical and non-critical processes. The results are resumed in the table in Figure 6.5. We warn the reader that this Chapter does not attain

a complete answer to the question: here we just present some preliminary results. Moreover we analize some further problems linked with the definition of avalanches from continuous activity variable processes, in order to shed light on possible misunderstandings that we encountered in the literature.

6.1.1 Beggs-Plenz procedure for avalanche measure

In this section we briefly explain the steps necessary to perform a measure of an avalanche's size and duration, starting from a raster plot, as usually done in experimental setups [9]. First of all, the Inter-Event-Interval (IEI) is measured, as the average time interval between two consecutive spikes of (whichever two elements of) the network. Then the raster plot is divided in contiguous bins of width equal to the IEI (see Fig.6.2). A bin is considered "empty" if no events are reported within it, and "occupied" otherwise. Consecutive series of occupied bins, preceded and ended by an empty one, define an avalanche. The avalanche duration is just the time interval between the preceding and the ending empty bins, and avalanche size is the total number of spikes that occurred in that time-interval.

6.2 Main Results: BP measure on known models

We already discussed in Chapter 2 the outcome of BP measure of avalanches in the Millman model: we learned that, when measuring avalanches on a state

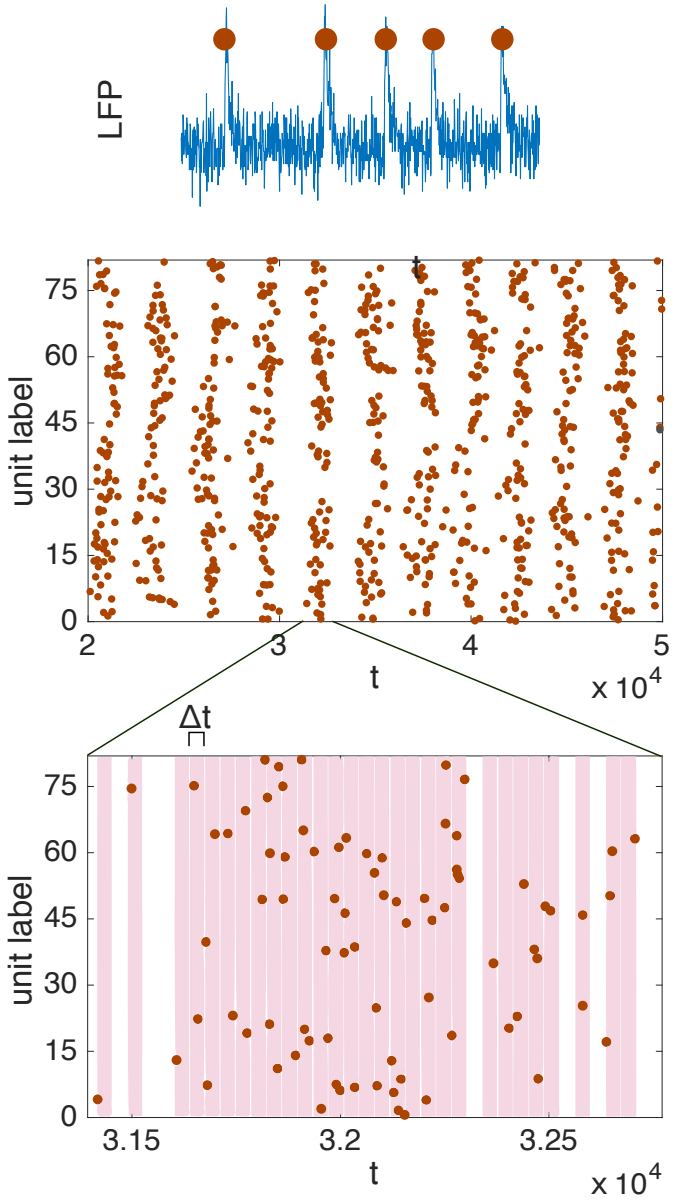

Figure 6.1: Sketch of the procedure for the definition of avalanches introduced in [9].

of sustained activity with BP-protocol (without precise causal information) no power laws appear: this is in agreement with criticality hypothesis, since Mill-

man system is not critical. Also in Chapter 4 we discussed a BP measure on our Landau-Ginzburg model, which also was in favour of BP measure as an unbiased interpretation of criticality (critical avalanches are power law distributed, whereas non-critical ones are less broadly-distributed –see Fig.4.5D–).

6.2.1 Avalanches in the Contact Process

We measured avalanches à la Beggs-Plenz (BP) in the Contact Process (see A.2). At the critical point avalanches result power-law distributed, with an exponent dependent on the time-bin, whereas in the subcritical phase avalanches have an earlier cutoff and on the supercritical phase avalanches are exponentially distributed. These results suggest that the method proposed by Beggs and Plenz is consistent with the correct definition of avalanches for the Contact Process[1].

6.2.2 Avalanches in Brunel model

In 2000 N.Brunel [22] proposed a microscopic model for neuronal spiking (see Appendix B.1), predicting various macroscopic behaviors –Synchronous Regular, Asynchronous Regular, Synchronous Irregular and Asynchronous Irregular phases– according to the level of synchronization of the spiking units and to the regularity of the firing (measured by the coefficient of variation of the inter-event intervals of each unit). In between the phases the model predicted

[1] Although also the subcritical phase is consistent with the power law behavior, but with a earlier cutoff.

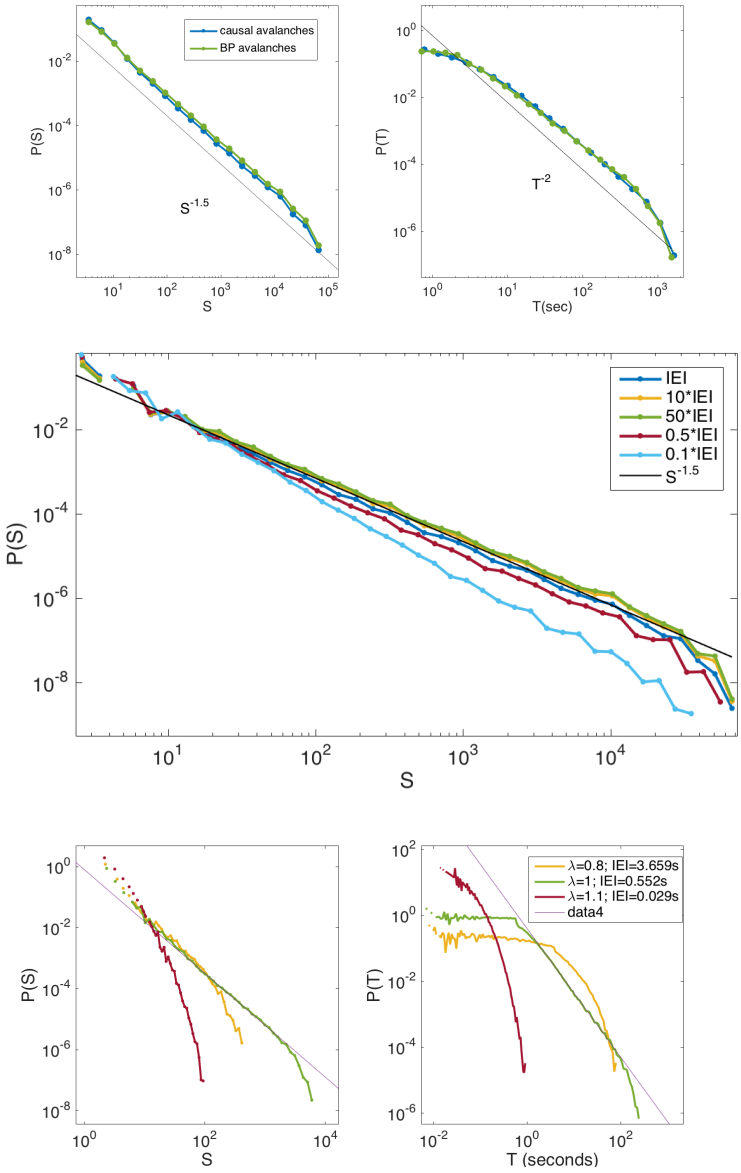

Figure 6.2: Upper Panel: Comparison between avalanches measured with causal information and avalanches measured by BP-protocol in a critical Contact Process. Central Panel: Avalanches à la BP in the critical Contact Process for varying bin sizes $\Delta t = \alpha IEI$ with $\alpha = 0.1, 0.5, 10, 50$. IEI stands for Inter-Event Interval. Lower Panel: Avalanches à la BP for subcritical, critical and supercritical Contact Processes ($\mu = 1, \lambda = 0.8, 1, 1.1$).

dynamical bifurcations, i.e. phase transitions. We reproduced Brunel's results and measured avalanches à la BP in the various phases. Avalanches in the Asynchronous phases (both AI and AR) are exponentially distributed, in agreement with the results in Chapter 2. Nevertheless avalanches measured in the whole SI phase (both close and far away from the bifurcation) result power law distributed (see Fig. 6.3).

Moreover, in the limit of very small integration step, we found some broadly distributed avalanches for the Synchronous Regular phase, whereas a meaningful measure would report delta-like distributed avalanches. This is because if the resolution of spiking is high enough, the neurons in the SR phase don't happen to fire exactly at the same time –as a consequence of the intrinsic stochasticity of external current arriving to each neuron–. The IEI of the whole network results of the order of the integration step[2] and the BP procedure splits into many smaller clusters what one would naturally call an avalanche. Those clusters result broadly distributed, as a consequence of the fact that external inputs are modeled as independent Poisson processes. This means that BP measure in this case only measures noise. This is definitely a problem of the method of Beggs-Plenz.

[2]Approximately one can evaluate that the units spike with an average delay of dt from each other, except for the first one of the cascade, which fires with a delay of T, i.e. the period of the regular spiking ($IEI \simeq ((N-1)dt+T)/N \simeq dt$). Instead one would naturally define an IEI of the order of T.

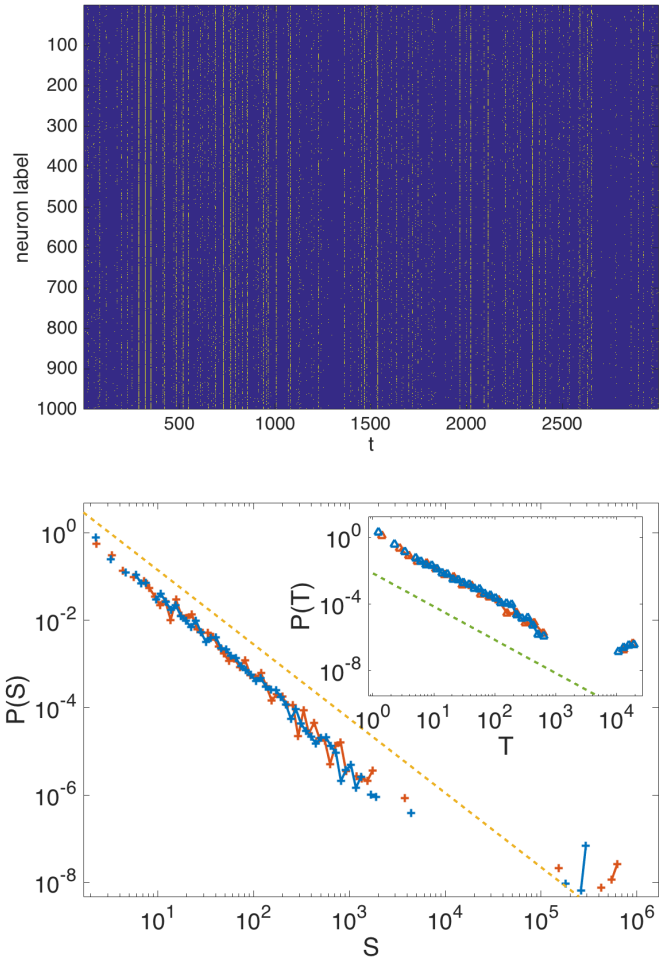

Figure 6.3: Upper Panel: Raster Plot of Brunel model in the Synchronous Irregular phase. Lower panel: Avalanche size (main figure) and duration (inset) distributions in Brunel's model for a system close to and far away from the bifurcation ($g = 6$ and $g = 8$ respectively). Other parameter values are $N = 10^4, J = 0.4, \tau_{rp} = 20ms, \tau = 200ms, V_r = 10mV, D = 30ms, C = 400, \theta = 20mV$, see [22].

6.2.3 Avalanches from an artificial distribution of spikes

The results on SR phase of the Brunel model exposed in the previous section suggest us to perform a measure on an artificially defined very simple model,

which evidently has nothing to do with criticality, but still shows power-law behavior. We construct a raster plot as follows: we define a period T, and N neurons firing exactly together with period T. Now we redefine the spiking time of each neuron, by adding to it a random delay extracted from a gaussian distribution centered in zero and with standard deviation σ. If σ is of the same order of T, then the system mimics an asynchronous regime and BP avalanches result exponentially distributed (see red crosses in Fig. 6.4), whereas if σ is smaller and the synchronicity between the units is not completely broken, BP avalanches result power-law, only by the effect of noise on the temporal distribution of spikes. Moreover, the results still hold if we substitute the gaussian distribution with a uniform distribution. This approach is suitable for analytical calculations, which we leave for future work.

6.3 Further Results: Misunderstandings on avalanches measure

As it has already been widely discussed in the literature, not all power laws are a signature of criticality [154, 33, 155]. In this Section we highlight some possible sources of error while investigating the relation between self-similarity and criticality in the brain.

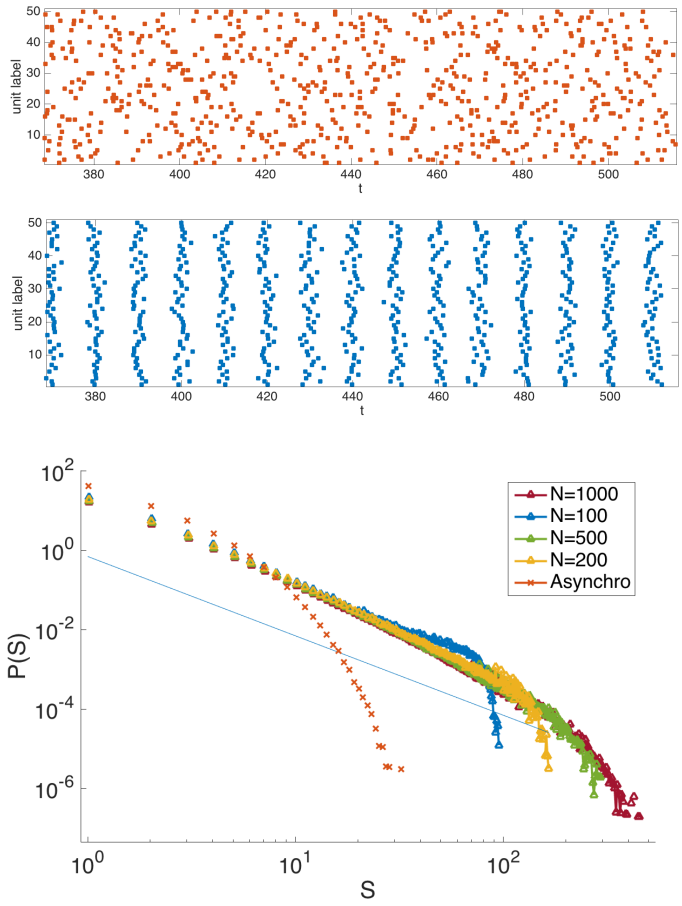

Figure 6.4: Upper Panel: Raster Plot as constructed by the artificial model, with $N = 50, T = 10$ and $\sigma = 10$ (asynchronous, red squares) and $\sigma = 1$ (synchronous, blue squares). Lower Panel: BP Avalanches from the artificial distribution of spikes. Triangles in different colors correspond to different sizes N and $\sigma = 0.1T$, red crosses correspond to $N = 200$ and $\sigma = 10$.

6.3.1 Non critical avalanches

In a simple continuous-time stochastic process describing the activity of a system, the duration of an avalanche could be defined as the extent of the time interval during which activity stays over a threshold (i.e. an avalanche begins/ends when the activity signal crosses beyond/below threshold). Let

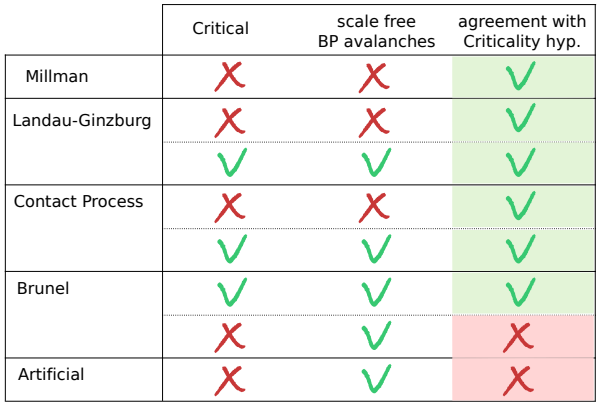

Figure 6.5: Scheme of results on BP measure in various models and evaluation . Millman model is not critical (the scale-invariance derives from a neutral dynamics, intead), as discussed profusely in Chapter 2. Consistently with this, avalanches a la BP result exponentially distributed. Also in Landau-Ginzburg model presented in Chapter 4, BP-measured avalanches give a good description of the dynamical behavior of the system, since avalanches are scale-invariant at the critical point, whereas far from it the distribution becomes less large. In the Contact Process BP measure of avalanches is almost undistinguishable from the usual definition including precise causal information: scale-free avalanches are measured only at the critical point. In Brunel's model, instead, one finds power-law distributed BPavalanches both at the critical point and in the whole Syncronous Irregular phase. Thus in this case BP measure is not a satisfying method, since it is not able to discriminate between critical and non-critical dynamics. Finally, we built a simple artificial model, showing that noise alone (together with a certain coherence) can generate scale-invariant BP avalanches. Thus the measure of power-law distributed BP avalanches does not guarantee that the system is at its critical point.

us suppose, for argument's sake that the original signal was a Wiener process (unbiased random walk), this would correspond to determining the statistics of first passage times through a barrier (i.e. the threshold); which is well known

(both numerically and analytically) to show scale-invariance, as a consequence of the lack of any characteristic length scale, but not critical in the sense of lying at the edge of a phase transition (see Chapter 5). Thus let us note that

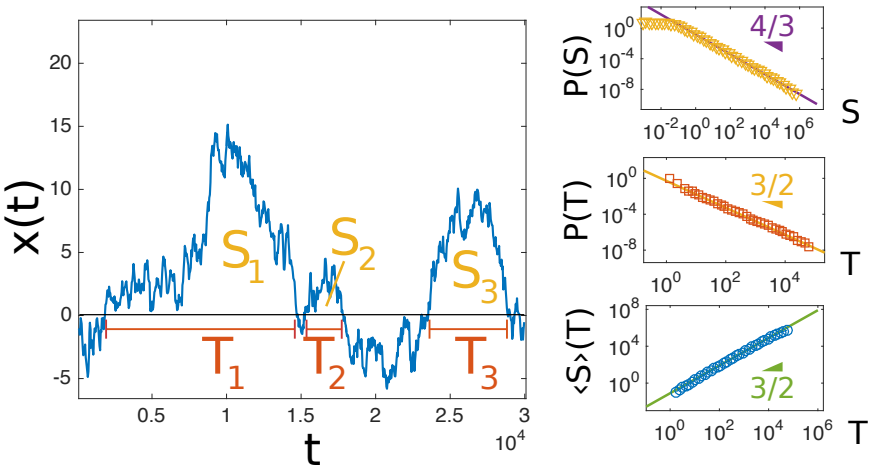

Figure 6.6: Illustration of the first return time statistics of a Random Walk. Left panel: a sketch of the process together with the illustration of the sizes and durations of three avalanches. Threshold is set to 0. Right panels (from up to down): distribution of size, duration and average size of a given duration, showing good agreement between numerical results (open symbols) and analytical ones (full lines).

if the global activity of a neural system happens to fluctuate around a stable sustained state, when performing an analysis of avalanching behavior through a thresholding procedure, cascades of activity would result scale free distributed, just as an effect of fluctuations. In fact, this scenario, at a macroscopic scale, is equivalent to an Ornstein-Uhlenbeck process:

$$\dot{x}(t) = -ax(t) + h + \sigma\eta(t), \tag{6.1}$$

where $\eta(t)$ is a delta-correlated, white noise with zero mean and unitary variance; the linear term (force) $-ax$ corresponds to the derivative of a parabolic potential bounding the walker close to h/a. Note that with $a = 0$ this is nothing but the usual free random walker or Wiener process [47]. The force introduces an upper cutoff in the first return times (i.e. avalanche duration) statistics, which, otherwise, follows the same exponents as the unbiased random walk. Thus, studying avalanches by analyzing fluctuations about a given threshold in a process with a well-defined steady-state value, one recovers power-laws, up to a scale controlled by $1/a$. These, however, are not critical in the sense of lying at the edge of a continuous phase transition.

6.3.2 On avalanche size

Also, particular attention is needed for the correct definition of the "size" of an avalanche: for example in a recent work by Poil et al. [16], where avalanche dynamics and oscillations were jointly reported in a network of excitatory and inhibitory neurons, the authors used a definition of *size*, which leads to a misclassification of the power law exponent and thus, to a possible misinterpretation of the results. Indeed, Poil et al. defined the size of an avalanche as the integral of the activity during the avalanche (instead of the integral of the activity *over threshold* during the avalanche); this is illustrated in Fig.6.7. Other works in literature show the same misdefinition of the size of avalanches[156]. Proceeding in this way, the actual size is corrected with an additional term proportional to the avalanche duration (as also illustrated in the Figure). This additional term complicates the scaling analysis.

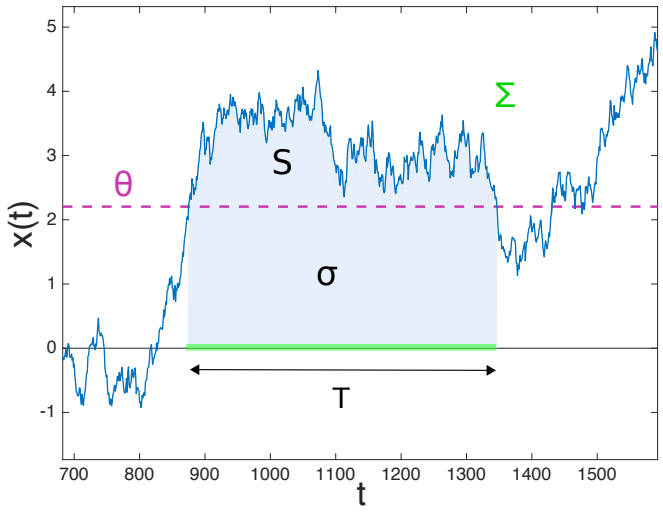

Figure 6.7: Analysis of first-passage times in a stochastic process; θ (magenta dashed line) is the threshold value employed to define crossings. S is the proper avalanche size (area above threshold, colored in blue in figure), T is its duration, Σ (delimited by the green contour) is the misleading definition of the avalanche size, as used in [16]. One has $\Sigma = S + \sigma$, with σ colored in orange in figure (note that $\sigma \propto T$).

In particular, given that a standard random walk (or a Ornstein-Uhlenbeck process describing fluctuations around a mean value) has first-return times distributed as $P(T) \sim T^{-3/2}$ ($\alpha = 3/2$), sizes measured as in Poil et al. have a correction to the true asymptotic behavior which scales with an exponent $\tau \approx 3/2$, which actually comes from including in the measure of the size an extra part proportional to the duration of the avalanche [16]. Observe, therefore, that this 3/2 has nothing to do with a critical branching process (beside the numerical coincidence): it is a spurious effect, coming from the first-passage time distribution of an effective Ornstein-Uhlenbeck process. In particular, both sizes and durations turn out to be distributed with the same

exponent with this definition of size, which is not the case in critical branching processes. One needs to go to huge system sizes, to see the actual scaling.

In order to illustrate the problem, we generate an Orstein-Uhlenbeck process and measure the avalanche size distribution ($P(S) \sim S^{-\tau}$) using this equivoque definition. In Fig. 6.8 we can see that, for low values of the threshold $\theta \simeq 0$, one finds the known avalanche exponent $\tau_{RW} = 4/3$ but, as the threshold grows, the exponent grows up to $\tau' \simeq 3/2$ (which, remarkably, is the avalanche size exponent of a Branching Process).

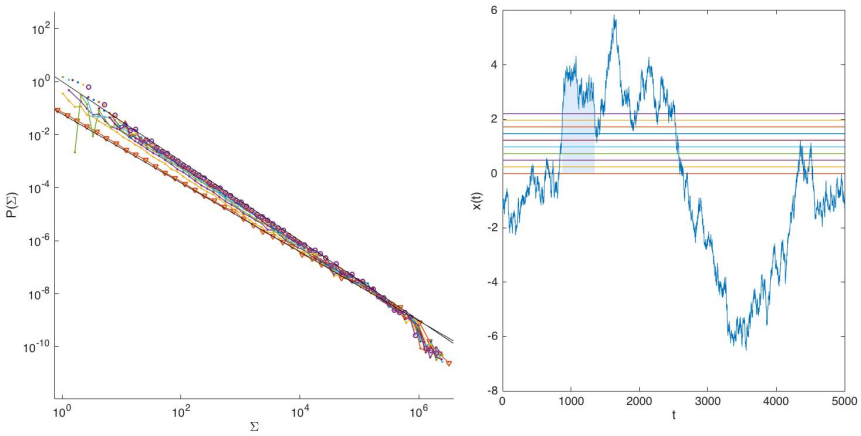

Figure 6.8: Avalanche pseudo-size distributions $P(\Sigma)$ for different threshold values (in different colors, as shown in the Right panel). Black continuous lines represent the power laws $P(\Sigma) = \Sigma^{-4/3}$ and $P(\Sigma) = \Sigma^{-3/2}$. We can see that for the smaller threshold value (red triangles), the correct RW statistics is recovered, while for the bigger threshold value (purple circles) the avalanche size statistics is well fitted by an exponent $\tau = 3/2$.

A couple of recent papers underline the "perils" associated with thresholding, which can certainly be a source of confusion [157, 158]. In what follows we will try to explain analitically how, if one, erroneously defines the size of an

avalanche as in Fig.6.7, the exponent of the avalanche size distribution results polluted by the exponent of the duration distribution. Referring to the Right panel of Fig.6.8, representing an avalanche of an Ornstein Uhlenbeck process, one has:

$$P(T) = \mathcal{N} T^{-3/2},$$

where $\mathcal{N}$ is a normalization constant. Now we want to calculate the distribution of the misdefined-size Σ. One has $\Sigma = S + \sigma = cT^{3/2} + \theta T$ and hence $d\Sigma = (cT^{1/2} + \theta)dT$, from which we can readily calculate

$$P(\Sigma) = P(T)\frac{dT}{d\Sigma} = \mathcal{N}\frac{T^{-3/2}}{cT^{1/2} + \theta}.$$

From this it follows that, if θ is small one has

$$P(\Sigma) \simeq \frac{\mathcal{N}}{c} T^{-2} \simeq \frac{\mathcal{N}}{c}[(\Sigma/c)^{2/3}]^{-2} = \mathcal{N}'\Sigma^{-4/3},$$

which is the correct result for the avalanche size distribution of an Ornstein-Uhlenbeck process. On the other hand, if θ is big, for small values of T, one has

$$P(\Sigma) \simeq \frac{\mathcal{N}}{\theta} T^{-3/2} \simeq \frac{\mathcal{N}}{\theta}[\Sigma/\theta]^{-3/2} = \mathcal{N}''\Sigma^{-3/2},$$

which would lead to the absurd that the original process is in the Branching Process universality class.

It is important to note that, if one had a good statistics for huge avalanches (and no cutoffs), he would recover the correct asymptotic value for the avalanche size exponent, $\tau = 4/3$, for any value of θ.

Chapter 7

Non-critical amplification of fluctuations in simple models of persistent neural dynamics

7.1 Introduction

The lack of striking arguments in favour of the criticality hypothesis, has fostered the growth of competing explanations for power-law like distributions of neural events. Given that criticality is not a must in order to obtain power-law distributions –which, on the contrary, can be generated by a variety of alternative mechanisms [155, 33, 159, 160, 161, 21]– some authors have highlighted that it is not clear wether the available empirical evidences actually call for criticality or alternative origins could be invoked. Some possible alternatives

have been already discudded along this Thesis: neutral theories, bistability and noise [162, 163]. In particular, the emergence of highly irregular bursts of activity has often been reported in association with balance between excitatory and inhibitory instances [22, 23], but it is not always clear whether or not implementing a balance condition can be interpreted as tuning the system close to the point of transition between two distinct phases.

In this context, Benayoun et al. [97] introduce an intriguingly puzzling, very general and solid machinery, giving rise to the emergence of self-similar bursts of activity in finite-size systems of spiking neurons. Poising the system in a regime of balance between excitation and inhibition results in an avalanching-like behaviour where the system wanders through an almost-linear phase space which is very wide with respect to the level of the demographic noise present. Here the results presented in [97] are confirmed for a much wider window of scales and extensively tackled. The intriguing phenomenon of balanced amplification of fluctuations that they introduce is deeply scrutinized, in order to uncover the interplay between the factors concurring to the appearance of non-critical avalanches of activity. In order to explain the phenomenon, we recover the mathematical rationale of "non-normal" forms and in particular we study the transient behaviour of "reactive" systems and try to explain the emergence of a non-differentiable manifold (a "scar") close to the fixed point. Also, this framework allows to precisely survey the relationship that exists between "balance" and "criticality" and to explain that the system being close to the transition between two phases is not a necessary nor sufficient condition for the emergence of the phenomenon. Although the specific meaning of the two

concepts of "balance" and "criticality" might vary in other contexts, clarifying the differences between them in a simple framework, may give a hint on how they can be correctly interpreted in more complex setups. Moreover we give specific quantitative insights on the exponents of the power laws, measured at a mesoscopic level and relate them to two different types of noise (multiplicative and additive –see Chapter 5–), that become dominant at different scales. Finally we show that the described mechanism is not a peculiarity of the excitatory/inhibitory underlying structure, but it applies to a wider scenario: a similar non-crtitcal scale-invariance can be obtained by changing the regulatory mechanism that drives the dynamics, i.e. excluding inhibition and introducing synaptic plasticity. As encountered before in this PhD thesis, also in this case inhibition and synaptic plasticity can be considered as alternative homeostatic mechanism. Finally we highlight that spatially (diffusively) coupled noisy reactive units are likely to show spatio-temporal patterns in a wide region of the parameter space.

7.2 Main Results

7.2.1 Simplified Wilson-Cowan model

Following [97], we consider here a version of the Wilson-Cowan model (see Appendix B.2) simplified and reduced to an elementary setting, where only one stable fixed point exists and depending on whether excitation or inhibition dominates, the steady state is respectively active or inactive. More specifically,

by considering that the coupling constants depend uniquely on the pre-synaptic cell type, i.e. $\omega_{EE} = \omega_{EI} = \omega_E$ and $\omega_{II} = \omega_{IE} = \omega_I$ (and fixing the decay constant α and the small external current h), the system is left with a two dimensional parameter space, which consists of the excitatory and inhibitory synaptic strengths. Under this symmetry, the unique steady state only depends on $\omega_0 = \omega_E - \omega_I$. In Fig.7.1 we plot the value of the fixed point, in the variable $\Sigma = (E + I)/2$, for different values of ω_0, while keeping $\omega_s = \omega_E + \omega_I$ constant. The system shows a phase transition in the critical value $\omega_0 = 0$ separating an active (excitation dominated) from an inactive (inhibition dominated) phase. Note that since a small external field h is present, the fixed point doesn't loose its stability at criticality. Strikingly, this remarkably simple and intuitive behavior is overturned when finite size effects are taken into account.

7.2.2 Phenomenology

Benayoun et al [97] showed that, in a regime of *balance between excitation and inhibition*, or, equivalently, when the difference between excitatory and inhibitory synaptic weights is very small with respect to their sum $\omega_0 \ll \omega_s$, low levels of noise (i.e. large but not infinite system sizes) generate highly bursty (pseudo-scale-invariant) behavior. This is in outstanding countertrend with respect to the mean field case, which, as stated above, would predict a single sustained steady state, while the former, on the contrary, shows an alternation of highly bursty time intervals, interspersed with periods of silence, extremely reminiscent of the experimental evidences showing self-similar bursts of activity in the resting state of cortical dynamics. In fact a measure of the

avalanches size and duration, defined in complete analogy with the experimental setup, gives power-law distributions. Thus the mechanism presented here is a candidate to model neuronal avalanches. It is noteworthy to stress that this avalanching behavior can be observed far from the critical point, establishing an alternative to the criticality hypothesis, which ascribes the scale-invariance observed in experiments to the system being poised close to a critical transition point.

7.2.3 Criticality and Balance

Here we address the problem of fully expliciting the difference between *critical* and *balanced*. First of all we should better talk about "quasi-criticality" [83], given both the inherent limitedness of the system size and the existence of a small external field h. The condition for the system to be quasi-critical is $\omega_0 \ll 1$, while the system is balanced when $\omega_0 \ll \omega_s$, thus quasi-criticality is not necessary nor sufficient for balance. In order to clarify this issue and discriminate the effects of criticality and balance we plot in Fig.7.2 the phase plane of the deterministic system (Eq.D.9). In the first row (Fig.7.2 a and b) the parameters set the system in a (close to) critical sate, (the stable fixed point, i.e. the point where the nullclines intersect, is evidenced with a red dot) corresponding to the the blue arrow in Fig.7.1, while in the second row (Fig.7.2 c and d) the deterministic system spontaneously evolves towards a stable highly active phase (red arrow in Fig.7.1). Moreover, the first column (Fig.7.2 a and c) shows non-balanced configurations (i.e. small values of the sum ω_s) while the second column (Fig.7.2 b and d) shows balanced ones.

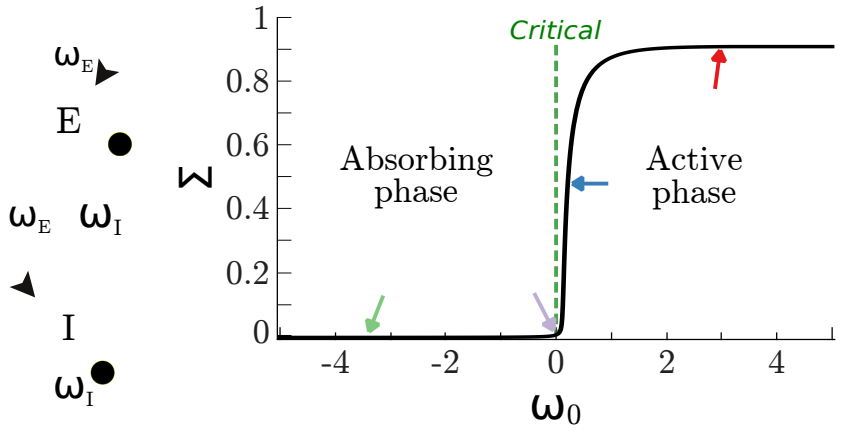

Figure 7.1: Left: sketch of the Wilson Cowan model. The excitatory population interacts with a single parameter, ω_E and the same applies to the inhibitory population, with ω_I. Right: Phase transition for the model, the phase of the system depends on the diference $\omega_0 = \omega_E - \omega_I$; if $\omega_0 > 0$ the system is in the active phase. From left to right the system is in the 'down' state, critical point, a 'weakly-stable' up state and in the 'up' state (green, purple, blue and red, respectively).

At this heuristic level we can remark that in the balanced case there is some sort of "scar" in the phase portrait, such that two shear stresses flowing in opposite directions, coexist very close to each other. In other words the vector field $(\vec{E}, \vec{I})$ shows a discontinuity all along a manifold (a line in this case) that corresponds to a whole (infinite) set of (unstable – or marginally stable –) points in which the nullclines superimpose. As we shall explain in further details in what follows, this "scar" is responsible for the amplification of the fluctuations around the fixed point introduced by demographic noise: as soon as a small noise drives the system "slightly" away from the fixed point, these strong flows hardly pull the system towards very low (or very high) levels of activity. Conversely, in the case of a critical, but non-balanced system

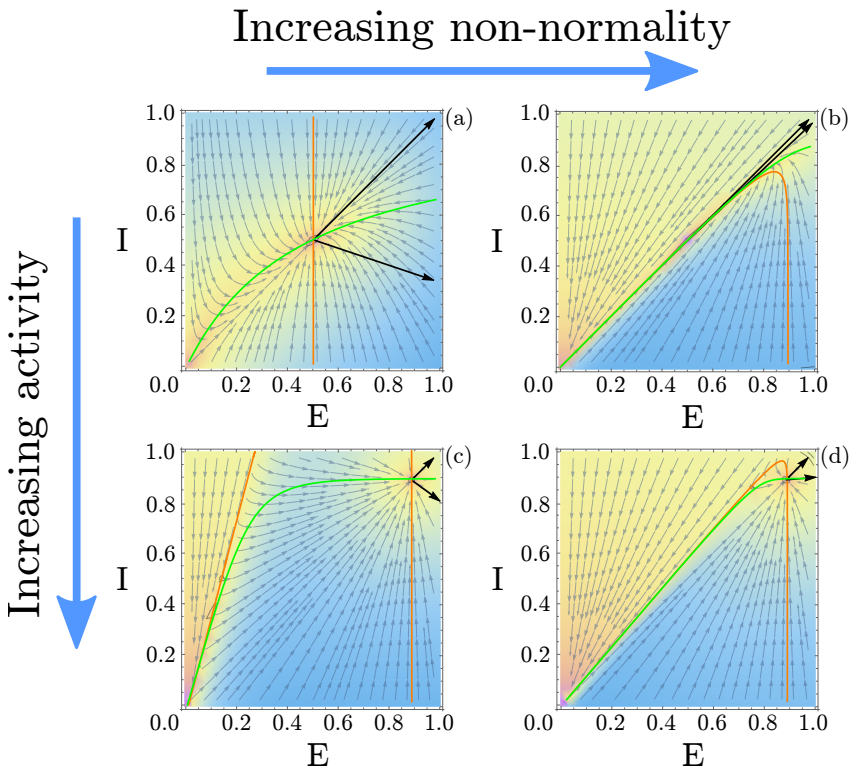

Figure 7.2: (a) E-I phase portrait for an stable state near the critical point ($\omega_E = \frac{1}{5}$, $\omega_I = 0$). The stable fixed point – wherein the nullclines intersect– is represented as a circle. The eigenvectors direction in the stable 'up' state are indicated by black arrows, (b) E-I phase portrait for a balanced-amplification condition ($\omega_E = 7$, $\omega_I = \frac{34}{5}$). The nullclines are in close proximity to each other, in contrast with the former case, (c) E-I phase portrait for a stable state far from the critical point ($\omega_E = 4$, $\omega_I = 1$). and, (d) E-I phase portrait for the same situation in the active phase but, with ($\omega_E = 20$, $\omega_I = 17$). The proximity between the nullclines makes it easy to see that the systems evolves, near the critical point, around a $(1+\epsilon)$-dimensional movement; i.e. any small perturbation results in great fluctuations from the 'up' state to the 'down' state.

(Fig. 7.2 a) it is immediately evident that the same mechanism causing brutal fluctuations is not at work.

7.2.4 Linearized dynamics is non-normal

Folowing Murphy et al. [164] this phenomenon can be explained under the rationale of *non-normal* dynamics. Considering that the dynamics in the balanced case naturally selects a preferential direction along the diagonal [97], let us change variables to $\Sigma = (E + I)/2$, $\Delta = (E - I)/2$. Eq. D.9 becomes

$$\begin{cases} \frac{d\Sigma}{dt} = & -\alpha\Sigma + (1 - \Sigma)\, f\,(\theta) \\ \frac{d\Delta}{dt} = & -\Delta\,(\alpha + f\,(\theta)) \end{cases}$$

with $\theta = \omega_0\Sigma + (\omega_s)\,\Delta + h$. Elementary algebra can be employed to verify that the fixed point lays in $(\Sigma_0, 0)$, i.e. always in the diagonal in the (E, I) reference frame. A standard linear stability analysis around the fixed point gives the Jacobian

$$J = \begin{pmatrix} -\lambda_1 & \omega_{ff} \\ 0 & -\lambda_2 \end{pmatrix}$$

where the eigenvalues are $\lambda_1 = (\alpha + f(s_0)) + (1 - \Sigma_0)\omega_0 f'(s_0)$ and $\lambda_2 = (\alpha + f(s_0))$ and $\omega_{ff} = (1 - \Sigma_0)(\omega_E + \omega_I)f'(s_0)$.

Note that if ω_0 is small and positive, so are λ_1 and λ_2. To see this, note that λ_2 is the sum of two small terms α, which is chosen to be small in this case ($\alpha = 0.1$) and $f(s_0) \approx s_0$. The extra term in λ_1 is also small, since $f' < 1$. Thus, the fixed point is *weakly stable*, and the linear stability of the fixed point depends on the weights only via the difference ω_0 [97]. Correspondingly, the stability is weak when the system is close to the critical point and it looses its stability ($\lambda_{1,2} = 0$) exactly at the critical point $\omega_0 = 0$. Nevertheless, the

structure of the Jacobian makes it visible that the eigenvalues does not enclose all the information of the dynamics, as the out-diagonal term (the so-called *feedforward* term) cannot be eliminated [1]. Triangular matrices such as J are called *non-normal*, meaning that $J^*J \neq JJ^*$, where J^* is the conjugate transpose of J[2]. The effect of a big feedforward term in Eq.7.2.4 is straightforward to verify: when operating on a small perturbation along the Δ direction, the linearized dynamics gives a small response in the same direction plus a much bigger response along the Σ direction, corresponding to the strong shear flows clearly visible in Fig. 7.2. Non-normal matrices are also said to be "reactive" [165], when the dynamics they describe shows unusually long-lasting transient behavior: the system is strongly driven away from the fixed point before coming to its steady state. We refer to Section D.5.1 for a brief overview on non-normal forms. Thus in this case, the stability of the fixed point has to be compared with the feedforward term ω_{ff}. A big feedforward term is able to strongly affect the dynamics when the stability of the fixed point is weak *with respect to the feedforward component* (even if the eigenvalues are not close to zero), i.e. when the non-normality is big with respect to the stability. Since the eigenvalues depend on the control parameters through ω_0, while ω_{ff} only depends on ω_s, the meaningful relation for the appearance of the mechanism discussed above is the balance condition $\omega_0 \ll \omega_s$. Through the mathematical aside above, we now try to clarify some details of the phenomenology presented. First of all, just as a matter of terminology, we remark that the change of variables $(E, I) \to (\Sigma, \Delta)$, that we performed for evident convenience, turns out

[1] Triangular matrices are not diagonalizable.

[2] Note that in the quantum mechanics all non-normal matrices are "explicitly forbidden", since all physical operators are Hermitian and all Hermitian matrices are normal

to be a Schur transformation, indeed generating a triangular Jacobian. The (non-orthogonal) basis of eigenvectors in the variabes (Σ, Δ) is

$$\begin{pmatrix} 1 \\ 0 \end{pmatrix}, \begin{pmatrix} 1 \\ \xi \end{pmatrix}$$

with $\xi = \frac{\omega_0}{(\omega_E + \omega_I)}$, the eigenvectors becoming more and more similar for $\xi \to 0$.

Moreover the weight of the non-normality is basically the weight of the feed-forward interaction with respect to the eigenvalues, which means that with a fixed ω_0 it grows with ω_s {*it goes (very) roughly as* $1 - \mathcal{O}(\omega_0)/\mathcal{O}(\omega_s)$}. In other words the balance condition $\omega_0 \ll \omega_s$ means exactly that the non-normality is big with respect to the stability of the fixed point. From the phase portrait of Figure 2 we can imagine that, in a case where the balance condition holds, if we perturbed the steady state slightly but sufficiently to exit from the basin of attraction of the stable fixed point, the trajectory would perform a big transient excursion in the direction of the scar.

7.2.5 The roles played by the noise

When the system is endowed with some small amplitude noise σ, then the effects of the transient regime are stabilized and the dynamics keeps wandering along the diagonal in the (E, I) reference-frame (Fig.7.2) resulting in the wild fluctuations of the firing rate shown in Fig. 7.3: the fluctuations generated by the noise are strongly amplificated under balance conditions by the mechanism of reactivity along the Σ direction. In particular, intermediate values of σ give

rise to up and down states, reminiscent of experimental findings of cortical areas in the brain. Moreover, numerical simulations suggest that the higher the value of the noise, the more time the system spends close to the origin, in between excursions to the 'up' state. Such avalanche-like dynamics allows a measure of duration and size of the mesoscopic activity over a small threshold, which confirms the result of [97], i.e. both duration and size of the avalanches follow a power law of the form $P(T) \sim T^{-\alpha}$ and $P(S) \sim S^{-\tau}$, where α and τ are the corresponding exponents (see lower panel of Figure 7.3). Furthermore, it allows for an accurate analysis of the exponent of the power-laws. Although the power law is composed by a mixture of different trends, for high values of the noise (or at least for small avalanche sizes), the exponents are compatible with the well known exponents for a standard random walk, i.e. $\alpha = 3/2$ and $\tau = 4/3$. Despite the fact that the mechanism that generates large fluctuations has been defined, the system shows large silent time-intervals (with extremely low activity as shown in Fig.7.3), whose existence is a necessary condition in order to define avalanches. However, the origin of such silent intervals is not in the picture yet but, as indicated by the temporal series it is related and (probably) induced by high values of noise. This problem is addressed in the next section.

7.2.6 The reduced system

The empirical observation that the system keeps wandering along the diagonal in the (E, I) reference-frame suggests to study a reduced one variable system, where the dynamics is strictly constrained to evolve along the diagonal (i.e.

$\Delta = 0$, $E = I = \Sigma$). Since in this approximation θ is small, we take the Taylor expansion $\tanh(\theta) \approx \theta$. The reduced system, in the variable ρ reads

$$\frac{d\rho}{dt} = h + (-\alpha - h + \omega_0)\,\rho - \omega_0\rho^2 + \sigma\sqrt{(\omega_0 + \alpha - h)\rho - \omega_0\rho^2 + h}\eta_\rho,$$

where η_ρ is a gaussian white noise variable. For very low levels of activity ($\rho \approx 0$), the noise amplitude in Eq. 7.2.6 is dominated by the square root term and the reduced dynamics is approximately equivalent to the Langevin equation for the Contact Process in a fully connected network (see Appendix A.2)

$$\dot{\rho} = h + a\rho - b\rho^2 + \tilde{\sigma}\sqrt{\rho}\eta,$$

with $a = (-\alpha - h + \omega_0)$, $b = \omega_0$ and $\tilde{\sigma} = \sigma\sqrt{(\omega_0 + \alpha - h)}$.

In Chapter 5 it has been shown that Eq.7.2.6 can be mapped into a random walk confined by a logarithmic potential, attracting the dynamics of the system to the noise-induced singularity in the origin. This would explain the unusually large permanence times of the original two-variable system into low activity regimes, responsible for the avalanching behavior.

The original dynamics of eq.B.2 can be directly compared with the simplified one introduced above (Fig.7.4). On one hand, the time series of the dynamics of the complete system (resulting from a numerical integration of the model) defines the effective bivariate probability distribution $P(\Sigma, \Delta)$. Marginalizing over Δ, one obtains the stationary distribution of the dynamics along the diagonal $P(\Sigma) = \int_0^\infty P(\Sigma, \Delta)d\Delta$, from which it is straightforward to define (the projection along the diagonal of) an effective potential, as $V_{eff}(\Sigma) = -\ln P(\Sigma)$.

On the other hand, the stationary potential for the reduced dynamics in ρ can be calculated through a Fokker-Planck approach [47] and reads:

$$V(\rho) \propto \left((1 - \frac{2h}{\sigma^2}) \ln \rho - \frac{2a}{\sigma^2}\rho + \frac{b}{\sigma^2}\rho^2 + c \right)$$

In Fig.7.4 the effective potentials deriving from the complete and the reduced dynamics are shown to be fairly similar. Thus we can conclude that the bistability of the potential, causing the system to remain trapped close to the origin, is generated by the square root multiplicative noise term. The presence of a small driving h makes sure that the system never falls into the absorbing state, but keeps trying to escape from the logarithmic potential well. Moreover, for the reduced system in Eq.7.2.6, it has been shown in Chapter 5 that the avalanche statistics can be fully determined calculating the first return time to the origin of the random walk confined to the logarithmic potential. The avalanches result to be power-law distributed, with continuously varying non-universal exponents depending on the driving h and on the noise amplitude σ: $\alpha = 2 - 2h/\sigma^2$ and $\tau = 1.5 - h/\sigma^2$. However, the avalanche statistics of the Wilson Cowan dynamics under balance condition (Eq.B.2) does not follow the same exponents. As shown in Fig.7.3, the statistics of avalanches in the full system is composed by a mixture of different trends, but at least for small avalanche sizes, the avalanche exponents are compatible with the well known exponents for a standard random walk (see Chapter 5), $\alpha = 3/2$ and $\tau = 4/3$. Thus, the problem of understanding the origin of the power law exponents of the avalanche distributions is still open: the diagonal dynamics is essential but not sufficient to describe the whole system.

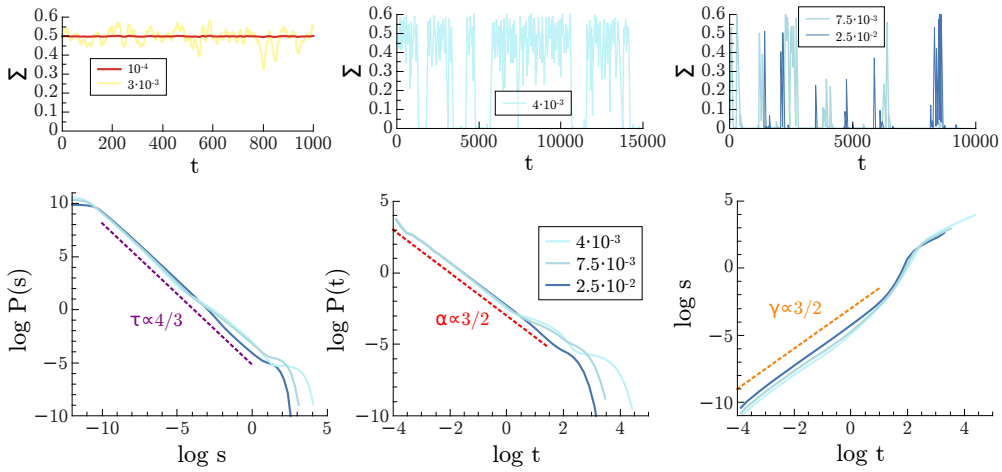

Figure 7.3: Temporal series showing avalanches under a "balance amplification" condition. Upper panel: Temporal series of Σ in a balanced-amplification condition ($\omega_E = 7$, $\omega_I = \frac{34}{5}$) for increasing levels of noise (from left to right). Above a certain threshold the system is allowed to reach the absorbing state, showing an avalanching behavior for high values of noise. Lower panel: Probability of different types of avalanches for different values of the noise amplitude (σ, see Legend); size avalanches, time avalanches and, size versus time avalanches. Note that, in the three cases, the nature of the avalanches highly depends on the noise amplitude. Other parameter values: $\alpha = 0.1, h = 10^{-3}$.

7.2.7 Beyond the diagonal

A possible reason for the random-walk-ike exponents found can be figured out observing the vector field $(\vec{E}, \vec{I})$ in Fig.7.2. Indeed, the whole semi-plane $I > E$ is attracted to the origin by a (roughly) parabolic potential. In an approximate way, it is possible to imagine that half of the vector field is compatible with an attractive parabolic well potential with a (virtual) minimum close to the origin, that joins discontinuously along the diagonal with the other half system, which is another attractive potential with a (true) minimum, i.e.

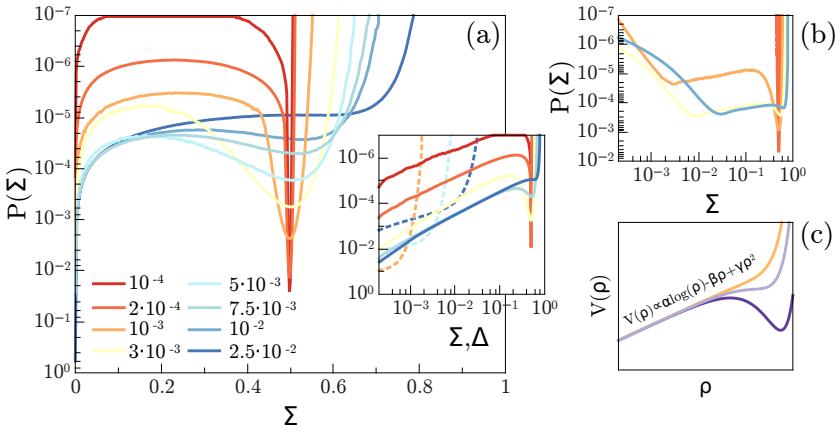

Figure 7.4: Histogram of the Σ-signal of one Wilson-Cowan column for different values of the noise amplitude. (a) Log-normal scale, y-axis is inverted. Histogram of the $\Sigma-signal$ of one Wilson-Cowan column for different values of the noise amplitude (σ, see legend). The potential change from a single potential well (for low noise, not shown) to a bistable situation alternating between 'up' and 'down' states and, finally, to a new single potential with absolute minimum on the 'down' state. Inset: same data but in log-log scale. Dashed lines corresponds to $\Delta-potential$, showing extremely small and parabolic-like potentials. (b) Histogram of the $\Sigma-signal$ of one Wilson-Cowan column for the additive noise case and different values of the noise amplitude (σ, same color code). (c) Theoretical potential from previous one-dimensional effective equations in ρ. The similarity among them is undeniable. Parameter values: $\omega_E = 7$, $\omega_I = \frac{34}{5}$, $\alpha = 0.1$, $h = 10^{-6}$.

the up-state. Therefore, when the system is trapped very close to the origin (by the logarithmic potential sketched above), the small fluctuations with inhibitory dominated activity ($I > E$) are subject to a quadratic-like potential generating an Ornstein-Uhlenbeck first-passage time distribution. On the contrary, when the fluctuation is excitatory dominated ($E > I$), the system is strongly pulled towards high activity states. In order to test this hypothesis, and corroborate our conjecture on the role played by the various ingredients

(i.e. non-normal dynamics, multiplicative and additive noise) cooperating to produce the noise induced bursty behavior in Wilson-Cowan balanced system, we propose a simple effective model, that contains an essential version of all the mechanisms described.

7.2.8 Minimal model

First, let us resume our understanding of the complete dynamics, keeping in mind Fig.7.2b. Let's say that the system is initially in the mean field steady state. Noise (deriving from the finiteness of the neural network) will produce a small perturbation that (if noise is big enough –i.e. if the system size is small enough–) eventually causes the system to exit from the basin of attraction of the (weakly) stable fixed point. If the noise on the excitatory variable prevails, the system performs a wild excursion towards higher activity levels (by the effect of the non-normal dynamics), before coming back to the vicinity of the fixed point. If the fluctuation is inhibitory dominated, instead, the non-normal dynamics strongly pulls the system towards the origin, suddenly shutting down the activity and leading the trajectory along the diagonal, where the system experiences the singularity of the potential generated by the (square root) multiplicative noise. At the same time, noise can perturb the system to slightly inhibitory states, causing Ornstein-Uhlenbeck distributed small avalanches, or to slightly excitatory states, where the non-normal dynamics immediately raises the activity level, eventually driving the system back close to the fixed point. The model we propose to mimic this behavior is the following:

- The system evolves according to the following set of effective equations:

$$\begin{cases} \dot{\rho} = h + a\rho - b\rho^2 + \sigma\sqrt{\rho} & \rho > T \\ \dot{\rho} = -a\rho + \sigma\eta & \rho < T \end{cases} \tag{7.1}$$

  where T is an arbitrary small threshold.

- The system can instantly take the value $\rho = 0$ or $\rho = \frac{a}{b}$ with probability p, mimicking the shear flow close to the diagonal and allowing some type of '*tunneling effect*'.

Setting up the system in the active phase (i.e. with $a > 0$) this 'toy' model are able to reproduce the complex behavior of the avalanches shown in Fig.7.3. Figure 7.5 shows the avalanche size and duration probability distributions for different values of p. Just as our original model, there is a region with a power-law behavior following the Random Walk universality class for small avalanches, and a 'bump' that reflects the existence of an Up (weakly) stable state of the system. Finally, for huge avalanches there exists an exponential cut-off.

7.2.9 Tsodyks Markram model for networks with synaptic plasticity.

We propose that this mechanism could actually be quite general in the neural dynamics, following the idea that avalanching behavior in resting state could be noise-induced. We conjecture that inhibition is not the only regulatory

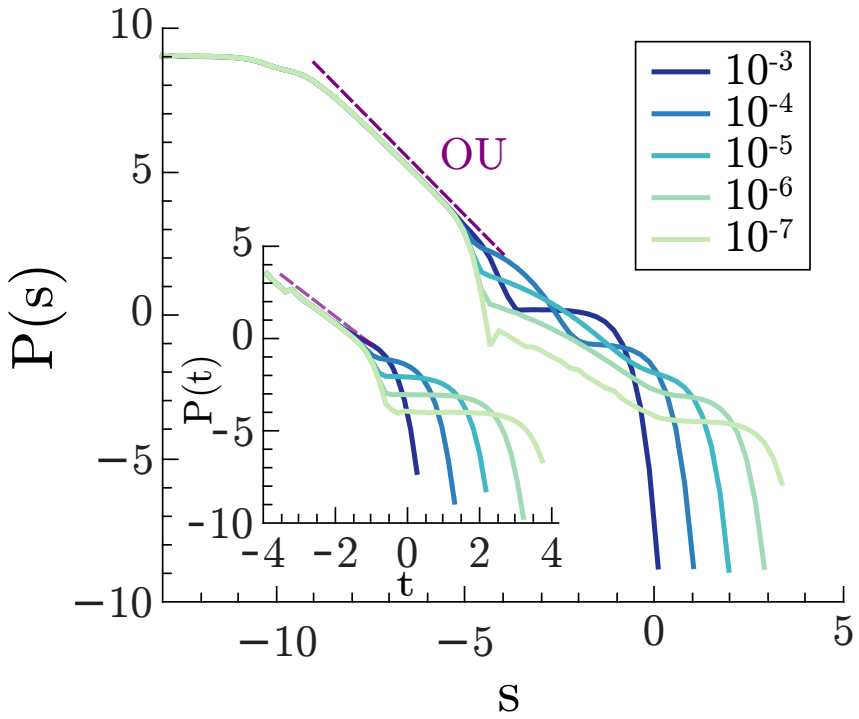

Figure 7.5: Avalanches for the $(1+\epsilon)$-dimensional minimal model. Avalanche size distribution for differents values of p. There is a region of random walk movement, followed by a bump related to the tunneling effect. Inset: Same behavior for the avalanche duration distribution. Parameters values: $a = 0.5$, $b = 1$, $\sigma = 10^{-3}$, $h = 10^{-3}$, $T = 2.5 \cdot 10^{-4}$.

mechanism that induces a reactive behavior: non-normal forms might be a common trait in neurophysics.

In this section we remove inhibition from the picture and consider a network of only excitatory spiking neurons, communicating through plastic synapses. More specifically we endow the system with Short-Term Synaptic Plasticity (STP) to show that this mechanism, under some homeostatic conditions, represented here by some particular choice of the synaptic and neuronal time scales, is sufficient for the emergence of highly untrivial reactive behaviors.

A density (Wilson Cowan-like) variable x describes the excitatory activity of the network, which, since the system is finite, is endowed with a demographic noise. The overall incoming current, though, is mediated by the synaptic density variable y, which describes the (short term) dynamic behavior of the synapses. A common way to model Short Term Plasticity is through the Tsodyks-Markram model [25] (see also Appendix B.3). As already mentioned in this thesis (see Chapter 4), this model describes the dynamics of the transmission of the electric signal from the spiking neuron to its neighbor through the neurotransmitter resources present in the pre-synaptic terminal. The Langevin equations for the system read:

$$\begin{cases} \dot{x} = -\alpha x + (1-x) f[yx + h] + \sigma\sqrt{x}\eta \\ \dot{y} = \frac{1}{\tau}(1-y) - uyx \end{cases}$$

where $f(x)$ is the same sigmoid function defined for the Wilson-Cowan dynamics, h is a small inhibitory external current and η is a gaussian white noise. In absence of activity, the synaptic variable recovers (up to saturation $y = 1$) with a time scale specified by τ, while in presence of activity, it gets consumed, proportionally to the overall activity, at a much faster time scale $1/u$.

By similarity with the Wilson-Cowan model, where only one fixed active/inactive point exists (depending on whether excitation or inhibition dominates, respectively), the specific parameters of the model above are chosen to be consistent with the case B described in Chapter 4. In such a case, between the up and the down states, a regime of bistability including three fixed points is found for intermediate values of ξ (in between two saddle-node bifurcations). In such

intermediate regime, for appropriate choices of the parameters, the reactive dynamics is present. In particular, this specific case is achieved by taking the limit of small (but non-vanishing) values of Θ, α, τ_D and τ_R and also, with some extra fine tuning (i.e. the condition $\frac{\tau_D}{\tau_R} \ll 1$ and $\frac{1}{\tau_D} \approx \alpha$, where the last equation represents a sort of balance between the synaptic depression timescale and the neuronal decay timescale) to reach the non-normal condition shown in Figure 7.6a. As in the Wilson-Cowan model, there exists a stable 'up' state with a characteristic 'shear' flow driving the system away from the stable fixed point and dropping it (by a noise-induce phenomenon) to the 'down' state (see Figure 7.6b).

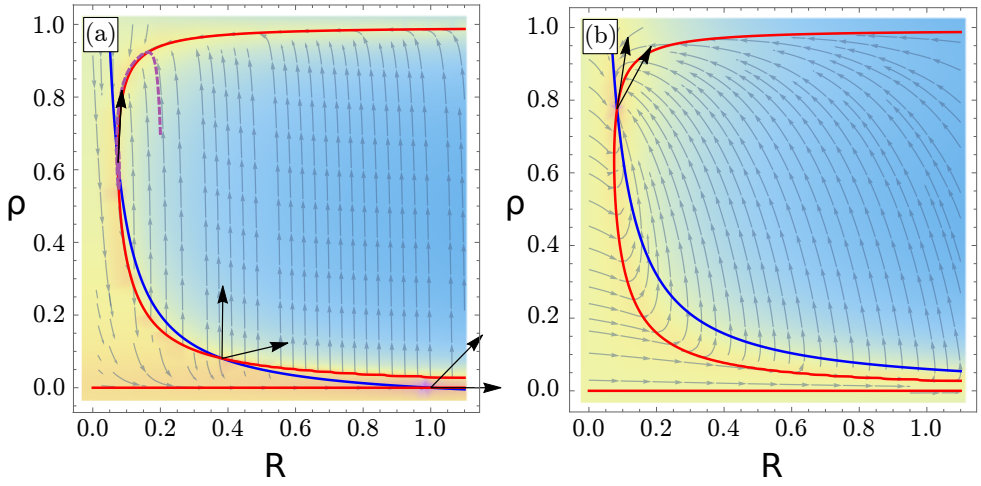

Figure 7.6: Phase portrait for the '*balanced*' TM model. (a) Non-normal condition with two fixed points showing reactive dynamics. A characteristic 'shear' flow surrounds the two stable fixed points, 'up' and 'down'. Parameters: $h = 10^{-6}$, $\Theta = 0.03$, $\alpha = 0.01$, $\tau_D = 100$, $\tau_R = 2000$, $\chi = 1$ (b) Stable fixed point with incoming flow in all directions. Parameters: $h = 10^{-6}$, $\Theta = 0.03$, $\alpha = 0.01$, $\tau_D = 0.2$, $\tau_R = 1000$, $\chi = 13$.

Numerical simulation of Eqs.(7.2.9) suggest that there exists a clear distinction

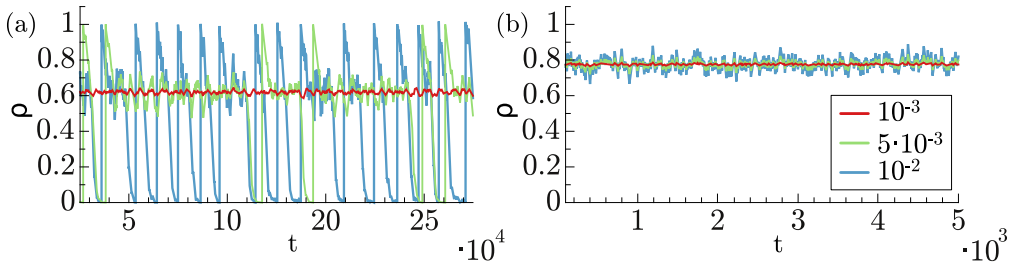

Figure 7.7: Temporal series for noisy system corresponding to parameters shown in the above figure. (a) Reactive system for different values of the noise amplitude (as in the legend). For the lower one (red line) the system features a stable 'up' state, that can be destabilized (green line) up to generate bursty dynamics (blue line) for increasing values of noise amplitude. Such fluctuations are excursions between the two metastable states. (b) For identical values of the noise amplitude, only an 'up' stable state exists. The lack of non-normal effects around the stable state prevents noise-induced fluctuations.

in the noisy dynamics corresponding to the two cases illustrated in Figure 7.6. As shown in Figure (7.7), both cases have two stable states but for the first case, the 'weak' stable 'up' state for relatively small amplitudes of the noise, can be easily destabilized, generating a clear bursty quasi-periodic dynamics with amplified fluctuations. Instead, for the second one (see Figure (7.7)b) the same values of the noise amplitude slightly perturb the dynamics of the system around the 'up' state, with no trace of amplification of fluctuations.

7.3 Summary and Conclusions

Scale-invariance has been proven to be ubiquitous in nature. Power-law distributed avalanches of activity are reported in very diverse phenomena, from

earthquakes and microfracturing phenomena, to solar flares, rainfall, or type II superconductors [166, 167, 168, 169, 170], as we already discussed in Chapter 1. Very often such a scale-invariant behaviour is considered as the fingerprint of underlying criticality, as widely overviewed along this thesis. Recently, some authors have been relating the emergence of power laws in cortical systems, with the existence of self-organized criticality [171, 21, 40, 20, 83], concerned with the existence of a slow regulatory mechanism that tunes the system to criticality. Nevertheless, the criticality hypothesis in cortical networks is still controversial [162, 87] (see also 6), and, occasionally, even the significance of their emergence in the experimental context has been questioned. The mechanism of balanced amplification, recently proposed by Benayoun et al. [97], and thoroughly scrutinized here provides a (non-critical) candidate to model some features of neuronal avalanches. Thus, the Wilson-Cowan model for excitatory and inhibitory neuron populations, placed in a condition of *balance* between excitatory and inhibitory couplings, is able to describe (without any need of fine tuning to a critical point) transitions between up (active) and down (quiescent) states as they occur in the brain during sleep or under anesthesia [88, 89], as well as large fluctuations that closely resemble the empirical scale-free avalanches of brain dynamics [9]. In other words, the effect of the regime of balance is an avalanching-like (finite size) behavior where the system wanders through an almost-linear phase space which is very wide with respect to the level of the noise introduced. However, temporal series suggests that the system, in order to show avalanching behavior, remains trapped very close to the origin, that is the effect of the logarithmic potential along the balanced dynamical trajectory, i.e. the one-dimensional trajectory where excitatory and

inhibitory activity are completely equal. Deviations from such diagonal drive the system from one minimum to the other, mimicking something similar to a 'tunneling effect', where the permanence time in each minimum depends on their relative depth, which in its turn is fully determined by the intensity of the noise. We evidenced how this mechanism is related to balance but not necessarily to criticality. In fact the singular behavior does not stem from the thermodynamic limit, on the contrary, the whole phenomenon is a finite-size effect. From another point of view, noise in an essential feature in order to observe the scale invariant behavior: the avalanches in this case stem from an amplification of noise-induced fluctuations in the system, while the deterministic system does not necessarily become unstable. Nevertheless, unlike the microscopic dynamics studied by Benayoun et al. [97], our mean-field description shows more clearly scale-free avalanches composed by, either a mixture of different trends or (for high values of the noise amplitude) exponents compatible with the standard random walk universality class, i.e. $\alpha = 3/2$ and $\tau = 4/3$. Thus, although reactive dynamics may be of key importance in neural mechanisms (such as in up and down states) and in fostering large fluctuations, it does not seem to be a plausible candidate to account for the scale-invariance belonging to branching-process universality class observed in experiments and already outlined in previous chapters. On the other hand, we have shown that the reactive dynamics applies to a wider scenario, extensible to different neural mechanisms, including synaptic plasticity as encoded in the Tsodyks-Markram model.

Chapter 8

Conclusions

The human cortex operates in a state of restless activity, whose meaning and functionality are still not well understoood.

Understanding the origin, nature and significance of complex patterns of neural activity, as recorded by diverse electrophysiological and neuroimaging techniques, is a central challenge in Neuroscience and the main target of this Thesis. These patterns include collective oscillations or rhythms, emerging out of partial synchronization, as well as highly-heterogeneous outbursts of activity intespersed by periods of quasi-quiescence called "neuronal avalanches". The sizes and durations of such avalanches have been consistently found to be scale-free and to obey scaling behavior, reminiscent of criticality. This empirical evidence seems to support the theoretical conjecture proposing that the cortex might obtain important functional advantages by operating at the edge of a continuous phase transition.

In this Thesis, we analyzed under different viewpoints this popular though controversial hypothesis.

Self-organized criticality elucidates the conditions under which physical and biological systems tune themselves to the edge of a second-order phase transition, entailing scale-invariant behaviors. Existing well-accepted models claim the occurrence of self-organized criticality in the brain: nevertheless either they are not biologically plausible, or they present some kind of shortcoming, so that, in our opinion, none of them do relate exhaustingly neuronal avalanches to self-organized criticality.

In particular, we focus on the celebrated model of Millman et al. [21], in which diverse neuronal avalanches, obeying scaling, can coexist simultaneously, even if the network operates in a regime far from the edge of any phase transition (thus being incompatible with criticality). Instead, we show that perturbations to the system state unfold dynamically according to a neutral drift (guided only by stochasticity) with respect to the background of endogenous spontaneous activity, and such a neutral dynamics –akin to neutral theories of population genetics and of biogeography– implies marginal propagation of perturbations, responsible for scale-free distributed causal avalanches. In other words, causal avalanches follow power-law distributions even if the system is not poised at criticality. We argue that causal information, not easily accessible to experiments, is essential to elucidate the nature and statistics of neural avalanches and that the possibility that neutral dynamics plays an important role in the cortex functioning, is a plausible *alternative* to the criticality hypothesis. We discuss the implications of these findings, in the attempt of designing new em-

pirical approaches to shed further light on the origin of neuronal avalanches, on how causality could be evaluated in an experimental framework and, ultimately, on how the brain processes and stores information.

Motivated by the empirical observation of bimodal distributions of activity in neuroscience and other fields, we proposed and analyzed a general theory for the self-organization to the point of phase-coexistence in systems exhibiting a first-order phase transition. The theory of Self-Organized Bistability explains the emergence of regular avalanches with attributes of scale-invariance which coexist with huge anomalous ones, with realizations in many fields. Following the footprints of the development of the theory of SOC, we build a microscopic toy model, the "fixed-energy" version of the theory, and a Langevin description of Self-Organized Bistability. Moreover we discuss the generation of system-size "king" avalanches, through a nucleation argument. We also take into account the effects of spatial and topological heterogeneities: while on a regular lattice the background field is able to compensate the quenched disorder on sites' behavior, on disordered network topologies, preliminary results suggest that heterogeneity is able to smoothen the first order transition and reduce SOB behavior to SOC.

The issue of the viability of SOC or SOB in cortical circuits still holds unsolved. We address it by inheriting ideas from the physics of phase transitions and in particular by following the principle of parsimony of Landau-Ginzburg, in order to analyze their possible collective phases and phase transitions. The resulting mesoscopic approach that we develop is similar in spirit to that of Wilson-Cowan, but, crucially, including stochasticity and space. Synaptic plasticity

or inhibition are scritinized as alternative key regulatory/homeostatic mechanisms, leading to very similar results. Detailed analyses reveal two types of phase diagrams, depending on parameters. A first scenario, that could be related to an awake state of the brain, includes four possible emergent phases: down state, synchronous, asynchronous, and up state; and reveal that all chief empirical findings for neural avalanches are consistently reproduced by tuning our model to the edge of synchronization. This is, the putative criticality of cortical dynamics does not correspond to a point of marginal propagation of activity (quiescent/active phase transition), as usually assumed, but to a synchronization phase transition, at which oscillations and scale-free avalanches coexist.

In the second scenario –achieved by a slower dynamics for synaptic resources– the model explains up and down states as they occur, e.g. during deep sleep and anaesthesia. The present approach constitutes a theoretical framework to rationalize the possible collective phases and phase transitions of cortical networks in simple terms, thus helping shed light into basic aspects of brain functioning from a very broad perspective.

Moreover, our Landau-Ginzburg approach allows to discuss the conceivability of self-organization in this simplified, though comprehensive model of the cerebral cortex. We show that this description corresponds to a non-conserved version of SOB, and that the conserved limit can be recovered by slowing down the dynamics of synaptic plasticity with respect to membrane potential activity. The biological inspiration of the model, allows to directly compare the parameters of the model with experimentally measured values. We found

that the synaptic timescales necessary in order to achieve self-organization are not compatible with the values deriving from experimental observations. We conclude that the empirically reported apparent criticality can only possibly come about if the cortex is tuned at the edge of a synchronization phase transition, where neuronal avalanches and oscillations coexist, and where dynamical diversity is maximal. Still, other possible scenarios could emerge within the self-organization framework if one considered additional/different homeostatic mechanisms.

The exponents measured for the distributions of neuronal avalanches are well-known to coincide with those of un-biased branching processes. This gave us the input to revisit the general problem of deriving the mean-field values of avalanche exponents in systems with absorbing states. Focusing on the generality of the result, we showed how exponents can be calculated analytically by mapping the corresponding Langevin equations describing the stochastic dynamics into a random walker confined to the origin by a logarithmic potential. We reported on the emergence of non-universal continuously-varying exponent values stemming from the presence of small external driving –that might induce avalanche merging– that gives a possible explanation of the deviations from the mean field exponents observed in real systems.

The lack of a strong physical criterion to set a parameter (the time binning) for the definition of avalanches is one of the main sources of skepticism on the universality of the measure of scale-invariance and, consequently, on the critical hypothesis. Moreover it is conceivable that the scale-invariant nature of the avalanches, could be induced by the protocol of clustering used to define

avalanches. In fact it could be plausible that determining the time-bin as the average time interval between two events recorded in the network, biased the measure, artificially creating time units such that the branching parameter of the resulting process is unitary, thus generating on average a fictitious branching process. We briefly discussed some preliminary findings on this topic. While it is not clear yet, BP method provides a biased measure and considering as well the difficulties in acquiring accurate data for several decades –which would be necessary to confirm the occurrence of precise finite size scaling or other signatures of criticality– different perspectives have been proposed, in alternative to the criticality hypothesis. For instance a different perspective relates the emergence of highly irregular bursts of activity with the condition of balance between excitation and inhibition in the cortex. We analyzed in detail this mechanism, which leads to the emergence of non-critical power laws for neuronal avalanches within realistic and simple modelling framework. Through analytical and computational tools, we made clear the role of balance in a Wilson-Cowan-like deterministic dynamics and how this can stem from a "non-normal" setup, under very general assumptions. Furthermore we elucidated how noise superimposes to this dynamics, creating an intriguing, very general and solid machinery, giving rise to the emergence of self-similar bursts of activity in finite-size systems of spiking neurons.

8.1 Summary of Thesis Achievements

In this PhD thesis we try to help elucidating the picture on the criticality hypothesis in the brain, starting from a unifying and rigorous perspective. The overall contribution of this thesis is an accurate analysis of the possibility of the existence of a phase transition in the brain (and the eventual self-organization to it). We identify that an essential element for the behavior of the synthetic neuron is the feature of integrating signal coming from many neighbors, and only when the total signal is above a certain value, the neuron transmits the information to its neighbors. This mechanism creates a positive feedback loop for the global activity, which generates a discontinuous phase transition.

Taking into account one of the most cited models that reproduce self-organized criticality in neural networks, the model of Millman et al. [21] – which shows the existence of a discontinuous phase transition– we show that it is not able to reproduce avalanches unless **causal information** is included, information which, very often, is not possible to evaluate or include in the experimental settings.

Under a general point of view (not related to neural context) we developed a theory for **self organization to a first order phase transition** in a spatially extended system, in full analogy with the paradigm of self-organized criticality. We characterize the dynamical behavior of the system, both through a microscopical toy-model description and through a stochastic mesoscopic Langevin description. We uncover that cascades of activity follow a bimodal distribution, where scale-invariance coexists with huge events, balistically invading the

whole system.

Moreover we construct a parsimonious Landau-Ginzburg theory of the brain, showing that if a phase transition exists in the brain, it should be a **synchronization phase transition**, instead of an absorbing/active one, as generally assumed. We were able to recover many of the phenomena described by experiments by setting our model at the critical point of this transition.

We give an insight on mean field Directed Percolation exponents (the exponents claimed to appear in neural avalanches experiments), how general they are, what are they related to.

Furthermore we discuss the possibility that experimental protocol for the measure of avalanches introduces a bias, even though much work is still necessary before we can draw conclusions on this point.

Finally we help shedding light on a mechanism for generation of non-critical scale-invariance, based on a so-called **reactive dynamics**. This also allows an exploration of the relation between criticality and balance between excitation and inhibition.

8.2 Resumen de los resultados de la tesis en Castellano

En esta tesis doctoral intentamos clarificar asuntos fundamentales sobre la hipótesis de la criticidad en el cerebro, a través de una perspectiva unificadora y rigurosa. La principal contribución de esta tesis es un análisis preciso de la posibilidad de la existencia de una transición de fase en el cerebro (y la eventual autoorganización del cerebro en el punto de transición de fase). Identificamos que un elemento esencial para el comportamiento de las neuronas sintéticas es la característica de integrar la señal proveniente de muchos vecinos, y transmitir la señal de output solo cuando la señal total en input está por encima de cierto umbral. Este mecanismo crea un circuito de retroalimentación positiva para la actividad global, que genera una transición de fase discontinua.

Basándonos en uno de los modelos más citados en Neurociencia, que reproduce la criticidad autoorganizada en las redes neuronales, el modelo de Millman et al. [17] –que involucra una transición de fase discontinua– mostramos que este modelo no es realmente capaz de reproducir avalanchas a menos que se incluya información causal sobre cuál neurona se activa por efecto de cuál, información que, muy a menudo, no es posible evaluar o incluir en los experimentos. Bajo un punto de vista general (no relacionado exclusivamente con el contexto neuronal) desarrollamos una teoría para la autoorganización a una transición de fase de primer orden en un sistema espacialmente extendido, en plena analogía con el paradigma de la criticidad autoorganizada (SOC). Caracterizamos el comportamiento dinámico del sistema, tanto a través de

una descripción microscópica como a través de una descripción mesoscópica de un proceso de Langevin. Descubrimos que las cascadas de actividad siguen una distribución bimodal, donde la invarianza de escala coexiste con grandes eventos, que invaden balisticamente el sistema entero. Además, construimos una teoría minimal del cerebro, siguiendo el metamodelo de Landau-Ginzburg, mostrando que si existe una transición de fase en el cerebro, debería ser una transición de fase de sincronización, en lugar de una entre estado absorbente y estado activo, como generalmente asumido en literatura. Tuneando nuestro modelo en el punto crítico de esta transición, pudimos recuperar muchos de los fenómenos descritos por los experimentos. Paralelamente, proporcionamos una visión unificadora sobre los exponentes de Percolación Dirigida (Directed Percolation) en campo medio (los exponentes que la comunidad neurocientífica afirma aparecer en experimentos de avalanchas neurales), explicando en detalle cuánto de general son, y con qué están relacionados. Además, discutimos la posibilidad de que el protocolo experimental para la medición de avalanchas pueda introducir un bias, aunque todavía es necesario mucho trabajo antes de sacar conclusiones sobre este punto. Finalmente ayudamos a arrojar luz sobre un mecanismo para la generación de invariancia de escala no crítica en el cerebro, basada en una dinámica reactiva producida por un balance entre excitación y inhibición.

Appendix A

Criticality in equilibrium and non-equilibrium systems

A.1 Criticality in equilibrium transitions

We briefly expose the fundamental concepts related to criticality in equilibrium systems, taking advantage of the Ising model and afterwards briefly describe how those concepts can be extended to the realm of non-equilibrium phase transitions, through the simple example of the Contact Process.

A.1.1 Elementary concepts on phase transitions

When some macroscopical property of a system change qualitatively as a response to a small change of the environmental conditions, the system is said

to undergo a *phase transition*. Usually the two phases are considered to be characterized by their degree of order (i.e., the transition is between an ordered and a disordered phase) so that the thermodynamic observable used to distinguish between them is called the *order parameter*, while the change in the environmental conditions is encoded in the variation of the *control parameter*. Formally, all macroscopic properties in equilibrium systems can be deduced from the free energy of the system. Since phase transitions involve dramatic (qualitative) changes of the macroscopic state of the system, they must correspond to *singularities of the free energy*. Moreover, given that the canonical partition function of a finite collection of particles is always analytic, phase transitions must emerge by taking the *thermodynamic limit*.

Undoubtedly, the phase transition which is more experienced in every-day life is the transition between states of water. When water is boiling in a kettle, a phase transition between its liquid and its gaseous state is occurring. The two states *coexist* and, at constant temperature and pressure, the volume of liquid decreases while the volume of gas increases. This situation is represented with a red line in Fig.A.1 and corresponds to a so-called *first order phase transition*. In a plot of the order parameter (that is, in this case, the density of the system) versus the control parameter, which, in this case, is the temperature, we would see a discontinuous jump at $T \simeq 100C$ (for $P = 1atm$), meaning that at constant temperature, one jumps from a phase with high density (liquid) to a phase with very low density (gas). The denomination of such transitions stems from the fact that first derivative of Gibbs free energy suffers a discontinuity at the transition point. If we would perform the same experiment at a lower pres-

sure (green line in Fig.A.1), the transition between liquid and vapour would be smooth, i.e. the order parameter would change continuously as a response to control parameter changes. The singular point in which the order parameter starts to grow in a *second order phase transitions* is called the *critical point* and the behavior of the system in the vicinity of this point is characterized by a divergence of the correlation length, meaning that there is no characteristic scale for the interactions in the system, fluctuations occur at all length scales and many quantities are described by power-law functions, since they are invariant under dilatations ($f(x) = x^{\alpha}$, $f(kx) = k^{\alpha} f(x)$). Close to criticality the fluid appears "milky" (the phenomenon is most commonly demonstrated in binary fluid mixtures), evidencing the existence of collective fluctuations in density at long enough wavelengths to scatter visible light (*critical opalescence*). At criticality the properties of the system can be described through a set of *critical exponents* which do not depend on the details or parameters of the system, but only on its fundamental symmetries and conservation laws. Remarkably transitions as diverse as the liquid/gas and ferromagnetic/paramagnetic can be described by the same set of critical exponents and are said to belong to the same *universality class*.

A.1.2 The Ising model

Let us express concepts reviewed in the previous section, in a more formal way, benefitting from the help of the Ising model. Ising model describes the magnetization of certain substances such as nichel or iron below a certain temperature (called the *Curie temperature*). Let us consider a lattice of N

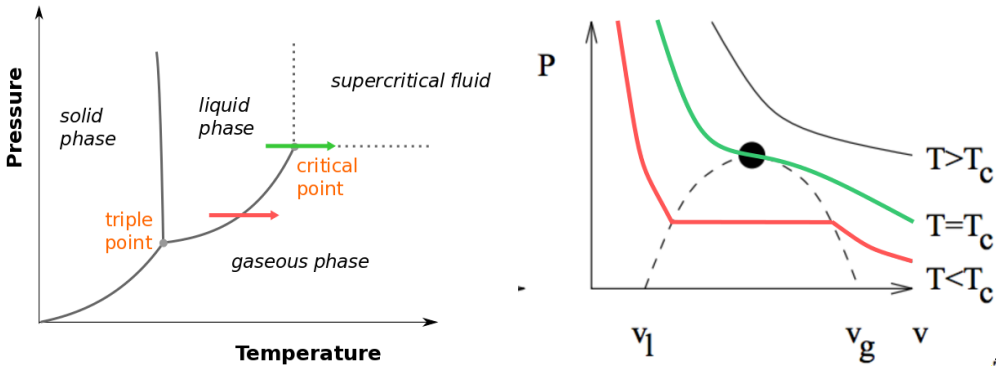

Figure A.1: Left: Sketch of the phase diagram of water in the space (P, T). Red and green curve indicate first and second order phase transitions respectively, at constant pressure and varying temperature. Right: phase transitions for constant temperatures $T < T_c, T = T_c, T > T_c$ and varying pressure, plotted as a function of the volume. The red curve, corresponding to the first order phase transition, evidences the phase coexistence between liquid and gaseous phase.

binary degrees of freedom representing the spin of particles $s_i = \pm 1$, $i = 1, ..., N$. The Hamiltonian of the system reads

$$\mathcal{H} = -J \sum_{\langle ij \rangle} s_i s_j - H \sum_i s_i, \tag{A.1}$$

where the sum runs over neighboring sites. The partition function reads

$$\mathcal{Z}(T, H) = \sum_{\{s_i\}} e^{-\beta \mathcal{H}}, \tag{A.2}$$

where the first sum runs over all the possible configurations of microstates $\{s_i\} = \{s_1, s_2, ..., s_N\}$, the energy scale $\beta = k_B T$ and the free energy is

$$F(T, H) = -\frac{1}{\beta} \log \mathcal{Z} = \langle E \rangle - TS. \tag{A.3}$$

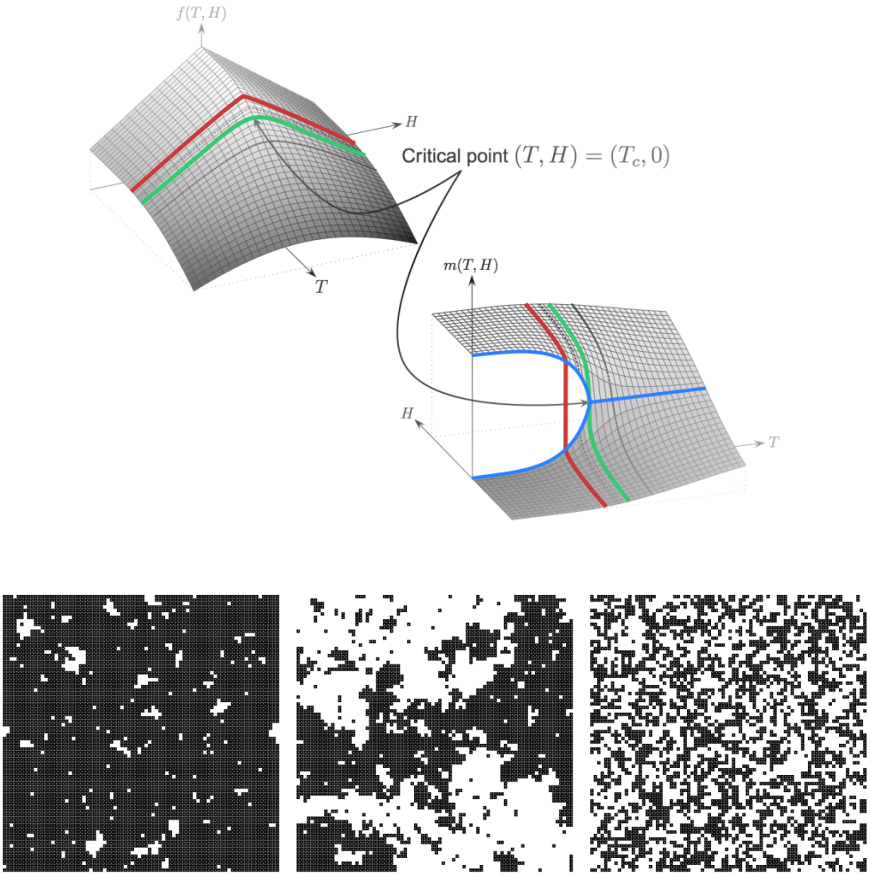

Figure A.2: Upper panel: diagram of the phase transitions for the Ising model: free energy per spin $f(T,H)$ and average magnetization per spin $m(T,H)$. Discontinuity of the free energy indicates a phase transition. Red line and green line evidence respectively a first order and second order phase transition at fixed temperature ($T<T_c$ and $T=T_c$, respectively) and varying external field. Blue line is the ferromagnetic/paramagnetic transition at fixed external field and varying temperature. Lower panel: example of steady-state configurations of the 2D Ising model for temperatures $T<T_c, T=T_c, T>T_c$ respectively showing ordered, critical and disordered phase.

A phase diagram for an Ising ferromagnet is reported in Fig.A.2 [172]. By changing the magnetic field at constant temperature, the system can undergo

a phase transition from a phase in which the magnetization is positive to a phase in which the magnetization is negative, both a first order ($T < T_c$, red curve in Fig.A.2), and a second order one ($T = T_c$, green curve in figure), as occurs in the liquid-gas phase transition. However, a second order phase transition is also achieved by changing the temperature at fixed zero magnetic field (marked by the blue line in Fig.A.2). Remarkably this second order phase transition is accompanied by a *spontaneous symmetry breaking* in which the system spontaneously chooses to be in either un up or a down-spin phase. The spontaneous emergence of magnetisation in zero external field as the temperature is lowered below a certain critical temperature in the Ising model is one of the simplest frameworks to study a phase transition (paramagnetic-ferromagnetic transition), so let us focus on it, in order to formalize the features of criticality [172]. The total magnetization, i.e. the difference between the number of spins pointing up and down, $M = \sum_{i=1}^{N} s_i$ is the easiest observable to measure, distinguishing between the ordered ferromagnetic phase at low temperatures and the disordered paramagnetic phase at high temperatures, where the magnetization is zero. Its average is the natural order parameter to consider,

$$\langle M \rangle = \frac{\partial \ln \mathcal{Z}}{\partial(\beta H)} = \frac{1}{\mathcal{Z}} \sum_{\{s_i\}} M e^{-\beta \mathcal{H}}, \tag{A.4}$$

but often one normalizes quantities of interest by the number of degrees of freedom, thus considers

$$m = \frac{\langle M \rangle}{N} = -\frac{\partial f}{\partial H}, \tag{A.5}$$

where $f = F/N$ is the free energy per spin. The sensitivity of the average magnetisation per spin to changes in the external field at a fixed temperature

is given by the susceptibility per spin

$$\chi(T,H) = -\frac{\partial m}{\partial H}, \tag{A.6}$$

and it is related to the variance of the total magnetization (fluctuation-dissipation theorem) through

$$\chi = \frac{\beta}{N}(\langle M^2\rangle - \langle M\rangle^2). \tag{A.7}$$

Moreover the sensitivity of the average energy per spin $\epsilon = \langle E\rangle/N$ to changes in the temperature at fixed external field is given by the heat capacity per spin, referred to as the specific heat:

$$c(T,H) = \frac{\partial \epsilon}{\partial T} = \frac{\beta}{N}(\langle E^2\rangle - \langle E\rangle^2). \tag{A.8}$$

The correlation function describes the correlations in the fluctuations of the spins s_i and s_j

$$g(\mathbf{r}_i,\mathbf{r}_j) = \langle (s_i - \langle s_i\rangle)(s_j - \langle s_j\rangle)\rangle = \langle s_i s_j\rangle - \langle s_i\rangle\langle s_j\rangle, \tag{A.9}$$

and it is related to the susceptibility by

$$\chi = \beta \sum_{j=1}^{N} g(\mathbf{r}_0,\mathbf{r}_j). \tag{A.10}$$

The correlation length ξ is the characteristic linear scale of the correlation function: $g(\mathbf{r}_i,\mathbf{r}_j) \propto e^{-|\mathbf{r}_i-\mathbf{r}_j|/\xi}$.

At relatively high temperatures, the entropic part of the free energy dominates

and the free energy is minimised (entropy is maximised) by randomising the orientation of spins. Meanwhile, at relatively low temperatures, the energy component dominates so that the free energy is minimised by minimising the energy, i.e. by aligning spins. When the thermal energy and the interaction energy are comparable, a phase transition from a disordered to an ordered state takes place, where

$$\lim_{H\to 0^{\pm}} m(T,H) \propto \begin{cases} 0 & \text{for } T \geq T_c, \\ \pm(T-T_c)^{\beta} & \text{for } T \to T_c^- \end{cases} \tag{A.11}$$

The *critical exponent* β characterises the pick-up of the magnetisation at $T = T_c$. At relatively high temperatures the variance per spin decays as β in zero external field, i.e. the spins can be considered non-interacting. As the temperature is lowered, the fluctuations away from the average magnetisation per spin ($m = 0$) increase and the spins become increasingly more interactive, and at the critical temperature the fluctuations diverge, meaning that the are correlated throughout the system and the system is extremely sensitive (responsive) to external perturbations:

$$\begin{aligned} \chi(T, H \to 0) &\propto |T - T_c|^{-\gamma} \quad \text{for } T \to T_c \\ c(T, H \to 0) &\propto |T - T_c|^{-\alpha} \quad \text{for } T \to T_c \end{aligned} \tag{A.12}$$

As a consequence of the divergence of the susceptibility, at the critical point the spin-spin correlation function cannot decay exponentially fast with distance.

Indeed, at $(T_c, 0)$ one finds

$$g(\mathbf{r}_i, \mathbf{r}_j) = |\mathbf{r}_i - \mathbf{r}_j|^{-(d-2+\eta)} \tag{A.13}$$

and

$$\xi(T, H \to 0) \propto |T - T_c|^{-\nu}. \tag{A.14}$$

A.1.3 Landau theory of phase transitions

Landau was awarded with the Nobel prize in physics 1962 for 'his pioneering theories for condensed matter, especially liquid helium' explaining the fluid-superfluid phase transition in ^4He [172]. He argued that if the free energy is analytic near the critical point, then it can be expanded in terms of the order parameter which is small in the vicinity of the phase transition.

$$f(T, H; \phi) = \sum_{k=0}^{\infty} \alpha_k(T, H)\phi^k \tag{A.15}$$

for $T \to T_c$ and $H \to 0$ where ϕ denotes a general order parameter and $\alpha_k(T, H)$ are coefficients that depend on the control parameters (for example in the Ising model those parameters are the temperature and the external field). Symmetry arguments can be used to constrain the coefficients $\alpha(T, H)$. For example, for the Ising model in zero external field, the free energy is an even function of the order parameter, since in the absence of any external field the spins are equally likely to be pointing up or down, on average: $f(T, 0; \phi) = f(T, 0; -\phi)$, so that $\alpha_k(T, 0) = 0$ for odd k in zero external field. In the

vicinity of the phase transition, the order parameter is small. Thus we expect the higher-order terms in the expansion of the free energy to be negligible. Therefore, in zero external field, the simplest possible form of the free energy that can describe a continuous phase transition is:

$$f(T, 0; \phi) = \alpha_0(T, 0) + \alpha_2(T, 0)\phi^2 + \alpha_4(T, 0)\phi^4. \tag{A.16}$$

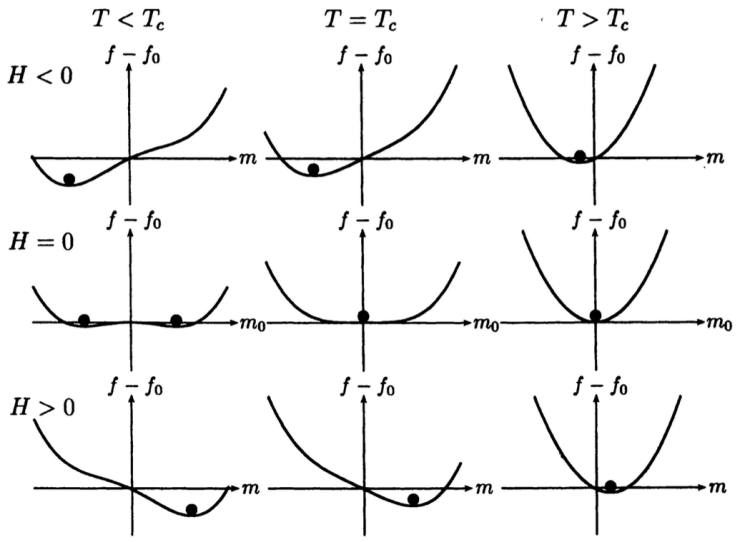

Figure A.3: A sketch of the free energy per spin, $f - f_0$, versus the average magnetization per spin, m. The balls indicate the position of the minimum of the free energy. The three panels in the top row are for negative external field and temperatures $T < T_c$, $T = T_c$,$T > T_c$, respectively. The three panels in the middle row are for zero external field and temperatures $T < T_c$, $T = T_C$, $T > T_c$, respectively. The three panels in the bottom row are for positive external field and temperatures $T < T_c$, $T = T_c$, $T > T_c$, respectively [172].

At $T = T_c$, the free energy has a unique extremum at $< \phi = 0$ which is a marginally stable minimum. Since $\alpha_2(T, 0)$ is positive for $T > T_c$ (since the

free energy has a unique extremum) and negative for $T < T_c$ (since the free energy has three extrema), it follows that $\alpha_2(T, 0)$ must be zero at $T = T_c$, while $\alpha_4(T, 0)$ remains positive to ensure that the extremum is a minimum. Assuming that the coefficients $\alpha_k(T, H)$ are analytic around $(T_c, 0)$, they can themselves be expanded in powers of $(T - T_c)$ and H. Close to the critical temperature and for small external fields, $\alpha_2(T, H) = \tilde{\alpha}_2(T - T_c)$. Moreover, if we restore a small external field, we can write the full Landau theory of continuous (second-order) phase transitions with order parameter ϕ (and up-down symmetry):

$$f(T, 0; \phi) = \tilde{\alpha}_0 + \tilde{\alpha}_2(T - T_c)\phi^2 + \tilde{\alpha}_4\phi^4, \tag{A.17}$$

from which one could derive the mean-field exponents for the Ising model. Since the Landau theory is an expansion of the mean-field model, it cannot be employed to evaluate quantitative results, but it is an amazingly powerful tool to straightforwardly catch the qualitative behavior of a system.

A.2 Criticality in non-equilibrium systems: The Contact Process

A system reaches equilibrium if it is completely isolated from external influences (thermal, mechanical, chemical, etc.) such that no external flux of mass or energy can pass through it. Such special conditions can be achieved in laboratory-designed systems, but almost never in Nature.

More formally, non-equilibrium systems are defined as systems for which detailed balance condition may not hold:

$$w_{ij}P_i^{eq} \neq w_{ji}P_j^{eq}, \tag{A.18}$$

where P_i^{eq} is the probability to find the system in the i-th stationary configuration and w_{ij} is the probability (rate) of transiting from configuration i to configuration j. This means that in steady-state conditions there is some sort of net probability flux between the configurations of the system, even though the system may appear macroscopically time-independent.

One of the simplest possible toy models presenting a non-equilibrium phase transition is the Contact Process. It is a birth-death stochastic process defined on a network of N binary units, which can be either occupied or empty: each occupied site dies with probability μ and has a probability λ to reproduce, creating a new occupied site at a randomly selected empty neighboring site. It was first proposed by Harris [173] as a model for epidemics spreading and, since then it has been largely used to model the dynamics of propagation of some type of "activity" (as e.g. infections in epidemic spreading, computer viruses in networks, etc.). It predicts two possible outcomes with a phase transition in between: if birth rates prevails, the infection spreads throughout the population, eventually reaching a stable percentage of infected individuals; if death rate prevails, then the recovering is fast enough and the infected percentage decreases until it vanishes, if birth and death rate are balanced, the system is critical. A fundamental[1] feature of the Contact Process is the

[1] A conjecture by Jannsen [124] and Grassberger [125] states that in every dimension,

existence of an *absorbing state*: if all active sites are dead, then the dynamics ceases. Thus, absorbing state acts as a probability sink, creating a net flow of probability, which is an example of how the detailed balance can be broken.

For simplicity, we consider here a fully coupled network. The Master equation reads

$$\begin{aligned}\dot{P}(n,t) &= W_{n-1\to n}P(n-1,t) + W_{n+1\to n}P(n+1,t) + \\ &\quad -W_{n\to n+1}P(n,t) - W_{n\to n-1}P(n,t) = \\ &= \lambda(n-1)\tfrac{N-n+1}{N}P(n-1,t) + \mu(n+1)P(n+1,t) + \\ &\quad -\lambda n\tfrac{N-n}{N}P(n,t) - \mu n P(n,t),\end{aligned} \tag{A.19}$$

where $W_{n_1\to n_2}$ is the transition rate between the state with n_1 occupied sites to the state with n_2 occupied sites. Introducing a density variable $\rho = n/N$ and renaming $\epsilon = 1/N$, Eq.A.19 becomes[2]

$$\begin{aligned}\dot{P}(\rho,t) &= \lambda N[(\rho-\epsilon)(1-\rho+\epsilon)P(\rho-\epsilon,t) - \rho(1-\rho)P(\rho,t)] + \\ &\quad +\mu N[(\rho+\epsilon)P(\rho+\epsilon,t) - \rho P(\rho,t)].\end{aligned} \tag{A.20}$$

Hence, performing a (second order) Taylor expansion[3] in the limit of big system sizes $\epsilon \to 0$ –which allows to approximately consider ρ as a continuous variable– one has:

$$\partial_t P(\rho,t) = \partial_\rho[(\lambda\rho(1-\rho)-\mu\rho)P(\rho,t)] - \frac{1}{2N}{\partial_\rho}^2[(\lambda\rho(1-\rho)+\mu\rho)P(\rho,t)]. \tag{A.21}$$

all models exhibiting a continuous transition to an absorbing/quiescent phase, without any additional symmetry or conservation law, belong to Directed Percolation universality class.

[2] $W_{n\to n+1} = W_{N\rho\to N\rho+1} = W_{\rho\to\rho+\epsilon}$

[3] i.e. using the formula $f(\rho-\epsilon) = f(\rho) - \epsilon\partial_\rho f(\rho) + \frac{\epsilon^2}{2}\partial_\rho^2 f(\rho)$, with $f(\rho) = \rho(1-\rho)P(\rho)$

The last equation is the Fokker Planck equation for the Contact Process (in a fully connected topology). The corresponding Langevin equation (à la Ito) reads [47]:

$$\dot{\rho}(t) = (\lambda - \mu)\rho - \lambda\rho^2 + \sigma\sqrt{(\lambda - \mu)\rho - \lambda\rho^2}\eta(t), \tag{A.22}$$

where $\eta(t)$ is a gaussian white noise with unitary variance and zero mean ($\langle\eta(t)\rangle = 0$ and $\langle\eta(t)\eta(t')\rangle = \delta(t - t')$).

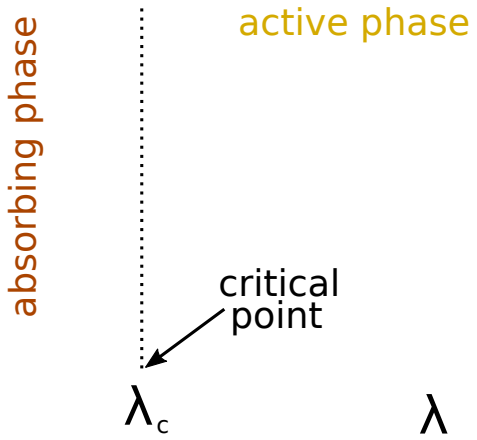

Figure A.4: Transition diagram $\rho(\lambda)$ of the mean field Contact Process in light green, susceptibility $\chi(\lambda)$ in dark green.

If we consider only the deterministic part of the equation above (i.e. the thermodynamic limit)

$$\dot{\rho}(t) = (\lambda - \mu)\rho - \lambda\rho^2, \tag{A.23}$$

also known as the Malthus-Verhulst equation, we can already highlight the qualitative features of the system, in particular the existence of a phase transition. In fact,

(i) for $\lambda/\mu < 1$, the system decays to an absorbing state, with null stationary

activity $\rho_{st} = 0$, (i.e. with no occupied sites), as $\rho(t) = \rho(0)\exp(-\frac{\Delta}{\mu}t)$, with $\Delta = |\lambda - \lambda_c|$

(ii) for $\lambda/\mu > 1$, the system is in the active regime and there are two stationary states: $\rho_{st} = 0$ and $\rho_{st} = 1 - \mu/\lambda$;

(iii) finally when $\lambda/\mu = 1$ the system undergoes a bifurcation: close to the critical point $\lambda = \lambda_c = \mu$

$$\rho_{st} = \frac{\lambda - \lambda_c}{\lambda} = \frac{\Delta}{\Delta + \lambda_c} = \frac{\Delta}{\lambda_c} + O(\Delta^2) \sim \Delta^{\beta}, \tag{A.24}$$

where Δ is the distance from the critical point and $\beta = 1$ is a critical exponent. Moreover, the dynamics shows critical slowing down at the critical point, since one obtains

$$\rho(t) = \frac{\rho(0)}{1 + \lambda\rho(0)t} \sim t^{-1} \tag{A.25}$$

for large times. One can also define the critical exponents $\nu_{\|}$ and $\nu_{\perp}$ for the the correlation time and correlation length, characterizing the divergence of the time and space[4] correlation functions close to the critical point. If we introduce a small driving field h to the dynamics, we are able to calculate the susceptibility

$$\chi \equiv \partial_h \rho_{st}|_{h\to 0} = \Delta^{-1}, \tag{A.26}$$

such that infinitesimal perturbations diverge at the critical point.

Moreover, non-equilibrium phase transitions show peculiar features in their dynamical behavior, which have no correspondence in standard equilibrium phase

[4]note that $\nu_{\perp}$ can only be defined out of the mean-field limit

transitions. Usually one can perform spreading experiments, i.e. set an initial condition with a single seed of activity on an absorbing background, on the full dynamics (including the fluctuation term), and measures the statistics of cascades of spatio-temporal activity, or 'avalanches' of activity. For subcritical values of the control parameter $\mu/\lambda < 1$, size and durations of the avalanches are exponentially distributed. For supercritical values $\mu/\lambda > 1$, on the contrary, a huge amount of the avalanches reach the whole system size. Right at the critical point $\lambda = \mu$, sizes and durations show maximal variability, i.e. they are power-law distributed, up to the system size, where an exponential cutoff usually appears. Results of spreading experiments on network of different sizes can be rescaled onto each other, or equivalently the size-dependent distributions can be expressed as:

$$P(s, N) \sim s^{-\tau}\mathcal{G}(s/N), \tag{A.27}$$

meaning that "finite size scaling", which is a signature of criticality, holds.

Finally when the Contact process is defined on a network, an additive diffusion term $D\nabla^2\rho$ appears in the Langevin equation. The avalanches of activity generated in a spatially explicit model are fractal at criticality.

A.3 Self-Organized Criticality

In the attempt to explain the ubiquity in nature of systems that exhibit features of criticality, as if they where posed in the vicinity of a second order phase tran-

sition, Bak, Tang and Wiesenfeld [6] came up with a toy-model –the sandpile–, pointing-out a mechanism by which dynamical systems can self-organize to the vicinity of a second-order phase transition, without needing to tune any parameter. The concept of Self-Organized Criticality encountered a huge resonance during the last decade of the twentieth century, many modified versions of the original sandpile were developed and used as toy-models to explain several phenomena, such as earthquakes and solar flares statistics, Barkhausen noise, vortices in type-II superconductors etc. [166, 167, 168, 169, 170]. The original sandpile model is as follows. Consider a network, let's say a square lattice with open boundaries, and let's drop randomly grains of sand or tokens of stress(/energy) –discrete units– until one site reaches a threshold value, θ. When a site reaches the threshold, the site "topples", meaning that it redistributes its grains of sand between its neighbors. This redistribution can eventually lead one of the neighbors to threshold, so that eventually a cascade of events –also called an "avalanche"– takes place. When a toppling event occurs at a boundary site, some grains of sand may fall off the system ("dissipate"), in such a way that each avalanche comes to an end at some point. When the cascade of events is over, the process starts from the beginning: new grains of sand are introduced into the system ("driving"), until a new avalanche occurs. It has been shown that such a system has all the features of a critical non-equilibrium phase transition, in fact it can be seen as a dynamical system whose fixed point is a critical point. Avalanche's statistics are scale-free (size, duration, average size given the duration), correlation lengths diverge, finite-size scaling holds, scaling relations between exponents can be found.

The key idea to elucidate how SOC works consists in "regularizing" sandpiles by switching off slow driving and boundary dissipation. In this way, the total amount of sand (that we call "energy", E) becomes a conserved quantity that can be used as a control parameter [30, 61, 7]. In the "*fixed-energy ensemble*" the system can be either in an *active phase* (with perpetual activity) for large values of E, or in an absorbing phase (where dynamics ceases) for sufficiently small values of E [62]. Separating these two phases, there is a critical point, E_c, at which a standard second-order phase transition occurs. In this setting, SOC is understood as a dynamical mechanism which, by exploiting slow driving and energy dissipation at infinitely separated timescales, self-tunes the system to E_c [6, 32, 28, 58]). To illustrate these ideas, let us recall how do they operate in the simplest possible mean-field framework [43]. For this, we consider, the minimal form $\dot{\rho}(t) = a\rho - b\rho^2$ for a (mean-field) continuous phase transition separating an absorbing phase with vanishing activity $\rho = 0$ (for $a < 0$) from an active one $\rho = a/b \neq 0$ (for $a > 0$); $b > 0$ is a constant. This equation is now coupled to an additional conserved "energy" variable E fostering the creation of further activity, $\dot{\rho}(t) = (a + \omega E)\rho - b\rho^2$, where $\omega > 0$ is a constant. For sandpiles, E represents the total density of sandgrains while ρ is the density of sites above threshold. In the fixed-energy variant, E is a conserved quantity, and the critical point lies at $E_c = -a/\omega$. Instead, in the SOC version, E is a dynamical variable, as an arbitrarily small driving rate, h, and activity-dependent energy dissipation, ϵ are switched on: $\dot{E} = h - \epsilon\rho$. In the double limit, $h, \epsilon \to 0$ with $h/\epsilon \to 0$ the steady-state solution is $E = E_c$, i.e. the system self-organizes to criticality.

To investigate how this simple mean-field picture changes in spatially-extended noisy systems, we briefly recap the stochastic theory of SOC. The phase transition of SOC systems, in their fixed-energy counterpart, is described by the following set of Langevin equations incorporating spatial coupling (diffusion) and noise in a parsimonious way:

$$\begin{aligned} \partial_t \rho(\vec{x},t) &= [a + \omega E(\vec{x},t)]\rho - b\rho^2 + D\nabla^2\rho + \sigma\eta(\vec{x},t) \\ \partial_t E(\vec{x},t) &= D\nabla^2\rho(\vec{x},t) \end{aligned} \tag{A.28}$$

where $\rho(\vec{x},t)$ and $E(\vec{x},t)$ are fields (some dependencies on $(\vec{x},t)$ have been omitted), $b > 0$, D and σ are the diffusion and noise constants, respectively, and $\eta(\vec{x},t)$ is a zero-mean multiplicative Gaussian noise with $\langle \eta(\vec{x},t)\eta(\vec{x'},t)\rangle = \rho(\vec{x},t)\delta(\vec{x}-\vec{x'})\delta(t-t')$ imposing the absorbing state condition. Eq.(A.28) was proposed on phenomenological grounds [61, 7] (see also [174]) but it can be rigorously derived from microscopic rules (using a coherent-state path-integral representation [175]) [5].

The fixed-energy theory described by Eq.(A.28) exhibits a continuous phase transition at $\bar{E}_c$ (where $\bar{E}$ is the spatially averaged energy). More remarkably, switching on slow-driving and boundary dissipation in Eq.(A.28)[6] it self-organizes to $\bar{E}^* = \bar{E}_c$. The width of the spatially-averaged energy distribution $P(\bar{E})$ in the SOC ensemble around $\bar{E}_c$ becomes progressively smaller as system size is enlarged, ensuring that in the thermodynamic limit the system self-

[5] Observe that the $E(\vec{x},t)$ field is a sort of dynamically-generated disorder, different from the "quenched" disorder appearing in other SOC-like phenomena such as Barkhaussen noise [135].

[6] This can be done in different ways; e.g. increasing both $\rho(\vec{x},t)$ and $E(\vec{x},t)$ at a given point by some amount (0.1) to create a new avalanche when the absorbing state has been reached and allowing for energy dissipation at open boundaries.

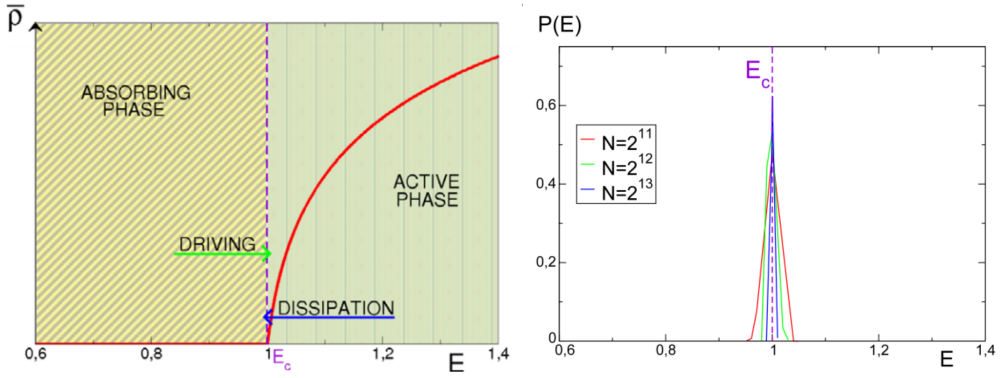

Figure A.5: Figures from [31]. Left: Sketched diagram illustrating the mechanism of self-organization. In the fixed-energy ensemble, there are an active phase and an absorbing phase, separated by a critical point, E_c. Slow driving and dissipation make sandpiles fluctuate around their associated fixed-energy counterpart critical point. Right: the distribution of E during avalanches, plotted for simulations of the conserving Langevin theory, using various system sizes (2^{11}, 2^{12}, and 2^{13}). The distributions become progressively peaked around E_c upon increasing the system size (the value of E has been normalized with E_c for each size), assuring that, in the thermodynamic limit, the system self-organizes sharply to E_c.

organizes exactly to its critical point[7]. This Langevin approach has allowed for establishing a connection between SOC and standard non-equilibrium phase transitions [30, 61, 7, 58], allowing for further computational and theoretical [67, 179] understanding.

A.4 Brief summary of neutral theory

The introduction by Kimura in 1968 of the neutral theory –hypothesizing that most evolutionary change is the result of genetic drift acting on neutral alleles

[7]See [31], and [176, 177, 178] for some lingering controversy.

[180]– caused much debate and a revolution in the way population genetics and molecular evolution were understood. In a similar endeavor, Hubbell proposed that most of the variability in complex ecological communities could be ascribed to neutral dynamics of similar species which expand or decline as a result of stochasticity [181, 182]. Neutral theories have in common that they neglect any *a priori* intrinsic difference between coexisting individuals, regardless of their "species" (allele, tree,...) type, implying that the dynamics is purely driven by random demographic effects. For instance, the introduction of a novel species within an established population triggers a random cascade of changes, or "avalanche", which –as a result of the implicit neutrality– does not have an inherent tendency to neither shrink nor to expand at the expenses of others. This marginal-propagation process generates scale-free avalanches, which resemble critical ones even if the system is not necessarily posed at the edge of a phase transition [182, 35]. Neutral models have been successfully employed to explain the emergence of scale-free distributions in (i) epidemic outbreaks with neutral microbial strains [35], (ii) viral-like propagation of neutral memes [183], (iii) the evolution of the microbiome [184], and (iv) the renewal of the intestinal epithelium from neutral stem cells [36].

Consider a fully connected network with N nodes (extensions to regular lattices, or more complex networks architectures are also possible but we stick here to the simplest case) and a number of possible states (be these species, alleles, opinions, etc.). The simplest neutral-dynamic model is the "voter model" (VM) [44, 120, 67, 131], also known as Moran process in the context of population dynamics and population genetics (see e.g. [185]). The VM assumes that

there are two types of species that we call A and B, respectively, and that the system/network is saturated, meaning that all nodes are always occupied, each one adopting one of the possible states at every time. The dynamics proceeds as follows: at each time step, one randomly chosen individual is "invaded" by a copy of another neighboring node at uniform rate, i.e. common to all the individuals in the population independently of their species labels. Without loss of generality we first consider the case with just two species, and later on we explain how this can be employed to analyze the case with multiple species.

The, so defined, 2-species VM has been profusely studied in the mathematical literature; some of its main relevant features are [44, 120, 67, 131, 185]: (i) it has no free parameters, (ii) it lacks any characteristic (length or time) scale and its dynamics exhibits scale-invariance, and (iii) it is characterized by purely noise-driven diffusive dynamics (see [67, 131] for more mathematical in-depth presentations).

Now, we derive the coarse-grained mean-field description of a voter model; similar derivations can be found in the literature [185]. For the sake of illustration, let us consider also a more generic model in which λ_A (resp. λ_B) is the probability for A (resp. B) to invade a site in state B (resp. A), with $\lambda_A \neq \lambda_B$ in general; the VM dynamics is recovered imposing the symmetrical or neutral condition $\lambda_A = \lambda_B$.

As the system is saturated, the number of individuals for the other species is $n_B = N - n_A$ and the state of the system can be determined by the total number of individuals of A, n_A. The model can be expressed as a branching

process [42], with transition rates $W(n_A \to n_A{+}1) = \lambda_A n_B n_A/N$ and $W(n_A \to n_A{-}1) = \lambda_B n_A n_B/N$. Using these rates, writing down the master equation for the probability of finding the system in a state n_A at time t –or alternatively with a density of individuals A, $\rho_A = n_A/N$– and performing a standard large N expansion, one readily obtains the following Fokker-Planck equation:

$$\begin{aligned}\frac{\partial P(\rho_A,t)}{\partial t} &= -(\lambda_A-\lambda_B)\tfrac{\partial}{\partial \rho_A}[\rho_A(1-\rho_A)P(\rho_A,t)] \\ &\quad +\tfrac{\lambda_A+\lambda_B}{2N}\tfrac{\partial^2}{\partial \rho_A^2}[\rho_A(1-\rho_A)P(\rho_A,t)],\end{aligned} \tag{A.29}$$

or its equivalent (Itö) Langevin equation

$$\dot{\rho}_A = (\lambda_A-\lambda_B)\rho_A(1-\rho_A) + \sqrt{\frac{\lambda_A+\lambda_B}{N}\rho_A(1-\rho_A)}\eta(t), \tag{A.30}$$

where η is a zero-mean Gaussian white noise with $\langle \eta(t)\eta(t')\rangle = \delta(t-t')$. The neutrality condition $\lambda_A = \lambda_B$ implies that the deterministic drift in Eq.A.30 vanishes thus $\langle \dot{\rho}_A \rangle = 0$, i.e. the average density of each species remains constant on average; i.e. its population does not grow nor shrink on average, but it just experiences stochastic demographic changes as described by

$$\dot{\rho}_A = \sqrt{\rho_A(1-\rho_A)}\eta(\tilde{t}), \tag{A.31}$$

where a factor $2\lambda_A/N$ has been absorbed into the new timescale $\tilde{t}$.

Observe that this last equation describes a stochastic process (random walk) with two absorbing barriers at 0 and 1, corresponding to either of the species A

or B, respectively, dominating the whole network. By neglecting the quadratic term in the noise (which is a valid approximation as far as the avalanche is small with respect to the much-larger system size), the avalanche-time exponent $\alpha = 2$ can be deduced from the first-passage time (return to the origin) statistics of this random-walk process, and using simple scaling arguments one can also easily derive $\tau = 3/2$ for the avalanche-size distribution [186], i.e. one recovers the mean-field exponents of the voter model (neutral theory) class (see e.g. [35]). These power-laws are truncated only by system size. The exponent values could also be analytically determined by employing the more standard generating function formalism for an unbiased branching process, as the rate of any cluster of A nodes to expand $\lambda_A n_A n_B/N$ coincides with its rate to contract $\lambda_B n_A n_B/N$ in the neutral case $\lambda_A = \lambda_B$ (see, e.g. [42, 43]).

Two apparently important differences between the VM dynamics and the multi-species contact-process-like one that we employed in Chapter 2 are: (i) that many species appear in our model and only two of them in the VM, and (ii) that in the VM the system is "saturated", in the sense that each single site is in one of the two possible opinions/alleles/species/labels/states, whereas in the model we study, some sites can be inactive, not belonging to any avalanche.

Regarding the first difference, for any given avalanche in the multi-species model, we can label it as "A" and the rest of species labeled together as "B", which is feasible given that they all obey the same dynamical rules, i.e. are neutral. In what respects the second point, general principles of statistical physics, relying on universality, indicate that such a difference should have little effect on avalanche exponents. As a matter of fact, looking at

the computational results for the dynamics of individual avalanches, such a difference is confirmed to be irrelevant.

Appendix B

Famous Models in Neuroscience

Here we briefly report notorious and successful models used in neuroscience, which succeeded in describing empirical behaviors of biological neural networks in a simple way, including minimal ingredients and catching the essential features of the system. To keep in mind those models will be useful in the following discussion.

B.1 Brunel Model

The model introduced by Nicolas Brunel in 2000 [22] defines the dynamics of a sparsely connected network of N excitatory and inhibitory leaky integrate-and-fire (LIF) neurons. On one hand, it allows an analytical approach to the description of the network and on the other hand, it unfolds and characterizes a reach repertoire of dynamical regimes, based on synchronization properties

of the underlying oscillating neurons. Leaky Integrate-and-Fire is one of the simplest dynamics to describe the membrane potential V_i of a neuron i. It reads:

$$\tau \dot{V}_i(t) = -V_i(t) + RI_i(t) \tag{B.1}$$

In words it states that the membrane potential $V_i(t)$ decays (polarizes) with time constant τ in absence of inputs, while it grows (depolarizes) by the effect of the incoming synaptic currents $I_i(t)$. Whenever the membrane potential reaches a threshold value θ, an action potential or "spike" is emitted (t_i^k indicates the time of the k^{th} spike of neuron i) and the membrane potential is reset to a value V_r, after a refractory period τ_{rp}, during which the potential is insensitive to stimulation. The synaptic current $I_i(t)$ is just the sum of all spikes contributions (modeled as delta functions):

$$RI_i(t) = \tau \sum_j J_{ij} \sum_k \delta(t - t_j^k - D), \tag{B.2}$$

where D is a transmission delay, $j = 1..C_{tot}$ runs over all connections to neuron i, i.e. excitatory, inhibitory and external $C_{tot} = C_E + C_I + C_{ext}$, with $C_{tot} \ll N$. External synapses (considered to be excitatory) are modeled as independent Poisson processes with rate ν_{ext} comparable to the frequency of spiking that would be generated if the system only had excitatory synapses and synaptic efficacy $J_{ij} = J$ for excitatory synapses and $J_{ij} = -gJ$ for inhibitory synapses.

In the limit in which a neuron needs many inputs to reach its threshold value, i.e. $J \ll \theta$, by virtue of Central Limit Theorem, the synaptic current can be

approximated by:

$$RI_i(t) = \mu(t) + \sigma\sqrt{\tau}\eta_i, \tag{B.3}$$

where $\mu(t)$ is related to the firing rate $\nu(t)$ (note that it is not dependent of the neuron index i) and η_i is a gaussian white noise such that, as a consequence of the sparse connectivity (every two neurons only share a small number of common inputs), $\langle \eta_i(t)\eta_j(t')\rangle = \delta(t-t')\delta_{ij}$. In other words this means that neurons can be considered as independent point processes sharing a common instantaneous firing rate: between t and $t+dt$, a spike has a certain probability to occur $\nu(t)$ for each neuron, but these events occur independently for different neurons. If the firing rate is time-dependent, then the network will show some degree of synchrony, since at times where $\nu(t)$ is big, statistically a big number of neurons spike. This change of perspective allows to define (and characterize) 4 different dynamical regimes:

- Synchronous Regular phase (SR): the firing rate is periodic; neurons are almost fully synchronized and their firing pattern is regular.

- Synchronous Irregular phase (SI): firing rate is time-dependent, although it does not oscillate in a periodic fashion; single nueron's spiking are irregular, as measured by an high *Coefficient of Variation* of Inter Spike Intervals[1].

- Asynchronous Regular phase (AR): the firing rate is sustained and its time dependence vanishes in the thermodynamic limit; neuron's spiking

[1]The Coefficient of Variation of a set $\mathbf{x}$ is defined as the ratio between the standard deviation and the mean of the set, $CV_{\mathbf{x}} = \frac{\sigma(\mathbf{x})}{\mu(\mathbf{x})}$

pattern is almost periodic ($CV_{ISI} \simeq 0$).

- Asynchronous Iregular phase (AI): the firing rate is sustained andstationary but with strongly irregular individual firing (high CV_{ISI}).

Versions of the model including different timescales for excitatory and inhibitory synapses were also considered, but this did not introduce any new dynamical regime.

B.2 Wilson Cowan Model

The Wilson-Cowan model considers mean field description of a large-scale neocortical homogeneous population of excitatory and inhibitory neurons [98]. Usually the equations are thought to describe a cortical column, a densely connected section of the cerebral cortex, composed by hundreds or thousands of neurons. The equations describing the dynamics of the activity (density of active neurons) for the two subpopulations E and I read [98]:

$$\begin{cases} \frac{dE}{dt} = -\alpha E + (1 - E) f(s) \\ \frac{dI}{dt} = -\alpha I + (1 - I) f(s), \end{cases}$$

where $f(s)$ is a sigmoid arbitrary response function, that for simplicity we fix to

$$f(s) = \begin{cases} \tanh(s) & s \geq 0 \\ 0 & s < 0 \end{cases}$$

and s is the incoming current

$$s = \omega_E E - \omega_I I + h.$$

which is simply the sum of all synaptic inputs, i.e. the sum of the whole excitatory and inhibitory activity weighted by their respective synaptic efficacy, plus an external small constant input current h. These simple equations state that for low incoming currents the activity of each population decays exponentially with a time scale specified by $1/\alpha$; on the other hand the activity grows up to a maximum saturation value $(E, I = 1)$ as a function of the incoming current s. According to this mean field approach, the connections between the cells within the described populations are assumed to be random and dense enough so that spatial heterogeneity can be neglected.

Despite its simplicity, the Wilson Cowan model encompasses a plethora of different possible scenarios, depending on the parameter values. The possibility to visually display and readily understand those scenarios using phase plane methods (together with the feasibility to analitically approach some issues) granted a big success to the model, considering that its collection of behaviors turned out to be very effective in describing a striking variety of experimentally observed neural behaviors, concerning both spontaneous and evoked activity, such as the existence of multiple stable states (Up-Down states), oscillatory behavior, simple and multiple hysteresis loops, together with the prediction that a weak stimulus produces dumped propagating waves whereas a stronger stimulus generates a more localized response [98, 187, 188, 189].

In a more recent work [97], Benayoun et al recovered WC model as the mean field limit of a coarse graining of a microscopic simple model. According to this model a spiking neuron is a binary unit, such that (i) each neuron is either active or quiescent (ii) the probability that each quiescent neuron becomes active depends on (a sigmoid function of) the total synaptic input and (iii) each active neuron decays at a constant rate. An all-to-all connectivity is considered at first, but the results are extended to a random sparse graph. Starting from this microscopic simple binary-neuron rate model Benayoun et al were able to recover Wilson-Cowan (mesoscopic) dynamics, through a Van Kampen system-size expansion [148]. Thus they determined the correct stochastic term to be added to D.9 to consider the effects of the finiteness of the population described. After a coarse graining of the master equation, the full stochastic equations read:

$$\begin{cases} \frac{dE}{dt} = -\alpha E + (1-E)\, f\,(s) + \sigma\sqrt{\alpha E + (1-E)\, f\,(s)}\eta_E \\ \frac{dI}{dt} = -\alpha I + (1-I)\, f\,(s) + \sigma\sqrt{\alpha I + (1-I)\, f\,(s)}\eta_I \end{cases}$$

where $\eta_{E,I}$ are gaussian white variables and the stochastic term is a demographic noise (given by the second moment of the jump probabilities), which decays with system-size and vanishes in the termodinamic limit.

B.3 Tsodyks-Markram model for Synaptic Plasticity

Synapses are the juctions between neurons, that is the points where neurons exchange information. Most of the time, electrical information traveling through the axon (*output terminal*) of the pre-synaptic neuron must be transformed into chemical activity, through the release of "neurotransmitters" that bind to receptors located in the membrane of the dendrite (*input terminal*) of the post-synaptic cell. It is a common belief that this synaptic dynamics, together with various mechanisms for its regulation are at the basis of memory storage and learning. In a celebrated paper [25] Misha Tsodyks and Henry Markram modeled, in a biologically plausible way, short term synaptic efficacy changes over time reflecting the history of presynaptic activity. In its simplified form TM model can be resumed into the dynamical equation for one variable, being the neurotransmitter resources $R(t)$ present in the presynaptic terminal:

$$R(t) = \frac{1}{\tau_R}(\xi - R(t)) - \frac{1}{\tau_D}S(t). \tag{B.4}$$

In words, this equation states that in absence of activity the synaptic resources recover to a baseline level ξ, with characteristic time $\frac{1}{\tau_R}$, whereas they get depleted with a timescale $\frac{1}{\tau_D}$ whenever the presynaptic terminal is emitting a spike. $S(t)$ is the spike train passing through the synapse, which can be seen as a sum of delta-like spikes (LIF model) $\sum_k \delta(t-t_k)$, where t_k is the k^{th} spiek of the presynaptic neuron, or, if considered in a coarse-grained fashion, $S(t)$ is

just the electrical activity of the network.

B.4 Millman Model

The model of Millman *et al.* [21] was introduced as a biologically realistic model able to reproduce robust SOC behavior in networks of non-conservative leaky integrate-and-fire neurons with short term synaptic depression, during Up states. We discuss largely about this model in Chapter 2 and analyse in detail the measure of the avalanches. This model consists of a population of N leaky integrate-and-fire excitatory neurons which are randomly connected in a directed graph to, on average, other K neurons in the population (i.e. forming a Erdős-Rényi network [190]). External inputs, $I_{\mathrm{e}}^{k}(t)$, are Poisson-distributed with rate f_e and internal inputs, $I_{\mathrm{in}}^{k}(t)$, are generated from spiking neurons in the network (k accounts for the input number). Both internal and external currents are modeled by exponentials functions of amplitude $w_{\mathrm{e/in}}$ and characteristic time τ_s, $I_{\mathrm{e/in}_i}^{k}(t) = w_{\mathrm{e/in}} \exp(-(t - t_{s_i}^{k})/\tau_s)$, where $t_{s_i}^{k}$ represents the corresponding spiking time of neuron i. Each individual neuron i is described by a dynamical variable V_i representing its membrane potential. When this value reaches a threshold value θ, the neuron spikes and it may open –with probability p_r– each of its n_r associated release sites per synapse, inducing a postsynaptic current. After spiking, the membrane potential is reset to the resting potential value, V_r, for a refractory period τ_{rp}, during which its dynamics is switched-off. Synaptic depression is implemented by means of a dynamical "utility" variable $U_{ij}(t) \in [0, 1]$ (for neuron i and release site j),

which modulates the release probability $p_r \to U_{ij}p_r$. The membrane potential obeys the following equation:

$$\begin{aligned}\dot{V}_i &= -\frac{V_i - V_r}{RC} + \sum_k \frac{I^k_{\mathrm{e}_i}(t)}{C} \\ &\quad + \frac{1}{C} \sum_{\substack{i' \in n.n.(i) \\ j,k}} \Theta(p_r U_{i'j}(t^k_{s_{i'}}) - \zeta^k_{i'j}) I^k_{\mathrm{in}_{i'}}(t),\end{aligned} \tag{B.5}$$

where R is the membrane resistance C its capacitance, k is the spike number, i' runs over presynaptic neurons linking to i, and j' over its release sites; $\zeta^k_{i'j'}$ is a uniform random number in $[0, 1]$ and $\Theta(x)$ the Heaviside step function. On the other hand, the synaptic utility U_{ij} is set to 0 immediately after a release and recovers exponentially to 1 at constant rate, τ_R:

$$\dot{U}_{ij} = \frac{1 - U_{ij}}{\tau_R} - \sum_k U_{ij}\Theta(p_r - \zeta^k_{ij})\delta(t - t^k_{s_i}). \tag{B.6}$$

As equations (B.5) and (B.6) are linear during successive events, they can be integrated exactly, which allowed us to implement both synchronous (or clock-driven) and asynchronous (or event driven) methods [191], leading to essentially indistinguishable results. Versions of the model including inhibitory couplings were also studied, but this did not alter the main conclusions.

Appendix C

Disclaimer on Up Down states

Originally Up and Down states refer to single neuron states in which the neuron, after firing, remains in two possible preferred subthreshold states: one very hyperpolarized, the so-called Down state and one more depolarized, so-called Up state. [54, 192, 98]. Nevertheless in [54] it was proposed that the existence of Up and Down states is fundamental and inherent property of a whole neural ensemble. Consequently a vast part of the literature (see for instance [89, 55, 21]) have assumed the use of the words "Up and Down states" for slow coherent oscillations in the cortex similar to those seen during deep sleep or anesthesia, or, more in general to a bistability shown at the whole-network scale, where the two stable states are characterized by high and low levels of activity respectively. Although it would be more correct to talk about high and low activity states, here for convenience we inherit the (slightly improper) use of "Up and Down states" when referring to collective properties of a whole network.

Appendix D

Supplementary informations

D.1 Supplementary information to Chapter 2: Neutral theory of neural avalanches

Here we discuss some details and minor results on the neutral theory of neural avalanches, discussed in Chapter 2.

D.1.1 Total density of activity at stationarity in the minimal model

Neglecting fluctuations from finite size effects, the dynamics of the total density of activity for the process described by Eq.(2.1) becomes deterministic in the limit $N \to \infty$:

$$\dot{\rho} = (\lambda(1-\rho) - \mu)\rho + \epsilon(1-\rho), \tag{D.1}$$

whose stationary solution, $\dot{\rho} = 0$, is

$$\rho^* = \frac{\lambda - \mu - \epsilon + \sqrt{4\epsilon\lambda + (\lambda - \mu - \epsilon)^2}}{2\lambda}. \tag{D.2}$$

Up to first order in ϵ, Eq.(D.2) can be written as

$$\rho^* \simeq \begin{cases} \dfrac{\epsilon}{\mu - \lambda} & \text{if} \quad \lambda < \mu \\ 1 - \dfrac{\mu}{\lambda} + \epsilon \dfrac{\mu}{\lambda(\lambda - \mu)} & \text{if} \quad \lambda > \mu. \end{cases} \tag{D.3}$$

D.1.2 Avalanche statistics for Down states in the model of Millman et al.

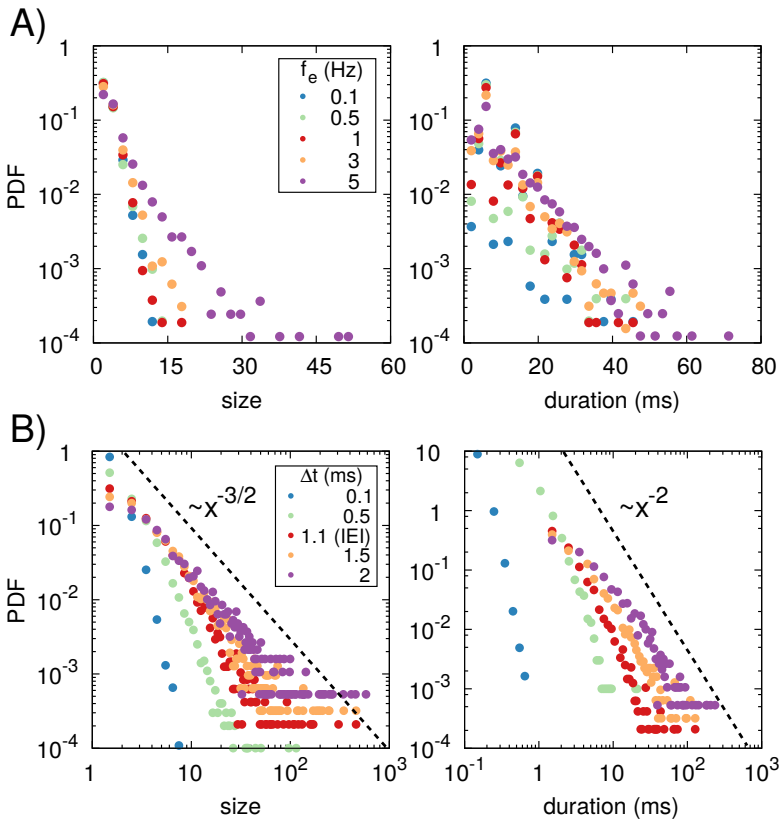

Figure D.1: Avalanche size and duration distributions relative to periods of low activity (Down states) for timeseries generated with the model of Millman *et al.* [21] using two different methods. Panel A (linear-logarithmic plot): "Causal" avalanches were defined using the same criterion as in [21], for several values of the external input f_e, confirming the observation that sizes and durations are exponentially distributed. Panel B (double logarithmic scale): "Time-correlated" avalanches, defined with the standard temporal binning method [9] (which ignores causal information), using five different time intervals Δt to bin the data, including one coinciding with the average interevent interval (IEI) as usually done in the analyses of empirical data [9], for $f_e = 5$ Hz. In all cases, simulations were performed in a network of $N = 3000$ neurons (model parameters as in [21]).

D.1.3 Causal avalanches in the model with inhibitory synapses

Main results presented above are robust under the introduction of inhibitory synapses. Following [21], we run simulations of the model for which 20% of the neurons are initialized as inhibitory (so their output current has amplitude $-w_{\text{inh}}$) and, to keep the network balanced, each single neuron receives $k_i = k = 10$ inputs, 2 of which are from inhibitory ones. The introducing of inhibitory currents increases the coefficient of variation of spiking times, leading to enhanced variability. Still, as above, there exists a wide region of the parameter space, within the Up state (active phase) where causal avalanches keep showing scale-invariant behavior (see Fig. D.2). More specifically, this happens whenever the amplitude of the inhibitory current is not too strong (so as to allow for the Up state to exist) and for values of the inhibitory synaptic timescale up to four times larger than the excitatory one.

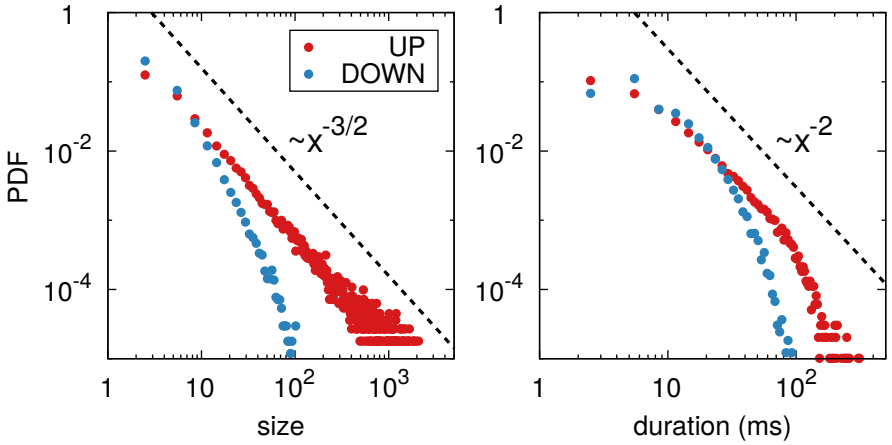

Figure D.2: "Causal" avalanche size (Left) and duration (Right) distributions in the model of Millman *et al.* including inhibitory synapses. The avalanche statistics exhibit a robust power-law scaling with the same exponents of a critical branching process (marked with dashed lines for comparison) with the Up state, while they are exponentials, with a characteristic scale in the Down state. Simulations were performed in a network of $N = 3000$ neurons setting the inhibition amplitude to $w_{\text{inh}} = 50$ pA, and other parameters as in [21].

D.1.4 Avalanche statistics in the minimal model for activity propagation

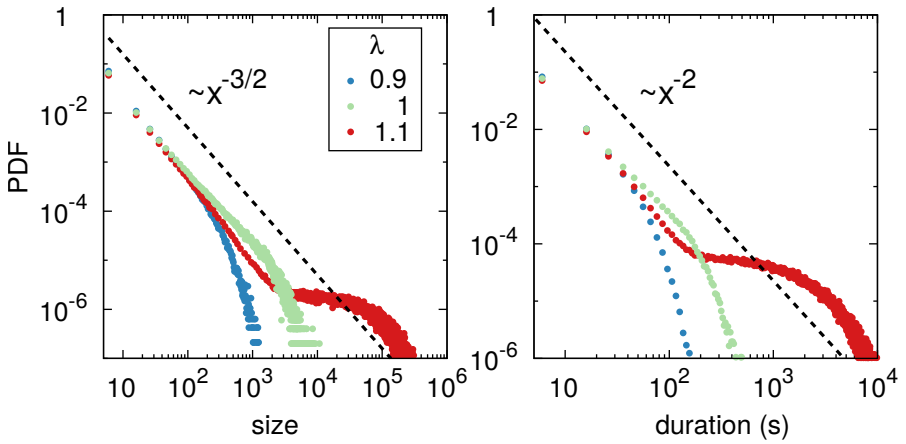

Figure D.3: Avalanche size (Left) and duration (Right) distributions in the minimal model for activity propagation when avalanches propagate in the network one at a time, i.e. without overlap between avalanches. This is done by setting $\epsilon = 0$ and introducing one single active node each time the activity stops. Distributions are plotted for different values of the activation rate λ in the quiescent phase ($\lambda = 0.9$), active phase ($\lambda = 1.1$) and at criticality ($\lambda = 1$), illustrating the PDFs are not scale-invariant, except right at the critical point. Parameter values are: $\mu = 1$, $N = 10^3$.

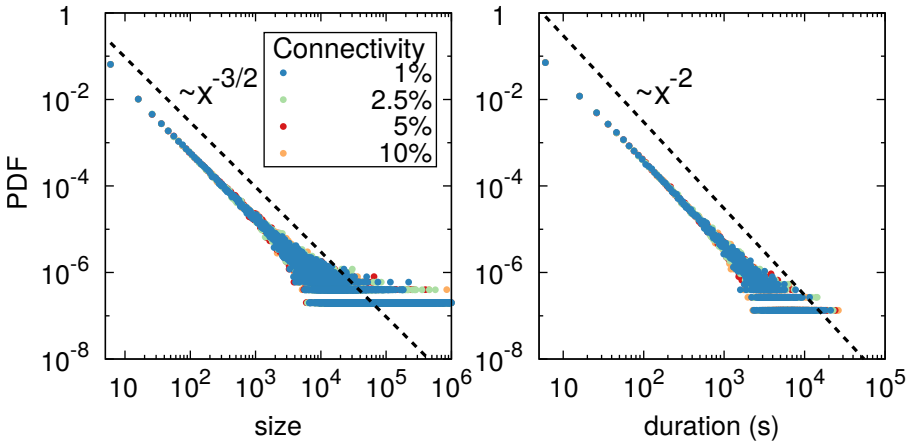

Figure D.4: 'Causal" avalanche size (Left) and duration (Right) distributions in the minimal model for activity propagation on a directed random network with limited connectivity. In all cases, avalanche statistics exhibit a robust power-law scaling with the same exponents of the fully-connected (undirected) network. Parameter values are: $\mu = 1$, $\lambda = 2$, $\epsilon = 10^{-3}$, $N = 10^4$ (the total activity is $\rho \simeq 0.5$).

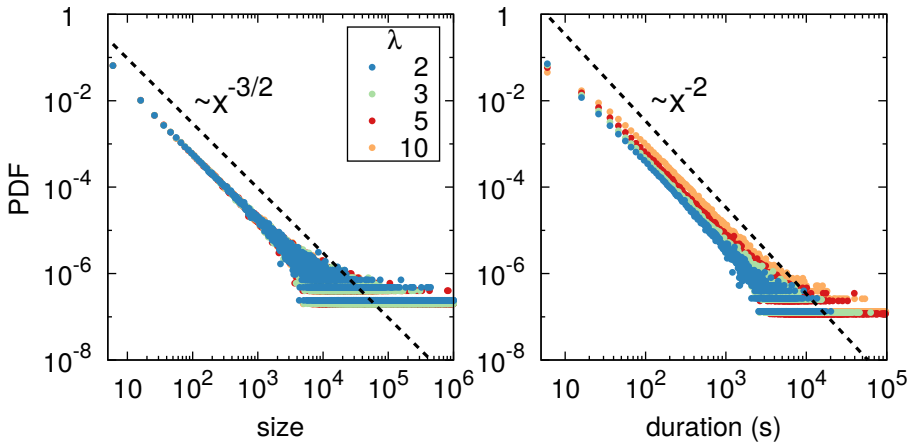

Figure D.5: "Causal" avalanche size (Left) and duration (Right) distributions in the minimal model for activity propagation when multiple avalanches coexist in the network, for different values of the activation rate λ along the active (UP) phase (corresponding to stationary densities around $\rho^* = 0.5$, 0.66, 0.8 and 0.9, respectively). In all cases, avalanche statistics exhibit a robust power-law scaling with the same exponents of a critical branching process (marked with dashed lines for comparison). Increasing the spreading rate results in an enlargement of the mean duration of avalanches, with negligible effect on the size distributions. Parameter values are: $\mu = 1$, $\epsilon = 10^{-3}$, $N = 10^4$.

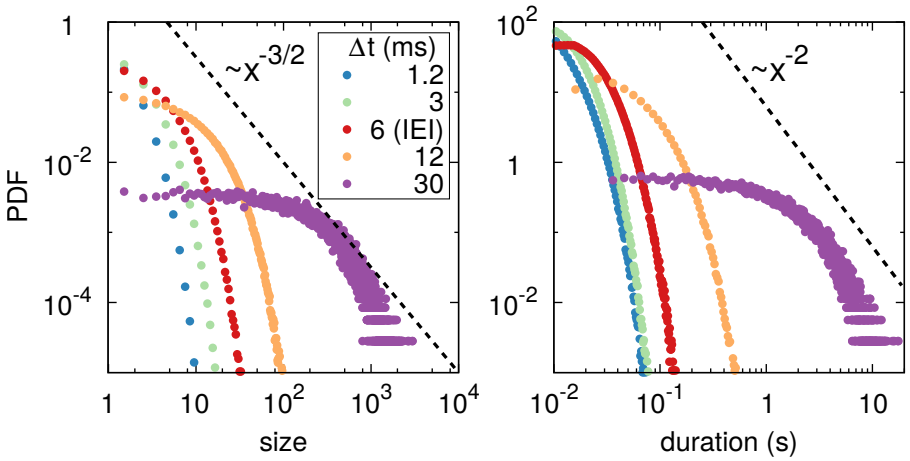

Figure D.6: "Time-correlated" avalanche size (Left) and duration (Right) distributions in the minimal model for activity propagation, computed with the standard temporal binning method [9], using five different time intervals Δt to bin the data, including one coinciding with the average interevent interval (IEI). In this case distributions do not obey a power-law distribution but have a characteristic scale. Parameter values are: $\mu = 1$, $\lambda = 2$, $\epsilon = 10^{-3}$, $N = 10^3$ (the total activity is $\rho \simeq 0.5$).

D.2 Supplementary information to Chapter 3: Self-organized bistability

D.2.1 The role of Spatial Heterogeneity

Spatial heterogeneity is ubiquitously present in real systems, and often it is an important ingredient to take into account, since it can change drastically the behavior of the system.

A general result in statistical mechanics proves that discontinuous transitions cannot possibly occur in 2D disordered systems at thermodynamic equilibrium [193, 194, 195]. This conclusion has been recently extended to more general systems, not necessarily at equilibrium, including stochastic systems undergoing phase transitions into absorbing states [196]. In fact local differences in environmental conditions can generate regions that are more prompt to collapse and others that are more resilient, giving rise to patchy and irregular activity patterns [68]. A recent work confirming the results in [196], investigates the prevention of catastrophic shifts on spatially extended noisy systems undergoing first order absorbing phase transitions [68], and shows that any amount of spatial heterogeneity smoothens the transition, so that the collapse from the active phase to the quiescent one occurs in a rather gradual way in the disordered system. Moreover the analysis reported in [68] explained the appearance of a Griffiths phase (i.e. a broad region around the transition point in which power law scaling is observed [114]) due to a progressive deterioration of the more unfavorable regions, generating successive collapses of the more

resilient zones, in a step by step fashion.

Here we want to briefly address this issue in the SOB framework focusing on quenched disorder (i.e. cases where disorder does not change with time): is environmental disorder a sufficient ingredient to smoothen the abrupt transition in presence of a self-organization dynamics? Or, in other words, does spatial heterogeneity transform SOB into SOC? To study explicitly the consequences of heterogeneity in a system described by Eq.(3.1), we include a spatial, quenched disorder into the system, more precisely we add disorder (separately) on the *facilitation parameter* b and on the *threshold parameter* D_E.

D.2.2 Disorder on the *facilitation parameter*

In this section we assume the facilitation parameter b to be position-dependent, i.e. $b \to b(x)$. The value of $b(x)$ at each location x is randomly extracted from a uniform distribution in the interval defined by β_1 and β_2:

$$P(b) = \mathcal{U}(\beta_1, \beta_2). \tag{D.4}$$

In Fig.D.7 we plot the distribution of duration and size of avalanches, comparing the dishomogeneous case with the homogeneous case $P_{homog}(b) = \delta(b - \bar{b})$. In particular, since we want to compare the avalanches stemming from dishomogeneous versus homogeneous case, we choose the fixed value $\bar{b}$ in the homogeneous case to coincide with the mean value of the uniform distribution of $b(x)$, i.e. $\bar{b} = \mathbb{E}[P(b)]$. We observe that there is no appreciable difference be-

tween the two cases, suggesting that this kind of quenched disorder is irrelevant for the SOB mechanism. Please note that also in the case where the uniform distribution is nonzero for positive values of b, meaning that some sites are not facilitated, the system behaves as if there was no spatial heterogeneity at all. This countertrend with respect to the previous evidences [68, 196] must be due to the presence of the energy field. In fact the existence of a background field may allow to compensate the spatial heterogeneity, rearranging locally in such a way to correlate with the values of $b(x)$ and thus balance the effects of the disorder. In order to test this idea, we analyze the correlations between $b(x)$ and $E(x,t)$ for the case of the upper panel of Fig.D.7. We evaluate the variable

$$C(t) = \frac{\langle E(x,t)b'(x)\rangle - \langle E(x,t)\rangle\langle b'(x)\rangle}{s[E(x,t)]s[b'(x)]}$$

where $\langle . \rangle$ and $s[.]$ represent respectively the average and the standard deviation, summing over x and $b'(x) = -b(x)$. In Fig.D.8 we see that $C(t)$ seems to tend to a value close to -1 for $t \to \infty$, meaning that in the stationary state the energy field anti-correlates with the *facilitation field* $-b(x)$, thus compensating the quenched disorder. Interestingly the small periodic jumps that we see in Fig.D.8 are compatible with the characteristic duration of king avalanches in this case $\sim 6.2 \times 10^3$.

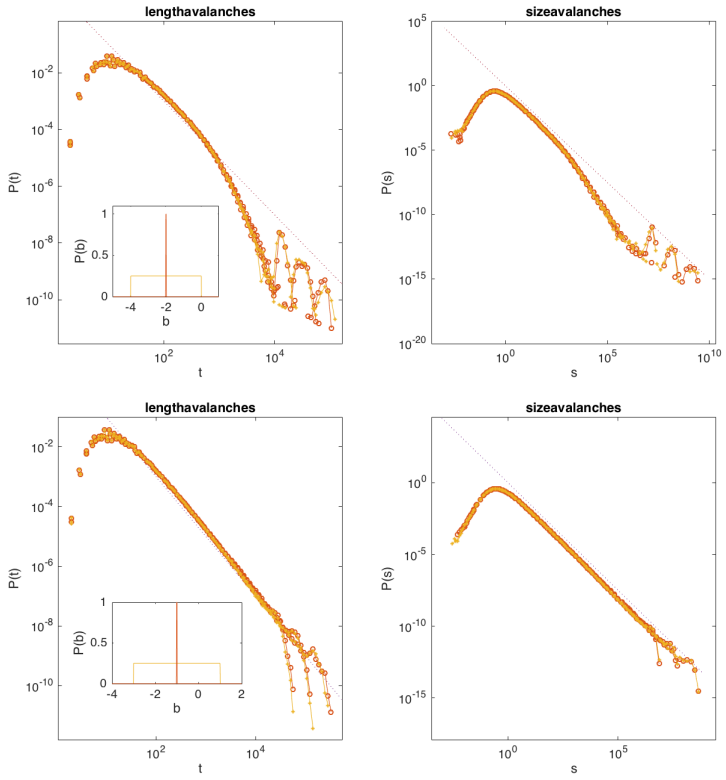

Figure D.7: Distribution of duration and size of avalanches for system sizes $L = 2^6, 2^7, 2^8$. We compare the avalanches for the homogeneous case $b(x) = \bar{b}$ (red) with the heterogeneous case, for which $b(x)$ is uniformly distributed (yellow). We plot distributions $P(b)$ in the insets with same color code. In the upper panel the choice of $\bar{b}$ sets the system in the *King-avalanche dominated regime*, whereas in the lower panel system is in the *Hybrid regime*. Other parameters are $a = -1.3, \omega = c = D = \sigma = 1$.

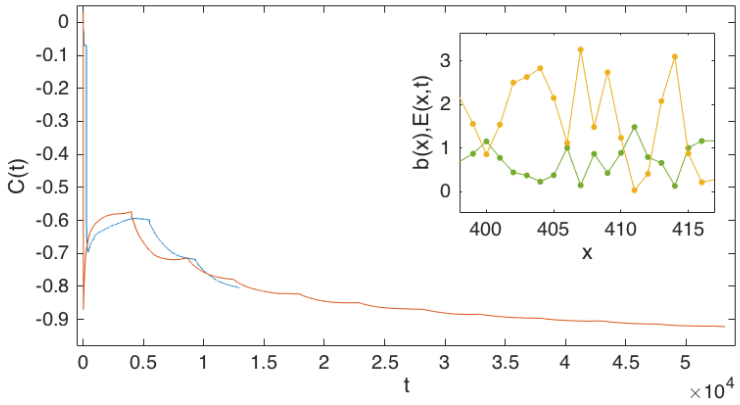

Figure D.8: Time evolution of the Correlation variable $C(t)$ for a system of linear size $L = 2^5$ and other parameters as in the upper inset of Fig.1. In the inset there is a sketch of the two fields $b'(x)$ and $E(x,t)$, for a particular choice of a $t \gg 1$: we see that where b' is big E is small and *vice versa.*

D.2.3 Disorder on the *threshold parameter*

Here we analyze the case $D_E \to D_E(x)$,

$$P(D_E) = \mathcal{U}(\Delta_1, \Delta_2). \tag{D.5}$$

Analogously to the previous case we make a comparison with the homogeneous case $P_{homog}(D_E) = \delta(D_E - \bar{D}_E)$, with $\bar{D}_E = \mathbb{E}[P(D_E)]$. Also in this case the disorder doesn't seem to affect qualitatively the avalanches statistics. As shown in Fig.D.9 the only difference is that the *kings* in the heterogeneous case are slightly bigger.

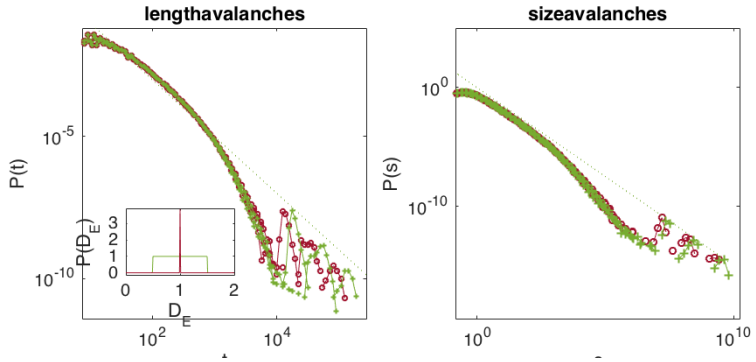

Figure D.9: Distribution of duration and size of avalanches for system sizes $L = 2^6, 2^7, 2^8$. Comparison between the homogeneous case $D_E(x) = \bar{D}_E$ (dark red) with the heterogeneous case (green).

D.2.4 Topological disorder

All of the results above have been obtained for 2D systems. However, some of the reported noise-induced effects might depend profoundly on the system dimensionality. Thus, we now discuss the dependence of the behavior of the system from the dimensionality of the underlying network topology. For 1D systems, fluctuation effects are expected to be extremely severe. Indeed, existing analytical arguments predict that stochasticity completely washes away discontinuous transitions into absorbing states, converting them into continuous ones [62]. Thus, catastrophic shifts into quiescent states cannot possibly occur in 1D systems.

As we are interested in shedding light on brain behaviour, we consider a hierarchical modular network (HMN) that has been recently found to play a crucial role in neural dynamics [197]. Here we use a simple structural model to build-up synthetic HMNs as follows: local densely connected moduli are used as building blocks; they are recursively grouped by establishing additional inter-

moduli links in a level- dependent way, as exemplified in Figure D.10. Further details of the construction methods can be found in [114]. A crucial feature of HMNs is represented by their finite topological dimension D. The topological dimension of a network can be defined as follows: starting from a single node, the number of neighbors N_z reachable after z steps is computed for increasing z until the entire network is covered [198]. The network is finite dimensional with dimension d if $\langle Nz \rangle \sim z^d$, generalizing the familiar behavior of regular lattices. The topological dimension of a HMN can be tuned easily, by changing the average number α of links between pairs of modules at each hierarchical level (see Fig.D.10 and [114]).

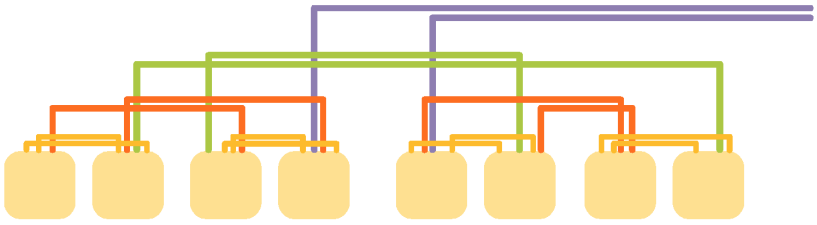

Figure D.10: Sketch of the HMN construction method. Given a positive integer s, consider 2^s basal fully connected moduli of size M. At the lowest hierarchical level, moduli are linked pairwise into super-moduli by establishing a fixed number α of random unweighted and undirected links between the elements of each modulus ($\alpha = 2$ in figure). Newly formed blocks are then iteratively linked pairwise with the same α for a total of s iterations, until the network becomes connected. The resulting network has size $N = 2^s M$.

We considered different HMNs, characterized by different topological dimensions d. In particular, we show results for $d = 1.6$ and $d = 2.8$ (networks with such properties are obtained by choosing $\alpha = 1$ and $\alpha = 4$ respectively.

Dissipation is included by declaring $4\sqrt{N}$ nodes as boundary nodes. First we plot the diagram of the transition in the fixed-energy ensemble (Fig.D.11). We observe that, while for $d = 2.8$ first order maintains and that the coexistence region is wider, for $d \sim 1.6$ the discontinuity smoothens and the transition becomes second order transition.

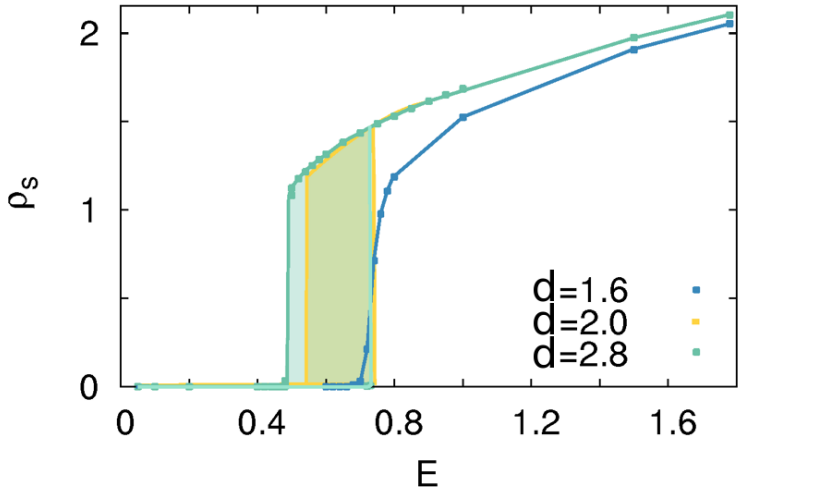

Figure D.11: Phase diagrams (steady-state density as a function of E) for different topological dimensions of the network, $d = 2.8, d = 2$, and $d = 1.6$. We plot in the fixed-E ensemble. Parameters: $b = 2, N = 212, a = 1.3, \omega = c = D = \sigma = 1$.

Secondly we analyzed the distribution of SOC avalanches for the considered topological dimensions. Preliminary results (not shown) for the exponents of the distributions are compatible with linear interpolation between SOC systems with closest integer dimensions. Then we explored the effect of topology on a SOB system (hybrid regime, $b = -1$). For $d = 2.8$, SOB behaviour is recovered and, interestingly, for $d = 1.6$, two different regimes seem to appear; SOB regime for smaller (and more densely connected) neighborhood and SOC

regime for larger (and sparser connected) scales. Those results are preliminary checks and further analyses are undoubtedly needed in order to elaborate firm conclusions.

In summary, whereas for quenched disorder the background field is able to counteract and compensate its effects, in the case of topologcal disorder on hierarchical modular networks, the smaller the spatial dimension, the more likely fluctuations play a fundamental role, potentially breaking SOB behavior and generating a much more gradual and smooth transition.

D.3 Supplementary information to Chapter 4: Synchronization phase transition

D.3.1 Model details

In the Wilson-Cowan model the dynamics of the average firing rate or global activity, ρ, is governed by the equation

$$\dot{\rho}(t) = -\rho\,(t) + (1-\rho)S\,(W\rho\,(t) - \Theta)$$

where W is the synaptic strength, Θ is a threshold value, and $S(x)$ is a sigmoid (transduction) function, e.g. $S(x) = 1/2(1 + \tanh(x))$ [98, 97]. We adopt this well-established model and, for simplicity, keep only the leading terms in a power-series expansion, yielding the deterministic part of Eq.(D.13). To this we add noise $\sqrt{\rho(t)}\eta(t)$ –which is a delta-correlated Gaussian white noise of zero mean and unit variance, accounting for stochastic/demographic effects in finite local populations as dictated by the central limit theorem; a formal derivation of such an intrinsic or demographic noise, starting from a discrete microscopic model can be found in [97]). A noise term could be also added to the equation for synaptic resources [55], but it does not significantly affect the results. Considering N mesoscopic units, and coupling them with some networked structure (e.g. a two dimensional lattice), we finally obtained the set of Eqs.(4.3).

D.3.2 Analytic signal representation

The Hilbert transform $\mathcal{H}(\cdot)$ is a bounded linear operator largely used in signal analysis as it provides a tool to transform a given real-valued function $u(t)$ into a complex analytic function, called the *analytic signal representation*. This is defined as $\mathcal{A}_u(t) = u(t) + i\mathcal{H}[u(t)]$ where the Hilbert transform of $u(t)$ is given by: $\mathcal{H}[u(t)] = h * u = \frac{1}{\pi}\lim_{\epsilon\to 0}\int_\epsilon^\infty \frac{u(t+\tau)-u(t-\tau)}{\tau}d\tau$. Expressing the analytic signal in terms of its time-dependent amplitude and phase (polar coordinates) makes it possible to represent any signal as an oscillator. In particular, the associated phase is defined by $\phi_k^{\mathcal{A}} = \arctan Im(\mathcal{A}_k)/Re(\mathcal{A}_k)$.

Let $u(t)$ be a real function such that $u(t) \in \mathbb{L}^p(\mathbb{R}), 1 \leq p < \infty$, then the Hilbert transform of $u(t)$ is given by the convolution $u(t)$ with the (non integrable) function $h(t) = 1/\pi t$:

$$\mathcal{H}[u(t)] = h * u = \frac{1}{\pi} p.v. \int_{-\infty}^{\infty} \frac{u(\tau)}{t-\tau}d\tau = \frac{1}{\pi}\lim_{\epsilon\to 0}\int_\epsilon^\infty \frac{u(t+\tau)-u(t-\tau)}{\tau}d\tau,$$

where $p.v.$ indicates the Cauchy principal value of the integral. The Hilbert transform $\mathcal{H}(\cdot)$ is a bounded linear operator largely used in signal analysis because it allows to transform real functions into analytic functions, the *analytic signal* $z_u(t)$ of the input $u(t)$ being defined as

$$z_u(t) = u(t) + i\mathcal{H}[u(t)].$$

Expressing the analytic signal in terms of its time-variant amplitude and phase (polar coordinates) allows us to look at the local signals of our problem as

oscilators, and thus measure their synchronization through the Kuramoto parameter. The envelope of the signal is just the amplitude of the analytic signal. The Hilbert transform is a particular case of the so called singular integral operators studied by Caldern and Zygmund and it is closely related to the Dirichlet problem, which consists of looking for a harmonic function that is continuous on a domain and assumes certain continuous values on the boundary of the domain. Here we will not get much into the mathematical details and we will not prove the particular form of the Hilbert transform, but we will illustrate a simple example of calculation of the envelope of a signal. Given a signal $u(t) = \sin \omega t$, its Hilbert transform is

$$\mathcal{H}[u(t)] = \frac{1}{\pi} \lim_{\epsilon \to 0} \int_{\epsilon}^{\infty} \frac{\sin \omega(t+\tau) - \sin \omega(t-\tau)}{\tau} d\tau = \tag{D.6}$$

$$= \frac{2 \cos \omega t}{\pi} \lim_{\epsilon \to 0} \int_{\epsilon}^{\infty} \frac{\sin \omega \tau}{\tau} d\tau = \cos \omega t. \tag{D.7}$$

Hence the analytic signal is

$$z_u(t) = \sin \omega t + i \cos \omega t$$

and its amplitude is $a(t) = 1$, which coincides with the envelope of the original function.

D.3.3 Phases from spiking patterns

An alternative method to define a phase at each unit can be constructed after the continuous timeseries has been mapped into a spiking series. In particular,

$\phi_k^{(\mathcal{B})}(t) = 2\pi(t - t_n^k)/(t_{n+1}^k - t_n^k)$ where $t \in [t_n^k, t_{n+1}^k)$ and t_n^k is the time of the n^{th} spike of node/unit k.

D.3.4 From continuous timeseries to discrete events

Local timeseries at each single unit, $\rho_k(t)$, can be mapped into time sequences of point-like ("unit spiking") events. For this, a local threshold $\theta \ll 1$ is defined, allowing to assign a state on/off to each single unit/node (depending on whether it is above/below such a threshold) at any given time. If the threshold is low enough, the procedure is independent of its specific choice. A single (discrete) "event" can be assigned to each node i, e.g. at the time of the maximal ρ_i within the on-state; a weight proportional to the integral of the activity time series spanned between two consecutive threshold crossings is assigned to each single event (see Fig.4.5A). Other conventions to define an event are possible, but results are not sensitive to it as illustrated in the SI.

D.3.5 Robustness of the results against changes the dynamics

In this Section we confirm the robustness of the results and conclusions presented in the main part with respect to the modification of various ingredients and modelling details. In particular, we first discuss the full model with synaptic plasticity (as in the Main Results Section), but without truncating the equation for activity, and second we consider inhibition as encapsulated in

the well-known Wilson-Cowan equations (rather than synaptic plasticity) as a chief regulatory mechanism.

Non-truncated excitatory-activity equation

The dynamics in a mesoscopic region of the cortex or "unit" is described by a Wilson-Cowan equation [98] for the excitatory activity –such that the activity grows with the incoming current through a sigmoid response function– together with the Tsodyks-Markram (TM) model for synaptic plasticity [81]:

$$\begin{cases} \dot{\rho} = & -\alpha\rho + (1-\rho)\tanh\left(a\rho R + p\right) + h \\ \dot{R} = & \frac{1}{\tau_R}\left(\xi - R\right) - \frac{1}{\tau_D}\rho R. \end{cases} \tag{D.8}$$

In Figure D.12, we show that a linear-stability analysis reproduces a Hopf bifurcation scenario, as in the most relevant case (case A) discussed in Chapter 4. When noise and spatial coupling are added, and the system is integrated on a two-dimensional lattice, a synchronous irregular regime of network spikes as well as an asynchronous irregular regime of nested oscillations are found. These regimes, which are graphically illustrated by the lower panels of Figure D.12, are fully analogous to their corresponding counterparts in the case of the Main Results Section, unveiling the existence of a synchronization transition in between them. This confirms that the simplified truncated equation for the activity considered in the text is a valid approximation of the full dynamics. Here we do not show a detailed analysis of the synchronization transition nor of the emergence of scale-free avalanches; but, let us remark that we have not

found any relevant difference with respect to the case discussed in the paper in any of our exploratory checks.

Inhibition as main regulatory mechanism

In this section we consider the Wilson-Cowan equations [98] , including both excitatory and inhibitory neural populations for each mesoscopic region or unit. In this case, inhibition plays the role of chief homeostatic mechanism, regulating the level of the overall network activity. More specifically, we consider a version of the Wilson-Cowan dynamics, including also intrinsic noise as corresponds to large but finite (mesoscopic) regions. Such a model was derived in a very interesting work from an underlying microscopic model [97], and is described by the following set of stochastic equations for the densities of excitatory (E) and inhibitory (I) neurons:

$$\begin{aligned}
\dot{E}_i &= -\alpha E_i + (1-E_i)\tanh\left[\omega_{EE}E_i - \omega_{IE}I_i + h\right] + \\
&+\sigma\sqrt{\alpha E_i + (1-E_i)\tanh\left[\omega_{EE}E_i - \omega_{IE}I_i + h\right]} \\
\dot{I}_i &= -\alpha I_i + (1-I_i)\tanh\left[\omega_{EI}E_i - \omega_{II}I_i + h\right] + \\
&+\sigma\sqrt{\alpha I_i + (1-I_i)\tanh\left[\omega_{EI}E_i - \omega_{II}I_i + h\right]}\,,
\end{aligned} \tag{D.9}$$

where α is the decay rate for the activity, h is an external driving field, σ is the noise amplitude, and ω_{ij} (with $i,j = E,I$) are the couplings between population i and j within a single unit; particularly important here is the auto-excitation coupling ω_{EE}, which we take as a control parameter. First of all, these equations are analyzed in the (noiseless) mean field limit. By increasing

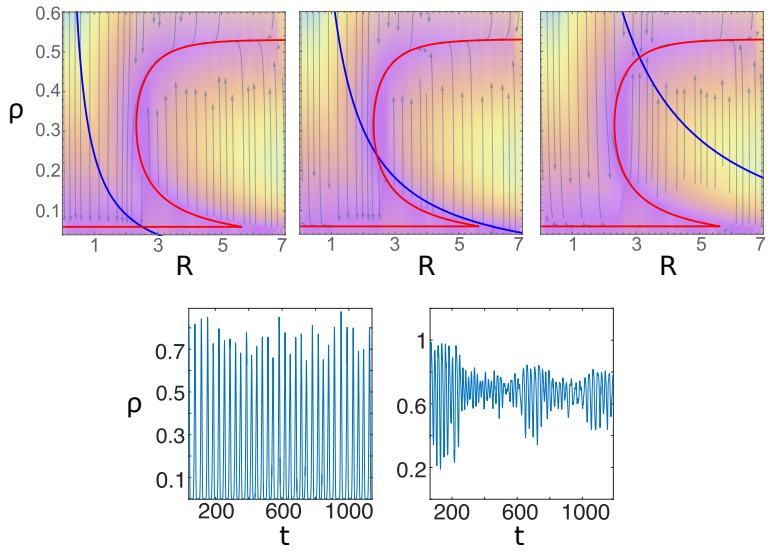

Figure D.12: Analysis of the model of Eq. D.8. Upper panels: deterministic phase portrait with $\xi = 5, 12, 28$ (from left to right). respectively. showing a down state, a limit cycle and up state regimes, as in the case A in Chapter 4. Other parameters are $\alpha = a = 1$, $\mu = 0.033$, $\tau = 500$, $p = -0.34$, $h = 0.06$. Varying parameter values, it is possible to find either a similar Hopf bifurcation (case A) or a saddle node bifurcation (case B), as in the model with the truncated expansion. Lower panels: Temporal evolution of the total activity $\rho(t)$ on a two-dimensional lattice with $N = 64^2$ (after having introduced noise and coupling); in the (left) synchronous (network spiking) and in the (right) asynchronous (nested oscillations) regimes, respectively, revealing the presence of a synchronization phase transition in between the two regimes; parameter values: $\xi = 5$ and $\xi = 13$, respectively.

ω_{EE}, the system exhibits a transition from a "down" state to an "up" state (see Fig. D.13). Thus, a saddle-node bifurcation separates a state of high activity from a state of low activity, we found no track of a possible Hopf bifurcation. However, very interestingly, as soon as noise is switched on (i.e $\sigma \neq 0$), a noise-induced phenomenon appears: trajectories nearby the up-state fixed point, can escape from its basin of attraction as a result of fluctuations, and are then almost deterministically driven towards the down state, where a similar mechanism makes them escape with some probability. This phenomenon has been recently scrutinized in a very interesting work, where the role of non-normal forms has been emphasized [97]. This mechanism, generates in an effective way a noise-induced limit cycle between up and down states, which plays the same role as the deterministic limit cycle (Hopf bifurcation) of case A described above. As a matter of fact, computer simulations of units described by Eq.(D.9), and coupled diffusively, give rise to the phenomenology illustrated in Fig.D.13: as the control parameter ω_{EE} is increased, the system undergoes a phase transition from a synchronous phase with very distinctive network spikes, to an asynchronous regime with nested oscillations, as it happens in the model with synaptic plasticity. Thus, also in this case, the phases are the same as in the Main Results Section and a synchronization transition appears between them.

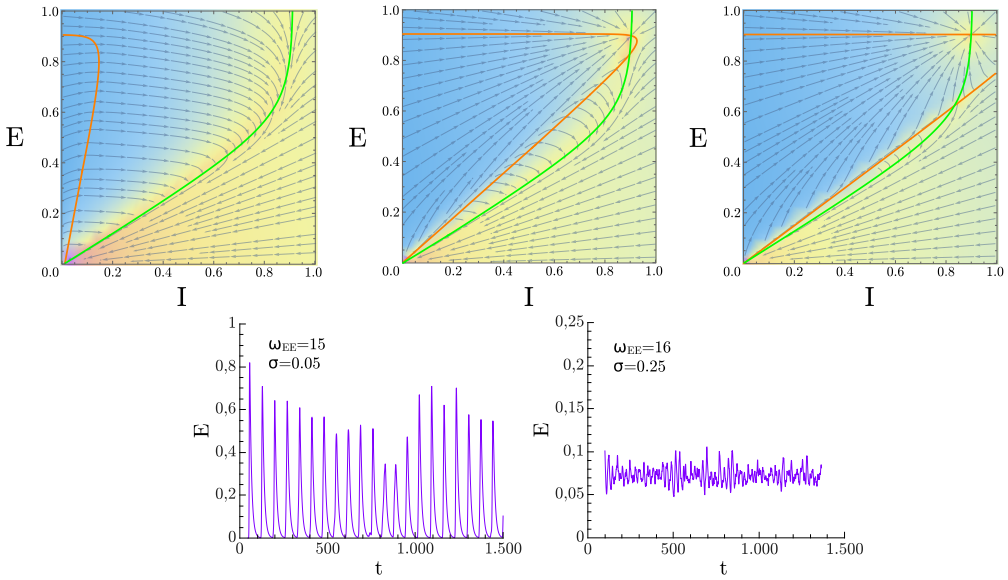

Figure D.13: Upper panels: mean-field analysis of the Wilson-Cowan set of Eqs. (D.9) describing both excitatory and inhibitory neural populations at each single unit, with parameters such that a noise-induced limit cycle (see [97]) in between a down and an up state can emerge once a non-vanishing noise is switched on. Observe that there is (left) a stable down-state fixed point ($\omega_{EE} = 4$) and a (right) stable up state ($\omega_{EE} = 16$); however the basin of attraction of the up state is small, and a relatively small fluctuation can induce the system state to go beyond the saddle-node line, where deterministic trajectories take the system toward the down state. In the lower panels we illustrate results of a computer simulation for a two-dimensional lattice of coupled noisy units, Eq.(D.9), corresponding to (left) synchronous/network-spiking and (right) asynchronous/nested-oscillation regimes. Parameter values: $D = 1$, $\omega_{EI} = 4.65$, $\omega_{IE} = 14.0$, $\omega_{II} = 2.8$, $h = 10^{-3}$ and $\alpha = 0.1$. Control parameter $\omega_{EE} = 15$ for SI regime and $\omega_{EE} = 16$.

D.3.6 SI2. Robustness against changes in synaptic time scales, diffusion and noise

As discussed in Chapter 4, there are two possible scenarios according to the relation between the timescales for the recovery and depletion (τ_R and τ_D, respectively). Namely, between the quiescent or 'down' state with $\rho^* \approx 0$ and the active or 'up' state with self sustained activity there exists a stable limit cycle (case A) or a regime of bistability (case B). Fixing parameter values while changing τ_R and τ_D, it is possible to construct a (mean-field or deterministic) phase diagram showing the different possible cases that emerge when the control parameter ξ is varied (cases A and B). As shown in Fig. D.14 when the recovery time (τ_R) is much bigger than the depletion time (τ_D) the system is in the case A, while for bigger values of the depletion time (τ_D) it falls into the case B with a transitions between up (active) and down (quiescent) states. We

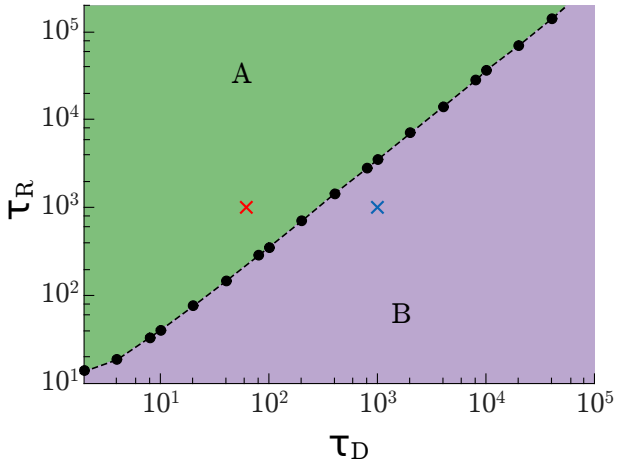

Figure D.14: Mean-field phase diagram showing the type of transition for different values of τ_R and τ_D. Red (blue) cross show the particular case chosen in the Fig.1 of the main text for the case A (B). Parameter values are $a = 0.6, b = 1.3, h = 10^{-3}$.

have also explored the behavior of the system against changes in the diffusion constant D. Figure D.15 shows the phase diagram for different values of D and some particular temporal series with the aim of characterize the different possible behaviors. As can be observed, there exists a transition from the synchronous irregular phase to the synchronous regular one for a wide range of D values (e.g. from $D = 0.01$ (red line) to $D = 2$ (violet line), and $D = 4$ (green line)). If D is set to very large values, the system falls into the mean field expected behavior, switching from the network spiking regime to the up state. Similar conclusions are obtained, by fixing D and decreasing the noise amplitude σ.

D.3.7 The effect of long-range connections and network heterogeneity

The detailed map of synaptic connections plays a central role in brain function [103]. Even if most of the neuronal connections occur within the local neighborhood, long-range white-matter connectivity allows for information to be distributed and processed across the whole cortex. Such long-range connections comprise only about 10% of the total connections in the brain, but their role is crucial for brain functionality [112, 103].

Small-world topology

As the simplest possible approximation beyond a lattice of nearest neighbor connections, and consistently with [112], we built a small-world network, as

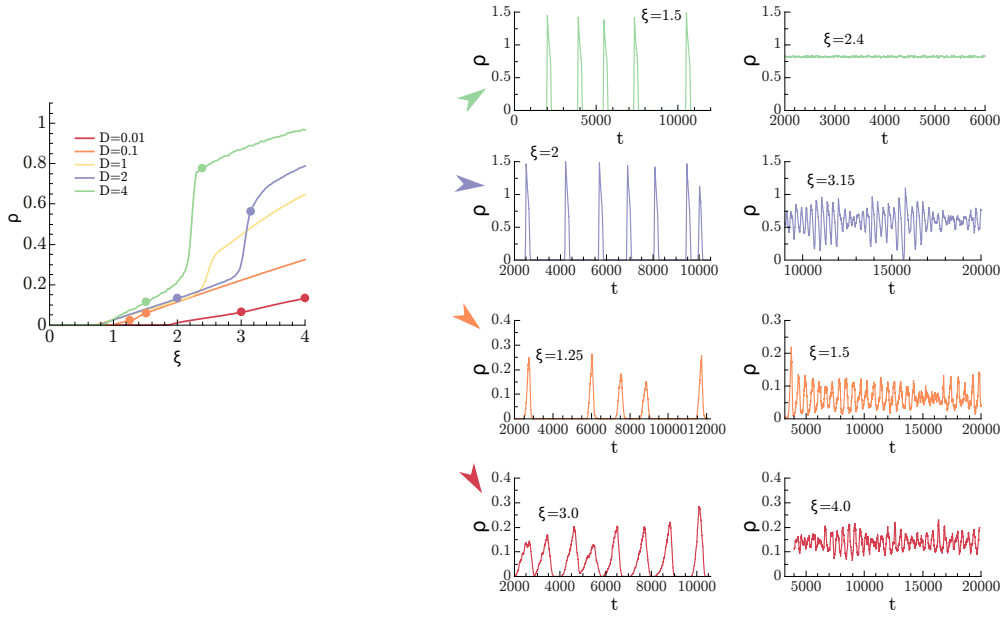

Figure D.15: Left panel: Order parameter as a function of the control parameter ξ for various values of the diffusion constant D. Right panel: Temporal series for two particular values of ξ for each value of D, (marked with colored points in the left panel), showing the expected behavior. Low values of D show a transition between the synchronous irregular phase to the asynchronous irregular one, as in the main text (red, orange, violet and green line). Parameter values: $a = 1.0, b = 1.5, \tau_R = 10^3, \tau_D = 10^2, h = 10^{-7}$.

done in the Watts-Strogatz model [199], by rewiring 10% of the links of a two-dimensional lattice. We explored the phase space of the model defined by Eqs. 1 and 2 of the main text, on this connectivity architecture (see Fig.(D.16) upper panel), and observed that the leading features described in the paper (i.e. phases and phase transitions) are preserved when long-range interactions are introduced. Indeed, as illustrated in the lower part of Fig.(D.16), our computational analyses reveal that the emergence of synchronous and an asynchronous phase, with a synchronization transition in between is a general intrinsic feature of our model, which is not modified by the small-world prop-

erty of the network. In any case, it is important to remark that even if the main phases remain unaffected, important details such as the extension of such phases, the specific shape of avalanches, the amplitude of nested oscillations, the broadness of the critical-like region etc. could be potentially sensitive to the introduction of network heterogeneity. Some of these aspects are explicitly illustrated in the forthcoming paragraphs.

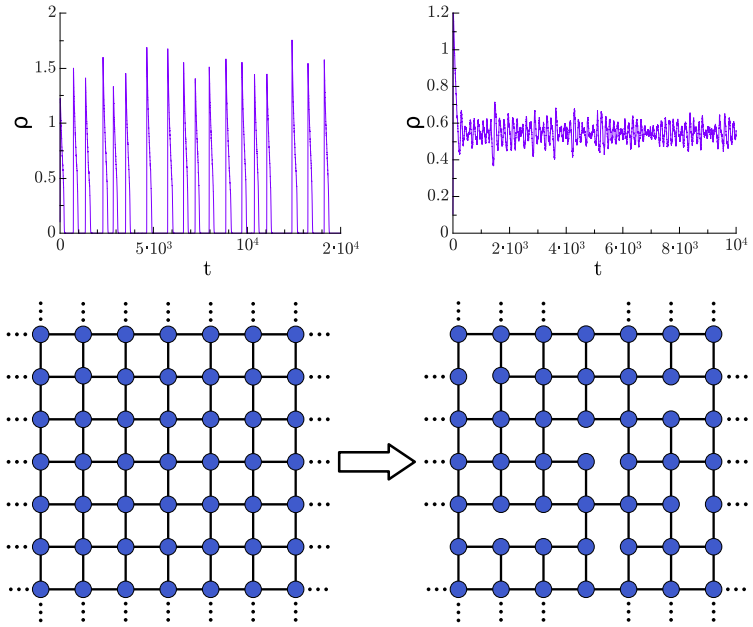

Figure D.16: Upper panel: sketch of the rewiring procedure defining a small-world network architecture: a ten percent of the links are rewired, in such a way that the average connectivity is preserved. Lower panel: Plots illustrating the results of computational analyses of the dynamics (main text, Eq. 1 and 2); in particular, temporal series of the global electrical activity in a small world lattice for two different values of control parameter ξ; (left, $\xi = 2.8$) synchronous/network-spike regime, and (right, $\xi = 2.96$) asynchronous/nested-oscillation regimes, respectively; a synchronization phase transition exists separating these two alternative regimes. Other parameter values: $a = 1.0, b = 1.5, \tau_D = 10^2, \tau_R = 10^3, h = 10^{-7}$.

D.3.8 Detrended Fluctuation Analysis

In this section we present an additional type of analyses to discriminate whether the system lays at a critical point or in either the subcritical or the supercritical phases. The method is based on the fact that, at the critical point of a (second order) phase transition, the (time-dependent) order parameter, as measured in any finite system, shows long-range temporal correlations (long-memory effects), which can be quantified by measuring its Hurst exponent [200]. The Hurst exponent of a time series is a measure of the dispersion of a process on a scaling support. For example the Hurst exponent of an uncorrelated signal (white noise) is $\alpha = 1/2$, since the root mean square translation distance after n steps of a Wiener process, i.e. an unbiased random walk (the process obtained by integrating white noise), is proportional to $\sqrt{n}$. For correlated signals (colored noises) one expects bigger Hurst exponents (as a reference, $\alpha \simeq 1$ is found for pink noise). The Hurst exponent can be calculated by splitting the time series into adjacent windows, plotting the square-root displacement from the mean as a function of the window size and evaluating the exponent of the resulting power law (see below). More specifically, "detrended fluctuation analysis" (DFA) is a technique for measuring the Hurst exponent in a non-stationary time series: the "detrending" operation allows to remove fictitious memory effects related to non-stationarity, and the method basically consists in subtracting the local "trend" (usually a linear fit approximation) of the signal before performing the analysis on each window [109, 201]. DFA consists of two steps: the data series $\rho(t)$ is shifted by its mean $\bar{\rho}$ and integrated

(cumulatively summed) in time:

$$\mathcal{P}(\tau) = \sum_{t=1}^{\tau} (\rho(t) - \bar{\rho})\,; \tag{D.10}$$

then segmented into windows of various sizes n, and in each window a fluctuation function $F(n)$ is calculated, as

$$F(n) = \sqrt{\frac{1}{T}\sum_{h=1}^{k}\sum_{\tau=1}^{n}\left(\mathcal{P}^{(n)}(\tau + (h-1)n) - X_{\mathcal{P}}^{(n)}\right)^2} \tag{D.11}$$

where $X_{\mathcal{P}}^{(n,h)}$ is the linear regression of $\mathcal{P}^{(n)}(\tau)$, with $\tau \in [(h-1)n, hn]$, the superscript indicates the dependence on the window size n and $T = kn$ is the total length of the time series. If $F(n) \sim n^{-\alpha}$, then α is the Hurst exponent [109, 110]. We performed a DFA on the global signal $\rho(t)$ coming out of our computer simulations for different values of the control parameter ξ (in the synchronous and asynchronous phases as well as at the critical point). Results are shown in Fig.D.17: (i) fluctuations in the asynchronous phase grow approximately as the square root of the window length, as expected for (uncorrelated) white noise; (ii) in the synchronous phase, above a certain characteristic length, the dependence is very weak, remarking the existence of a certain degree of order, i.e. a characteristic time scale at which there is order, i.e. synchronization; (iii) just at the critical point the growth of the fluctuations is anomalously large, confirming the existence of long-range correlations: a signature of criticality. Therefore, from the global activity signal we are able –through a DFA analysis– to conclude that long-range correlations, characteristic of criticality, emerge at the transition point.

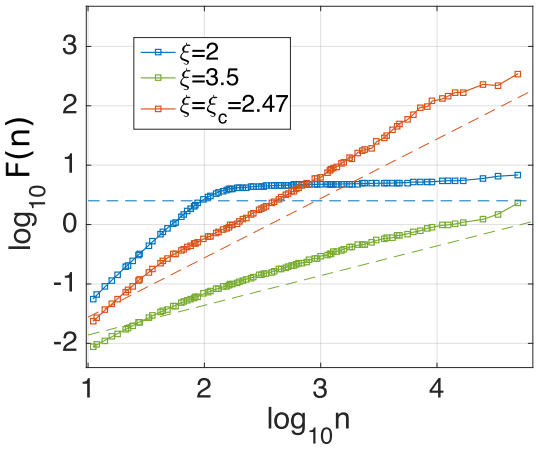

Figure D.17: Detrended fluctuation analysis of the macroscopic signal for different values of the control parameter $\xi = 2$ (synchronous phase) $\xi = 2.47$ (critical point), and 3.5 (asynchronous phase), respectively. Close to the transition point the DFA shows an Hurst exponent close to 1 (orange dashed line) implying long-range autocorrelations, a fingerprint of criticality, while the white noise value $\alpha = 1/2$ (green dashed line) emerges in the asynchronous regime, and an asymptotically almost flat curve is obtained in the synchronous phase, revealing the existence of a characteristic time scale. Parameter values are taken as in the main text and $N = 2^{14}$.

D.3.9 The nature of nested oscillations

In order to unveil the nature of the nested oscillation (asynchronous irregular) phase and to determine whether it is a finite size effect or it survives in the thermodynamic limit, the existence of a second phase transition separating it from the up state is investigated here. In other words: are the asynchronous irregular phase and the up-state phase two different phases, or are they just the same phase, with only a quantitative difference in the amplitude of the variability around the mean value? As we illustrate in what follows the correct answer is this second one. The fraction of inactive units, ρ_0, can thus be chosen as an order parameter for the putative phase transition between the AI and the active phase. In Figure D.18 we plot the average over time of ρ_0 in function of ξ and we verify that this alternative order parameter detects the same phase transition already characterized in the main text, by employing synchronization order parameters. This implies that, in the large system-size limit, there exists no macroscopic difference between the asynchronous/nested-oscillation regime and the up state. Therefore, the nested oscillations can be understood as the result of partial synchronization of local regions; the superposition of a few regions gives rise to complex waves as those in Fig.2 (A3) of the main text. However, when the system becomes progressively large, the number of such locally synchronized regions grows, and their interference leads to a standard up state, in which fluctuations around the mean density decay as a function of the system size.

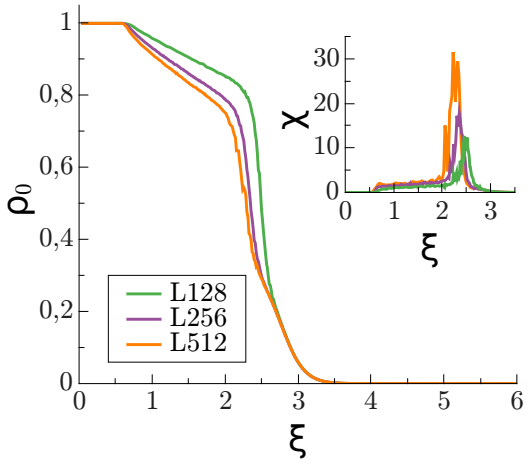

Figure D.18: Main: averaged fraction of inactive sites in the system ρ_0 as a function of the control parameter ξ, revealing the presence of a phase transition. Inset: Variance over runs of a given fixed duration of the average value of the control parameter multiplied by $\sqrt{N}$ in order to highlight possible deviations with respect to central limit theorem (CLT); as a result of which, a decay with $\sqrt{N}$ is expected; thus multiplying by $\sqrt{N}$ a convergence to a constant should be expected if the CLT holds. Observe, however, the increase in peak height as the system size is enlarged revealing a violation of the CLT, as expected at the critical point of a second order phase transition. Note that for all the system sizes the peaks are located approximately in the same spots as in Fig.4.3; thus ρ_0 is an alternative order parameter that leads to the same results as the previously considered synchronization order parameters: it detects the synchronization phase transition, and reveals that there is no difference between the AI and the active phase in the limit of infinitely-large network sizes.

D.3.10 On the definition of Avalanches

Since the individual signal in our analysis stems from a coarse grained section of neural tissue, we assign a weight to each event, representing the number of spikes in the section and determined by the integral of the signal during the event (see 4.5A). Thus the only difference between the procedure we employ and the experimental one [9] (see Chapter 6) is that the size of an avalanche is defined in our case as the *weighted* sum of the events during an avalanche.

On the definition of spiking events

In the analysis of avalanches presented in the Main Results Section, a particular (and reasonable) criterion has been chosen to convert each local (continuous) time signal into a discrete series of spikes, allowing to build up the raster plot, from which avalanches are measured using the standard experimental protocol consisting on a time-clustering the events [9]. Here, we employ a different criterion to define spikes, thereby illustrating the robustness of our main findings against such a choice. In particular, the alternative discretization criterion is sketched in Figure D.19 and is as follows: a threshold θ is established at each single unit, and every unit is declared to be in its *spiking* state whenever its activity is over threshold. Thus, the main difference with the protocol in the Main Results Section is that now, in between two-consecutive time steps in which the unit is below threshold, the site is considered to be "on" not just not just at one time step (at its maximum of activity, as in the method of the main text), but possibly during many time steps, in a full time interval.

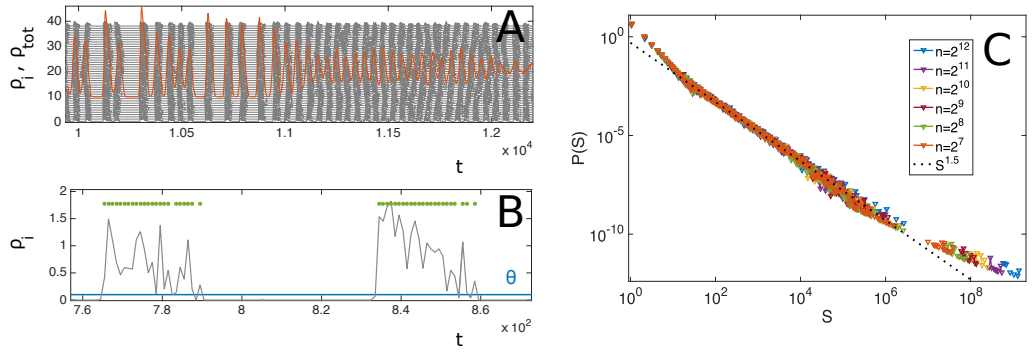

Figure D.19: A.Sample of local temporal signals are plotted in grey (shifted for convenience of visualization) together with the global signal $\rho(t)$ (shifted and rescaled) represented in red color, for a lattice of $N = 64^2$ units. B. illustration of the alternative method employed here to define "spike events" from a local temporal signal. Green dots represent times during which the unit is in its spiking state; obviously, a discrete (integration) time is required to have a finite number of spikes per interval of local activity. C. Distribution of avalanche sizes for various subsampling trials, using the criterion sketched in B to define events. The black dotted line is the power law with exponent 3/2 plotted as a guide to the eye.

Considering these spiking events, avalanches are defined through the same experimentally inspired protocol that we used in the Main Results Section; the size of an avalanche is simply the number of spike counts during an avalanche. Figure D.19 shows that the avalanche size distribution at the critical point is preserved by employing this alternative definition of the spikes. Moreover if a (random) subsampling of the units is performed, the distribution keeps following a power law consistent with experimentally measured exponent 3/2.

Threshold effects

The standard empirical method to detect avalanches, as defined in [9], is intrinsically affected by some arbitrariness in parameter choices, that has been already discussed in the literature [9, 10] (see Chapter 6). In particular, one arbitrary parameter is the threshold value θ above which the state "on" or "spiking" is declared In order to avoid spurious effects and consistently with the definition of avalanches as activity propagating marginally before falling into an absorbing state ($\rho = 0$), we choose a small value $\theta \ll 1$ (namely $\theta = 10^{-4}$). The common belief is that if, as a matter of fact, the system is scale-invariant, this value should not affect the large scale properties, such as exponent values. However, one has to be particularly careful with any thresholding procedure. For example, while for a standard one-dimensional random-walk process the avalanche exponents are independent of the threshold value chosen, this is not the case for other stochastic processes, e.g. birth-death processes [158]. Moreover the threshold value should not be chosen too high relatively to the amplitude of the signal in order to avoid splitting an event into multiple (correlated) ones [157]. Recording a spike every time that the system crosses a very small threshold exposes the measurements to the effects of small fluctuations around the origin, induced by the multiplicative demographic noise term in Eq.4.3 in the main text (see Fig. D.20). In order to avoid such a problem, it is possible to set also a second threshold value A_{min} for the minimal area for a spiking event to be considered as such; below such a threshold, activity is considered just a noise effect (not a proper spike) and, hence, disregarded. As illustrated in Figure D.21 the statistics of avalanches

does not depend significantly on the value chosen for such a threshold, A_{min}.

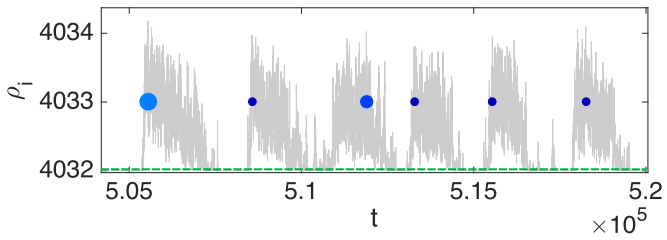

Figure D.20: Illustration of small events in the signal of the activity of one unit. Events covering a very small area (marked with red crosses) are neglected, while proper spikes are marked with blue full dots (smaller darker dots correspond to spikes with smaller area).

System-size dependence

At the critical point of a phase transition, scale-invariant behavior is expected to be only limited by system size. This effect, which was also reported to be observed in experiments on neural avalanches, e.g. reducing the number of electrodes used for the data analyses [9], is also a hint in favor of true scale invariance, since finite size scaling holds when the system is at its critical point. In Figure D.22 avalanche size and duration distributions are compared for various system sizes. Apart from the underlying structure (which is discussed in D.3.10), as expected, larger systems show larger avalanches with progressively larger cut-off scales, while the overall size (resp. time) distribution keeps following a power law trend with the usual exponents $\tau = 3/2$ (resp. $\alpha = 2$; see inset).

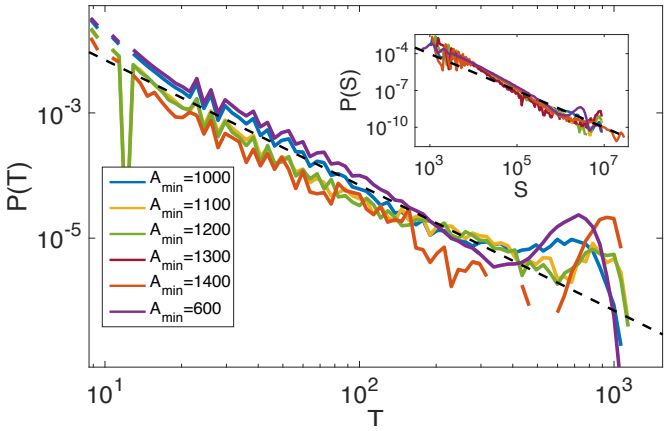

Figure D.21: Independence on the avalanche exponent values on the value chosen for the threshold on the minimal area A_{min}, used to declare "activity". Apart from the details of the substructure of the distribution, no qualitative dependence can be found by varying the value of A_{min}, both in avalanche-time (main plot) and avalanche-size (inset) distributions.

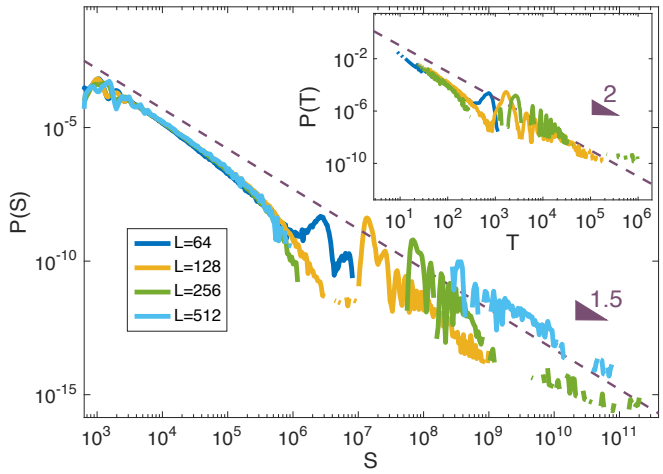

Figure D.22: Avalanche size S and duration T distributions for system sizes $L = 2^6, 2^7, 2^8, 2^9$. Although finite size scaling is not perfect, as the system size grows bigger, bigger avalanches are found. Dashed lines represent an hypothetic power law trend with $\tau = 3/2$ and $\alpha = 2$.

Oscillations coexisting with scale invariance

Usually, scale-free avalanches of activity can be measured at the critical point of an *absorbing-state phase transition*. When the concept of "avalanche" is employed to describe the critical point of a synchronization phase transition, the marginal oscillatory nature of the system unavoidably introduces a characteristic time scale –i.e. the period of the oscillation– which, in principle, is in contrast with the idea of scale-invariance. However, the two concepts can coexist –at least within certain limited scales– as illustrated in Figure D.24. Here we show how the structure (e.g. the peaks) in the avalanche-time distribution (inset) corresponds to the period of oscillation of a macroscopic variable (the total number of spikes, in the main plot); for instance, an isolated network synchronization event has a typical duration of 2000 (in arbitrary units), a sequence of two, about 5000, etc. On the other hand, the whole distribution, once these peaks are ignored can be approximately described as a power law with the expected exponent values.

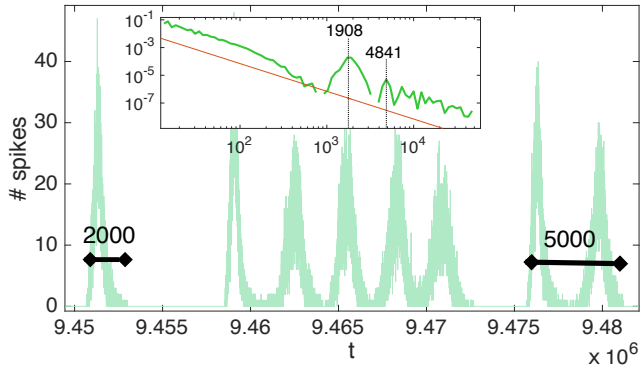

Figure D.23: Analysis of the structure underlying the avalanche-duration distributions. The main figure shows the total number of spikes at time t. Irregular oscillations of the global activity can be recognized, as the system is close to the edge of the synchronization phase transition. The characteristic period of an isolated oscillation corresponds to the peak in the avalanche duration distribution, while its multiples correspond to smaller peaks. System size $N = 128^2$.

D.4 Supplementary information to Chapter 5: A simple unified view of branching process statistics: random walks in balanced logarithmic potentials

D.4.1 Irrelevance of non-linear terms

For the directed percolation class in the mean-field limit, where spatial heterogeneity is neglected, Eq.(5.1) reduces to

$$\dot{\rho}(t) = a\rho - b\rho^2 + \sqrt{\rho}\eta(t). \tag{D.12}$$

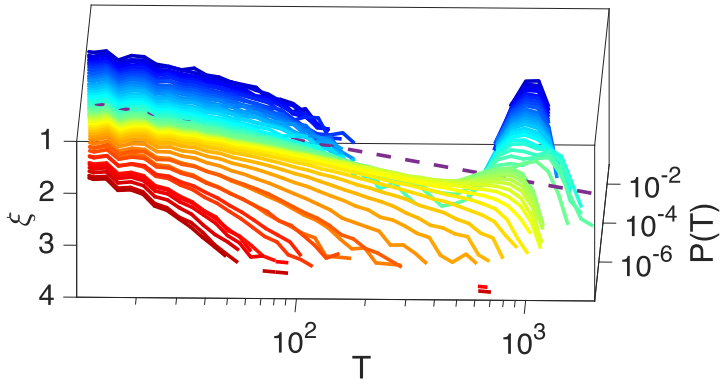

Figure D.24: Duration distribution for various values of the control parameter ξ. Only close to the critical point the distribution is (almost) scale-free with exponent consistent with the value 2 reported in experimental literature. Supercritical distributions show marked peaks corresponding to single oscillations of the whole network and subcritical settings show exponential cutoff for relatively low values of avalanche durations. System linear size L=64.

At criticality, i.e. $a = 0$, there is still a non-linear (saturation) term $-b\rho^2$ which introduces a characteristic maximal activity scale, thus apparently precluding scale-invariance. The way out of this apparent conundrum is that when studying avalanches in discrete/particle models, activity is created at a single location, and in the continuous limit, this corresponds to vanishing density of activity, $\rho = 0$. Thus, one needs to consider a large but finite system size, say Ω (e.g. one could think of a fully connected network with Ω nodes), and perform a finite-size scaling analysis. Defining y by $\rho = y/\Omega$ then –up to leading order in Ω– Eq.(D.12) reduces to $\dot{y}(\tilde{t}) = \sqrt{y}\eta(\tilde{t})$ where $\tilde{t} = \Omega t$. In other words, employing the correct rescaled variables y and $\tilde{t}$ the saturation term is never "seen" by the expanding avalanche, which is compatible with the density being equal to zero, as the avalanche invades an infinitely large system. Observe that in the main text we keep the notation with ρ and t, for

the sake of simplicity.

Similarly, the voter-model (or compact directed percolation [70] or neutral theory) class –characterized by two symmetric absorbing states– is described, as said above, by the Langevin equation [131]

$$\dot{\rho}(t) = D\nabla^2\rho(\mathbf{r},t) + \sqrt{\rho(1-\rho)}\eta(\mathbf{r},t), \tag{D.13}$$

which, again, ignoring spatial dependencies and rescaling the variables, readily becomes the DRW equation, Eq.(5.6). The very same reasoning applies also to the other universality classes discussed in the Introduction (i.e. dynamical percolation and the Manna class); also in these cases the corresponding non-linear terms, describing saturation effects vanish upon properly rescaling the system.

On the other hand, beyond the mean-field limit, the non-linearities are essential and control the "renormalized" values of the avalanche exponents (see e.g. [202]), which differ for the various universality classes [65, 138], and avalanches can develop non-symmetric shapes [203].

D.4.2 First-return time distributions

Following the general result of A. Bray [150] (see also F. Colaiori [72]), here we summarize the computation of avalanche exponents for a random walk in

a logarithmic potential. The general Fokker-Plank equation reads [47]

$$\frac{\partial P(x,t)}{\partial t} = \mu \frac{\partial}{\partial x}\left(\frac{\partial P(x,t)}{\partial x} + \frac{\beta}{x}P(x,t)\right). \tag{D.14}$$

To calculate the probability distribution $F(T)$ of the return times at which a walker starting close to the origin ($P(x,0) = \delta(x-\epsilon), \epsilon \to 0$) first hits back the origin, the absorbing boundary condition $P(0,t) = 0$ needs to be imposed. Note that $F(T)$ is minus the probability flux at 0, $F(T) = -j(0, t = T)$, with

$$j(0, t = T) = -\mu \left[\frac{\partial P(x,t)}{\partial x} + \frac{\beta}{x}P(x,t)\right]_{x=0}. \tag{D.15}$$

One can try a solution of the Eq.(D.32) of the form $P(x,t) = r(x)\exp(-\mu k^2 t)$ and note that the resulting equation can be converted into a Bessel Equation with the change of variable $r(x) = x^{\frac{1-\beta}{2}}R(x)$,

$$x^2 R''(x) + xR'(x) + \left(k^2x^2 - \nu^2\right)R(x) = 0, \tag{D.16}$$

where $\nu = (1+\beta)/2$. The general solution of this last equation is a linear combination of Bessel functions of the first kind of order $\pm\nu$. Putting the pieces back together, employing the orthogonality property of the Bessel functions, and imposing the initial condition, leads to

$$\begin{aligned} P(x, t \mid \epsilon, 0) &= \left(\frac{x}{\epsilon}\right)^{1-\nu} \epsilon \int_0^\infty dk k [A J_\nu(k\epsilon) J_\nu(kx) \\ &+ B J_{-\nu}(k\epsilon) J_{-\nu}(kx)] e^{-\mu k^2 t}, \end{aligned} \tag{D.17}$$

where A and B are numerical constants. The integral in Eq.(D.34) gives the modified Bessel function of the first kind $I_{\pm\nu}$ and, it is easy to compute the flux at the origin in the small ϵ limit [150, 72], leading to Eq.(5.10).

Following the general result of Bray[150] and Colaiori [72], we revise the analytics behind the calculus of avalanche exponents of a Random Walk in a Logarithmic Potential, from a different point of view.

The corresponding Fokker-Plank equation reads [47]

$$\frac{\partial P(x,t)}{\partial t} = \mu \frac{\partial}{\partial x}\left(\frac{\partial P(x,t)}{\partial x} + \frac{\beta}{x} P(x,t)\right) \tag{D.18}$$

From this equation we can readily calculate the stationary distribution $P_{st}(x)$ such that $\partial_t P_{st}(x) = 0$:

$$P_{st}(x) = \mathcal{N} x^{-\beta}$$

We observe that if we put in our Langevin equation a constant shift term h, it gave here as an exponential cutoff term $\exp(-hx)$.

As we stated above, our aim is to calculate the distribution of avalanches, that, stated in other words, is the probability distribution of the times at which the particle first reaches the origin (*first passage time probability*), having started its motion close to the origin. This determines the initial condition that we need:

$$P(x,0) = \delta(x-\epsilon), \tag{D.19}$$

where we will take the limit $\epsilon \to 0$.

To complete the definition of our system we need a boundary condition that we choose to be absorbing.

$$P(0,t) = 0 \tag{D.20}$$

This choice means that the probability current (defined as $\partial_t P(x,t) = -\partial_x j(x,t)$) calculated in the origin must be incoming ("something might arrive into the origin, but nothing will exit"), hence $j(0,t) \leq 0$.

We also note that this probability current (with the opposite sign) coincides exactly with what we need: the probability of entering into the origin at time t, which will necessarily be the first passage into the origin because after being absorbed we remove the particle from the system.

So, once we solve the time-dependent Fokker-Plank equation, our result will follow straightforward as:

$$F(0,t) = -j(0,t) = \mu \left[\frac{\partial P(x,t)}{\partial x} + \frac{\beta}{x} P(x,t) \right]_{x=0}. \tag{D.21}$$

In order to solve the Fokker Plank equation, first of all we note that it is homogeneous, thus we can assume a solution of the form $P(x,t) = r(x)\exp(-\mu k^2 t)$. Now our Fokker-Planck equation reads

$$x^2 r''(x) + \beta x r'(x) + (k^2 x^2 - \beta) r(x) = 0$$

The latter equation can be converted into a Bessel Equation with the change

of variable $r(x) = x^{\frac{1-\beta}{2}} R(x)$:

$$x^2 R''(x) + xR'(x) + \left(k^2 x^2 - \nu^2\right) R(x) = 0, \tag{D.22}$$

where we defined $\nu = (1+\beta)/2$. The general solution for the previous equation is a linear combination of Bessel Functions of the First Kind of order $\pm\nu$. Hence, putting the pieces back together, we can write an implicit full solution of the form

$$P(x,t) = x^{1-\nu} \int_0^\infty dk \left[\phi(k) J_\nu(kx) + \psi(k) J_{-\nu}(kx)\right] \exp(-\mu k^2 t).$$

If we remember now the orthogonality property of the Bessel functions

$$\int_0^\infty dk k J_a(kx_1) J_b(kx_2) = \delta_{ab} \frac{\delta(x_1 - x_2)}{x_1},$$

imposing the initial condition will give us the expression for $\phi(k)$ and $\psi(k)$. Indeed we have

$$P(x,0) = \delta(x-\epsilon) = \left(\frac{x}{\epsilon}\right)^{1-\nu} \epsilon \int_0^\infty dk k \left[J_\nu(k\epsilon) J_\nu(kx) + J_{-\nu}(k\epsilon) J_{-\nu}(kx)\right] \tag{D.23}$$

and solving the integral for the time dependent full solution we finally get to:

$$P(x,t \mid \epsilon, 0) = \left(\frac{x}{\epsilon}\right)^{1-\nu} \epsilon \int_0^\infty dk k \left[A J_\nu(k\epsilon) J_\nu(kx) + B J_{-\nu}(k\epsilon) J_{-\nu}(kx)\right] e^{-\mu k^2 t} =$$

$$= \frac{\epsilon}{2\mu t} \left(\frac{x}{\epsilon}\right)^{1-\nu} \exp\left(-\frac{x^2+\epsilon^2}{4\mu t}\right) \left[A I_\nu\left(\frac{\epsilon x}{2\mu t}\right) + B I_{-\nu}\left(\frac{\epsilon x}{2\mu t}\right)\right] = \tag{D.24}$$

$$= AP_\nu(x,t \mid \epsilon,0) + BP_{-\nu}(x,t \mid \epsilon,0),$$

where I_ν is the modified Bessel Function of the First Kind and A and B are numerical constants. Remembering the power series expression for the modified Bessel Function, and that we are interested in the limit of small ϵ, we get

$$I_\nu\left(\frac{\epsilon x}{2\mu t}\right) = \left(\frac{\epsilon x}{4\mu t}\right)^\nu \sum_{m=0}^{\infty} \frac{1}{m!\Gamma(m+\nu+1)} \left(\frac{\epsilon x}{4\mu t}\right)^{2m} =$$

$$= \frac{1}{\Gamma(m+1)} \left(\frac{\epsilon x}{4\mu t}\right)^\nu \left(1+\mathcal{O}(\epsilon^2)\right).$$

By performing some substitutions, we easily get to the result

$$P_\nu(x,t \mid \epsilon,0) \simeq \frac{4\mu\epsilon^{2\nu}}{\Gamma(\nu-1)} x(4\mu t)^{-\nu-1} e^{-\frac{x^2}{4\mu t}}, \tag{D.25}$$

where the approximation means that we are neglecting terms $\mathcal{O}(\epsilon^2)$, and thus by straightforward substitution into the definition we get:

$$j_\nu(0,t) \simeq -\frac{4\mu\epsilon^{2\nu}}{\Gamma(\nu-1)}(1+\beta)(4\mu t)^{-\nu-1} e^{-\frac{x^2}{4\mu t}}. \tag{D.26}$$

The other part of our solution, after some simple algebra, gives

$$P_{-\nu}(x,t \mid \epsilon,0) = \frac{4}{\Gamma(\nu-1)} x^{1-2\nu}(4t)^{\nu-1} e^{-\frac{x^2}{4t}} \left(1+\mathcal{O}(\epsilon^2)\right)$$

and

$$j_{-\nu}(0,t) = 0.$$

So our result is precisely

$$F(0,t) = \frac{4\mu\epsilon^{2\nu}}{\Gamma(\nu-1)}(1+\beta)(4\mu t)^{-\nu-1}e^{-\frac{x^2}{4\mu t}} \sim t^{-\nu-1} = t^{-\frac{3+\beta}{2}}. \tag{D.27}$$

For $\beta = 0$ we would recover of course the Random walk exponent for avalanches' duration (as the case $\beta = 0$ is precisely a standard Random Walk).

For the case we are discussing here we have $\beta = 1$, instead, and we get

$$F(0,t) = t^{-2} \tag{D.28}$$

that is precisely the distribution of duration of avalanches for a Branching Process.

This means that despite the fact that a Random Walk in a Logarithmic Potential gives non-universal exponents for avalanches, for the case presented here, in which the logarithmic Potential derives from a change It-Stratonovich, there exist a relation between the coefficients of the equation. Both of them only depend on noise amplitude, compensating each other and hence generating Branching Process exponents.

We also remark that this result was also calculated by Feller in [141], more

precisely he solved the equation

$$\frac{\partial u(\rho,t)}{\partial t} = \frac{\partial}{\partial \rho}\left(a\rho u(x,t) - \frac{\partial}{\partial \rho}(b\rho + c)u(x,t)\right) \tag{D.29}$$

that is the Fokker Plank equation that corresponds to our Langevin interpreted la Ito, plus a constant plus a linear term, namely it would be:

$$\dot{\rho} = bx + c + \sqrt{x}\xi$$

with $\langle \xi(t)\xi(t')\rangle = 2a\delta(t-t')$. He found the result:

$$F(0,t) = -\frac{b}{\Gamma\left(-\frac{c}{a}+1\right)}\frac{e^{-bt}}{1-e^{-bt}}\left\{\frac{\chi b}{a(1-e^{-bt})}\right\}^{\frac{-c+a}{a}}\exp\left(-\frac{\chi b}{a(1-e^{-bt})}\right) \tag{D.30}$$

where $\chi > 0$ is a parameter such that a foundamental solution $u(\rho,t;\chi)$ assumes initial values 0 whe $\rho < \chi$ and 1 when $\rho > \chi$. {*I don't understand what this means*}

It is easy to check that for t small enough we recover

$$F(0,t) \simeq t^{-2+\frac{c}{a}} \tag{D.31}$$

and if we plot the whole formula in Mathematica (Figure D.25), we see that the power law holds for all values of t up to a cutoff determined by b.

To calculate the probability distribution $F(T)$ of the return times at which a walker starting close to the origin ($P(x,0) = \delta(x-\epsilon), \epsilon \to 0$) first hits back the origin, the absorbing boundary condition $P(0,t) = 0$ needs to be imposed.

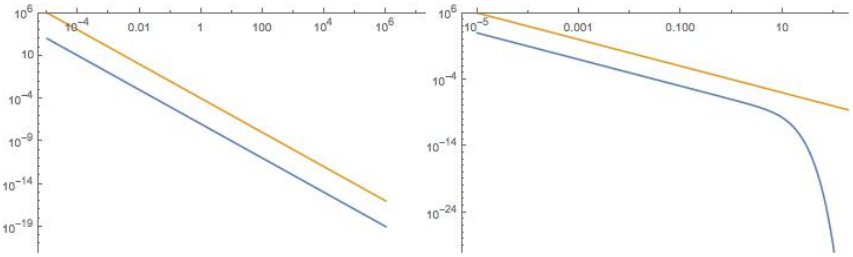

Figure D.25: Plot of the result for $F(0,t)$ by Feller in blue, in orange a reference guide for the eye of a power law t^{-2}. Left is for $b = 10^{-8}$, right $b = 0.5$. Other parameters fixed $a = 1, c = 0$.

Note that $F(T)$ is minus the probability flux at 0, $F(T) = -j(0, t = T)$, with

$$j(0, t = T) = -\mu \left[\frac{\partial P(x,t)}{\partial x} + \frac{\beta}{x} P(x,t) \right]_{x=0}. \tag{D.32}$$

One can try a solution of the Eq.(D.32) of the form $P(x,t) = r(x)\exp(-\mu k^2 t)$ and note that the resulting equation can be converted into a Bessel Equation with the change of variable $r(x) = x^{\frac{1-\beta}{2}} R(x)$,

$$x^2 R''(x) + xR'(x) + \left(k^2 x^2 - \nu^2\right) R(x) = 0, \tag{D.33}$$

where $\nu = (1+\beta)/2$. The general solution of this last equation is a linear combination of Bessel functions of the first kind of order $\pm\nu$. Putting the pieces back together, employing the orthogonality property of the Bessel functions, and imposing the initial condition, leads to

$$\begin{aligned} P(x, t \mid \epsilon, 0) &= \left(\frac{x}{\epsilon}\right)^{1-\nu} \epsilon \int_0^\infty dk k [A J_\nu(k\epsilon) J_\nu(kx) \\ &+ B J_{-\nu}(k\epsilon) J_{-\nu}(kx)] e^{-\mu k^2 t}, \end{aligned} \tag{D.34}$$

where A and B are numerical constants. The integral in Eq.(D.34) gives the modified Bessel function of the first kind $I_{\pm\nu}$ and, it is easy to compute the flux at the origin in the small ϵ limit [150, 72], leading to Eq.(5.10).

D.5 Supplementary information to Chapter 7: Non-critical amplification of fluctuations in simple models of persistent neural dynamics

D.5.1 Insights in Non-Normal Matrices

In this section the mathematical notion and some of the properties and details of non-normal matrices are briefly reviewed. Normal matrices are usually defined as the ones that commute with their adjoints $\mathcal{N}^*\mathcal{N} = \mathcal{N}\mathcal{N}^*$ [204]. One could restate this more practically saying that normal matrices have a most convenient property: there exists an orthonormal basis consisting purely of eigenvectors. The unitary matrix, which has the eigenvectors as columns, transforms the original matrix into a diagonal one. Since the transformation is unitary, the lengths and the angles between the vectors are preserved when passing from the original basis to the eigenvectors one. This makes it most convenient to study the dynamics in the eigenvector basis, since the components of a vector in the eigenvector basis, evolve independently from each other.

Conversely non-normal matrices are either *deficient*, in which case there are not even enough linearly independent eigenvectors to build a basis, or, if they are diagonalizable, there certainly exists a basis consisting purely of eigenvectors, even normalized ones, but not orthonormal ones [204]. This means that some directions are poorly (or even not at all) represented i.e. they have small

(or zero) dot product with all eigenvectors in the basis. So if one evolves an initial vector in the eigenvectors basis (given that it exists), the amplitudes of its components will evolve independently (by definition of eigenvectors), but the eigenvectors themselves are not independent (since their dot product is not 0), making it misleading to study the dynamics in this basis [204, 164]. From another perspective, non-normal matrices are *non diagonalizable by a unitary transformation* (or, if they are deficient, they are non diagonalizable at all). Since the matrix that (supposing that it is invertible) transforms the initial matrix into the eigenvectors non-orthogonal basis (and which contains the eigenvectors as columns) is not unitary (i.e. the eigenvectors are not orthogonal), then the length and the angles between vectors are not preserved by the transformation and thus, representing the trajectory in the basis of the eigenvectors makes it stretched and sheared.

The Rayleigh quotient of a matrix for a non-zero vector $|x\rangle$ is defined as

$$R(A, x) \equiv \frac{\langle Ax|x\rangle}{\langle x|x\rangle}.$$

For any normal matrix

$$R(A, x) = \frac{\sum_i \lambda_i x_i^2}{\sum_i x_i^2},$$

where x_i is the i-th component of $|x\rangle$. It is easy to see that the Rayleigh quotient reaches its maximum (minimum) value when $|x\rangle$ coincides with the eigenvector relative to the largest (smallest) eigenvalue $\lambda_{max}(A)$ ($\lambda_{min}(A)$) and $\max(R(A, x)) \equiv \lambda_{max}(A)$ holds (respectively $\min(R(A, x)) \equiv \lambda_{min}(A)$). This means that for a normal matrix the strongest magnification that can occur

must take place in the eigenspace belonging to the eigenvalue with the largest modulus; for all other vectors the magnification will be smaller. This property (also called Rayleigh principle [205]) does not hold for a non-normal matrix. This means that in the non-normal case, the eigenvalue with the largest modulus must by no means necessarily represent the strongest amplification factor or, conversely, that there might exist directions that are unexpectedly strongly amplified.

Moreover, it has been shown in [165] that, whereas the asymptotic behavior of the system is determined by the eigenvalues of the matrix of the dynamics, the instantaneous behavior is determined by the eigenvalues of the Hermitian part of A, defined as[1]

$$H(A) = \frac{1}{2}(A + A^T).$$

If the equilibrium itself is stable $\Re[\lambda_{max}(A)] < 0$, but the Hermitian part of A has positive eigenvalues ($\lambda_{max}(H(A)) > 0$), then the equilibrium is said to be *reactive* and the magnitude of some perturbations will initially grow before decaying.

In fact, given a perturbation (of magnitude $\|v_0\|$) to an asymptotically stable equilibrium of a linear system, *reactivity* is defined as the maximum amplification rate, over all initial perturbations, immediately following the perturbation [165]:

$$\text{reactivity} \equiv \max_{\|v_0\| \neq 0} \left(\frac{1}{\|v\|} \frac{d}{dt} \|v\| \right) \Bigg|_{t=0}.$$

[1]Note that a normal matrix with real eigenvalues is an Hermitian matrix and that the Hermitian part of an Hermitian matrix coincides with the matrix itself.

Since we can write:

$$\frac{d}{dt}\|v\| = \frac{d}{dt}\sqrt{v^T v} = \frac{v^T(A+A^T)v}{2\|v\|} = \frac{v^T H(A) v}{v^T v}\|v\|, \tag{D.35}$$

then, reactivity coincides with the maximum Rayleigh quotient of the Hermitian part of the matrix, which, by Rayleigh principle, coincides with $\lambda_{max}(H(A))$:

$$\text{reactivity} = \lambda_{max}(H(A)). \tag{D.36}$$

Even if non-normal matrices cannot be diagonalized by a unitary transformation, on the other hand Schur Theorem guarantees that any square matrix is unitarily equivalent to a triangular matrix (let's say upper triangular) with the eigenvalues on the diagonal (Schur transformation). This triangular matrix is also diagonal if and only if the original matrix is normal. The strictly upper triangular part of the matrix corresponds to connectivity flows from node j to node i with $j > i$ and therefore it is often referred to as *feedforward interaction* [164].

Finally, although the Schur decomposition is not uniquely specified (since it derives from a Graham-Schmidt orthogonalization approach, starting from whichever eigenvector), it is possible to uniquely characterize the overall strength of the feedforward connectivity of a matrix. Indeed it can be defined by means of two unitary invariants: the sum of the absolute squares of all of the elements of a matrix (it is easy to check that it is invariant under a unitary transformation) and the sum of absolute squares of the eigenvalues (the eigenvalues

of a matrix themselves are unitary invariants). So we can define unambiguously the weight of the non-normality as the sum of the absolute squares of the feedforward elements of any Schur decomposition:

$$f = \frac{\sum_{n=1}^{N^2} m_n^2 - \sum_{i=1}^{N} |\lambda_i|^2}{\sum_{n=1}^{N^2} m_n^2}$$

where λ_i are the eigenvalues of the $(N \times N)$ matrix and m_n are the single entry values of the matrix.

D.5.2 Turing patterns

Following [206] we prove here that, in a spatially explicit version of Wilson-Cowan model, if balance condition holds, it is possible to observe persistent pattern activity formation through Turing instabilities.

Let's imagine that we want to couple various cortical columns, disposed in a square lattice, for instance. If we assume that we can neglect inter-columnar mixed coupling, i.e. excitatory (inhibitory) subpopulation of a column only interacts with excitatory (inhibitory) subpopulation of its neighbors, and we choose diffusion-like coupling, then (after linearizing the dynamics close to the fixed point $\bar{v}$) we have something of the form [165]:

$$\frac{\partial v}{\partial t} = Av + D\nabla^2 v,$$

where D is a diagonal matrix containing the diffusion coefficients on the diagonal and A is the linearizd dynamics. If we apply a Fourier transform and

define $J = A - \|\omega\|^2 D$, the equation above can be written as

$$\frac{d\tilde{v}}{dt} = J\tilde{v}.$$

Let's assume that $\lambda_1(A) < 0$, or equivalently that the individual dynamics is linearly stable around the fixed point $\bar{v}$. If there exist some values of ω such that $\Re[\lambda_1(J)] > 0$, it means that the equilibrium $\bar{v}$ can be destabilized by diffusion, a phenomenon called *Turing instabilities* [207]. Hence (heterogeneous) perturbations with those spatial frequency ω will grow and produce stable spatial patterns. This typically occurs when the diffusion coefficients of the two populations are very different from each other.

If we write

$$H(J) = H(A) + \left(-\frac{\|\omega\|^2}{2} D\right)$$

and we remember that, by Weyl's theorem, the largest eigenvalue of the sum is less than or equal to the sum of the largest eigenvalue of each matrix, then we immediately see that, if A is not reactive ($\lambda_1(H(A)) < 0$), then J is not reactive ($\lambda_1(H(J)) < 0$) and Turing instabilities are impossible ($\frac{d}{dt}\|v\| < 0$). Thus reactivity is a prerequisite for transient Turing instabilities.

As pointed out in [206], adding noise on top of this picture, has the effect of stabilizing those transient instabilities, allowing stable Turing patterns for a wide range of diffusion constants [207].

We verified that in our toy-model for the cortex, there exist spatial patterns of excitation and inhibition, or, under a different point of view, spatial patterns

of activity (see Figure D.26).

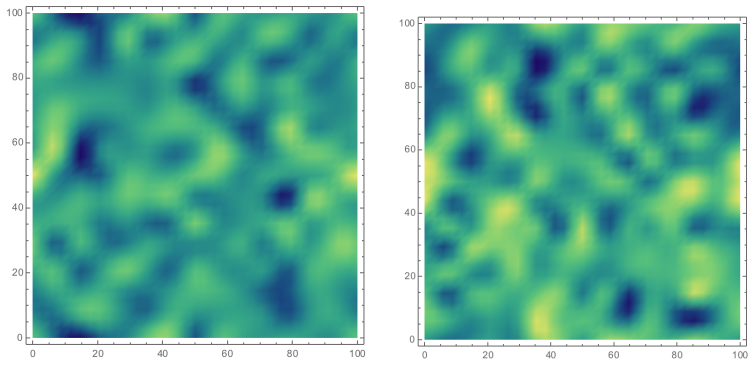

Figure D.26: Left: Turing patterns in Wilson-Cowan. Right: Turing pattern in Tsodyks-Markram

Pattern formation in the visual cortex has already been reported in Wilson-Cowan model, in association with the production of hallucinations by the visual cortex [208]. Hallucinations are geometric images that many observers see after taking hallucinogens such as LSD, cannabis, mescaline or psilocybin. The fact that in most cases they are seen in both eyes and move with them, suggests that they are generated in the brain [208]. The geometrical patterns seen when the eyes are closed could reflect spatial patterns produced in the visual cortex, generated by a mechanism of Turing instability.

Our model allows to relate the possibility of creating geometrical patterns of activity discussed in [208] to the reactivity provoked by balance between excitation and inhibition.

Bibliography

[1] Miguel A Muñoz. Colloquium: Criticality and dynamical scaling in living systems. *arXiv preprint arXiv:1712.04499*, 2017.

[2] T. Mora and W. Bialek. Are biological systems poised at criticality? *J. Stat. Phys.*, 144(2):268–302, 2011.

[3] Ariel Haimovici and Matteo Marsili. Criticality of mostly informative samples: a bayesian model selection approach. *Journal of Statistical Mechanics: Theory and Experiment*, 2015(10):P10013, 2015.

[4] Joaquín Marro. *Physics, nature and society: a guide to order and complexity in our world*. Springer Science & Business Media, 2013.

[5] C.G. Langton. Computation at the edge of chaos: Phase transitions and emergent computation. *Physica D: Nonlinear Phenomena*, 42(1):12–37, 1990.

[6] Per Bak, Chao Tang, and Kurt Wiesenfeld. Self-organized criticality: An explanation of the 1/f noise. *Phys. Rev. Lett.*, 59(4):381, 1987.

[7] Alessandro Vespignani, Ronald Dickman, Miguel A Muñoz, and Stefano Zapperi. Driving, conservation, and absorbing states in sandpiles. *Physical review letters*, 81(25):5676, 1998.

[8] Juan A Bonachela, José J Ramasco, Hugues Chaté, Ivan Dornic, and Miguel A Muñoz. Sticky grains do not change the universality class of isotropic sandpiles. *Physical Review E*, 74(5):050102, 2006.

[9] John M Beggs and Dietmar Plenz. Neuronal avalanches in neocortical circuits. *J. of Neurosci.*, 23(35):11167–11177, 2003.

[10] Thomas Petermann, Tara C Thiagarajan, Mikhail A Lebedev, Miguel AL Nicolelis, Dante R Chialvo, and Dietmar Plenz. Spontaneous cortical activity in awake monkeys composed of neuronal avalanches. *Proc. Natl. Acad. Sci. U.S.A.*, 106(37):15921–15926, 2009.

[11] Alberto Mazzoni, Frédéric D Broccard, Elizabeth Garcia-Perez, Paolo Bonifazi, Maria Elisabetta Ruaro, and Vincent Torre. On the dynamics of the spontaneous activity in neuronal networks. *PLoS One*, 2(5):e439, 2007.

[12] Ariel Haimovici, Enzo Tagliazucchi, Pablo Balenzuela, and Dante R Chialvo. Brain organization into resting state networks emerges at criticality on a model of the human connectome. *Phys. Rev. Lett.*, 110(17):178101, 2013.

[13] Enzo Tagliazucchi, Pablo Balenzuela, Daniel Fraiman, and Dante R Chialvo. Criticality in large-scale brain fMRI dynamics unveiled by a novel point process analysis. *Front. Physiol.*, 3(15), 2012.

[14] Oren Shriki, Jeff Alstott, Frederick Carver, Tom Holroyd, Richard NA Henson, Marie L Smith, Richard Coppola, Edward Bullmore, and Dietmar Plenz. Neuronal avalanches in the resting meg of the human brain. *Journal of Neuroscience*, 33(16):7079–7090, 2013.

[15] Timothy Bellay, Andreas Klaus, Saurav Seshadri, and Dietmar Plenz. Irregular spiking of pyramidal neurons organizes as scale-invariant neuronal avalanches in the awake state. *Elife*, 4:e07224, 2015.

[16] Simon-Shlomo Poil, Richard Hardstone, Huibert D Mansvelder, and Klaus Linkenkaer-Hansen. Critical-state dynamics of avalanches and oscillations jointly emerge from balanced excitation/inhibition in neuronal networks. *J. Neurosci.*, 32(29):9817–9823, 2012.

[17] Massobrio Paolo, De Arcangelis L., Pasquale Valentina, Jensen Henrik J., and Plenz Dietmar. Criticality as a signature of healthy neural systems. *FRONTIERS IN SYSTEMS NEUROSCIENCE*, 9:–, 2015.

[18] Dan Oprisa and Peter Toth. Criticality and deep learning, part I: theory vs. empirics. *CoRR*, abs/1702.08039, 2017.

[19] Dan Oprisa and Peter Toth. Criticality & deep learning II: momentum renormalisation group. *CoRR*, abs/1705.11023, 2017.

[20] Anna Levina, J Michael Herrmann, and Theo Geisel. Dynamical synapses causing self-organized criticality in neural networks. *Nature Phys.*, 3(12):857–860, 2007.

[21] Daniel Millman, Stefan Mihalas, Alfredo Kirkwood, and Ernst Niebur. Self-organized criticality occurs in non-conservative neuronal networks during 'up' states. *Nat. Phys.*, 6(10):801–805, 2010.

[22] Nicolas Brunel. Dynamics of sparsely connected networks of excitatory and inhibitory spiking neurons. *J. Comput. Neurosci.*, 8:183–208, 2000. 10.1023/A:1008925309027.

[23] C Van Vreeswijk. Partially synchronized states in networks of pulse-coupled neurons. *Phys. Rev. E*, 54:5522–5537, 1996.

[24] Fabrizio Pittorino, Miguel Ibáñez Berganza, Matteo di Volo, Alessandro Vezzani, and Raffaella Burioni. Chaos and correlated avalanches in excitatory neural networks with synaptic plasticity. *Phys. Rev. Lett.*, 118:098102, Mar 2017.

[25] Misha V Tsodyks and Henry Markram. The neural code between neocortical pyramidal neurons depends on neurotransmitter release probability. *Proc. Natl. Acad. Sci. USA*, 94(2):719–723, 1997.

[26] Per Bak. *How nature works: the science of self-organized criticality.* Copernicus, New York, 1996.

[27] James P Sethna, Karin A Dahmen, and Christopher R Myers. Crackling noise. *Nature*, 410(6825):242–250, 2001.

[28] Henrik Jeldtoft Jensen. *Self-organized criticality: emergent complex behavior in physical and biological systems.* Cambridge university press, Cambridge, 1998.

[29] Gunnar Pruessner. *Self-organised criticality: theory, models and characterisation*. Cambridge University Press, 2012.

[30] Ronald Dickman, Miguel A Muñoz, Alessandro Vespignani, and Stefano Zapperi. Paths to self-organized criticality. *Brazilian Journal of Physics*, 30(1):27–41, 2000.

[31] J. A. Bonachela and M. A. Muñoz. Self-organization without conservation: true or just apparent scale-invariance? *J. Stat. Mech.*, page P09009, Sep 2009.

[32] G Grinstein. Generic scale invariance and self-organized criticality. In *Scale invariance, interfaces, and non-equilibrium dynamics*, pages 261–293. Springer, 1995.

[33] Mark E. J. Newman. Power laws, Pareto distributions and Zipf's law. *Contemp. Phys.*, 46(5):323–351, 2005.

[34] Pavel L Krapivsky, Sidney Redner, and Eli Ben-Naim. *A kinetic view of statistical physics*. Cambridge University Press, 2010.

[35] Oscar A Pinto and Miguel A Muñoz. Quasi-neutral theory of epidemic outbreaks. *PloS one*, 6(7):e21946, 2011.

[36] Carlos Lopez-Garcia, Allon M Klein, Benjamin D Simons, and Douglas J Winton. Intestinal stem cell replacement follows a pattern of neutral drift. *Science*, 330(6005):822–825, 2010.

[37] Larry F Abbott and Sacha B Nelson. Synaptic plasticity: taming the beast. *Nat. Neurosci.*, 3:1178–1183, 2000.

[38] Mircea Steriade and Igor Timofeev. Neuronal plasticity in thalamocortical networks during sleep and waking oscillations. *Neuron*, 37(4):563–576, 2003.

[39] Jorge Hidalgo, Luís F Seoane, Jesús M Cortés, and Miguel A Munoz. Stochastic amplification of fluctuations in cortical up-states. *PloS one*, 7(8):e40710, 2012.

[40] Anna Levina, J Michael Herrmann, and Theo Geisel. Phase transitions towards criticality in a neural system with adaptive interactions. *Phys. Rev. Lett.*, 102(11):118110, Mar 2009.

[41] Rashid V. Williams-Garcia, John M. Beggs, and Gerardo Ortiz. Unveiling causal activity of complex networks. *arXiv preprint arXiv:1603.05659*, 2016.

[42] Theodore E Harris. *The theory of branching processes*. Courier Corporation, 2002.

[43] Stefano Zapperi, Kent Bækgaard Lauritsen, and H Eugene Stanley. Self-organized branching processes: mean-field theory for avalanches. *Phys. Rev. Lett.*, 75(22):4071, 1995.

[44] J. Marro and R. Dickman. *Nonequilibrium Phase Transitions in Lattice Models*. Collection Aléa-Saclay. Cambridge University Press, 2005.

[45] M. Henkel, H. Hinrichsen, and S. Lübeck. *Non-equilibrium Phase Transitions: Absorbing phase transitions*. Theoretical and mathematical physics. Springer London, Berlin, 2008.

[46] Daniel T Gillespie. Exact stochastic simulation of coupled chemical reactions. *J. Phys. Chem.*, 81(25):2340–2361, 1977.

[47] C. W. Gardiner. *Handbook of stochastic methods : for physics, chemistry and the natural sciences*. Springer series in synergetics, 13. Springer, Berlin, 2002.

[48] Heinz Georg Schuster, Dietmar Plenz, and Ernst Niebur. *Criticality in neural systems*. John Wiley & Sons, New Jersey, 2014.

[49] Kurt Binder. Theory of first-order phase transitions. *Rep. Prog. Phys*, 50(7):783, 1987.

[50] J.J. Binney, N.J. Dowrick, A.J. Fisher, and M.E.J. Newman. *The Theory of Critical Phenomena*. Oxford Univ. Press, Oxford, 1993.

[51] Andrea Pigorini, Simone Sarasso, Paola Proserpio, Caroline Szymanski, Gabriele Arnulfo, Silvia Casarotto, Matteo Fecchio, Mario Rosanova, Maurizio Mariotti, Giorgio Lo Russo, et al. Bistability breaks-off deterministic responses to intracortical stimulation during non-rem sleep. *Neuroimage*, 112:105–113, 2015.

[52] David Angeli, James E Ferrell, and Eduardo D Sontag. Detection of multistability, bifurcations, and hysteresis in a large class of biological positive-feedback systems. *Proc. Nat. Acad. of Sci.*, 101(7):1822–1827, 2004.

[53] Sanjay Tyagi. Tuning noise in gene expression. *Mol. Syst. Biol.*, 11(5):805, 2015.

[54] David Holcman and Misha Tsodyks. The emergence of up and down states in cortical networks. *PLoS Comput. Biol.*, 2(3):e23, 2006.

[55] Jorge F Mejias, Hilbert J Kappen, and Joaquin J Torres. Irregular dynamics in up and down cortical states. *PLoS One*, 5(11):e13651, 2010.

[56] L De Arcangelis. Are dragon-king neuronal avalanches dungeons for self-organized brain activity? *Eur. Phys. J. Spec.Top.*, 205(1):243–257, 2012.

[57] F de Los Santos, MM Telo da Gama, and MA Muñoz. Nonequilibrium wetting transitions with short range forces. *Phys. Rev. E*, 67(2):021607, 2003.

[58] Katy J Rubin, Gunnar Pruessner, and Grigorios A Pavliotis. Mapping multiplicative to additive noise. *J. Phys. A*, 47(19):195001, 2014.

[59] S S Manna. Two-state model of self-organized criticality. *J. Phys. A: Math. Gen.*, 24(7):L363–L369, 1991.

[60] K. Christensen, A. Corral, V. Frette, J. Feder, and T Jssang. Tracer dispersion in a self-organized critical system. *Phys. Rev. Lett.*, 77(1):107–110, 1996.

[61] Alessandro Vespignani, Ronald Dickman, Miguel A Muñoz, and Stefano Zapperi. Absorbing-state phase transitions in fixed-energy sandpiles. *Phys. Rev. E*, 62(4):4564, 2000.

[62] Haye Hinrichsen. Non-equilibrium critical phenomena and phase transitions into absorbing states. *Adv. Phys.*, 49(7):815–958, 2000.

[63] Naoto Yoshioka. A sandpile experiment and its implications for self-organized criticality and characteristic earthquake. *Earth Planets Space*, 55(6):283–289, 2003.

[64] Didier Sornette and Guy Ouillon. Dragon-kings: mechanisms, statistical methods and empirical evidence. *Eur. Phys. J. Spec. Top.*, 205(1):1–26, 2012.

[65] Miguel A Muñoz, Ronald Dickman, Alessandro Vespignani, and Stefano Zapperi. Avalanche and spreading exponents in systems with absorbing states. *Phys. Rev. E*, 59(5):6175, 1999.

[66] Kurt Wiesenfeld, Frank Moss, et al. Stochastic resonance and the benefits of noise: from ice ages to crayfish and squids. *Nature*, 373(6509):33–36, 1995.

[67] Ivan Dornic, Hugues Chaté, and Miguel A Muñoz. Integration of langevin equations with multiplicative noise and the viability of field theories for absorbing phase transitions. *Phys. Rev. Lett.*, 94(10):100601, 2005.

[68] Paula Villa Martín, Juan A Bonachela, Simon A Levin, and Miguel A Muñoz. Eluding catastrophic shifts. *Proc. Natl. Acad. Sci. USA*, 112(15):E1828–E1836, 2015.

[69] P Grassberger. Tricritical directed percolation in 2+ 1 dimensions. *J. Stat. Mech.*, 2006(01):P01004, 2006.

[70] JW Essam. Directed compact percolation: cluster size and hyperscaling. *J. of Phys. A*, 22(22):4927, 1989.

[71] Baruch Meerson and Pavel V Sasorov. Extinction rates of established spatial populations. *Phys. Rev. E*, 83(1):011129, 2011.

[72] Francesca Colaiori. Exactly solvable model of avalanches dynamics for barkhausen crackling noise. *Adv. Phys.*, 57(4):287–359, 2008.

[73] Fabrizio Lombardi, Hans J. Herrmann, Dietmar Plenz, and Lucilla De Arcangelis. On the temporal organization of neuronal avalanches. *Front. Syst. Neurosci.*, 8, 2014.

[74] Dante R Chialvo. Critical brain networks. *Phys. A*, 340(4):756–765, 2004.

[75] D. R. Chialvo. Emergent complex neural dynamics. *Nat. Phys.*, 6:744–750, 2010.

[76] Elakkat D. Gireesh and Dietmar Plenz. Neuronal avalanches organize as nested theta- and beta/gamma-oscillations during development of cortical layer 2/3. *Proc. Natl. Acad. Sci. USA*, 105(21):7576–7581, May 2008.

[77] Hongdian Yang, Woodrow L Shew, Rajarshi Roy, and Dietmar Plenz. Maximal variability of phase synchrony in cortical networks with neuronal avalanches. *J. Neurosci.*, 32(3):1061–1072, 2012.

[78] Lucilla de Arcangelis, Carla Perrone-Capano, and Hans J. Herrmann. Self-organized criticality model for brain plasticity. *Phys. Rev. Lett.*, 96:028107, Jan 2006.

[79] Nigel Stepp, Dietmar Plenz, and Narayan Srinivasa. Synaptic plasticity enables adaptive self-tuning critical networks. *PLOS Comput. Biol.*, 11(1), 2015.

[80] Daniel Harnack, Miha Pelko, Antoine Chaillet, Yacine Chitour, and Mark CW van Rossum. Stability of neuronal networks with homeostatic regulation. *PLoS Comput. Biol.*, 11(7):e1004357, 2015.

[81] H. Markram and M.V. Tsodyks. Redistribution of synaptic efficacy between pyramidal neurons. *Nature*, 382:807–810, 1996.

[82] Chang-Woo Shin and Seunghwan Kim. Self-organized criticality and scale-free properties in emergent functional neural networks. *Phys. Rev. E*, 74(4):045101, 2006.

[83] JA Bonachela, S. de Franciscis, J.J. Torres, and M. A. Muñoz. Self-organization without conservation: are neuronal avalanches generically critical? *J. Stat. Mech.Theory E.*, 2010(02):P02015, 2010.

[84] Daniel J Amit and Nicolas Brunel. Model of global spontaneous activity and local structured activity during delay periods in the cerebral cortex. *Cereb. Cortex*, 7(3):237–252, 1997.

[85] N. Brunel and V. Hakim. Sparsely synchronized neuronal oscillations. *Chaos*, 18(1):015113, 2008.

[86] Shree Hari Gautam, Thanh T Hoang, Kylie McClanahan, Stephen K Grady, and Woodrow L Shew. Maximizing sensory dynamic range by tuning the cortical state to criticality. *PLoS Comput. Biol.*, 11(12):e1004576, 2015.

[87] Jonathan Touboul and Alain Destexhe. Power-law statistics and universal scaling in the absence of criticality. *Phys. Rev. E*, 95:012413, Jan 2017.

[88] A Destexhe. Self-sustained asynchronous irregular states and up down states in thalamic, cortical and thalamocortical networks of nonlinear integrate-and-fire neurons. *J. Comput. Neurosci.*, 27(3):493–506, 2009.

[89] Mircea Steriade, A Nunez, and F Amzica. A novel slow (¡ 1 hz) oscillation of neocortical neurons in vivo: depolarizing and hyperpolarizing components. *J. Neurosci.*, 13(8):3252–3265, 1993.

[90] H Eugene Stanley. *Introduction to phase transitions and critical phenomena*. Oxford University Press, Oxford, 1987.

[91] John Toner, Yuhai Tu, and Sriram Ramaswamy. Hydrodynamics and phases of flocks. *Ann. Phys.*, 318(1):170–244, 2005.

[92] Michael A Buice and Jack D Cowan. Field-theoretic approach to fluctuation effects in neural networks. *Phys. Rev. E*, 75(5):051919, 2007.

[93] Paul C Bressloff. Metastable states and quasicycles in a stochastic wilson-cowan model of neuronal population dynamics. *Phys. Rev. E*, 82(5):051903, 2010.

[94] P C Bressloff. Spatiotemporal dynamics of continuum neural fields. *J. Phys. A Math. Theor.*, 45(3):033001, 2012.

[95] Eric R Kandel, James H Schwartz, Thomas M Jessell, Steven A Siegelbaum, and A James Hudspeth. *Principles of neural science*, volume 4. McGraw-hill New York, 2000.

[96] Peter Dayan and LF Abbott. Theoretical neuroscience: computational and mathematical modeling of neural systems. *J. Cogn. Neurosci.*, 15(1):154–155, 2003.

[97] Marc Benayoun, Jack D Cowan, Wim van Drongelen, and Edward Wallace. Avalanches in a stochastic model of spiking neurons. *PLoS Comput. Biol.*, 6(7):e1000846, 2010.

[98] Hugh R Wilson and Jack D Cowan. Excitatory and inhibitory interactions in localized populations of model neurons. *Biophys. J.*, 12(1):1–24, 1972.

[99] Maurizio Mattia and Maria V Sanchez-Vives. Exploring the spectrum of dynamical regimes and timescales in spontaneous cortical activity. *Cogn. Neurodyn.*, 6(3):239–250, 2012.

[100] Gustavo Deco and Viktor K Jirsa. Ongoing cortical activity at rest: criticality, multistability, and ghost attractors. *J. Neurosci.*, 32(10):3366–3375, 2012.

[101] Michael Breakspear. Dynamic models of large-scale brain activity. *Nature neuroscience*, 20(3):340–352, 2017.

[102] Gustavo Deco, Viktor K Jirsa, Peter A Robinson, Michael Breakspear, and Karl Friston. The dynamic brain: from spiking neurons to neural masses and cortical fields. *PLoS Comput. Biol.*, 4(8):e1000092, 2008.

[103] O. Sporns. *Networks of the Brain*. MIT Press, USA, 2010.

[104] Joaquin J Torres and Pablo Varona. Modeling biological neural networks. In *Handbook of Natural Computing*, pages 533–564. Springer, 2012.

[105] Shan Yu, Andreas Klaus, Hongdian Yang, and Dietmar Plenz. Scale-invariant neuronal avalanche dynamics and the cut-off in size distributions. *PloS one*, 9(6):e99761, 2014.

[106] Jon P Hobbs, Jodi L Smith, and John M Beggs. Aberrant neuronal avalanches in cortical tissue removed from juvenile epilepsy patients. *J. Clin. Neurophysiol.*, 27(6):380–386, 2010.

[107] Fernando Lopes da Silva. Neural mechanisms underlying brain waves: from neural membranes to networks. *Electroencephalogr. Clin. Neurophysiol.*, 79(2):81–93, 1991.

[108] Joel Tabak, Walter Senn, Michael J O'Donovan, and John Rinzel. Modeling of spontaneous activity in developing spinal cord using activity-dependent depression in an excitatory network. *Journal of Neuroscience*, 20(8):3041–3056, 2000.

[109] C.K. Peng, Shlomo Havlin, H. Eugene Stanley, and Ary L. Goldberger. Quantification of scaling exponents and crossover phenomena in nonsta-

tionary heartbeat time series. *Chaos: An Interdisciplinary Journal of Nonlinear Science*, 5(1):82–87, 1995.

[110] Klaus Linkenkaer-Hansen, Vadim V. Nikouline, J. Matias Palva, and Risto J. Ilmoniemi. Long-range temporal correlations and scaling behavior in human brain oscillations. *Journal of Neuroscience*, 21(4):1370–1377, 2001.

[111] Arkady Pikovsky, Michael Rosenblum, and Jürgen Kurths. *Synchronization: a universal concept in nonlinear sciences*, volume 12. Cambridge university press, Cambridge, 2003.

[112] Saad Jbabdi, Stamatios N Sotiropoulos, Suzanne N Haber, David C Van Essen, and Timothy E Behrens. Measuring macroscopic brain connections in vivo. *Nat Neurosci*, 18(11):1546–1555, 11 2015.

[113] Samora Okujeni, Steffen Kandler, and Ulrich Egert. Mesoscale architecture shapes initiation and richness of spontaneous network activity. *Journal of Neuroscience*, 37(14):3972–3987, 2017.

[114] Paolo Moretti and Miguel A Muñoz. Griffiths phases and the stretching of criticality in brain networks. *Nature communications*, 4, 2013.

[115] Gyorgy Buzsaki. *Rhythms of the Brain*. Oxford Univ. Press, Oxford, 2009.

[116] RS Zucker and WG Regehr. Short-term synaptic plasticity. *Annu Rev Physiol*, 64(1):355–405, 2002.

[117] Julijana Gjorgjieva, Guillaume Drion, and Eve Marder. Computational implications of biophysical diversity and multiple timescales in neurons and synapses for circuit performance. *Current Opinion in Neurobiology*, 37:44 – 52, 2016. Neurobiology of cognitive behavior.

[118] U. C. Täuber. *Critical dynamics: a field theory approach to equilibrium and non-equilibrium scaling behavior*. Cambridge University Press, 2014.

[119] Henry Markram, Eilif Muller, Srikanth Ramaswamy, Michael W Reimann, Marwan Abdellah, Carlos Aguado Sanchez, Anastasia Ailamaki, Lidia Alonso-Nanclares, Nicolas Antille, Selim Arsever, et al. Reconstruction and simulation of neocortical microcircuitry. *Cell*, 163(2):456–492, 2015.

[120] T.M. Liggett. *Interacting Particle Systems*. Classics in Mathematics. Springer, Berlin, 2004.

[121] Géza Ódor. *Universality in Nonequilibrium Lattice Systems: Theoretical Foundations*. World Scientific Publishing Company Incorporated, 2008.

[122] G Grinstein and Miguel A Muñoz. The statistical mechanics of absorbing states. In *Fourth Granada Lectures in Computational Physics*, pages 223–270. Springer, 1997.

[123] Kazumasa A Takeuchi, Masafumi Kuroda, Hugues Chaté, and Masaki Sano. Directed percolation criticality in turbulent liquid crystals. *Phys. Rev. Lett.*, 99(23):234503, 2007.

[124] Hans Karl Janssen. On the nonequilibrium phase transition in reaction-diffusion systems with an absorbing stationary state. *Z. Phys. B.*, 42(2):151–154, 1981.

[125] Peter Grassberger. On phase transitions in schlögl's second model. *Z. Phys. B.*, 47(4):365–374, 1982.

[126] G Grinstein, Miguel A Muñoz, and Yuhai Tu. Phase structure of systems with multiplicative noise. *Phys. Rev. Lett.*, 76(23):4376, 1996.

[127] Walter Genovese, Miguel A Muñoz, and José M Sancho. Nonequilibrium transitions induced by multiplicative noise. *Phys. Rev. E*, 57(3):R2495, 1998.

[128] Miguel A Muñoz, Francesca Colaiori, and Claudio Castellano. Mean-field limit of systems with multiplicative noise. *Phys. Rev. E*, 72(5):056102, 2005.

[129] Ronald Dickman and Alex Yu Tretyakov. Hyperscaling in the domany-kinzel cellular automaton. *Phys. Rev. E*, 52(3):3218, 1995.

[130] Ivan Dornic, Hugues Chaté, Jérôme Chave, and Haye Hinrichsen. Critical coarsening without surface tension: The universality class of the voter model. *Physical Review Letters*, 87(4):045701, 2001.

[131] Omar Al Hammal, Hugues Chaté, Ivan Dornic, and Miguel A Muñoz. Langevin description of critical phenomena with two symmetric absorbing states. *Phys. Rev. Lett.*, 94(23):230601, 2005.

[132] Peter Grassberger. On the critical behavior of the general epidemic process and dynamical percolation. *Math. Bio.*, 63(2):157–172, 1983.

[133] Hans Karl Janssen. Renormalized field theory of dynamical percolation. *Z. Phys. B.*, 58(4):311–317, 1985.

[134] Leo P Kadanoff, Sidney R Nagel, Lei Wu, and Su-min Zhou. Scaling and universality in avalanches. *Phys. Rev. A*, 39(12):6524, 1989.

[135] Olga Perković, Karin Dahmen, and James P Sethna. Avalanches, barkhausen noise, and plain old criticality. *Phys. Rev. Lett.*, 75(24):4528, 1995.

[136] Andrea Baldassarri, Francesca Colaiori, and Claudio Castellano. Average shape of a fluctuation: Universality in excursions of stochastic processes. *Phys. Rev. Lett.*, 90(6):060601, 2003.

[137] JA Bonachela. *Universality in self-organized criticality*. PhD thesis, Ph. D. Thesis, University of Granada, Granada, Spain, 2008.

[138] Sven Lübeck. Universal scaling behavior of non-equilibrium phase transitions. *International Journal of Modern Physics B*, 18(31n32):3977–4118, 2004.

[139] Hoai Nguyen Huynh and Gunnar Pruessner. Abelian manna model in three dimensions and below. *Phys. Rev. E*, 85:061133, Jun 2012.

[140] Henry William Watson and Francis Galton. On the probability of the extinction of families. *J. Roy. Anthropol. Inst.*, 4:138–144, 1875.

[141] William Feller. Two singular diffusion problems. *Annals of mathematics*, pages 173–182, 1951.

[142] Peter Hilton and Jean Pedersen. Catalan numbers, their generalization, and their uses. *Math. Intell.*, 13(2):64–75, 1991.

[143] Nachum Dershowitz and Christian Rinderknecht. The average height of catalan trees by counting lattice paths. *Math. Mag.*, 88(3):187–195, 2015.

[144] Michael Plischke and Birger Bergersen. *Equilibrium statistical physics*. World Scientific, Singapore, 2006.

[145] Richard Otter. The multiplicative process. *Ann. Math. Stat.*, 20:206–224, 1949.

[146] Miguel A Muñoz, G Grinstein, and Yuhai Tu. Survival probability and field theory in systems with absorbing states. *Phys. Rev. E*, 56(5):5101, 1997.

[147] Hans Karl Janssen. Survival and percolation probabilities in the field theory of growth models. *J. Phys. Cond. Matter*, 17(20):S1973, 2005.

[148] N.G. Van Kampen. *Stochastic Processes in Physics and Chemistry*. North-Holland Personal Library. Elsevier Science & Tech, 2007.

[149] Mingzhou Ding and Weiming Yang. Distribution of the first return time in fractional brownian motion and its application to the study of on-off intermittency. *Phys. Rev. E*, 52:207–213, Jul 1995.

[150] AJ Bray. Random walks in logarithmic and power-law potentials, nonuniversal persistence, and vortex dynamics in the two-dimensional xy model. *Phys. Rev. E*, 62(1):103, 2000.

[151] Satya N Majumdar and Alain Comtet. Airy distribution function: from the area under a brownian excursion to the maximal height of fluctuating interfaces. *J. Stat. Phys.*, 119(3-4):777–826, 2005.

[152] Stefanos Papanikolaou, Felipe Bohn, Rubem Luis Sommer, Gianfranco Durin, Stefano Zapperi, and James P Sethna. Universality beyond power laws and the average avalanche shape. *Nat. Phys.*, 7(4):316–320, 2011.

[153] Damian Berger, Sunghoon Joo, Tom Lorimer, Yoonkey Nam, and Ruedi Stoop. Power laws in neuronal culture activity from limited availability of a shared resource. In *Emergent Complexity from Nonlinearity, in Physics, Engineering and the Life Sciences*, pages 209–220. Springer, 2017.

[154] John Beggs and Nicholas Timme. Being critical of criticality in the brain. *Frontiers in Physiology*, 3:163, 2012.

[155] Michael Mitzenmacher. A brief history of generative models for power law and lognormal distributions. *Internet Math.*, 1(2):226–251, 2004.

[156] Daniel B Larremore, Woodrow L Shew, Edward Ott, Francesco Sorrentino, and Juan G Restrepo. Inhibition causes ceaseless dynamics in networks of excitable nodes. *Physical review letters*, 112(13):138103, 2014.

[157] Lasse Laurson, Xavier Illa, and Mikko J Alava. The effect of thresholding on temporal avalanche statistics. *J. Stat. Mech. Theory E*, 2009(01):P01019, 2009.

[158] Francesc Font-Clos, Gunnar Pruessner, Nicholas R Moloney, and Anna Deluca. The perils of thresholding. *New J. Phys.*, 17(4):043066, 2015.

[159] Didier Sornette. *Critical Phenomena in Natural Sciences: Chaos, Fractals, Selforganization and Disorder: Concepts and Tools (Springer Series in Synergetics)*. Springer, 2006.

[160] John C Willis and G Udny Yule. Some statistics of evolution and geographical distribution in plants and animals, and their significance. *Nature*, 109(2728):177–179, 1922.

[161] Dimitrije Marković and Claudius Gros. Power laws and self-organized criticality in theory and nature. *Physics Reports*, 536(2):41–74, 2014.

[162] Jonathan Touboul and Alain Destexhe. Can power-law scaling and neuronal avalanches arise from stochastic dynamics? *PLoS ONE*, 5(2):e8982, 2010.

[163] Nir Friedman, Shinya Ito, Braden AW Brinkman, Masanori Shimono, RE Lee DeVille, Karin A Dahmen, John M Beggs, and Thomas C Butler. Universal critical dynamics in high resolution neuronal avalanche data. *Phys. Rev. Lett.*, 108(20):208102, 2012.

[164] Brendan K. Murphy and Kenneth D. Miller. Balanced amplification: A new mechanism of selective amplification of neural activity patterns. *Neuron*, 61(4):635 – 648, 2009.

[165] Ariane Verdy and Hal Caswell. Sensitivity analysis of reactive ecological dynamics. *Bulletin of Mathematical Biology*, 70(6):1634–1659, 2008.

[166] Per Bak, Kim Christensen, Leon Danon, and Tim Scanlon. Unified scaling law for earthquakes. *Phys. Rev. Lett.*, 88(17):178501, 2002.

[167] Stefano Zapperi, Alessandro Vespignani, and H Eugene Stanley. Plasticity and avalanche behaviour in microfracturing phenomena. *Nature*, 388(6643):658–660, 1997.

[168] FY Wang and ZG Dai. Self-organized criticality in x-ray flares of gamma-ray-burst afterglows. *Nat. Phys.*, 9(8):465–467, 2013.

[169] Ole Peters, Christopher Hertlein, and Kim Christensen. A complexity view of rainfall. *Phys. Rev. Lett.*, 88(1):018701, 2001.

[170] Stuart Field, Jeff Witt, Franco Nori, and Xinsheng Ling. Superconducting vortex avalanches. *Phys. Rev. Lett.*, 74(7):1206, 1995.

[171] Mikail Rubinov, Olaf Sporns, Jean-Philippe Thivierge, and Michael Breakspear. Neurobiologically realistic determinants of self-organized criticality in networks of spiking neurons. *PLoS Comput. Biol.*, 7(6):e1002038, 2011.

[172] K Christensen and NR Moloney. *Complexity and criticality*. Imperial College Press, London, 2005.

[173] Theodore E Harris. Contact interactions on a lattice. *The Annals of Probability*, pages 969–988, 1974.

[174] M Paczuski, S Maslov, and P Bak. Field theory for a model of self-organized criticality. *EPL (Europhysics Letters)*, 27(2):97, 1994.

[175] Kay J. Wiese. Coherent-state path integral versus coarse-grained effective stochastic equation of motion: From reaction diffusion to stochastic sandpiles. *arXiv preprint arXiv:1501.06514*, 2015.

[176] Anne Fey, Lionel Levine, and David B. Wilson. Driving sandpiles to criticality and beyond. *Phys. Rev. Lett.*, 104:145703, Apr 2010.

[177] Hang-Hyun Jo and Hyeong-Chai Jeong. Comment on driving sandpiles to criticality and beyond. *Phys. Rev. Lett.*, 105(1):019601, 2010.

[178] Su S Poghosyan, VS Poghosyan, VB Priezzhev, and Philippe Ruelle. Numerical study of the correspondence between the dissipative and fixed-energy abelian sandpile models. *Phys. Rev. E*, 84(6):066119, 2011.

[179] Juan A. Bonachela, Mikko Alava, and Miguel A. Muñoz. Cusps, self-organization, and absorbing states. *Phys. Rev. E*, 79:050106, May 2009.

[180] Motoo Kimura. *The neutral theory of molecular evolution*. Cambridge University Press, 1984.

[181] Stephen P Hubbell. *The unified neutral theory of biodiversity and biogeography (MPB-32)*, volume 32. Princeton University Press, 2001.

[182] Sandro Azaele, Samir Suweis, Jacopo Grilli, Igor Volkov, Jayanth R. Banavar, and Amos Maritan. Statistical mechanics of ecological systems: Neutral theory and beyond. *Rev. Mod. Phys.*, 88:035003, Jul 2016.

[183] James P Gleeson, Jonathan A Ward, Kevin P Osullivan, and William T Lee. Competition-induced criticality in a model of meme popularity. *Phys. Rev. Lett.*, 112(4):048701, 2014.

[184] Qinglong Zeng, Jeet Sukumaran, Steven Wu, and Allen Rodrigo. Neutral models of microbiome evolution. *PLOS Comput. Biol.*, 11(7):e1004365, 2015.

[185] Richard A Blythe and Alan J McKane. Stochastic models of evolution in genetics, ecology and linguistics. *J. Stat. Mech. Theor. Exp.*, 2007(07):P07018, 2007.

[186] Serena di Santo, Pablo Villegas, Raffaella Burioni, and Miguel A. Muñoz. Simple unified view of branching process statistics: Random walks in balanced logarithmic potentials. *Phys. Rev. E*, 95:032115, Mar 2017.

[187] Carl Van Vreeswijk, LF Abbott, and G Bard Ermentrout. When inhibition not excitation synchronizes neural firing. *Journal of computational neuroscience*, 1(4):313–321, 1994.

[188] Roman M Borisyuk and Alexandr B Kirillov. Bifurcation analysis of a neural network model. *Biological Cybernetics*, 66(4):319–325, 1992.

[189] Frank C Hoppensteadt and Eugene M Izhikevich. *Weakly connected neural networks*, volume 126. Springer Science & Business Media, 2012.

[190] Mark E. J. Newman. The structure and function of complex networks. *SIAM Rev.*, 45(2):167–256, 2003.

[191] Romain Brette, Michelle Rudolph, Ted Carnevale, Michael Hines, David Beeman, James M Bower, Markus Diesmann, Abigail Morrison, Philip H Goodman, Frederick C Harris Jr, et al. Simulation of networks of spiking neurons: a review of tools and strategies. *J, Comput. Neurosci.*, 23(3):349–398, 2007.

[192] Charles Wilson. Up and down states. *Scholarpedia journal*, 3(6):1410, 2008.

[193] Yoseph Imry and Shang-keng Ma. Random-field instability of the ordered state of continuous symmetry. *Physical Review Letters*, 35(21):1399, 1975.

[194] Michael Aizenman and Jan Wehr. Rounding of first-order phase transitions in systems with quenched disorder. *Physical Review Letters*, 64(11):1311, 1990.

[195] A Nihat Berker. Critical behavior induced by quenched disorder. *Physica A: Statistical Mechanics and its Applications*, 194(1-4):72–76, 1993.

[196] Paula Villa Martín, Juan A Bonachela, and Miguel A Muñoz. Quenched disorder forbids discontinuous transitions in nonequilibrium low-dimensional systems. *Physical Review E*, 89(1):012145, 2014.

[197] Pablo Villegas, Paolo Moretti, and Miguel A Muñoz. Frustrated hierarchical synchronization and emergent complexity in the human connectome network. *Sci. Rep.*, 4:5990, 2014.

[198] Miguel A Muñoz, Róbert Juhász, Claudio Castellano, and Géza Ódor. Griffiths phases on complex networks. *Physical review letters*, 105(12):128701, 2010.

[199] Duncan J. Watts and Steven H. Strogatz. Collective dynamics of 'small-world' networks. *Nature*, 393(6684):440–442, 06 1998.

[200] Rosario N Mantegna and H Eugene Stanley. *Introduction to econophysics: correlations and complexity in finance*. Cambridge university press, 1999.

[201] Kun Hu, Plamen Ch Ivanov, Zhi Chen, Pedro Carpena, and H Eugene Stanley. Effect of trends on detrended fluctuation analysis. *Phys. Rev. E*, 64(1):011114, 2001.

[202] Alexander Dobrinevski, Pierre Le Doussal, and Kay Jörg Wiese. Avalanche shape and exponents beyond mean-field theory. *Europhys. Lett.*, 108(6):66002, 2015.

[203] Lasse Laurson, Xavier Illa, Stéphane Santucci, Ken Tore Tallakstad, Knut Jørgen Måløy, and Mikko J Alava. Evolution of the average avalanche shape with the universality class. *Nat. Comm.*, 4, 2013.

[204] Lloyd Nicholas Trefethen and Mark Embree. *Spectra and pseudospectra: the behavior of nonnormal matrices and operators*. Princeton University Press, 2005.

[205] Roger A Horn and Charles R Johnson. *Matrix analysis*. Cambridge university press, 2012.

[206] Michael G. Neubert, Hal Caswell, and J.D. Murray. Transient dynamics and pattern formation: reactivity is necessary for turing instabilities. *Mathematical Biosciences*, 175(1):1 – 11, 2002.

[207] Alan Mathison Turing. The chemical basis of morphogenesis. *Bulletin of mathematical biology*, 52(1-2):153–197, 1990.

[208] Paul C Bressloff, Jack D Cowan, Martin Golubitsky, Peter J Thomas, and Matthew C Wiener. What geometric visual hallucinations tell us about the visual cortex. *Neural Computation*, 14(3):473–491, 2002.